PALEOCLIMATOLOGICAL APPROACH TO PLIO-QUATERNARY PALEOSOL-CALCRETE SEQUENCES IN BALA AND GÖLBAŞI (ANKARA) BY USING MINERALOGICAL AND GEOCHEMICAL PROXIES

A THESIS SUBMITTED TO
THE GRADUATE SCHOOL OF NATURAL AND APPLIED SCIENCES
OF
MIDDLE EAST TECHNICAL UNIVERSITY

BY

CEREN KÜÇÜKUYSAL

IN PARTIAL FULFILLMENT OF THE REQUIREMENTS
FOR
THE DEGREE OF DOCTOR OF PHILOSOPHY
IN
GEOLOGICAL ENGINEERING

SEPTEMBER 2011

Approval of the thesis:

PALEOCLIMATOLOGICAL APPROACH TO PLIO-QUATERNARY PALEOSOL-CALCRETE SEQUENCES IN BALA AND GÖLBAŞI (ANKARA) BY USING MINERALOGICAL AND GEOCHEMICAL PROXIES

submitted by **CEREN KÜÇÜKUYSAL** in partial fulfillment of the requirements for the degree of **Doctor of Philosophy in Geological Engineering Department, Middle East Technical University** by,

Prof. Dr. Canan Özgen _____
Dean, Graduate School of **Natural and Applied Sciences**

Prof. Dr. Zeki Çamur _____
Head of Department, **Geological Engineering**

Prof. Dr. Asuman G. Türkmenoğlu _____
Supervisor, **Geological Engineering Dept., METU**

Examining Committee Members:

Prof. Dr. Selim Kapur _____
Soil Department., Çukurova Üniversity

Prof. Dr. Asuman G. Türkmenoğlu _____
Geological Engineering Dept., METU

Prof. Dr. Fred J. Longstaffe _____
Geology Dept., UWO

Assoc.Prof. Dr. İsmail Ömer Yılmaz _____
Geological Engineering Dept., METU

Assis.Prof. Dr. Zehra Karakaş _____
Geological Engineering Dept., HÜ

Date: 28/09/2011

I hereby declare that all information in this document has been obtained and presented in accordance with academic rules and ethical conduct. I also declare that, as required by these rules and conduct, I have fully cited and referenced all material and results that are not original to this work.

Name, Last name:

Signature:

ABSTRACT

PALEOCLIMATOLOGICAL APPROACH TO PLIO-QUATERNARY PALEOSOL-CALCRETE SEQUENCES IN BALA AND GÖLBAŞI (ANKARA) BY USING MINERALOGICAL AND GEOCHEMICAL PROXIES

Küçükuysal, Ceren

Ph.D., Department of Geological Engineering

Supervisor: Prof. Dr. Asuman G. Türkmenoğlu

September 2011, 246 pages

The major goal of this study is to define the paleoclimatic conditions in Ankara region during Plio-Pleistocene period by evaluating the mineralogical and geochemical proxies carried from the paleosols and their calcretes. The field observations, mineralogical, micromorphological, geochemical and stable isotope investigations were all conducted to achieve a paleoclimatic approach.

As pedogenic minerals in calcretes, presence of dolomite with palygorskite in the Karahamzalı section and calcite with palygorskite in the Bala section together with high salinity and calcification values reveal the semi-arid and dry climatic conditions.

The geochemical signatures of the paleosols are consistent with each other indicating low clastic input during the dry seasons favouring the formation of calcretes. The $\delta^{13}C$ and $\delta^{18}O$ values indicate the formation of calcretes from percolating soil-water under predominantly C4 to C3:C4 association type vegetation. Temperature

calculations show that paleoclimatic conditions favouring the formation of calcretes in the region are semi-arid and seasonally dry with approximately 25°C soil depositional temperature.

This study is the first to give both a radiometric age data to the calcretes of Central Anatolia, Ankara and document their stable isotope compositions. Dated calcretes having ESR ages of 419±69ka and 761 ±120ka point the formation during Middle Pleistocene when Mid-Brunches Event (MBE) was happened and the periodicity changed affecting the climatic control over the European continent. Like the Mediterranean calcretes, this study suggests that calcretes in the study area started to develop with MBE warmth between Marine Isotope Stages of 13-11 and 19-17.

Keywords: Paleosol, calcrete, paleoclimate, Ankara, Plio-Quaternary

ÖZ

BALA VE GÖLBAŞI (ANKARA) PLIYO-KUVATERNER PALEOTOPRAK-KALKRİT SERİLERİNE MİNERALOJİK VE JEOKİMYASAL VERİLER KULLANARAK PALEOİKLİMSEL YAKLAŞIM

Küçükuysal, Ceren

Doktora, Jeoloji Mühendisliği Bölümü

Tez Yöneticisi: Prof. Dr. Asuman G. Türkmenoğlu

Eylül 2011, 246 sayfa

Bu çalışmanın amacı, Ankara bölgesi paleosol ve kalişlerinin mineralojik ve jeokimyasal özelliklerini değerlendirerek Pliyo-Pleyistosen döneminde bölgenin iklim koşullarını tanımlamaktır. Arazi çalışmaları, mineralojik, mikromorfolojik, jeokimyasal ve duraylı izotop analizlerinin tümü paleoiklimsel yorumlamada kullanılmıştır.

Kalişlerde pedojenik olarak bulunan dolomit ile paligorskit (Karahamzalı kesiti) ve kalsit ile paligorskit (Bala kesiti) , yüksek tuzluluk ve kalsifikasyon değerleri ile birlikte yarı kurak iklimi işaret etmektedir.

İki kesit için jeokimya değerleri birbirleri ile uyumlu olup, yarı-kurak dönemlerde malzeme geliminin az olduğunu ve kalişlerin geliştiğini işaret etmektedir. $\delta^{13}C$ ve $\delta^{18}O$ değerleri kalişlerin yarı-kurak dönemlerde C4 ve C3:C4 tipi bitki örtüsü altında toprak profili boyunca süzülen toprak-suyunda oluştuğunu göstermektedir. Bu koşullar için hesaplanan sıcaklık değeri 25°C'dir.

Bu çalışma ilk defa İç Anadolu ve Ankara'da bulunan kalişlerin duraylı izotop değerleri ve radyometrik yaş verisi elde edilmiştir. 419±69ka and 761 ±120ka olarak yaşlandırılan kalişler Orta Pleyistosen dönemi Orta Brunches Olayı (MBE) zamanına denk gelmekte aynı zamanda dönemselliğin değişerek ısınmanın Avrupa kıtasını etkilediği döneme denk gelmiştir. Akdeniz bölgesi kalişleri gibi, bu çalışma da Ankara Bölgesi'nde çalışılan kalişlerin, 13-11 ve 19-17 Okyanusal İzotop Dönemleri arasında MBE ısınması döneminde geliştiğini önermektedir.

Anahtar Kelimeler: Paleotoprak, kalkrit, paleoiklim, Ankara, Pliyo-Kuvaterner

TO MY BELOVED FAMILY…

ACKNOWLEDGMENTS

To begin with, I would like to express my deepest gratitude to my supervisor, Prof.Dr. Asuman G. Türkmenoğlu for all of the help that she has given in the development of this study. She has had a memorable impact on my life. All the contributions of her in each step of the research is deeply appreciated.

I had the honor of working with Prof.Dr. Selim Kapur, Assoc. Prof.Dr. İsmail Ömer Yılmaz and Asiss. Prof.Dr. Zehra Karakaş during the thesis study. Their guidance, support and encouragment are gratefully acknowledged.

Saying thank you to Prof.Dr. Fred J. Longstaffe will never be enough. He made the mineralogical and stable isotope analyses feasible by providing the equipment and the backup. His guidance and help during this study are also deeply appreciated.

During 2007–2008, I had TÜBİTAK 2214 Visiting Scientist Fellowship so that I had a chance to work at University of Western Ontario to carry my analysis under the supervision of Prof. Longstaffe. The tremendous help of Kim Law, Li Huang and Grace Yau are acknowledged.

Funding for the analyses of this study are provided by The Scientific and Technological Research Council of Turkey (TUBITAK) Grant No: 106Y172.

Assoc. Prof. Dr. Nurdan Yavuz Işık and Dr. Zühtü Batı carried pollen analysis of this thesis study. The valuable helps of them are greatly acknowledged.

Assoc. Prof.Dr. Birol Engin and Dr. Canan Aydaş dated the calcretes and provided incredible benefit for the improvement of this study. Their valuable contribution is also acknowledged.

I owe my deepest gratitude to my friends and colleagues Dr. M. Deniz Küstü, Dr. Selin Süer, Dr. Şebnem Ökten and Dr. Huriye Demircan. They showed tremendous support and encouragement throughout the study.

It is a pleasure to thank Dr. Kathleen Nicoll for her encouragement and guidance in developing a structure of any kind of academic writing.

My mother, Muazzez Akbay, my brother Cem İpekgil and his wife Neşe İpekgil and my aunt Sadiye Tangör have provided unconditional love and encouragement throughout my life. Without their support, this study would not have been so valuable.

Most importantly, I would like to thank my husband Onur Küçükuysal and my son Atalay Küçükuysal for their tremendous patience, understanding and encouragement in each step of my life. Your smiling eyes have enlightened my way all the time…

TABLE OF CONTENTS

ABSTRACT…… iv

ÖZ…….. vi

ACKNOWLEDGEMENTS…… ix

TABLE OF CONTENTS…… xi

LIST OF TABLES…… xv

LIST OF FIGURES…… xvii

CHAPTERS

1. INTRODUCTION……..... 1

1.1 PURPOSE…… 1

1.2. LOCATION OF THE STUDY AREA…… 2

1.3. PALEOCLIMATOLOGY CONCEPT…… 2

1.4. PALEOSOLS AND CALCRETES IN CLIMATE STUDIES…….. 5

1.5. ROLE OF SOIL CLAYS IN PALEOCLIMATE STUDIES 15

1.6. CLIMATE DURING PLIO-PLEISTOCENE…… 17

2. LITERATURE REVIEW…… 20

2.1. PREVIOUS STUDIES CONDUCTED ON THE ANKARA REGION……..... 20

2.2. PREVIOUS STUDIES RELATED WITH PALEOSOLS AND CALCRETES …….. 25

3. DESCRIPTION OF THE STUDY AREA……... 37

3.1. GEOLOGY OF THE REGION……. 37

3.2. DESCRIPTION OF THE SAMPLING SITES…….. 42

3.2.1. Karahamzalı Section…… 42

3.2.2. Bala Section……. 48

3.2.3. Other Sampling Sites……... 49

4. METHODOLOGY……. 54

4.1. FIELD SAMPLING……... 54

4.2. THIN SECTION PREPARATION…… 54

4.3. ANALYTICAL TECHNIQUES…… 57

4.3.1. Separation and X-ray Diffraction of the <2µm Size-Fraction……... 58

4.3.2. Preparation of Samples For The Stable Isotope Analysis…….. 62

4.3.3. Geochemical Analysis…… 63

4.3.4. Electron Spin Resonance Technique…….. 64

4.3.5. Scanning Electron Microscopy…….. 66

5. MINEROLOGY…….. 67

5.1. MINERALOGY OF THE KARAHAMZALI SECTION … 69

5.2. MINERALOGY OF THE BALA SECTION ……... 75

5.3.MINERALOGY OF İNCEK, DODURGA, METU, ÇİĞDEM SAMPLES…….. 87

5.4.SCANNING ELECTRON MICROSCOPE INVESTIGATIONS……..... 91

5.4.1. SEM Study on Karahamzalı Samples…… 93
5.4.2. SEM Study on Bala Samples…… 100

5.4.3. SEM Study on İncek, Dodurga, Çiğdem and METU Samples…….. 104

5.5. DOLOMITE AND ITS STOICHIOMETRY…… 108

6. MICROMORPHOLOGY……. 116

6.1. THIN SECTION DESCRIPTIONS ……. 116

6.2. TERMINOLOGY…….. 116

6.3.MICROMORPHOLOGY OF THE KARAHAMZALI PALEOSOLS AND CALCRETES…… 117

6.4.PETROGRAPHY OF OTHER SAMPLES…… 132

7. GEOCHEMISTRY…… 141

7.1. INTRODUCTION ……. 141

7.2. GEOCHEMISTRY OF KARAHAMZALI SECTION……. 146

7.3. GEOCHEMISTRY OF BALA SECTION…… 167

7.4.GEOCHEMISTRY OF CALCRETES FROM OTHER SAMPLING SITES…… 186

7.5. STABLE ISOTOPE GEOCHEMISTRY…….. 188

7.5.1 Stable Isotope Values of Carbonates in Karahamzalı and Bala Sections…… 190

8. GEOCHRONOLOGY…….. 196

9 DISCUSSION……. 200

9.1. AGE CONSTRAIN…….. 200

9.2. AN APPROACH TO THE MINERALOGY…… 201

9.3. AN APPROACH TO THE GEOCHEMISTRY…… 206

9.3.1. Karahamzalı Data…….. 206

9.3.2. Bala Data…… 208

9.4. AN APPROACH TO STABLE ISOTOPES……. 210

9.5. INTERPRETATION OF ALL PROXY DATA USED IN THIS STUDY……. 212

10. CONCLUSION…… 220

REFERENCES…….. 223

CURRICULUM VITAE……. 244

LIST OF TABLES

TABLES

Table 1.1. List of proxy used for paleoclimate reconstructions (Bradley, 1999)…… 3

Table 5.1. Semi-quantitative analysis of bulk composition of samples from Karahamzalı section…… 76

Table 5.2. Semi-quantitative analysis of clay fraction of samples from Karahamzalı section…… 78

Table 5.3. Semi-quantitative analysis of bulk composition of samples from Bala section……. 84

Table 5.4. Semi-quantitative analysis of clay fraction of samples from Bala section……. 84

Table 5.5. Semi-quantitative analysis of bulk composition of samples from İncek, Dodurga, METU, Çiğdem locations…… 92

Table 5.6. Semi-quantitative analysis of clay minerals from İncek, Dodurga, METU, Çiğdem locations…….. 92

Table 5.7. Table listing the samples including dolomite and their Ca:Mg ratio calculations……. 111

Table 5.8. Table showing the dolomite included samples with their d_{104} and Nca_{CO3} calculations. …….. 112

Table 7.1. Molecular weathering and pedogenesis ratios (Sheldon and Tabor, 2009 and Retallack, 2001)…….. 145

Table 7.2. Weight percentages of common oxides in paleosols and calcrete levels of Karahamzalı Section……. 151

Table 7.3. Trace element concentrations in paleosols and calcretes of Karahamzalı Section……... 152

Table 7.4. REE concentrations in paleosols and calcerets of Karahamzalı Section……. 153

Table 7.5. Weight percentages of common oxides in paleosols and calcrete levels of the Bala Section…… 170

Table 7.6. Trace element concentrations in paleosols and calcretes of Bala Section…….. 171

Table 7.7. REE concentrations in paleosols and calcerets of Bala Section…. 172

Table 7.8. Major element values of the samples from other sampling sites… 187

Table 7.9. $\delta^{13}C$ and $\delta^{18}O$ isotope compositions of Karahamzalı Section…… 191

Table 7.10. $\delta^{13}C$ and $\delta^{18}O$ isotope compositions of Bala Section……... 192

Table 8.1. The geochemical compositions of the calcretes from Bala section (Küçükuysal et al., 2011)……. 197

Table 8.2. The radioactivity and dating results of C1 and C2 samples (Küçükuysal et al., 2011)……. 198

Table 8.3. Pollen results of Karahamzalı paleosols……. 199

Table 9.1. The calculated $\delta^{18}O$ values of the fluids responsible for the formation of the Carbonates in Karahamzalı and Bala paleosols…… 213

LIST OF FIGURES

FIGURES

Figure 1.1 Location of the study are on (a) Turkey map ; (b) on Ankara map (not to scale) (1: Karahamzalı site; 2: Bala site; 3: METU, Çiğdem, İncek and Dodurga)…… 4

Figure 1.2. Schematic diagram of major components of the climatic system (Bradley, 1999)…… 5

Figure 1.3. Master horizons on soil profile (Retallack, 2001)……. 8

Figure 1.4. Calcrete classification based on the stages of development (Machette, 1985)…….. 12

Figure 1.5. Calcrete classification according to hydrological setting by Carlisle, 1980; 1983)…… 12

Figure 1.6. Global deep-sea oxygen and carbon isotope records based on data compiled from more than 40 DSDP and ODP sites (Zachos et al., 2001). …….. 19

Figure 3.1. The terrane map of Turkey showing the position of Ankara in a complex geological texture (Göncüoğlu et al., 1997)…….. 38

Figure 3.2. Geological map of Ankara produced by MTA (Akyürek et., 1997)…… 43

Figure 3.3. Maps showing the location of the Karahamzalı section…… 44

Figure 3.4. a & b) Field views of Karahamzalı section; c) sharp contact between red colored mudstone and the overlying channel deposit (the hammer is 33cm long). …….. 45

Figure 3.5. Columnar section of Karahamzalı section with field descriptions and soil properties. …… 47

Figure 3.6. Maps illustrating the location of the Bala section……. 50

Figure 3.7. Field views of Bala section showing alternations of red colored mudstones with channel deposits and the development of calcretes…….. 51

Figure 3.8. Columnar section of Bala section with field observations and soil properties……... 52

Figure 3.9. İncek sampling site with a powdery carbonate developed within a red colored mudstone layer of Late Pliocene age……. 53

Figure 3.10. Dodurga section showing alluvial fan deposists with channel deposist alternation. ……..... 53

Figure 4.1. Drilling operation in Karahamzalı sampling site…….. 55

Figure 4.2. Drilling operation in Bala sampling site…… 56

Figure 4.3. The pictures of freeze-dryer and the high-speed centrifuge in the Sample Preparation Laboratory of the Department of Geology at University of Western Ontario, Canada……. 60

Figure 4.4. Multiprep working mechanism…… 64

Figure 5.1. X-Ray diffraction of ethylene glycol solvated K-41 basaltic substrate (Sm: Smectite; Pla: Plagioclase)…….. 70

Figure 5.2. X-ray diffraction of powder paleosol from the lower part of the Karahamzalı Section (Sm: Smectite; Pal: Palygorskite; Qua: Quartz; Cal: Calcite)……. 71

Figure 5.3. X-ray diffraction of powder paleosol (carbonate-rich) from the Karahamzalı Section (Sm: Smectite; Chl: Chlorite; Kao: Kaolinite; Qua: Quartz; Pla: Plagioclase; Dol: Dolomite). ……. 71

Figure 5.4. X-ray diffraction of air dried and ethylene glycol solvated K-1 paleosol from the Karahamzalı Section. (Sm: smectite; Chl: chlorite; Pal: palygorskite; Qua: quartz; AD: air dried; EG: ethylene glycol solvated)….. 73

Figure 5.5. Changes in amounts of bulk mineral compositions (wt in %) of the Karahamzalı section with respect to depth (m)……. 77

Figure 5.6. Changes in amounts of clay minerals of samples (wt in %) in the Karahamzalı section with respect to depth (m)…… 79

Figure 5.7. X-ray diffraction of powder B-2 sample from the Bala section (Sm: smectite; Pla: plagioclase; Qua: quartz; Cal: calcite). …… 80

Figure 5.8. X-ray diffraction pattern of the B-2 sample from the Bala section (Sm: smectite; AD: air dried; EG: ethylene glycol; 300° and 550°C: heating treatments)…….. 81

Figure 5.9. X-ray diffraction pattern showing v/p ratio indicating smectite crystallinity…….. 81

Figure 5.10. X-ray diffraction pattern of the sample with AD, EG and heating treatments of the Bala section (Sm: smectite; Chl: chlorite; Kao: kaolinite; Qua: quartz; Cal: calcite; AD: aird dried; EG: ethylene glycolated: 300°C and 550°C : heating treatments)…… 82

Figure 11. X-ray diffraction pattern of palygorskite bearing sample from the Bala section (Sm: smectite; Pal: palygorskite; AD: air dried; EG: ethylene glycolated; 300°C and 550°C: heating treatments)……. 82

Figure 5.12. Changes in amounts of bulk mineral compositions of Bala section with respect to depth…… 85

Figure 5.13. Changes in amounts of clay fraction of samples in Bala section with respect to depth…… 86

Figure 5.14. X-ray diffraction pattern of a calcrete sample from Çiğdem area (Qua: quartz; Pla: plagioclase; Cal: calcite)…… 87

Figure 5.15.X-ray diffraction patterns of K–1, 14, 370–1 and 370–2 samples from Çiğdem and METU areas (Qua: quartz; Pla: plagioclase; Cal: calcite). …… 88

Figure 5.16. X-ray diffraction pattern of powder Dodurga sample (Qua: quartz; Pla: plagioclase; Cal: calcite). …… 89

Figure 5.17. X-ray diffraction pattern of clay fraction of Dodurga sample (Sm: smectite; I: illite; Kao: kaolinite; AD: air dried; EG: ethlene glycol; 300°C and 550°C: heat treatments). …… 89

Figure 5.18. X-ray diffraction pattern of paleosol sample from İncek area (Qua: quartz; Pla: plagioclase)……. 90

Figure 5.19. X-ray diffraction pattern of a paleosol from İncek area (Sm: smectite; I: illite; Kao: kaolinite; AD: air dired; EG: ethylene glycol; 300°C and 550°C: heating treatments). ……. 90

Figure 5.20. SEM-EDX on Karahamzalı paleosol revealing palygorskite fibers on dolomites…….. 94

Figure 5.21. Bridge-like morphology of palygorskite fibers on paleosols of the Karahamzalı section……... 95

Figure 5.22. Rhombohedral dolomites forming calcretes of the Karahamzalı section. 95

Figure 5.23. Short and thick illite fibers together with long and thin palygorskite fibers developed within Karakamzalı palesols. ……. 96

Figure 5.24. SEM image of paleosols from Karahamzalı section revealing the presence of smectite with corn-flake morphology covered by palygorskite fibers; feldspar grain next to them…….. 97

Figure 5.25. SEM image of chlorite observed with its flaky morphology within the Karahamzalı paleosols……. 97

Figure 5.26. SEM image of a feldspar grain and palygorskite on Karahamzalı paleosols with EDX analysis…… 98

Figure 5.27. SEM image of dolomites filling the pore space within Karahamzalı paleosol……. 99

Figure 5.28. SEM image of dolomites with their fresh surcaes not covered with any palygorskite fiber……. 99

Figure 5.29. SEM image of clay minerals and palygorskiye fibers developed within Bala paleosols…… 101
Figure 5.30. SEM image of a detrital quartz and cubic pyrite……..... 102
Figure 5.31. SEM image of smectite developed on Bala sample…… 103
Figure 5.32. SEM image of fresh quartz grain with conchoidal fracture surfaces together with smectite on Bala sample……. 104
Figure 5.33. SEM image of feldspar grain surrounded by semctite and palygorskite fibers on Bala paleosol…….. 105
Figure 5.34. SEM image of Bala paleosol revealing authigenic formation of clay mineral most possibly smectite with fibrous palygorskite…….. 106
Figure 5.35. SEM image of palygorskites developed on calcite grains……... 107
Figure 5.36. SEM image of Dodurga calcrete revealing the contact between calcite and clay minerals…….. 107
Figure 5.37. SEM image of clay minerals and calcite forming the cement of Dodurga sample……. 108
Figure 5.38. SEM image of rhombohedral calcites in Dodurga sample…… 109
Figure 5.39. Photomicrographs of dolomites found in Karahamzalı samples revealing their a) Group III and b) Group II characteristics…… 115
Figure 6.1.The general view of the caliche sample of the A-15 level from Karahamzalı section……. 118
Figure 6.2. Micritic carbonate minerals lining (a) the voids, (b) grains and (c) the channels of Karahamzalı paleosol……..... 119

Figure 6.3. Photomicrographs of (a) dense and continous infilling of MnO_2 within a void space and around a feldspar fragment within a calcrete sample of Karahamzalı succession; (b) clusters of broken/beaded MnO_2 coatings within a void space in calcrete sample of the Karahamzalı succession with probable organic infill. …… 120

Figure 6.4. Photomicrographs of sparry carbonate mineral infillings within the void spaces of calcretes in Karahamzalı succession (a,b) U-shaped lining of the voids are filled with coarse grained carbonates; (c) two almost parallel void spaces surrounding a rock fragment are filled with sparry carbonate and include MnO_2 clusters……. 121

Figure 6.5. Sparry carbonate minerals (a) surrounding a carbonate nodule and (b) coating the void space left from faunal activity. The sparry carbonates with sharp edges are the dog-tooth cement. ……. 122

Figure 6.6. Pore spaces developed due to dissolution processes remain unfilled but surrounded by coarse grained carbonate minerals…….. 123

Figure 6.7. Subangular blocky microstructure and well accomodated ped structure of the paleosols within the Karahamzalı succession. The photographs belong to the samples from the A-5 levels…… 124

Figure 6.8. Photomicrographs of (a) the primary partially accomodated subangular blocky peds and (b)granular to subangular smaller partially accomodated peds of the paleosols within the Karahamzalı succession. ….. 125

Figure 6.9. The voids morphologically classified as planar voids within the paleosols of the Karahamzalı succession……. 126

Figure 6.10. (a) spherical and (b) oval faunal chambers connected to elongated channels of Karahamzalı paleosols. ……... 126

Figure 6.11. Feldspar fragments floating in the calcrete sample (a) quartz and feldspar grains and rock fragments of andesite floating in the paleosol sample (b)……. 128

Figure 6.12. MnO_2 and clay coatings as (a) external quasi-coating of a carbonate in a paleosol sample of the calcrete sample of the Karahamzalı section…….. 129

Figure 6.13. Plant parts faecal excrements within the U-11 paleosol sample of Karahamzalı succession. …… 130

Figure 6.14. The disturbance within the paleosol matrix due to the expandable clay mineral contents of the paleosola of the Karahamzalı section. …… 131

Figure 6.15. Spheroidal microstructure of the paleosol in Karahamzalı section……. 131

Figure 6.16. Photomicrographs of the calcretes of the Dodurga-Türkkonut area revealing (a) Micritic calcite cement and microspar surrounding the rock fragment; (b) dog-tooth cement type microspar develeopment and (c) presence of calcite together with clay illuviations. Iron oxide linings are also observeable in calcrete samples……... 134

Figure 6.17. Iron oxide lining and clay cutans, micritic cement and polycrytsalline quartz grain of Dodurga calcrete. …….. 135

Figure 6.18. The elongated voids surrounded by sparry calcite crystals and infilled with humified material…… 135

Figure 6.19. Chalcedony infilling within an irregular shaped void of calcrete from the Dodurga area. ……. 136

Figure 6.20. Mineral grains and rock fragments surrounded by sparry calcite crystals and cemented with micrite. Rare subrounded to oval fragments in calcrete of Dodurga area. ……... 136

Figure 6.21. Pore spaces lined by secondary vermiform kaolinite and feldspars weathered to kaolinite……. 137

Figure 6.22. Clay coatings in the siltstone matrix from the Dodurga area. ... 138

Figure 6.23. A fine grained clastic rock fragment with rounded edges and quartz and feldspar grains with subangular edges…….. 138

Figure 6.24. Dense micritic cement and sparry calcite surrounding the fragments of the Çiğdem area. …… 139

Figure 6.25. Different forms of sparry calcites coating the rock fragments of the calcretes from Çiğdem area. (a) long-prismatic form, (b) fibrous form both pointing to the vadose zone of precipitation. ……. 140

Figure 7.1. Ti-normalized major oxide values of Karahamzalı samples…… 154

Figure 7.2. Ti-normalized trace element values of Karahamzalı samples….. 166

Figure 7.3. Ti-normalized REE values of Karahamzalı samples…… 158

Figure 7.4. Upper Crust and Shale European normalized REE values of Karahamzalı samples…….. 160

Figure 7.5. Trace element ratios of provenance estimation for Karahamzalı samples…….. 161

Figure 7.6. Molecular weathering ratios calculated for Karahamzalı samples…… 165

Figure 7.7.Chemical index of alteration values of Karahamzalı paleosols and carbonates……. 166

Figure 7.8. A-CN-K triangular plot of Nesbitt and Young (1984, 1989)….. 167

Figure 7.9. Ti-normalized major oxide values of Bala samples……. 173

Figure 7.10. Al-normalized trace element values of Bala samples……. 176

Figure 7.11. Al-normalized REE values of Bala samples…….. 178

Figure 7.12 Trace element ratios of provenance estimation for Bala samples…… 180

Figure 7.13. Upper Crust and Shale European normalized REE values of Bala samples…… 182

Figure 7.14. Molecular weathering ratios calculated for Bala samples…….. 184

Figure 7.15. Chemical index of alteration values of Bala paleosols and carbonates……. 185

Figure 7.16. A-CN-K triangular plot of Nesbitt and Young (1984, 1989)….. 186

Figure 7.17. δ13C and δ18O values of Karahamzalı samples plotted with respect to depth…… 193

Figure 7.18. $\delta^{18}O$ versus δ^{13} C values of Karahamzalı section…… 194

Figure 7.19. δ13C and δ18O values of Bala samples plotted with respect to depth……. 195

Figure 7.20. $\delta^{18}O$ versus $\delta^{13}C$ values of Bala section…….. 195

Figure 9.1. Relative changes between calcite, dolomite, palygorskite and smectite with respect to depth. …… 204

Figure 9.2. Relative changes between smectite, palygorskite and calcite with respect to depth…… 205

Figure 9. 3. Comparison of the stable isotope values of both sections studied…… 215

Figure .9.4. Interpretation of all proxy data of Karahamzalı section……... 216

Figure 9.5. Interpretation of all proxy data of Bala section……. 217

Figure 9.6. Global Stack $\delta^{18}O$ data showing marine isotope stages…… 218

Figure 9.7. Schematic model representing two different climatic conditions in the region (a) semi-arid, (b) wet conditions (modified from Armenteros and Huerta, 2006)…… 219

CHAPTER 1

INTRODUCTION

1.1. PURPOSE

The purpose of this study is (i) to document the role of Plio-Quaternary paleosols and their carbonates of Ankara region in paleoclimate studies, (ii) to explain the field characteristics of the paleosols and calcretes, (iii) to reveal the mineralogical compositions of the paleosols with their micromorphological properties defining the pedogenic features, (iv) to present oxygen and carbon isotope analysis of the carbonates in the studied paleosols to emphasize their potential to reconstruct the climatic conditions during the Plio-Pleistocene in the region, (v) to test whether the proxies used show evidences of Mid-Brunhes Event (warm period in Middle Pleistocene) occurred in the region and (vi) to evaluate the relevance of the proxy data gathered in this study to compare with the worldwide data to assess whether the paleoclimatological conditions are locally affected or have the global climatic signals of the Plio-Pleistocene.

The scope of work is summarized as:

- to evaluate the worldwide literature having the paleosols and calcretes as a dominant proxy for paleoclimate reconstruction;
- to assess the mineralogical and geochemical proxies of the paleosols and their calcretes to be used for the climatic expressions;
- to constrain a paleoclimatic history of the region for the Plio-Pleistocene by giving the first radiometric age data of the calcretes in Central Anatolia and to compare it with the pollen ages.

1.2. LOCATION OF THE STUDY AREA

The study area is composed of three separate sites located within Ankara, Central Anatolia, Turkey (Figure 1.1a). The first site in the south of Ankara near Kulu is in Karahamzalı village, 80km away from METU campus. The second sampling area is close to Çavuşlu Village, Bala in the southeast of Ankara. The last study area is a group of Çiğdem, METU, İncek and Dodurga areas in the southwest of Ankara (Figure 1.1b).

1.3. PALEOCLIMATOLOGY CONCEPT

Climate is the end-product of a several subsystems - the atmosphere, oceans, biosphere, land surface and cryosphere - which collectively make up the climate system (Figure 1.2) (Bradley, 1999). This means it is naturally dependent on geological factors which leads to the use of geological proxies for assessing past climates. As climate changes, the studies about the global climate conditions and the future predictions become more popular and important recently. These studies can be multi-disciplinary and geology is one of the important disciplines dealing with both past and present climatic conditions. Present climatic conditions can be predicted mostly by meteorological instruments; however land forms and processes are very important factors which cause sudden changes in climate. Knowing the principle of "the past is key to the future", the identification of past climates is very important to predict future climates accurately.

Bradley (1999) defined paleoclimatology as a the study of climate prior to the period of instrumental measurements and indicated that those instrumental records could only measure very recent climatic changes. Therefore, climate-dependent parameters, which are also called as proxy data, are very important in reconstructing paleoclimate of a region. The major types of proxy data are listed in the Table 1.1.

Table 1.1. List of proxy used for paleoclimate reconstructions (Bradley, 1999).

1. Glaciological (Ice cores)
    - Geochemistry (major ions and isotopes of oxygen and hydrogen)
    - Gas content in air bubbles
    - Trace elements and microparticle concentrations
    - Physical properties (e.g. ice fabrics)

2. Geological

i. Marine (ocean sediment cores)

- Oxygen isotopic compostion, Morphological variations
- Faunal and floral abundance, Alkenones (from diatoms)

ii. Inorganic sediments

- Terrestrial (aeolian) dust and ice-rafted debris
- Clay mineralogy

iii. Terrestrial

- Glacial deposits and features of galical erosion
- Periglacial features, Aeolian depsoits (loess and dune
- Shorelines (eustatic and galico-eustatic features)
- Lacustr s) ine sediments and erosional fetaures (shorelines)
- Pedological features (relict soils)
- Speleothems (age and stable isotope composition)

3. Biological
    - Tree rings (width, denstiy, stable isotope compositions)
    - Pollen (type, relative abundance, and/or absolute concentration)
    - Plant macrofossils (age and distribution)
    - Insects (assemblage characteristics)
    - Corals (geochemistry)
    - Diatoms, ostracods and other biota in lake sediments (assemblages, abundance, and/or geochmeistry)
    - Modern population distribution (refugia and relict populations of plants and animals)

4. Historical
    - Written records of environmental indicators

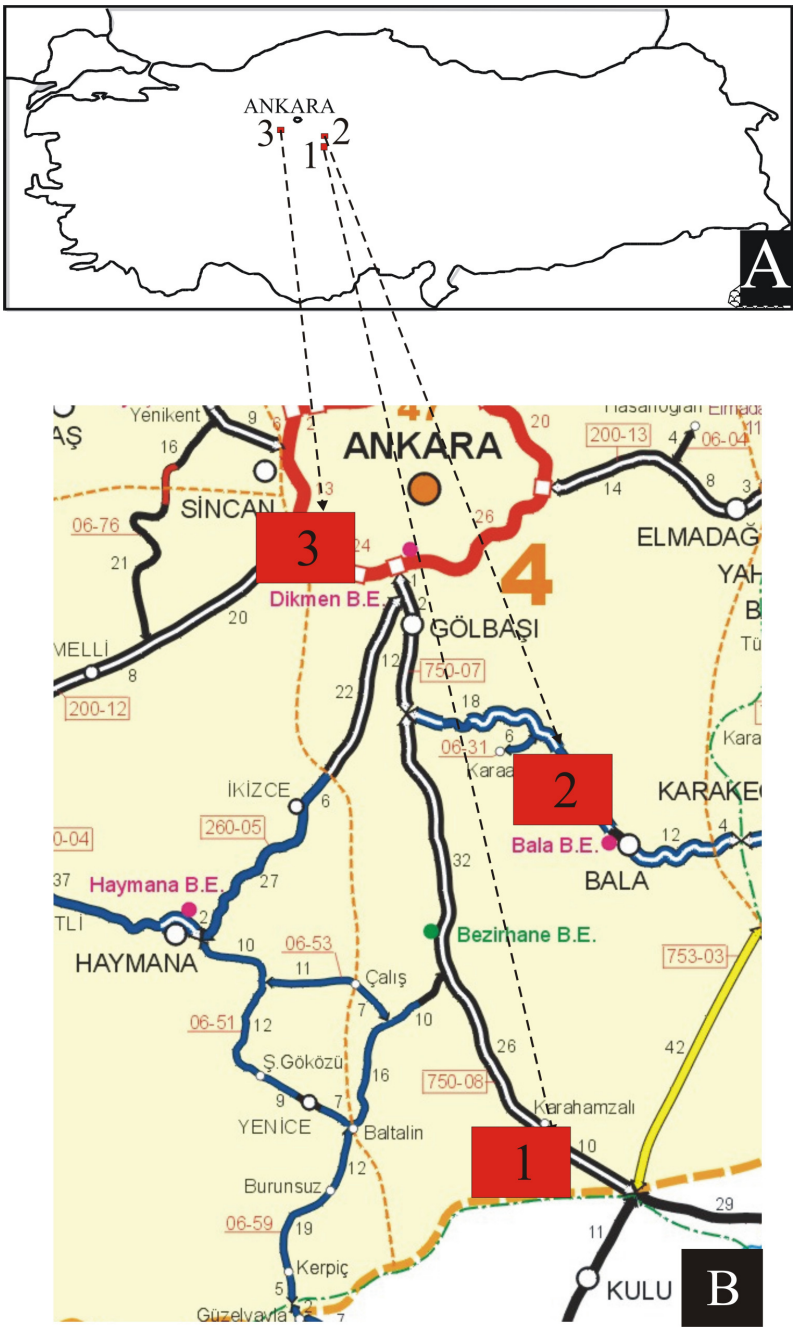

Figure 1.1 Location of the study area on (a) Turkey map and (b) Ankara map (not to scale) (1: Karahamzalı site; 2: Bala site; 3: METU, Çiğdem, İncek and Dodurga).

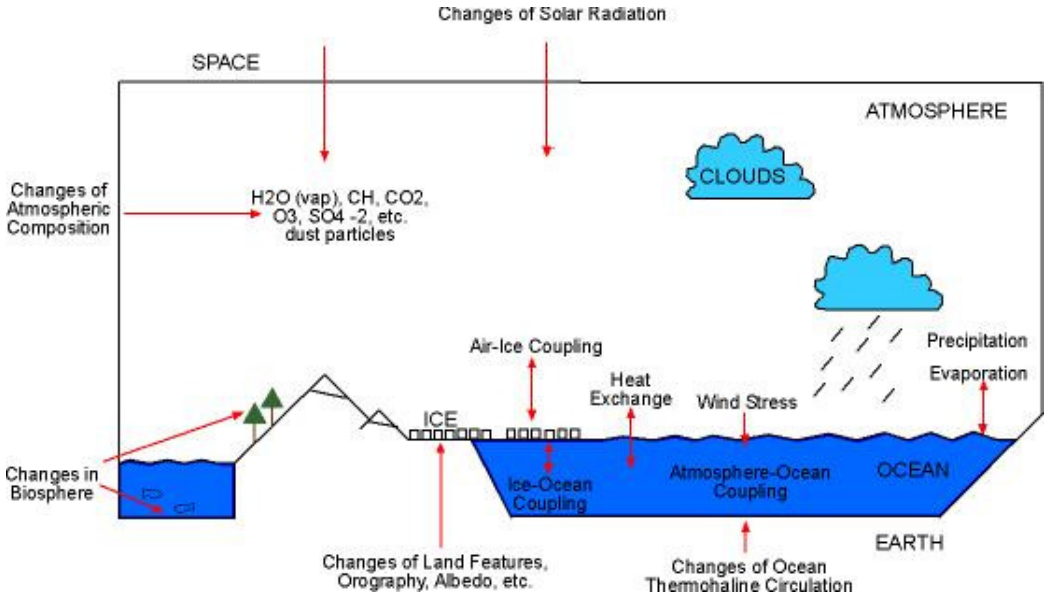

Figure 1.2. Schematic diagram of major components of the climatic system (Bradley, 1999).

1.4. PALEOSOLS AND CALCRETES IN CLIMATE STUDIES

Paleosols are used to interpret the past climates. By definition, a paleosol or fossil soil is a soil that formed on a landscape of the past (Kraus, 1999). In the paleopedological point of view of Retallack (2001), soil has a definition of a material forming the surface of a planet or similar body and altered in place from its parent material by physical, chemical or biological processes. Due to their structures and properties, as Morozova (1995) summarized, paleosols have complex informations about i) soil processes shaping the soil profile itself during pedogenesis in the warm interglacials and interstadials, (ii) natural processes which characterise the transition to cold semicycles (glacial stages) and (iii) diagenetic processes. Many unconformities show evidence of paleosols unless they were scoured clean by fluvial or marine erosion before being covered by later sediment.

Paleosols are also abundant in some sedimentary and volcanic successions (Retallack, 2001). In aggradational systems, as Kraus (1999) pointed out, if erosion is limited and sedimentation is rapid and unsteady, then weakly developed-compound paleosols are formed; on the other hand, if the rate of pedogenesis is greater than the rate of deposition, then composite paleosols which are vertically successive are formed. In contrast, if sedimentation is steady and erosion is insignificant, thick cumulative soils can easily form.

Although they seem featureless at first sight, paleosols have three major distinctive properties: 1) traces of life, 2) soil horizons, and 3) soil structure (Retallack, 1988, 1992, 2001). The best field criteria to distinguish paleosols from other sedimentary deposits is having fossil root traces which show that plant once grew in the sediment while the conditions are stable and were preserved under highly reducing (negative Eh) conditions. There are also some criteria which can be used as evidence for the presence of past organisms without having any organic preservation: 1) irregular tubular shapes, tapering downward and branching downward or outward from a center, and 2) concertina-like shape due to the compaction of surrounding sediment around lateral rootlets. Concentrations of other trace fossils such as burrows also can be used because they record periods of reduced or no deposition during which sediment was extensively modified at the surface (Retallack, 2001; 1997). Opal phytoliths, calcareous phytoliths, leaves and fructifications, pollen and spores, bones, teeth, wood and charcoal are the materials that can possibly be preserved in the old soils revealing the pH and Eh conditions (Retallack, 1997). Soil horizons of paleosols are one of the most useful features to recognize them within sedimentary sequences.

Generally, soil horizons show gradual changes in texture, colour or mineral content down into the parent material from the truncated ancient land surface (Retallack, 1997). Horizons of paleosols are distinct from many kinds of geological layering in

that the top of the uppermost horizon of a paleosol is usually truncated sharply whereas boundaries between lower horizons and underlying parent material commonly are gradational (Retallack, 2001).

The soil horizons vary with many subordinate properties. There are seven master horizons (Retallack, 2001; Soil Survey Staff, 1975; 1998). The O horizon is the upper-most horizon with surface accumulation of organic matter overlying clayey or sandy part of soil (Figure 1.3). The A horizon is the level where humified organic matter mixed with mineral fractions are accumulated. It usually occurs at the surface or below the O horizon. The E horizon underlies O or A horizon and is characterized by less organic matter, less sesquioxides or less clay than the underlying horizon. It is usually light colored due to abundance of quartz. The B horizon underlies an O, A or E horizons and shows enrichment in clay, carbonate, sesquioxides or organic matter. The K horizon is a subsurface horizon which is impregnated with carbonate such that it forms a massive layer. The C horizon is the subsurface horizon that is more weathered than bedrock and lacks the degree of weathering of A, E, and B horizons. R is the lowermost horizon and it represent the consolidated and unweathered bedrock. (Figure 1.3)

The master horizons can be recognized and identified in the field; however, to have a best description of paleosol, each subordinates of the master horizons must be defined with all mineralogical, morpholgical and geochemical properties.

The third criteria is the soil structure that is developed to different degrees and progressively overwhelmed pre-existing structures of parent material (Retallack, 2001). Soils can have open cracks and hollows. Burrows and root traces are tubular features of soils. Glaebules or naturally hardened soil lumps are another general classes of soil structures. Peds are very important features for soils. They are the

aggregates of soil: the clods of earth between cracks, burrows and other soil openings (Retallack, 2001). They are generally classifed according to their size, angularity and shape. Therefore, seven types of peds are characterized: they are platy, prismatic, columnar, angular blocky, subangular blocky, granular and crumb structures. All of the ped structures have distinctive features recognizable from the other ped structures. Additionally, the formation of ped structures are also related to the environmental and climatic conditions therefore are good indicators of the conditions at the time of soil formation. Cutans are modified surfaces of peds, clasts or crystals (Retallack, 2001). There are many kinds of cutans varying in composition. Argillan is a term used for clay cutans.

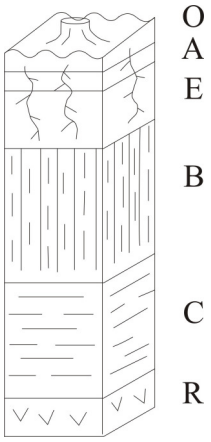

Figure 1.3. Master horizons on a soil profile (Retallack, 2001).

Ferran is cutan of sesquioxides of iron. Cutans for iron or manganese oxides are called mangan. There are mainly three types of formation mechanisms for cutans: 1) washing down of material into cracks (illuviation cutans); 2) progressive alteration

inward from a surface (diffusion cutans); 3) differential shear forces within the soil (stress cutans). Also microfabric of soils and paleosols are used to differ them. The details of microfabrics are available in Retallack (2001).

Nettleton et al. (1998) classified paleosols into three: buried, exhumed and relict soils. Relict paleosols are soils that formed on pre-existing landscapes, but were not buried by younger sediment. Buried ones are the soils that were buried by younger sediment/rock. Exhumed paleosols are soils that were buried but have been re-exposed on the land surface by erosion. In his study it is also stated that exhumed and relict soils are not easy to recognize. Then Nettleton et al. (2000) added a new order for paleosols: lithified paleosols that are commonly buried although some may be exhumed.

Particles size analysis which is informative for the diagnostics of the pedogenesis, total chemical anaylses providing information about the contact of chemical elements in the parent material, amount of CO_2 of carbonates, humus content and composition of clay minerals to identify processes of soil formation are the physico-chemical analyses that can be hold to identify the paleosols (Morozova,1995).

Many studies about paleosols use modern soil classification systems including the Soil Taxonomy (Soil Survey Staff, 1975; 1998) and the Food and Agriculture Organization of the United Nations (FAO, 1974) classification. The Mack et al. (1993) classification system is based on the field identifications of paleosols which makes classification more simpler and objective according to Kraus (1999).

However, as Retallack (1993) stated that using such restricted classification systems has disadvantages, Kraus (1999) confirmed using modern soil classification systems. Nettleton et al. (2000) proposed a paleosol taxonomy providing field-observable and

micromorphological features, chemical and clay mineralogical properties of paleosol orders (Retallack, 2001).

Paleosol carbonates which are generally called as calcretes or caliches are very important materials for interpreting the semi-arid to arid climatic conditions (James, 1972; Goudie, 1973; Goudie, 1983; Tucker, 1991). Calcrete is defined as a product of terrestrial within the zone of weathering in which calcium carbonate ($CaCO_3$) has accumulated in and/or replaced a pre-existing soil, rock, sediment or weathered material to give a substance which may ultimately develop into an indurated mass (Eren et al., 2011; Goudie, 1973; Salomons et al., 1978; Wright and Tucker, 1991).

This study uses the definiton of calcretes defined by Wright and Tucker (1991) that calcrete is a near surface, terrestrial accumulation of predominantly calcium carbonate, which occurs in a variety of forms from powdery to nodular to highly indurated, resulting from the cementation and displacive/replacive introduction of calcium carbonate into soil profiles, bedrock and sediments in areas where vadose and shallow phreatic groundwaters become saturated with respect to calcium carbonate.

If the main carbonate mineral is dolomite, then the name of the encrustation is called as dolocrete (Wright and Tucker, 1991). In the same study, the two basic types of calcretes are given as pedogenic calcretes formed in soil profiles beneath soil in the vadose zone and groundwater calcretes (or phreatic) developed around the water table. Before starting to classify the calcretes, it should be stated that the calcretes are not soil but occur within soil profiles containing discrete subhorizons (Wright and Tucker, 1991). It is also stated in Wright and Tucker (1991) that calcretes can only occur within certain types of paleosols which are Aridisols, Vertisols and Mollisols (Soil Survey Staff, 1975). Five basic classification schemes are used to classify the

calcretes. The first classification is based on the morphology of the calcretes by Netterberg (1967; 1980) and Goudie (1983). It starts with calcareous soils as an immature stage and continues with calcified soil, powder calcrete, pedotubule calcrete. Then as a semi-mature stage, nodular and honeycomb calcretes are classified. The mature stage includes hardpan, laminar and boulder/cobble calcretes (Wright and Tucker, 2001).

The second classification of calcretes is based on the stages of development by Machette (1985). This systems classifies the calcretes in terms of whether they are developed on gravel rich or gravel poor substrate, $CaCO_3$ distribution and maximum $CaCO_3$ content (Figure 1.4). The classification starts with stage 1 and 2 calcretes which are very immature ones and include very minor amount of $CaCO_3$ with respect to the others. Then, stage 3 calcretes are semi-mature calcretes with pronounced amount of $CaCO_3$ and generally the nodular calcretes are of this stage of development. Stage 4 up to 6 are the mature stages with very high amount of $CaCO_3$ and very dense, indurated and complex fabrics of calcretes (Figure 1.4) (Wright and Tucker, 2001).

The third classification is based on the hydrological setting by Carlisle (1980; 1983). This scheme classifies the calcretes as pedogenic, non-pedogenic, vadose and phreatic zone calcretes (Figure 1.5).

The mineralogical classification of calcretes defined by Netterberg (1980) is based on % dolomite content and approximate equivalent of % $MgCO_3$. This system names the calcretes as dolocrete if they include more than 90% dolomite and calcitic dolocrete if it is between 50–90%. It is followed by dolomitic calcrete and magnesian calcrete if the dolomite content between 5–10%. The name calcrete is relevant if dolomite content is less than 5%. (Wright and Tucker, 2001).

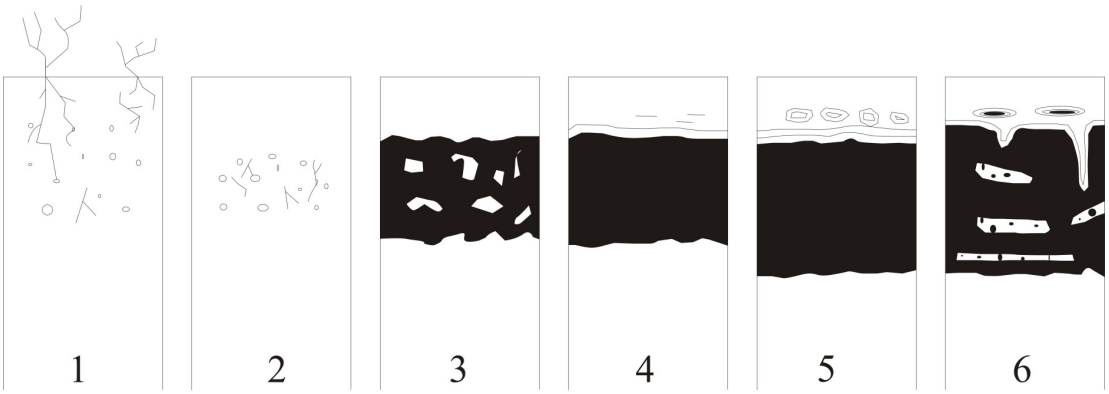

Figure 1.4. Calcrete classification based on the stages of development (Machette, 1985).

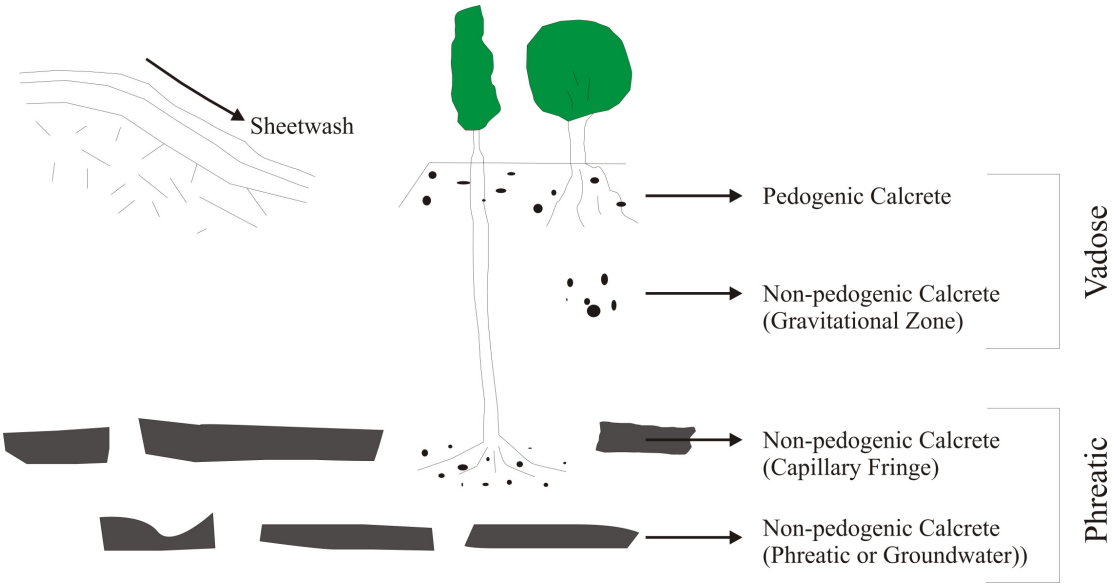

Figure 1.5. Calcrete classification according to hydrological setting by Carlisle, (1980; 1983).

Another means of classification is based on microstructure by Wright (1990). There are two kinds of calcretes in terms of this classification. The first end member is alpha calcrete which corresponds the K-fabrics of Gile et al. (1966). It consists of dense continuous masses of micrite to microsparitic groundmasses with floating etched or exploded skeloton grains, large euhedral crystals, crystal size mottling and displacive growth features. The second end-member of microstructural classification is beta calcretes. It is dominated by biogenic features such as rhizocretions, needle-fiber calcites, microbial tubes, alveolar septal structures and microcodium.

Defining the kinds of calcretes is as important as assessing the driving mechanism for the formations of calcretes and figuring out the source of carbonate is crucial for such studies. The main mechanisms and sources for the carbonate precipitation as calcretes are evaporation, evapotranspiration, common ion effect, degassing of CO_2 and microbial activity. Almost all of these factors are also climatically controlled and therefore very important in paleoclimate studies. The sources of $CaCO_3$ are varied (Goudie, 1973; 1983) and include rainfall, surface runoff, groundwater, dust, bioclast, vegetation litter and rock (Wright and Tucker, 2001). The mechanism of downward movement of dissolved $CaCO_3$ to form calcretes developed above the water table on non-calcareous substrates is named as per descensum model (Goudie, 1983). The reverse mechanism triggered by capillary action is referred as per ascencum.

According to the formation mechanism and place, calcretes are classified into two as pedogenic and groundwater types (Wright and Tucker, 2001). Groundwater calcretes (calcrete or dolocrete) are typically micritic and densely crystalline. The carbonate may contain authigenic silica, clays (sepiolite and palygorskite) and gypsum. They are generally of nodular and massive types. Groundwater calcretes usually do not produce mature profiles comparable to those in pedogenic calcretes. Most groundwater calcretes are formed below the zone of biological activity and thus

exhibit alpha fabrics. On the other hand, pedogenic calcretes have distinct profiles within the host profile meaning that the accumulation of carbonate can be subdivided into soil horizons. Carbonate precipitation occur over a relatively narrow depth range. Displacive growth, clay illuviation, pseudo-anticlinal features, brecciation, peloids and black pebbles are the ones which are characteristic for pedogenic calcretes (Wright and Tucker, 2001).

As mentioned before, in paleoclimotology studies, paleosols and paleosol carbonates are widely used to do interpretations. However, there are some limitations on using paleosols and pedogenic carbonates in paleoclimotology studies. Three limitations are mentioned by Kraus (1999). First one is climatic overprinting which could possibly happens when more than one climatic regime was effective during the formation of paleosols. Secondly, oxygen isotope composition of soil minerals are less resistant to diagenetic alterations than carbon isotopes. Third limitation is that not all the soils include pedogenic carbonates which are used in isotopic reconstruction. At this time, $\delta^{18}O$ values of clay minerals in soils are used for the interpretations. Morozova (1995) also stated some limitations in accuracy of paleoclimatic reconstructions as follows: (1) isomorphism or similar structures of soil profiles located in different natural regions, (2) an impossibility of the application of the principle of actualism, (3) polygenetic features of recent soils, (4) main stable soil properties emerged during the climatic optimum, (5) If it is possible to analyze the soil profile to down to its genetic types, then high level reconstruction can be carried out.

Despite having widespread occurrences of paleosols and calcretes in the central and southern parts of Turkey, still there has been very little attention to them. Calcretes and their evolution in Adana by Kapur et al. (1987; 1990; 1993) and in southern Anatolia by Atalay (1996); Kapur et al. (2000), in the Kırşehir region by Atabey et al. (1998), in the Mersin area by Eren et al. (2008); Eren (2011); Kadir and Eren (2008);

Eren (2007) have been published. The age of the calcretes in the Mersin area are is based on the previous studies. ESR and TL dating methods were employed to present the age of the calcretes in the Adana region which were dated from 250 to 782 ka BP (Özer et al., 1989; Atalay, 1996), corresponding the middle Pleistocene time. This age is also accepted for the calcrete formation by Kapur et al. (1987, 1990, 1993, 2000) for the Adana region and Eren et al. (2008) for the Mersin area.

1.5. ROLE OF SOIL CLAYS IN PALEOCLIMATE STUDIES

Clay minerals are hydrous silicates (Chamley, 1989) occurring under a limited range of conditions in geologic space and mainly found at the surface of the Earth (Velde, 1995). Tabor (2002) defines the soils as clay factories. The mineralogical and chemical composition of pedogenic phyllosilicates, which form in a soil through alteration of detrital clays or by primary precipitation, are strongly controlled by the chemical activity of the soil solution, which in turn is influenced by the amount and seasonality of rainfall (Buol et al., 1997; Tabor, 2002). This relationship clearly points the sensitivity of clay minerals to the climatic conditions at the time of formation. If clay minerals are pedogenic in origin, then they can be used as very good proxy for the environmental conditions.

Clay minerals can also be used as a good indicator of long-term climatic fluctuations because the clay mineral composition of weathering profiles and soils largely depends on the climatic conditions. But, as in the case of paleosols, the use of clay minerals for the paleoclimate interpretations is limited by the existence of diagenetic changes.

If the sources of clay minerals correspond to distinct petrographic and pedologic features and have changed in the course of time, the climatic signals may be deformed or even obliterated (Chamley, 1989). Chamley (1989) also stated some basic limitations for the use of clay minerals in reconstructing paleoclimates. The

major and the first limitation is shown as the existence of diagenetic changes which can easily alter the climatic signals. Second limitation is to use the precise, discriminant and highly reproducible techniques to get accurate results in such studies. Additionally, any changes in petrographic and pedologic features of soil clays may deform or even obliterate the climatic signal.

Singer (1980) points five assumptions which are also defined as limiting factors for the use of clay minerals in paleoclimate reconstructions. First one is that clay minerals and climatic paramaters are quantitatively related. Secondly, the study assumes the clay minerals as stable as long as the climatic and tectonic regimes do not change. Third assumption points the uniform character of clay minerals throughout the weathering profile. Additionaly, it assumes that clay minerals, once formed and buried, are stable. Final assumption mentions the sensitivity of clay minerals towards environmental changes.

Principally, the origin of clay minerals should be determined before interpretation. Soil weathering causes changes in clay mineralogy with increasing pedogenesis. The degree of pedogenesis is directly controlled by climatic conditions. The stable isotope compositions of the pedogenic phyllosilicates and pedogenic carbonates reflect $\delta^{18}O$ composition of the local meteoric water since they are accepted to precipitate in isotopic equilibrium with the soil water (Cerling, 1984; Deutz et al., 2001).

Comparing the studies related with pedogenic carbonates and phyllosilicates in association with paleoclimate, it has been recognized that pedogenic phyllosilicates have not been studied very much due to the difficulty of separating the pedogenic, detrital, burial and diagenetic phases in fine fraction of the soils. Combining the clay composition of the soil with the other proxy data allow to reconstruct the past climates.

1.6. CLIMATE DURING PLIO-PLEISTOCENE

As Zachos et al. (2001) emphasized, Earth's climate has undergone a significant and complex evolution since 65 million years and this evolution includes gradual trends of warming and cooling driven by tectonic processes on time scales of 10^5 to 10^7 years, rhythmic or periodic cycles driven by orbital processes with 10^4- to 10^6-year cyclicity, and rare rapid aberrant shifts and extreme climate transients with durations of 10^3 to 10^5 years. Much of the information until now about Cenozoic climate change has been driven from high-resolution deep-sea oxygen and carbon isotope records. Figure 1.6 represents the global deep-sea oxygen and carbon isotope records by pointing the major climatic, tectonic and biotic events compiled with 40 DSDP and ODP site data by Zachos et al. 2001.

Most Plio–Pleistocene climate research has focused on two relatively abrupt climate transitions, the onset of major northern hemisphere glaciation at approximately 2.7 Myr and the mid-Pleistocene transition (MPT) when the dominant periodicity of glacial response changes from 41 to _100 kyr (Lisiecki and Raymo, 2007).

As Millard et al. 2006 documented in their study, Messinian salinity crisis with a sharp sea level fall which occurred at the end of Miocene strongly affected the physiography of the Mediterranean Region. It was followed by the Pliocene which has the most recent sustained global warmth (IPCC, 2007) and is very crucial to both Plio-Pleistocene climate change and its effects on local weather patterns as well as future climates (Peryam et al., 2011). As Ermolli and Cheddadi (1997) explained, during the Late Pliocene and Early Pleistocene (from 2.47 Ma BP to 0.735 Ma BP) the dominant climatic periodicity was 41,000 yrs. Thereafter, this periodicity shifted to 100,000 yrs (Ruddiman et al., 1989). This has a great effect on the temperature and precipitation patterns over the European continent from interglacial to glacial (Ermolli and Cheddadi, 1997).

A recent study to summarize the climates of the Plio-Pleistocene is Peryam et al. (2011). In this study it is stated that one of the most recent large climatic changes in the Earth's history took place during Pliocene to Pleistocene time, when early Pliocene warmth was replaced by a cooler and strongly variable late Pliocene to Pleistocene climate regime marked by the onset of Northern Hemisphere glaciation (Haug et al., 2001; Zachos et al., 2001; Ravelo et al., 2004; Haug et al., 2005; Lisiecki and Raymo, 2005).

During the Pleistocene, two major changes in amplitude and frequency of glacial/interglacial cycles took place (Candy et al., 2010). The first event is the transition from 40 ka to 100 ka climate cycles which is known as Mid-Pleistocene revolution or MPR (Candy et al., 2010; Pisias and Moore, 1981; Ruddimon et al., 1989; Imbrie et al., 1993). The second event is known as Mid-Brunhes Event (MBE) that occurred between the marine isotope stages 13-11. It is a climatic transition that separates two climatic models: 1) early Middle Pleistocene interglacials (780-450 ka) characterized by only moderate warmth; 2) Middle and Late Pleistocene interglacials (after 450 ka) characterized by greater warmth consistent with or warmer than the Holocene. However, it is still unclear that this MBE is a global phenomenon or is restricted to specific regions. For example, there are long sedimentary records covering a large part of the Quaternary in Southern Europe, Ioannina, Tengahi Phillipon in Greece (Tzedakis, 1994; Tzedakis et al., 2006). There are also many Late Pleistocene to Holocene records from Turkey as such Gölhisar lake records (10-0 ka BP; Eastwood et al., 2007), Akgöl lake records (16-4 ka BP; Leng et al., 1999), Lake Nar (2-0 ka BP; Jones et al., 2006), Eski Acıgöl (>20-0 ka BP; Roberts et al., 2001), Lake Van (15-0 ka BP; Wick et al., 2003 and Litt et al., 2009) and Sofular Cave records (>20-0 ka BP; Göktürk et al., 2011). Although there are many records from Turkey, none of them has shown the MBE until this study.

Interglacial warming were not globally comparable during the early Middle Pleistocene and some regions of the world experienced cooler conditions. The implication is that during the period 780 ka – 450 ka the climate system of the southern hemisphere and the Northern Atlantic regions must have become decoupled. In North Europe and the North Atlantic interglacial climates underwent enhanced warming (Candy et al., 2010).

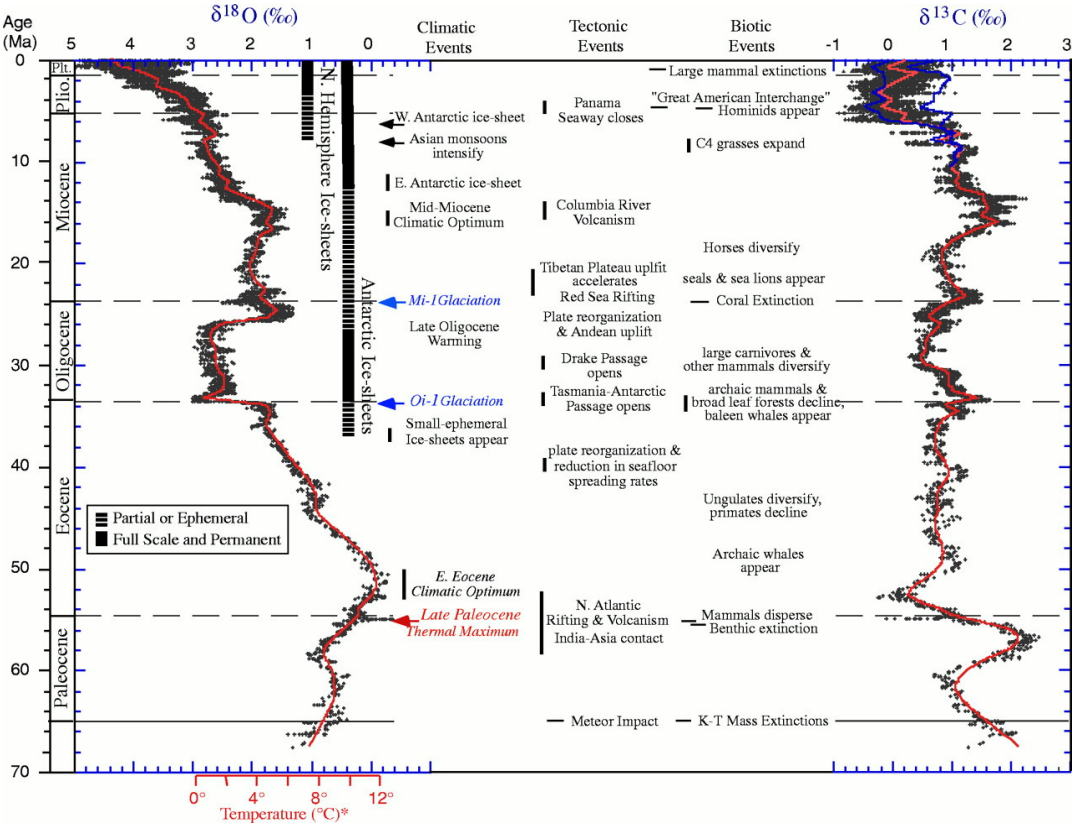

Figure 1.6. Global deep-sea oxygen and carbon isotope records based on data compiled from more than 40 DSDP and ODP sites (Zachos et al., 2001).

CHAPTER 2

LITERATURE REVIEW

2.1. PREVIOUS STUDIES CONDUCTED ON THE ANKARA REGION

There have been various geological, geomorphological and geotechnical studies about the Ankara region. The detailed literature survey was conducted and summarized in this chapter. The oldest studies in the region started in 1930s. One of them was carried by Chaput (1936). This study points the geological importance of Ankara within Central Anatolia and explained the geomorphological features in the region. Salomon-Calvi and Kleinsorge (1940) studied the geology and hydrology of the Central Anatolian Plains. Salomon-Calvi and Kleinsorge (1940) pointed the age of Gölbaşı Formation as Late Pliocene because of the presence of some mammalian fossils. At the same time, in 1949, Lahn also published a work on the geology of Central Anatolia mentioning also Ankara fan which originates in the Anatolide folds.

Many paleontological studies have been carried out within and around Ankara region, especially in Çalta. Şen et al. (1974) reported the results of the fossil investigations in Çalta region, northwest Ankara. The vertebrate fossils pointing Pliocene age were found in sandstones with calcerous cement. After that, Şen (1978) investigated the Rodentia fauna of Pliocene age. This fauna is stated to indicate the step environment and low humidity during Pliocene in Çalta region. Şen and Rage (1979) studied the composite vertebrate fauna in Çalta region. Ozansoy (1957) worked and revised the mammalian fossils of Turkey of Tertiary in age. In Ankara, around Elmadağ-Gökdere Küçükyozgat and Ayaş-İlhançay, fossils of Lower Pliocene age were reported. Middle Pliocene fossils of marl levels were found in Sarılar region. Conglomerate, marl and soil levels in

Yassıören location have mammalian fossils giving an age of Late Pliocene. Tekkaya (1974) reported the vertebrate fossils of Turkey found in association with the paleontologic and geologic investigations in Turkey from 1970 to 1973. In this study, Ayaş-Ilıca Village, Ayaş-Avşı and Kızılcahamam-Ağaöz places were mentioned as the locations of vertebrate fossil in the vicinity of Ankara and gave ages of Upper Pliocene, Ponsien and Upper and Middle Miocene, respectively.

Although paleosols and their carbonates are very abundant in Ankara, very little literature have been published. One of the most important pedological studies was carried by Cangir and Kapur (1983). It explains the toposequential relationships between the Ankara-Dikmen Paleosol and the environmental pedoliths. The studied areas are Kavaklıdere, Ayrancı, Dikmen, Öveçler, Balgat, Çukurambar, Atatürk Forestry Farm, MTA and METU. Four profiles from Çal Mountain, from tectonic steps and river terraces were physically, chemically and mineralogically examined. Total geochemical analysis of first profile from Çal Mountain shows an increasing trend in SiO_2, Al_2O_3 and Fe_2O_3 but a decrease in CaO and $CaCO_3$ amounts from the parent rock to the upper horizons. Cangir and Kapur (1983) defined these changes in the chemical composition as decalcification which is a typical process for red Mediterranean soils. Parent rocks have smectite as a major clay mineral, whereas in horizon B, kaolinite and illite become dominant. Profile 2 represents a degraded Mediterranean soil and formed from the material transported from the Çal Mountain. In this profile $CaCO_3$ is leached. Also, clay mineral amounts are much higher at the lower horizons as a typical characteristic of red Mediterranean soils. Smecite is the dominant clay mineral in profile 2. Profile 3 and 4 represent reddish-brown soils. They include carbonate concretions in B horizons. The host material of those two profiles can be the mixture of greywacke, limestone and red mediterranean soils found in and around Dikmen. In conclusion, Cangir and Kapur (1983) stated that these soils from four profiles do not show modern soil characteristics and they named profile 1 as a paleosol and the rest as pedoliths.

In neotectonic viewpoint, Koçyiğit (1987), (1991) and (2000) presented the evolution of Karakaya Orogen, the neotectonic evolution of Ankara and neotectonic characteristics of Central Anatolia, respectively. According to Koçyiğit (1991), the youngest rock units in the Ankara region are fluvial-lacustrine deposits of Late Miocene-Pliocene age and associated calcalkaline volcanic rocks. This study classifies them into two as: (1) Yuva Group and (2) Yalıncak Formation. Yuva Group is defined as formed by alluvial fan, braided plain, meandering plain and lake sediments in a tectonically active system and overlain by Yalıncak Formation. It is made up of gray and unsorted loose conglomerate, red-brown silty mudstone with carbonate concretions and lensoidal stream-channel conglomerates deposited in alluvial fans, braided to meandering river plains and playa lakes. Koçyiğit (1991) described the Haymana-Poltalı basin as an example of an accretionary forearc basin in Central Anatolia. This study also outlines the stratigraphy of the Ankara Region. According to Koçyiğit (1991), there are five major categories of the rock units: (1) Karakaya Complex, (2) Ankara Group, (3) Anatolian Complex, (4) Memlik Group (sedimentary fill of the forearc basin) and (5) the younger cover rocks (Maltepe Formation and Yuva Group). This study suggested the age of Maltepe Formation as Miocene and Yuva Group as Pliocene.

Another valuable contribution to the paleosol/calcrete literature of Ankara was on the geomorphological evolution of the Ankara region studied by Erol (1956, 1961, 1973 and 1983). The geology and geomorphology of Elmadağ and its surroundings were the subjects of Erol (1956). After this study, Erol (1961) dealt with the orogenic phases of the Ankara region. The phases were classified as Pre-Apline, Apline and Epeirogenic Movements in this study. It was stated that the Pleistocene river terraces may be the result of both vertical movements and of the Quaternary climatic changes. Erol (1973) outlined the major geomorphologic units in Ankara area and produced a geomorphological map of the region in 1/100 000 scale. The study classifies the basins and plains as valley floors (Holocene),

basin floor (Holocene), lower terraces (Young Plesitocene) and higher terraces (Older Pleistocene). Plateaus are defined as DI (highest plateau - End of Miocene), DII (high plateau – Middle Pliocene), DIII (middle plateau – Upper Pliocene) and DIV (lower plateau- Villafranchian). Among them, the most recent study about the region was Erol (1983). This study presents the landform generations and their correlated geological formations of Ankara Region. According to the study, Upper Miocene was a humid and hot period during which volcanism also occurred and denudation surfaces and lake basins formed. Messinien, however, was a period of arid and semi-arid climate which leads to the formation of gypsiferous lake systems. During transition from Miocene to Pliocene, tectonic movements were very effective for the new landform generations. Fluvial denudation processes became dominant during Pliocene.

Akyürek et al. (1997) presented the compilation and revision work on the environmental geology and natural resources of the province of Ankara and provided a geological map of Ankara in scale of 1/100 000. Then, in 2003, Akyürek et al. published a field book of Ankara-Elmadağ-Irmak-Kalecik region with providing a geological map in 1/100 000 scale. Additional works are carried by Dönmez et al. (2008) and Akçay et al. (2008) in which some of the studied locations are included. They also named and mapped the studied units as Late Miocene-Pliocene aged fluvi-lacustrine series.

Koçyiğit and Türkmenoğlu (1991) stated that clay minerals of smectite, illite, chlorite and kaolinite and white carbonate concretions with growth-faulted lensoidal to rectangular channel conglomerates are the diagnostics of the unstable fluvial setting with seasonal climate. They also mentioned that the pedogenic episodes interrupting frequently sedimentation of the Ankara Basin Fill is so called the “Ankara Clay Formation”. Ankara Clay has been selected a subject of many studies. One of them was done by Aras (1991) studied the clayey levels of Upper Pliocene deposits in Ankara Plain and Mogan depression to determine the

mineralogy and depositional environment of Ankara Clay as masters thesis. Another study by Sezer (1998) and Sezer et al. (2003) presented the cation exchange capacity and contaminant uptake properties of some natural clays as potential landfill liners. As a case study area, Sincan Çadırtepe Sanitary Landfill site was examined. This study explains the contaminant uptake properties which can be engineered as a component of barrier system. Additionally, Sağlam (2002) showed the oxide and clay minerals of Ankara Clay and maghemite, hematite, ilmenite and goethite were detected as iron oxides in her Masters Thesis. Then Sezer et al. (2003) published this work stating the Ankara Clay's suitable chemical and mineralogical characteristics and also high abundance and low-cost of extraction and supply for use of barrier design. Ankara Clay has been studied by many workers according to its geotechnical properties. Ordemir et al. (1977) stated the swelling problems of Ankara Clay. Kasapoğlu (1982) worked on the engineering properties of grounds (soils and rocks) in Ankara.

Aras et al. 1991 presented the mineralogy and depositional environment of Ankara Clay. Four sections from Ankara Plain and Mogan Depression were selected for this study. The clastics of Ankara Plain were suggested to be deposited as debris flow and flood plain deposits. The deposits from Mogan depression were described from recent debris flow and alluvial fan environment. Smectite-illite-chlorite and kaolinite represent the clay minerals of the studied samples from four profiles. Aras et al. (1991) stated that all of them were inherited from the source rocks of greywacke, schist and limestone. The absence of chlorite towards the northern parts of the basin is pointed in the study which indicates that the red mudstones were alluvial fan deposits of the rivers eroding Mesozoic source rocks in the region.

The paleo-ridge between Ankara and Etimesgut-Batıkent Basins during Pliocene was defined by Kiper (1984). For this study, the isopach and structure-contour maps of the region were prepared by Kiper (1984). The paleoridge which

separates the Ankara and Etimesgut-Batıkent basins was shown on the maps. Major difference between basins is given as follows: one of the basins was filled with lake deposits; on the other hand, the other basin was filled with fluvial deposits. This difference is stated as evidence of the paleoridge. The age of the red-brown Balgat Member is given as Upper Pliocene and that of gray Macun Member as Lower Pliocene.

Tankut (1985) published a work on the geochemistry of the Neogene volcanics around Ankara. This study points that the Ankara region is an important center of Tertiary volcanism occurred between Oliogocene and Pleistocene in Anatolia. Study shows that Neogene volcanics in four main areas in Ankara: city center, Elmadağ, Çubuk and Sincan. Those volcanics are classified as calcalkaline and alkaline characteristics. This study suggests within plate tectonic setting for the mafic volcanics around Ankara.

2.2. PREVIOUS STUDIES RELATED WITH PALEOSOLS AND CALCRETES

Paleosols and their carbonates have been studied with their paleopedological properties. More recent works have proved the efficiency of using the old soils and their carbonates to trace the paleoclimatic, paleoenvironmental and paleoecologic conditions over time. Many parameters can be used to study paleosols. The stable isotopic composition of pedogenic minerals from paleosols record key climatic parameters during soil formation (Stern et al., 1997; Vitali et al., 2002).

Arakel (1982) examined the genesis of calcrete developments in Hutt and Leeman lagoons, western Australia by determining the parameters that control formative processes, constructing a genetic model for coastal soil profiles and devising a generalized classification for calcrete types. Field and laboratory observations

indicate that vadose diagenesis in both study areas produced a variety of microtextural elements. Vadose diagenesis including precipitation and alteration causes calcrete developments in the study area. Precipitation is stated to cause the development of low Mg calcite, needle fibers and micritization. Alteration, on the other hand, promotes the maturity of the soil profiles by modifying the calcrete fabrics.

As stated by Cerling and Hay (1986), the stable isotopic composition of soil carbonates and other carbonates from terrestrial settings can give very useful paleoclimatic information, and paleosol carbonates from fluvial and eolian deposits give the best paleoclimatic signal. To find paleoclimatic history of East Africa during Plio-Pleistocene, oxygen and carbon isotope values of carbonates in Olduvai Gorge were studied and the values suggest major climatic changes at about 1.67, 1.3 and 0.6 myr within overall drift toward aridity.

Kapur et al. (1987) studied eight surfaces from the Taurus mountains to the south of Adana formed during Tertiary and Pleistocene periods due largely to fluviatile and tectonic processes. This study examined the micromorhology of the column horizon in the soils of the S2 surface in order to ascertain its genesis. Soils were stated as having polygenetic development and formed in two stages; first the initial rapid formation of micrite giving small grains and then formation of subspherical units or massive material. Kapur et al. (1990) aimed to describe the types of calcretes with three toposequences on Quaternary geomorphic surfaces formed in/on different materials of Northern Adana Basin. Those toposequences are found in Handere Formation which is Late Miocene-Pliocene fluvio-deltaic formation composed of calcareous claystone-shales as well as bentonic and massive.

Kapur et al. (1987) described the various types of calcretes developed on Quaternary geomorphic surfaces in Anatolia and compared them with the

Mediterranean soils. In this study, the evolution of calcretes are given in six stages. The evolutionay sequence of Pedogenic calcretes starts with a deposition of Pliocene clays first. Then, cracking of the clayey material and the formation of the large cuboidal structural units occurred. Stage 3 is the leaching proceeding in the Pleistocene pluvials and calcification occurring along vertical continuations of the structural units. In stage 4, verticle calcite columns in the interpluvial of the Pleistocene were developed and moderately calcareous soils were formed. After that, intense pluvials/interpluvials caused to increase decalcification of soil and calcification along rubefaction of the column horizon resulted in the formation of massive calcrete with change. The sources of carbonate enrichment were stated to be probably the aeolian additions of calcite in the interpluvials and the surface waters during pluvials. The last stage, stage 6 includes rubefaction to red hues of 2.5YR and 10YR with a hard thin crust forming over the massive calcrete which preserves the geomorphological surface it has formed in/on. The same study also mentioned that although the evolutionary sequence of the central Anatolian pedogenic calcretes is similar to the sequences in the west, south and southeast, the intermediate stage – the column horizon – is rarely determined to develop with diffuse calcite columns in brown to dark brown very thin column horizons, underlying massive calcretes. The weakly developed column horizons are shown to be possibly result of leaching through coarser particles.

Robinson and Wright (1987) studied the pedogenic minerals in a Lower Carboniferous paleosols in South Wales. Mixed-layer clay minerals of illite/smectite and I/S ordering, kaolinite-smectite and a three-component variety with kaolinite-smectite-chlorite-like material are found in paleosols of South Wales. Also, in this study the possible mechanism of illitization to produce the interlayered illite-smectite was stated as repeated wetting and drying cycles causing irreversible K-fixation. A year after, Wright and Robinson (1988) published another work on Early Carboniferous floodplain deposits from South Wales. Two paleosol sequences from an alluvial sediments were selected to

display the changes in profile characteristics interpreted as being caused by both intrinsic (channel migration) and extrinsic (marine transgression) processes. The carbonate nodules -having sharp boundaries with the mudstone matrix- found in the pofiles were interpreted as calcrete (caliche) nodules. Having a variety of many soil types, the paleosols were classified differently. Wright and Robinson (1988) concluded that the kaolinite-smectite and a three component variety with kaolinite/smectite/chlorite-like material are the dominant clays in the horizons lacking prominent calcrete nodules and interpreted as the products of leaching on the floodplain deposits due to a possible change to more humid conditions.

The study summarizing the importance of stable isotopes of caliches for paleoclimatic reconstructions was carried by Mack et al. (1991). In this study, caliches of the Abo Formation, south-central New Mexico, USA were investigated according to their mineralogy and stable isotope compositions. Fluvial caliches are stated here as consisting of low-Mg calcite nodules, micrite supported matrix, brecciation, ooids/pisoliths, alveolar-septal structure and peloids which indicate pedogenic origin in well-oxidized vadose zone. Contrastingly, the supratidal paleosols have drab colors, horizontal rhizoliths and paucity of vadose textures. The results of this study shows that the $\delta^{13}C$ values for both environments increase with a decrease in caliche age, indicating the relation between temperature increase and rainfall decrease with time.

Dinç et al. (1991) studied the formation, distribution and chemical properties of saline and alkaline soils of the Çukurova Region. Nine soil pits were sampled. pH in all soil profiles are 7.4-8.2 which indicates slightly alkaline character. Sodium adsorption ratio and extractable Cl increases with depth. Soils were classifed into three as highly saline soils occurring on the delta; moderatley saline soils in bottom lands and slightly saline soils of bottom lands and delta. The same year, Dinç et al. (1991) explained the soil relationships in the Çukurova region by pedo-geomorphological criteria. The region is stated to contain six different

geomorphic units from Late Pleistocene to Holocene. Fluvio-marine terraces have formed under continental-shallow conditions and consist of calichified conglomerates. River terraces are stated as to be formed on rubified and calichified Pliocene marls.

Billard (1993) discussed whether the Middle Pleistocene climatic optimum was recorded in the loess-paleosol sequences of Eurasia or not? A correlation and comparison between major Eurasian loess-paleosol sequences were the goals of this study. The Italian piedmont of Alps, loess accumulated in Normandy, the Carpathian foredeep, Hungarian Plain, Central Asia and Loess plateau of China were studied in terms of their pedological features. As a result, it is stated in this publication that the main periods of pedogenesis in Europe did not occurred at the same time with central Asia and loess plateau of China.

Another study showing the use of pedogenic clay minerals in paleosols is from Stern al. (1997). In this work, the oxygen isotope values of pedogenic clay minerals as smectite and kaolinite in a stratigraphic sequence of paleosols in the Siwalik Himalayan molasse, northern Pakistan are documented. The parallel increase in $\delta^{18}O$ values of smectites and that of calcite at 8.5-6.5 Ma indicates a climatic influence rather than a diagenetic effect. This climatic influences is summarized in this study as either aridity due to increasing soil water evaporation or a change from continental to more marine-sourced precipitation.

Andrews et al. (1998) presented the terrestrial Late Pleistocene climatic record of India by studying oxygen and carbon stable isotopes in pedogenic carbonates from Thar Desert. The present climate is mentioned as semi arid monsoonal climate with annual rainfall between 300 and 400 mm. Quartz, feldpsar and lithic detrital grains are commonly found. Due to lack of biogenic features, calcretes are classified as alpha calcretes. $\delta^{18}O$ values vary between -2.1 and -6.5‰ indicating aridity. $\delta^{18}O$ additionally, ranges from 0.0 to -1.7‰.

Another work is from national literature. The study area is very close to our area in regional scale. Atabey et al. (1998) published a work on the sedimentology of calcretes in Kırşehir area. Calcretes were found in alluvial fan, braided river and lacustrine deposits of Miocene age. Petrographic, SEM, XRD and staining studies were carried out. The calcretes are classified as transition zone calcrete, nodular chalky and laminar calceretes. Formation of the calcretes in Kırşehir region is summarized by Atabey et al. (1998) as follows: carbonate within the parent rocks is dissolved by carbonic acid (formed by CO_2 in atmosphere and water) and the calcium bicarbonate is formed. This solution is transported to the alluvial fan, fluvial and lacustrine deposits and percolated downward until water table. In arid and semiarid periods, due to capillarity, it rises and interact with the atmosphere, so loses CO_2 so $CaCO_3$ is precipitated.

Han et al. (1998) researched on the climatic implications of the S5 paleosol complex on the Southernmost Chinese Loess Plateau. Grain-size distribuiton of the profile shows that clay-sized particles first increases with depth until Bt horizon then decreases to C horizon. Coarse grains are much more abundant in the upper horizons. Quartz, feldspar and mica are found as non-clay minerals. Clay minerals are detected as illite, chlorite, kaolinite, smectite and mixed-layer clay minerals. SiO_2 and Al_2O_3 and CaO are the major oxides which vary throughout the profile. C_3 vegetation has $\delta^{13}C$ values ranging from -35 to -22‰, on the other hand, C_4 plants have $\delta^{13}C$ values of -17 to -8‰. According to the whole results, the climatic conditions are stated as drier during the Holocene.

McCarthy and Plint (1998) suggested three-part approach to define the complex interfluve sequence boundaries in non-marine successions and to integrate the paleopedology and sequence stratigraphy and then applied this approach to Dunvegan Formation in Alberta and British Columbia, Canada. First approach is to use the regional stratigraphy to predict the position of the paleosols. Second one is that field observations such as thickness, structure, color and degree of rooting

may reveal the paleosol profile. The third approcah is to define the micromorphological features such as bioturbation, fabric, clay coatings, ferruginous features, siderite and barite to understand the soil processes related to changes in water table, biological activity, weathering and accomodation. Those approaches are well-fit with the regional changes in the study area so this study proposed that this approach can be applicable to sequence boundary recognition of other non marine successions.

Khadkikar et al. (1998) classified the calcretes in Gujarat, western India into three as grounwater calcretes, pedogenic calcretes and calcrete conglomerates. Pedogenic calcretes are stated to be formed by carbonate saturated waters travelling preferentially along the stratification planes. Calcrete conglomerates, however, occur as ribbons, sheets and lenses due to reworking of both pedogenic and groundwater calcretes.

Karakaş and Kadir (1998) studied Neogene (Upper Miocene-Pliocene) lacustrine sediments of northern Konya Basin. This study States that the paragenesis and textural features of the minerals determined in the study area indicate precipitation due to climate fluctuations ranging from arid, semi-arid, and wet conditions. It is also mentioned in this study that sepiolite and palygorskite form authigenically as a result of the calcretion of carbonate units in alkaline conditions, high Si and Mg activity, and low Al.

Retallack (2001) has studied fossil soils and published papers and books on this topic. Among the most recent ones, Soils of the Past was published in 2001. It explains paleopedology concept, features of fossil soils, soil forming processes, soil classification and factors affecting the formation of soil. In this study soil is defined as the material forming the surface of a planet or similar body and altered in place from its parent material by physical, chemical or biological processes. It is also stated that since soils are complex zones of interaction between sediment

or solid rock and the ecosystem or atmosphere, defining a soil is a problematic issue.

Ufnar et al. (2001) studied the stratigrafic use of sphaerosiderite $\delta^{18}O$ values in paleosols of the Cretaceous Boulder Creek Formation, Canada. It is stated that $\delta^{18}O$ and $\delta^{13}C$ values of sphaerosiderites record the formation in meteoric phreatic fluids recharged by local precipitation. In this study, pyrite abundance with sphaerosiderites suggests marine influence on pedogenesis and increased siderite Mg/(Ca+Mg) and Mg/Fe ratios also suggest marine-meteoric fluid mixing. Paleosol micromorphology and geochemistry of siderites provide information about relative sea-level rise. Then, Ufnar (2007) proposed a tool for estimating the relative age of well-drained paleosols. The purpose of the study is summarized as to estimate the rates of illuvial clay accumulation in Bt horizon by using the dated fluvial sedimentary deposits from a humid-subtropical environment. Blue light optically stimulated luminescence (OSL) ages are proposed by Ufnar (2007) to be used to indicate the illuvial clay accumulation.

Deutz et al. (2001) illustrated that the stable isotope values of pedogenic carbonates can be used for paleoenvironmental reconstructions. Pedogenic carbonates from relict soils and paleosols from the Rio Grande Rift region of New Mexico were studied in this study. Coupled high-resolutton radiocarbon dating and stable isotope analysis were carried out. $\delta^{18}O$ values of pedogenic carbonates tend to increase with decreasing age but δ^{13} C values show almost no variation with depth and age. According to Deutz et al. (2001) the results show the presence of C_4 vegetation during the glacial and late-glacial periods and progressive increase in aridity.

Vitali et al. (2002) published a study of stable isotopic composition and clay mineral content of an interfluve paleosol from Cenomanian Dunvegan Formation, Canada. Clay minerals in the <2µm size fraction were found as detrital kaolinite

and illite, complex dioctahedral mixed-layer clay minerals. Randomly interstratified illitic and hyroxy-interlayer vermiculitic layers occured in <0.2µm size-fraction. TEM studies suggested that <0.2µm size-fraction comprises pedogenic clays which were used for the stable isotope investigations. Ancient soil water isotope values were found as δD -93‰ to -81‰ and $\delta^{18}O$ -12.9‰ to -11.6‰. Vitali et al. (2002) suggested that these values are higher than those of present precipitation, and suggestive of warmer and more humid conditions during the early Late Cretacous than at present.

Robinson et al. (2002) studied the calcrete nodules present in overbank facies of nonmarine deposits in Wealden Beds of southern England. Floating detrital grains, corroded grain margins and circumgranular cracks are the major features of the calcretes in the region. $\delta^{13}C$ values of diagenetic ferroan calcite is -15‰ which is consistent with early burial cementation, that of well-preserved micrite is -10.2‰ indicating C_3 -dominated vegetation.

Quaternary pedogenesis in a paleosol sequence in Hungary was reconstructed by Üveges et al. (2003). This study comprises of mineralogical, chemical and micromorphological analyses and SEM identifications. Four distinct horizons were identified as follows: first one includes chernozem brown forest soil, second one has yellowish red color, silty clay texture, third unit is a silty-sandy mixture of different materials and the last one is an alluvial formation. Particles size distribuiton shows sand content less than 5%, clay content is between 41–50%. So the distribution is stated as having no strong enrichment or depletion of any particle sizes. TiO_2/ZrO_2 ratio is given to state the heterogeneity of the parent material, and differences can be recognized from the results. $SiO_2/(Al_2O_3+Fe_2O_3)$ and $MgO+Na_2O+K_2O)/Al_2O_3$ ratios are used to indicate the intensity of the weathering and eluviation processes. Dominant clay minerals are found to be smectite with kaolinite, illite, vermiculite, chlorite, I/S and chlorite/vermiculite. Smectite amount shows variations throughout the profile. Vuggy pore and

vesicles are recognized as micromorphological features indicating wetting and drying cycles. Clay coatings were also found and indicate illuviation procceses. Carbonate concretions found in the upper horiozons were mentioned as to formed by chemical precipitation, pedogenic leaching and re-precipitation. All the data gathered from anaylses indicate that the studied section is the result of the superposition of a series of complex events, which roughly reflect the change of environmental conditions.

Genesis of calcretes in Mediterranean colluvial carbonate systems from southeast Spain were investigated by Jimenez-Espinoza and Jimenez-Millan (2003). Three different horizons-cemented gravels, chalky and massive laminar- from calcretes were examined by SEM revealing the presence of calcified filaments, rounded peloids and coated grains indicating that calcrete formation was controlled by the microbial activity related with plant roots. Mineralogy of the calcretes were analysed by XRD and composition shows the presence of smectite and hematite, suggesting a semi-arid climate.

Dolomitized calcrete, known as a diagenetic feature, is a subject of Fu et al. (2004). This study interpreted the calcretes as formed by diagenetic alteration of the host carbonate during subaerial exposure of the mud mounds. The studied calcretes lack the root-related structures which suggest a limited influence of macrophytes.

The dating of calcretes is another broad subject. Candy et al. (2004) published a work on quatifying time scales of pedogenic calcretes using U-series equilibria. Samples from hardpan and laminar horizons of a mature calcretes from an alluvial terrace within the Sorbas basin, southeast Spain were investigated by firstly determining their U and Th contents. The presence of high concentrations of ^{232}Th within all samples pointed the presence of detrital contamination. Dating results show that carbonate below the lower surface of the clasts were formed 207±11ka

BP; carbonates from within the infilled pores formed 155±9 la BP and laminar crust was formed 112±15 ka BP. Those results imply that time range of 72-32 ka is required for hardpan formation and time range of 121-69 ka is required for hardpan calcrete with an associated laminar crust.

Gong et al. (2005) defined four subaerial exposure surfaces in the Pleistocene carbonate sequences in Nansha Islands, south China Sea. Those surfaces are characterized by caliche formations and resulted from global sea-level changes. Dissolution cavities, mineral stabilization, porosity rimming and drusy cementation of low Mg calcite are the features of clacretes in the region. Also, alveolar texture, micro-rhizolith and caliche laebules are observed in all four diagenetic zones. $\delta^{13}C$ values range between -1.15 and -10.06‰, and $\delta^{18}O$ values which have a narrow variation range is between -4.44 to -8.68‰. Those values are stated as typical of meteoric diagenesis. This study concluded that central China Sea experienced episodes of significantly drier climate during Pleistocene sea-level lowstands than present (Gong et al., 2005).

Schellenberger and Veit (2006) studied the pedological, pedostratigraphic and geochemical characterization of Las Carreras loess-paleosol sequence. The studied section includes 32 paleosols, thirty of which has Bt horizons but 2 of them have Bw(k) horizon indicating no illuviation argillans. Geochemical analysis, as a general comment, is stated not to vary due to post-depositional pedogenic processes. Macro and micromorphological observations reveal that the major pedogenic processes are carbonate leaching, reprecipitation, soil aggregate formation, translocation and pseudogleization. Very low geochemical variations in major and trace elements also suggest thorough sedimentary mixing processes in dust source region.

One of the recent studies on paleosol carbonates was published by Kaakinen et al. (2006). Stable carbon and oxygen isotope values of carbonates in paleosols were

studied and their paleoclimatic and paleovegetational implications were stated in this study. Almost no variation in $\delta^{13}C$ and $\delta^{18}O$ values of carbonates from the fluvial part of the Chinese Loess Plateau suggest that no marked change in vegetation and climate during 10-6.8Ma. But at the boundary between fluvial and aeolian formations, there is a shift in both carbon and oxygen isotope values suggesting vegetation change and intersification of the Asian monsoon system.

Due to the rareness of the studies about the applications of mineralogical and stratigraphic analyses to charaterization of Chinese loess-paleosol section, Jeong et al. (2008) worked on the quantitative mineralogical, geochemical and microscopic analysis of bulk samples and single particles. Mineral compositions were determined by XRD as quartz, plagioclase, K-feldspar, phyllosilicates, calcite, dolomite and amphiboles. Clay minerals are found to be dominated by illite and illitic expandable clay minerals with minor chlorite, kaolinite and smectite.

A recent study from Eren et al. (2008) revealed the presence of Quaternary calcrete formations in Mersin, southern Turkey. The calcretes in this study are divided into two major groups as mature and immature profiles. Calcrete samples are stated as having dominantly calcite and palygorskite as a minor component. $\delta^{13}C$ and $\delta^{18}O$ values of calcretes are -6.03 to -9.65‰ and -4.31 to -6.82‰ PDB, respectively. Eren et al. (2008) indicated that those isotope values are evidence of formation from percolating meteoric water at or near the surface setting supporting a thin column of a soil and existence of beta fabrics of calcretes also show pedogenic origin.

Another study was conducted by Çobanoğlu et al. (2008). This study expresses the microstructural and geochemical properties of hard caliche deposits in the northern Adana basin. This work classified the calcretes of the region into three: massive, red caliche and calcium carbonate cemented caliche.

CHAPTER 3

DESCRIPTION OF THE STUDY AREA

3.1. GEOLOGY OF THE REGION

Covered with a complex mixture of magmatic, sedimentary and metamorphic rocks, Central Anatolia is a structurally triangular-shaped area (Koçyiğit, 1991, Göncüoğlu et al., 1996) and has experienced many tectonic and magmatic phases which led to the formation of units with different characteristics. Located on a collision system, the Ankara Region is bounded by Eurasian Plate to the north, Gondwana to the south and the intervening Sakarya continent (Figure 3.1). According to Koçyiğit and Deveci (2007), Ankara region has very complicated geology due to the tectonic juxtaposition of remnants of the Sakarya continent, Kırşehir block, the Menderes-Tauride platform, the intervening sutures and the superimposition of rock assemblages ranging in age from pre-Triassic to early Pliocene. The same study describes the rock assemblages of Ankara region from oldest to youngest as (1) pre-Triassic Lalahan nappe, (2) Triassic Karakaya Nappe, (3) Upper Hettangian–Lower Campanian Ankara Group, (4), Lower Campanian Anatolian Nappe, (5) Middle Campanian–Middle Eocene Memlik Group, (6) Upper Campanian–Lower Pliocene Kızılcahamam magmatic arc complex, (7) Oligo–Miocene fluviolacustrine and volcano-sedimentary sequences, and (8) Plio–Quaternary neotectonic units.

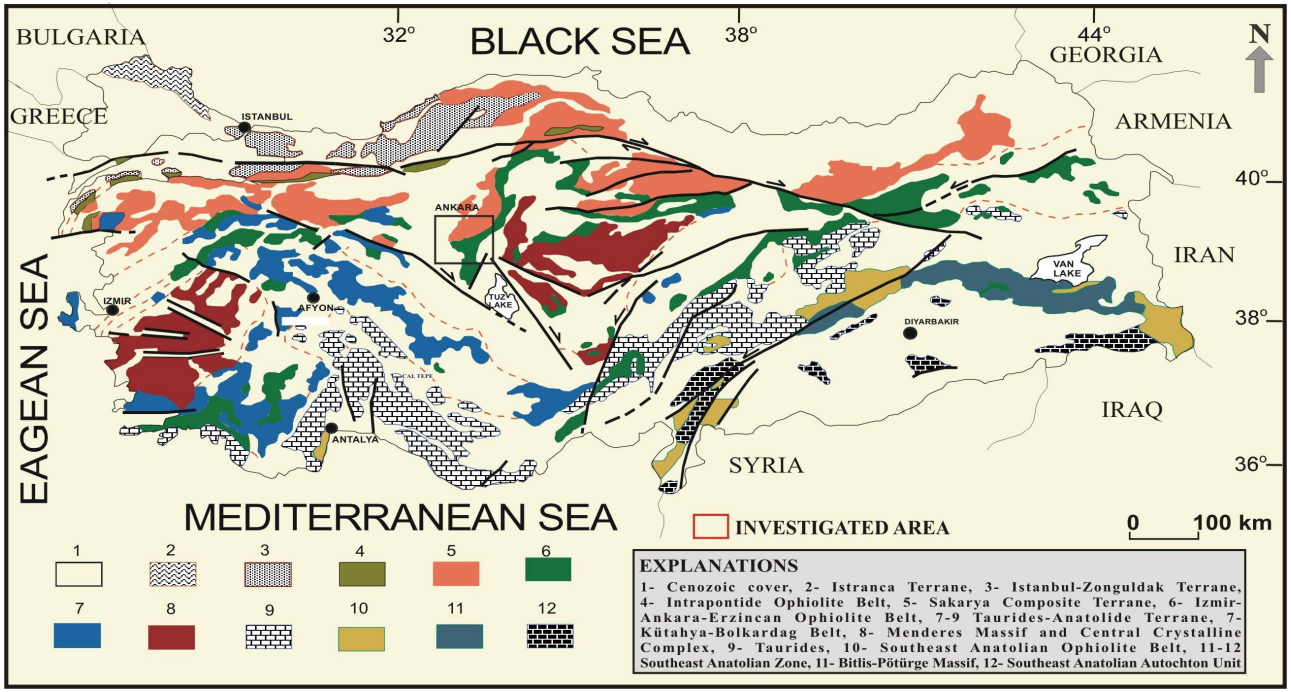

Figure 3.1. The terrane map of Turkey showing the position of Ankara in a complex geological texture (Göncüoğlu et al., 1996).

The following stratigraphic summary of Ankara Region (Figure 3.2) is referenced from Akyürek et al. (1997 and 2003) and Koçyiğit (1991).

The oldest unit of the region is composed of muscovite-quartz schist, sericite-chlorite-quartz schist, sericite-chlorite schist, phyllite, calc-schist, metavolcanics and metaconglomerate (Emir Formation) (Erol, 1956; Çalgın et al. 1973; Norman, 1973; 1982, 1984, Akyürek and Soysal, 1978; 1983). The age of the unit is assigned as Lower Triassic by Akyürek et al. (1979 a, b; 1980) and Akyürek (1981). Overlying unit consists of metaconglomerate, metasandstone, sandy limestone, sandstone, limestone, volcanogenic sandstone, agglomerate and metavolcanics (Elmadağ Formation) (Erol, 1956; Schmit, 1960; Çalgın et al., 1973; Erk, 1977, 1980; Bingöl et al., 1973; Akyürek and Soysal, 1978, 1983; Akyürek et al., 1979b, 1980). This formation also includes limestone blocks of Carboniferous, Permian and Permo-Carboniferous age. It is laterally transitive with Ortaköy Formation (Akyürek et al., 1979b, 1980; Bingöl et al., 1973; Akyürek and Soysal, 1978, 1983; Çalgın et al., 1973) of Middle-Upper Triassic age (Akyürek et al., 1997) which is made up of spilite, diabase, tuff, volcanogenic sandstone and agglomerate. It also includes İmrahor Limestone Member and Radiolarite Member. This formation is overlain by Keçikaya Formation of Middle-Late and Late Triassic age (Akyürek et al., 1997) and formed from grey, white colored limsetone. Rock units within the Ankara Group are cut by diabase dikes.

Above rocks of Triassic age, the units of Jurassic age are found. One of them is composed of conglomerate, sandstone, siltstone and sandy limestone (Hasanoğlan Formation: Akyürek et al., 1982) of Lias age (Akyürek et al., 1997). As overlying unit, limestone with silicified band and nodules (Akbayır Formation): Bilgütay, 1960; Batman, 1978) is observed. The lateral equivalent of Hasanoğlan Formation consists of volcanics with large feldspars, agglomerate, volcanogenic sandstone and limestone with ammonites (Günalan Formation: Müller (1957); Akyürek et

al., (1979b, 1980). It also includes reefal limestones which are Hörç Limestone Member. Both Akbayır Formation and Günalan Formation have tectonic contacts with Cretaceous ophiolites. Eldivan Ophiolite Complex, one of the ophiolites in the area, is composed of serpentinized ultramafics, ultramafics of dunite, pyroxenite, amphibolite, gabbro-diabase, cherty limestone and volcanics composed of spilite, basalt and diabase (Akyürek et al., 1979b, 1980; Akyürek, 1981). It outcrops to the southeast of Ankara. Dereköy Ophiolitic Melange (Ünalan et al., 1976; Batman, 1977), lateral continuation of Eldivan Ophiolite Complex, is comprised of serpentinite, gabbro, diabase and volcanics; limestone blocks of Upper Jurassic age belonging to the Mollaresul Formation; limestone blocks of unknown ages and limestone blocks of Permian age. It mostly crops out to the southwest of Ankara.

Kılıçlar Group of Cenomanian-Campanian age unconformably overlies the ophiolites. This group of sedimentary, volcanogenic-sedimentary and volcanic rocks which are laterally and vertically transient with each other is divided into Hisarköy (Norman, 1972; Özkaya; 1982; Akyürek et al., 1979b, 1980; Akyürek, 1981) and Karadağ (Norman, 1972; Birgili et al., 1975; Ünalan et al., 1976; Akyürek et al., 1979b, 1980; Akyürek, 1981) Formations. The former is composed of conglomerate with gravels of volcanics, sandstone, mudstone and limestone. The Kocatepe Limestone Member and olistostrome including the rocks derived from the Eldivan Ophiolite Complex are also part of the Hisarköy Formation which is laterally transient to the Karadağ Formation including alternation of sandstone, conglomerate, mudstone and calciturbidite interbeds.

Haymana Formation (Norman, 1972; Birgili et al., 1975; Çapan and Buket, 1975; Akyürek et al., 1982, 1984, 1988) of Maastrichtian age displays the alternation of conglomerate, sandstone and shale, and is transient with both Hisarköy and Karadağ Formations. Additionally, volcanics within the formation are differentiated as leucite, phonolitic-tephrite, tephritic-melaphonolite and crystal-

lithic tuffs. Another member of Kılıçlar Group is Malboğazı Formation (Ünalan et al., 1976; Yüksel, 1970; Hakyemez et al., 1986; Akyürek et al., 1988) which is composed of reefal limestone and sandstone. The Paleocene rocks in the region are defined as Çaldağ Formation (Yüksel, 1970; Akarsu, 1971, Schmit, 1960, Norman, 1972, Hakyemez et al., 1986) and Dizilitaşlar Formation (Yüksel, 1970; Ünalan et al., 1976; Schmit, 1960; Çapan and Buket, 1975). Çaldağ Formation of Monsian age (Sirel and Gündüz, 1976) is made up of algal limestones. It is laterally and vertically transient (transgressive) with the Dizilitaşlar Formation. The early Eocene aged Eskipolatlı Formation (Ünalan et al., 1976; Yüksel, 1070; Batman, 1978) is comprised of sandstone, marl and limestone. Comformably above, the sedimentary Çayraz Formation (Norman, 1972; Akyürek et al., 1982, 1984; Birgili et al., 1975; Yoldaş, 1982; Hakyemez et al., 1986) is found through the succession and the age of the unit is assigned as Küviziyen-Lütesiyen (Ünalan et al., 1976). The Miskincidere Formation (Norman, 1972; Çalgın et al., 1973; Çapan and Buket, 1975; Birgili et al., 1975) of Oligocene age is composed of alternation of conglomerate, sandstone, mudstone, marl and gypsum. It is unconformably overlain by Miocene rocks. Tekke volcanics (Çalgın et al., 1973); Akyürek et al., 1980) including andesite, trachyandesite, tuff, agglomerate and Oğulbey dacite (Kalkan et al., 1992) are the products of Miocene volcanism in the region. They are intertonguing with the sedimentary rocks of Kumartaş Formation (Çalgın et al., 1973; Arıkan, 1975; Ünalan et al., 1976; Akyürek et al.,1980, 1984); Hançılı Formation (Erol, 1956; Çalgın et al., 1973; Akyürek et al., 1982, 1984); Mamak Formation (Çalgın et al., 1973; Akyürek et al., 1980); Kızılırmak Formation (Birgili et al., 1975) and Bozkır Formation (Birgili et al., 1975).

Pliocene rocks unconformably overlie the Miocene rocks. The last volcanic product in the region is the Bozdağ basalt (Çalgın et al., 1973, Akyürek et al., 1980). Gölbaşı Formation (Çalgın et al., 1973, Akyürek et al., 1980) is composed of conglomerate, sandstone and mudstone. According to the stratigraphic

positions and previous works, the age of the Gölbaşı Formation is defined as Pliocene by Akyürek et al. 1997. As the youngest unit in the region, alluvium is found unconformably above the Pliocene rocks (Figure 3.2).

3.2. DESCRIPTION OF THE SAMPLING SITES

Before presenting the description of the sampling sites, what paleosol and calcrete mean for this study should be emphazied first. Paleosol is an old soil or fossil soil which is not related with the modern environmental and geochemical conditions, whereas it carries information about the time of its formation. Therefore, they play an important role in identifying the past paleogeological conditions. The presence of some features which are going to be defined in later Chapters of this contribution allow us to call the red-brownish colored mudrocks studied as paleosols for this study. The carbonate accumulations are also compatible with the explanations above. Therefore they are named as calcretes. The detailed information about the paleosols and calcretes of the studied samples are given in the following subchapters.

3.2.1. Karahamzalı Section

The road cut very close to Türkiye Şoförler Odası Federasyonu Dinlenme Tesisleri in Karahamzalı village has been selected as the first sampling site. It is located in southwest of Ankara and approximately 80km away from METU campus. 39 16 30.56''N and 32 57 30.70''E are the coordinates of the sampling location. There has been 2 separate sampling perfomed in this area, the first from outcrop and the second one by drilling operation. From the first one almost 12m height succession was sampled. Then by drilling up to 27 m, totally 39m succession is recorded (Figure 3.3). Red-brown colored mudstones with carbonate accumulations alternate with channel deposits (Figure 3.4a,b). There is a sharp contact between mudstones and the channel deposits (Figure 3.4c).

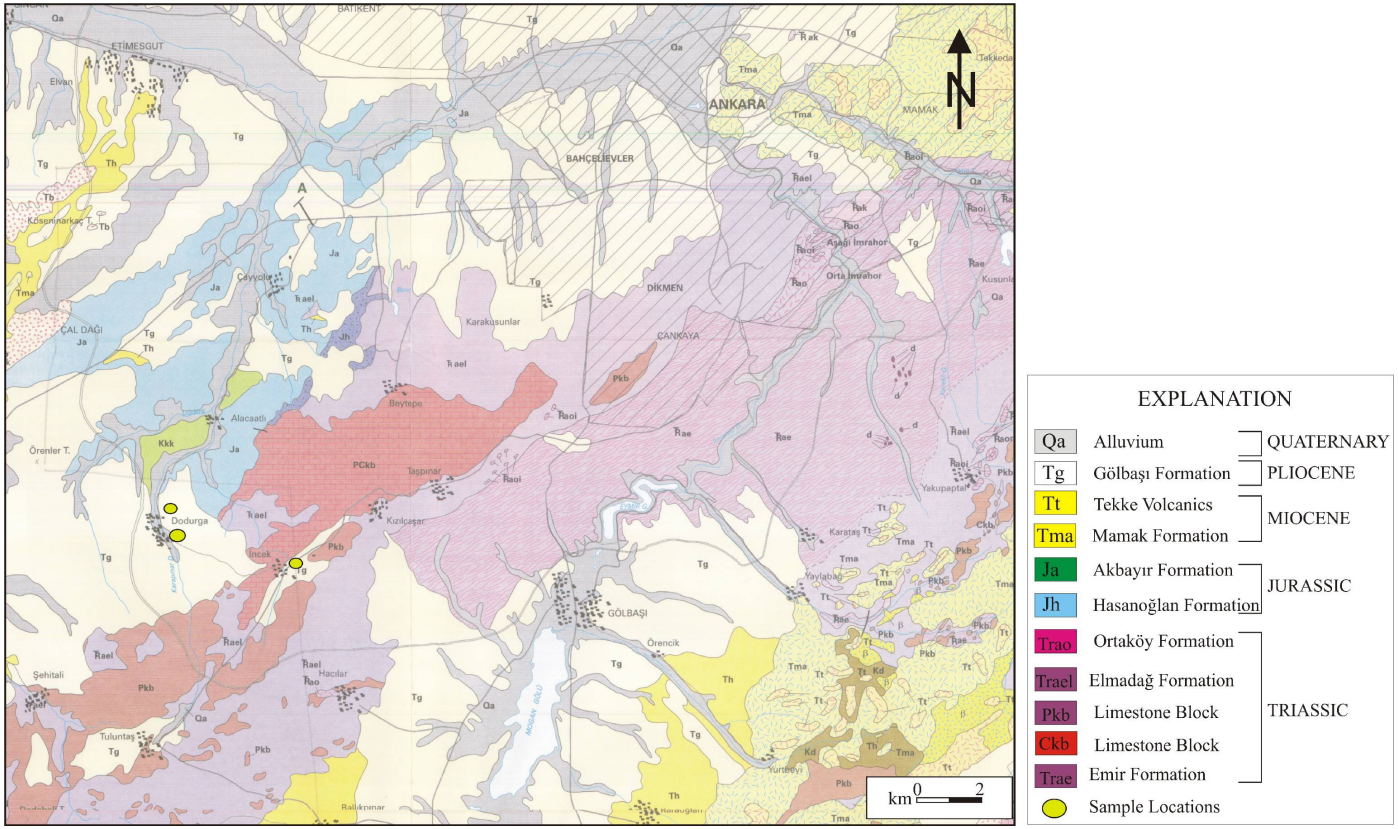

Figure 3.2. Geological map of Ankara in 1/100 000 (Akyürek et al., 1997)

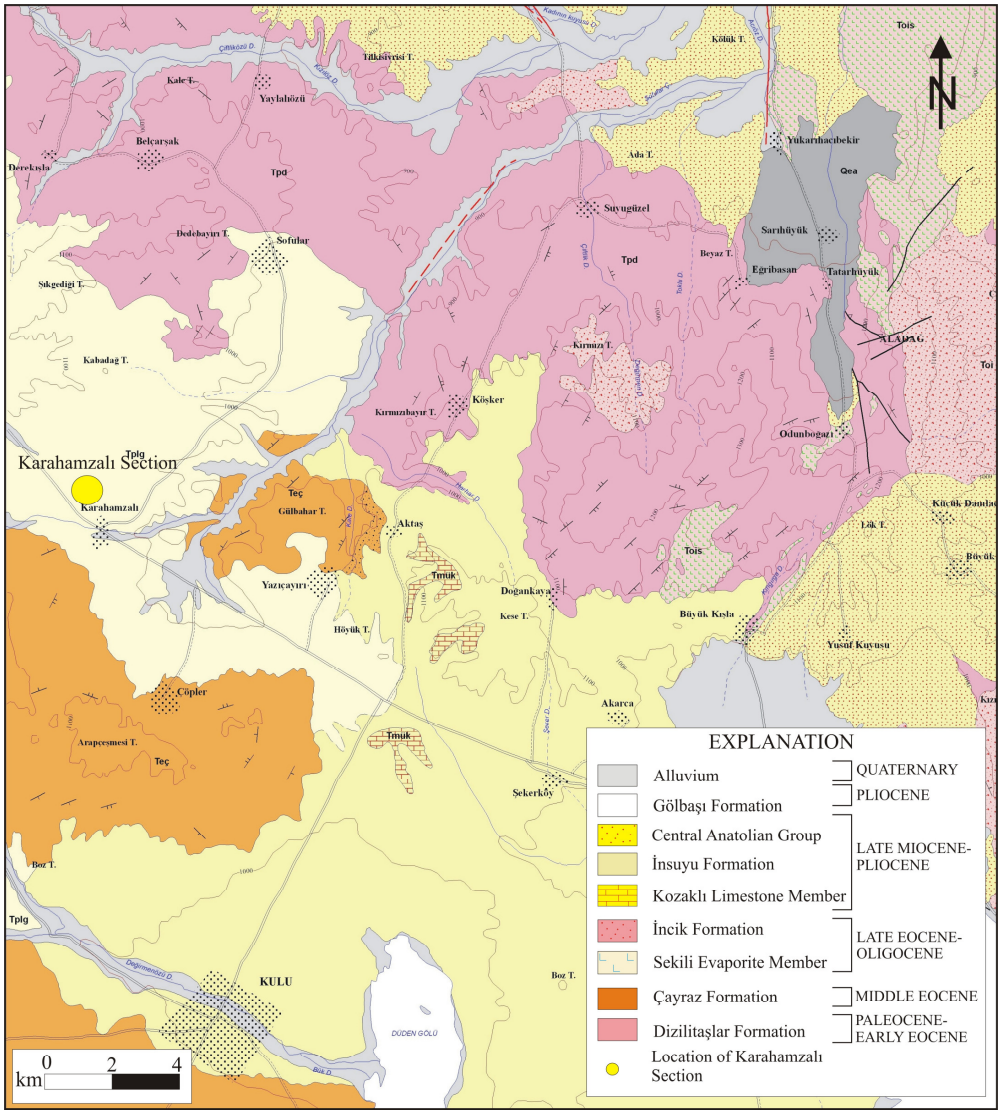

Figure 3.3. Map showing the location of the Karahamzalı section (Akçay et al., 2008).

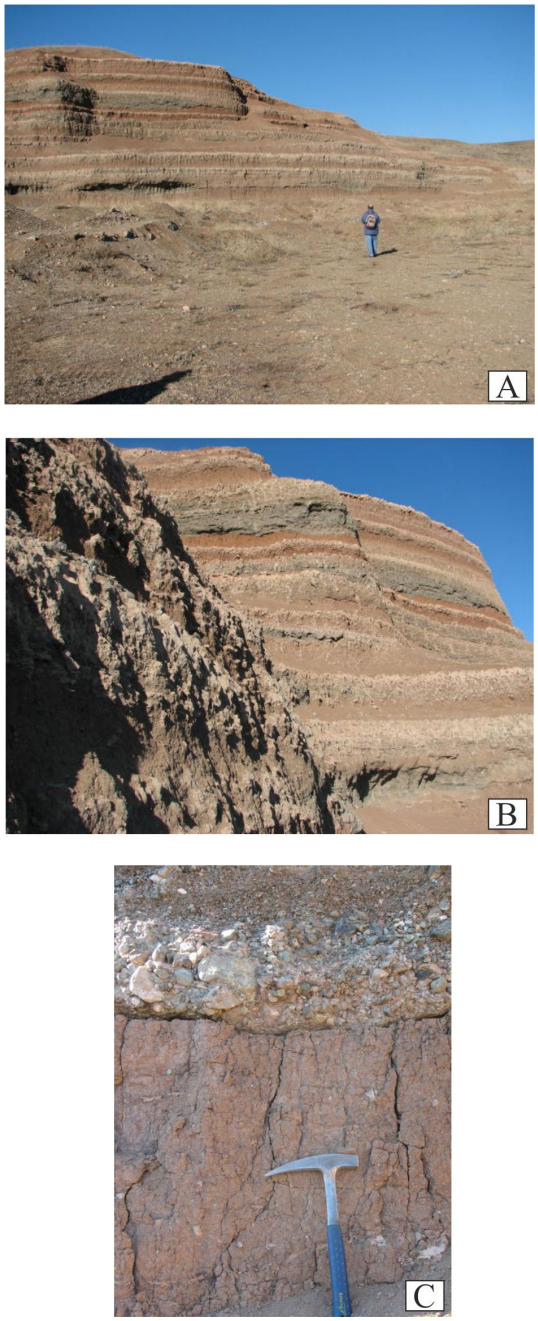

Figure 3.4. a & b) Field views of Karahamzalı section; c) sharp contact between red colored mudstone and the overlying channel deposit (the hammer is 33cm long).

The columnar section defines the stratigraphic relation of the lithologies with their field observations, soil morphologies and Munsell Colors (Figure 3.5). The lowermost unit is Evciler Basalt which has been assigned to be in Mio-Pliocene age by Dönmez et al. (2008) with K-Ar dating method. Unconformably above this unit, brownish red colored mudstones with paleosol characteristics starts to alternate with channel deposits up to 4m depth. However, the paleosols are divided into 3 separate groups in terms of their macrostructures through the section. The first group from bottom to 13m depth has almost only subangular blocky ped structure with relativey low amount of faunal and floral passages. The recorded Munsell colors of the units within this range are 5YR 7/2 and 5YR 6/3. Calcretes have sharp upper contact and transitional lower contact with the old soils. They show a small profile development from powdery calcrete to nodular calcretes (Figure 3.5).

From 13m to 4m depth, the second group of paleosols are recorded with both subangular blocky and prismatic ped structures. They become more reddish relative to the lower levels and still show alternation with channel deposits (Figure 3.5). This group of paleosols have more faunal and floral passages with respect to the lower paleosols but illustrates the same contact features. The Munsell colors observed within this range for paleosols and their carbonates are 7.5YR 8/2, 2,5YR 3/4, 5YR 7/2, 7.5YR 7/3 and 5YR 6/3.

At the top of the section, paleosols become more reddish in color with subangular blocky, prismatic and also granular structural units. Faunal and floral passages are the highest within this range. The Munsell colors recorded area 5YR 5/3, 7.5YR 5/3, 2.5YR 4/4, 5YR 6/3, 7.5YR 6/3 (Figure 3.5). The youngest unit is the recent soil deposit observed with red color and high carbonate accumulation.

On the basis of the stratigraphic position of the paleosols and the age of the underlying vocanic unit, the age of the paleosols is interpreted as Plio-Quaternary.

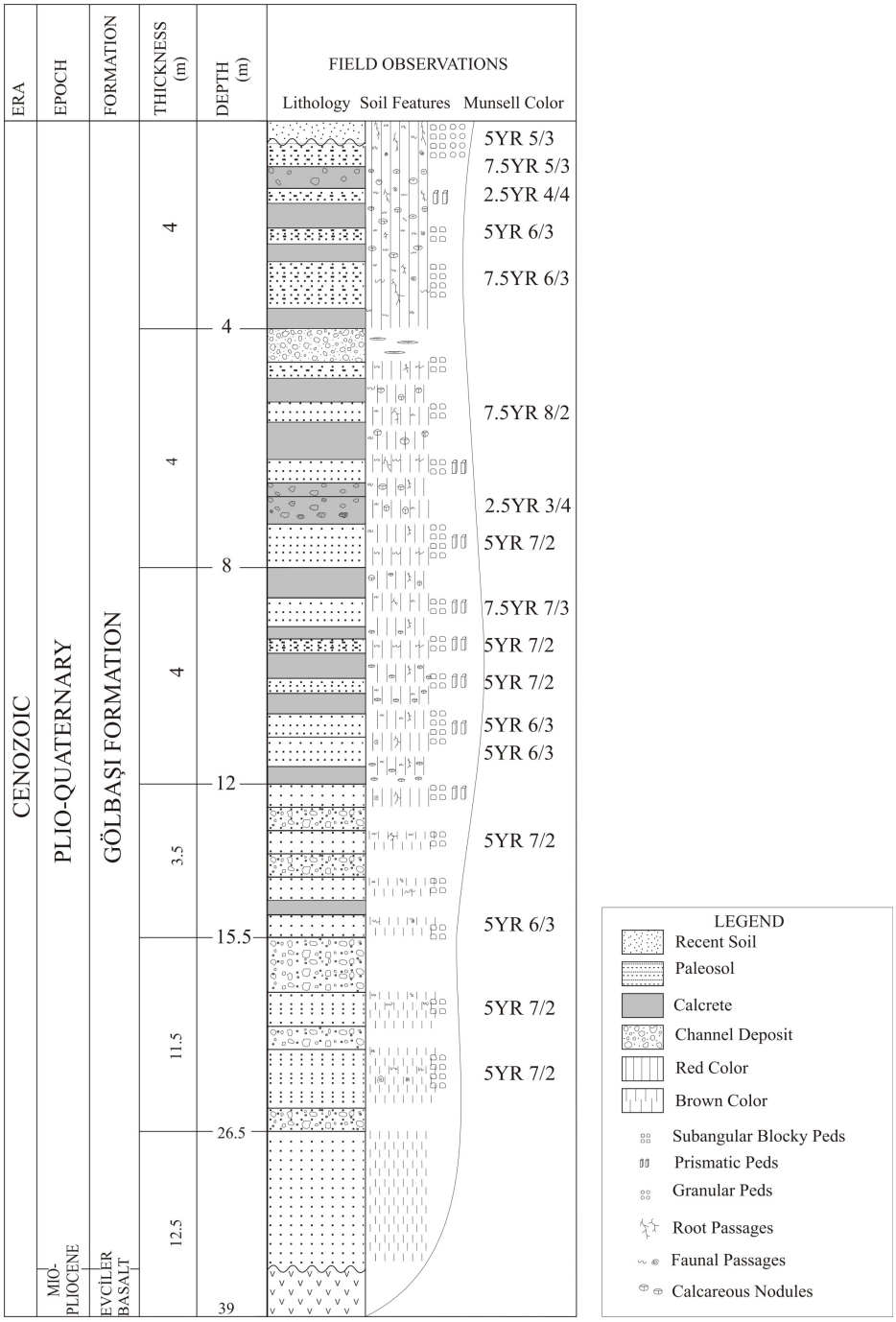

Figure 3.5. Columnar section of Karahamzalı section with field descriptions and soil properties.

3.2.2. Bala Section

The second sampling location is in Bala area, very close to the Çavuşlu Village. It is located to the southeast of Ankara and has coordinates of 39 40 20.04 N and 33 1 9.00 E (Figure 3.6). Due to the unavailability, the section could not totally be sampled from the outcrop, while only some lower levels are sampled and combined with the drilling operation from surface to 25 m depth. This section presents similar physical properties as the Karahamzalı section in that they both have red colored mudstone layers alternating with channel deposits (Figure 3.7a). Also they show calcrete developments within mudstone layers (Figure 3.7b). These mudstone layers like in Karahamzalı section show paleosol properties therefore called as paleosol for this study. The paleosol layers have sharp upper contact with the overlying channel deposits. The calcretes are nodular, tubular and powdery form presenting mostly downward transitional gradtion with a sharp upper parts (Figure 3.7c). The calcrete levels in Bala section are more common in outcrop samples while the ones gathered from drilling operation are mostly mudstones some of which have high carbonate accumulation layers.

From drilling operation 25m depth from ground could be sampled. At the bottom of the sampled section, channel deposists are found. They are made up of similar sized gravels with subangular to subrounded edges. Basalt and andesitic basalt fragments are common in these levels. At the bottom layers, the mudstone are more brownish and have Munsell colors of 7.5 YR 6/6. Up to section the brown colored mudstone layers start to show blocky to subagular blocky ped structures with a Munsell color of 2.5YR 4/4 and 5YR 7/2 (Figure 3.8). These were all developed during Late Pleistocene, since Middle Pleistocene was time of formation of C1 and C2 calcrete layers which are dated by ESR technique (given in Chapter 8). Peds within this time duration had started to show subangular blocky to prismatic structures implying dry conditions happened once. The color of the mudstones (paleosols) become more reddish and the frequency of the

calcrete layers are more up through the section (Figure 3.8). Unfortunately, above C2 level, the paleosols could not be sampled however their physical properties were recorded during field studies.

3.2.3. Other Sampling Sites

Other than Karahamzalı and Bala sections, calcretes from Çiğdem, İncek, METU and Dodurga areas were sampled (Figure 3.2). The calcretes from Çiğdem, İncek and METU areas are very similar in that they are all developed within red colored mudstones of Late Pliocene age (Aras, 1991). These mudstones have almost the same physical properties with Karahamzalı and Bala samples. On the other hand, calcretes from Dodurga area are found in yellowish- grayish colored fine grained siliciclasitc sedimentary rocks. They are mostly brecciated and different than the other calcretes physically. İncek, one of the sites having powdery calcrete development within a red colored mudstone layers was investigated (Figure 3.9). The coordinates of the sampling location are 36 474 024E- 44 058 51N and the eleveation is 1150 m. The field observation with HCl drops on the calcrete levels show high carbonate content. Unfortunately, due to its powdery nature, the calcrete samples could not be examined petrographically.

The second sampling site is Dodurga with the coordinates of the first location as 36 471 056E - 44 086 36N (Figure 3.2). Here, the alluvial fan sediments alternate with channel deposits (Figure 3.10). The red-yellowish mudstone layers show development of calcretes. Samples from Çiğdem and METU areas (Figure 3.2) are nodular calcretes with subrounded forms and a irregular bottom parts. The calcretes of these sites are also found in powdery form. These are accepted to be the early stages of the nodular calcrete developments. Towards the top, the maturity of the calcretes increases with increasing aridity and increasing carbonate content. These calcretes could be investigated petrographically.

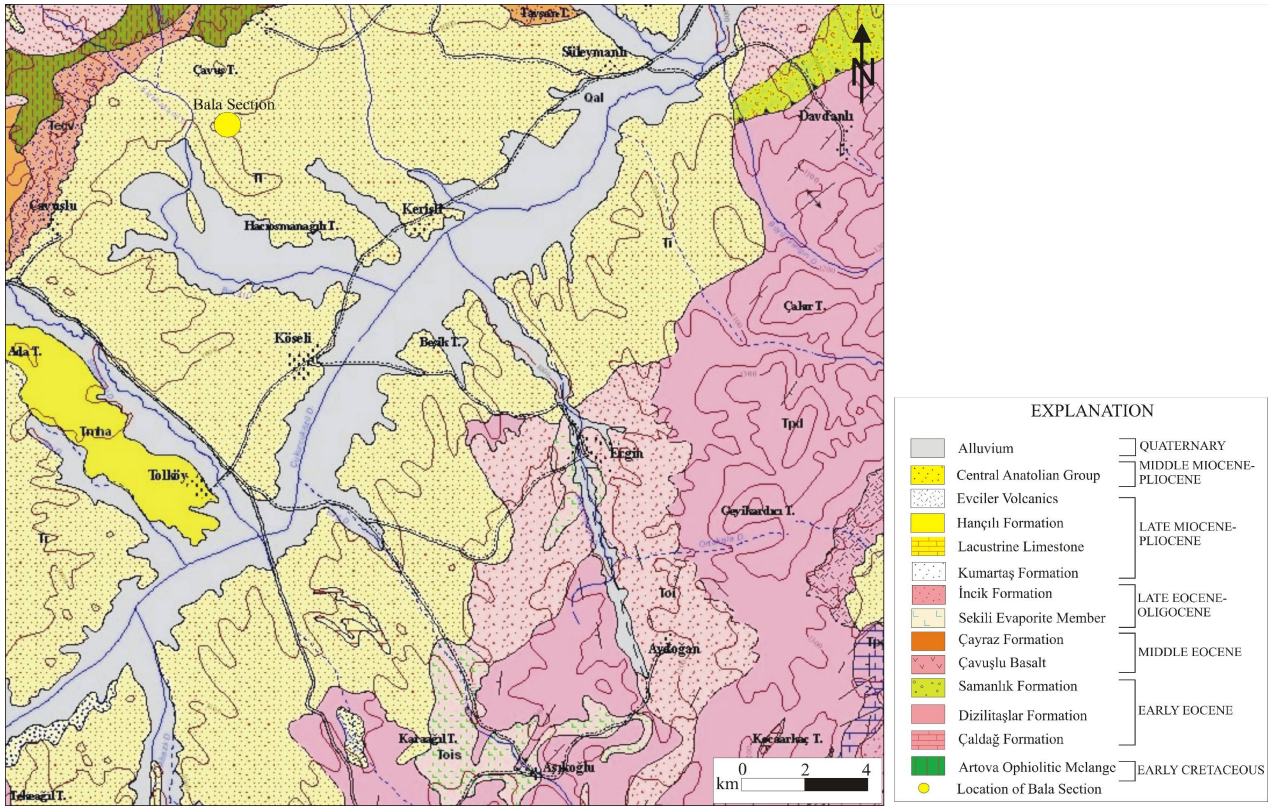

Figure 3.6. Geological map illustrating the location of the Bala section (Dönmez et al., 2008).

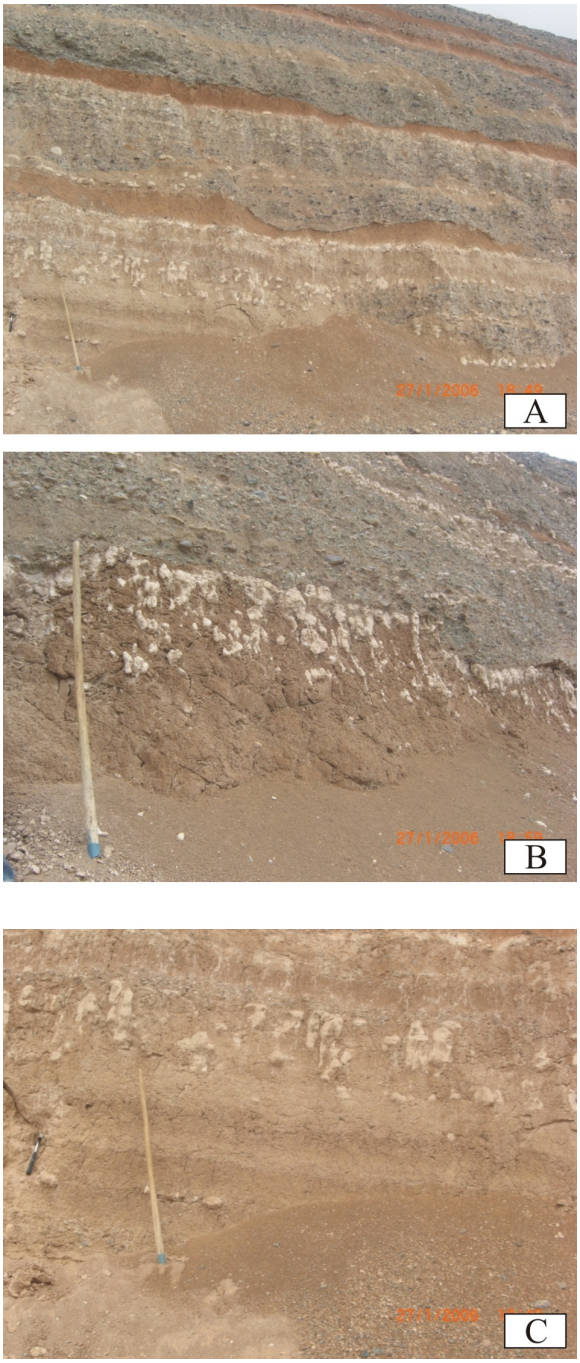

Figure 3.7. Field views of Bala section showing alternations of red colored mudstones with channel deposits and the development of calcretes.

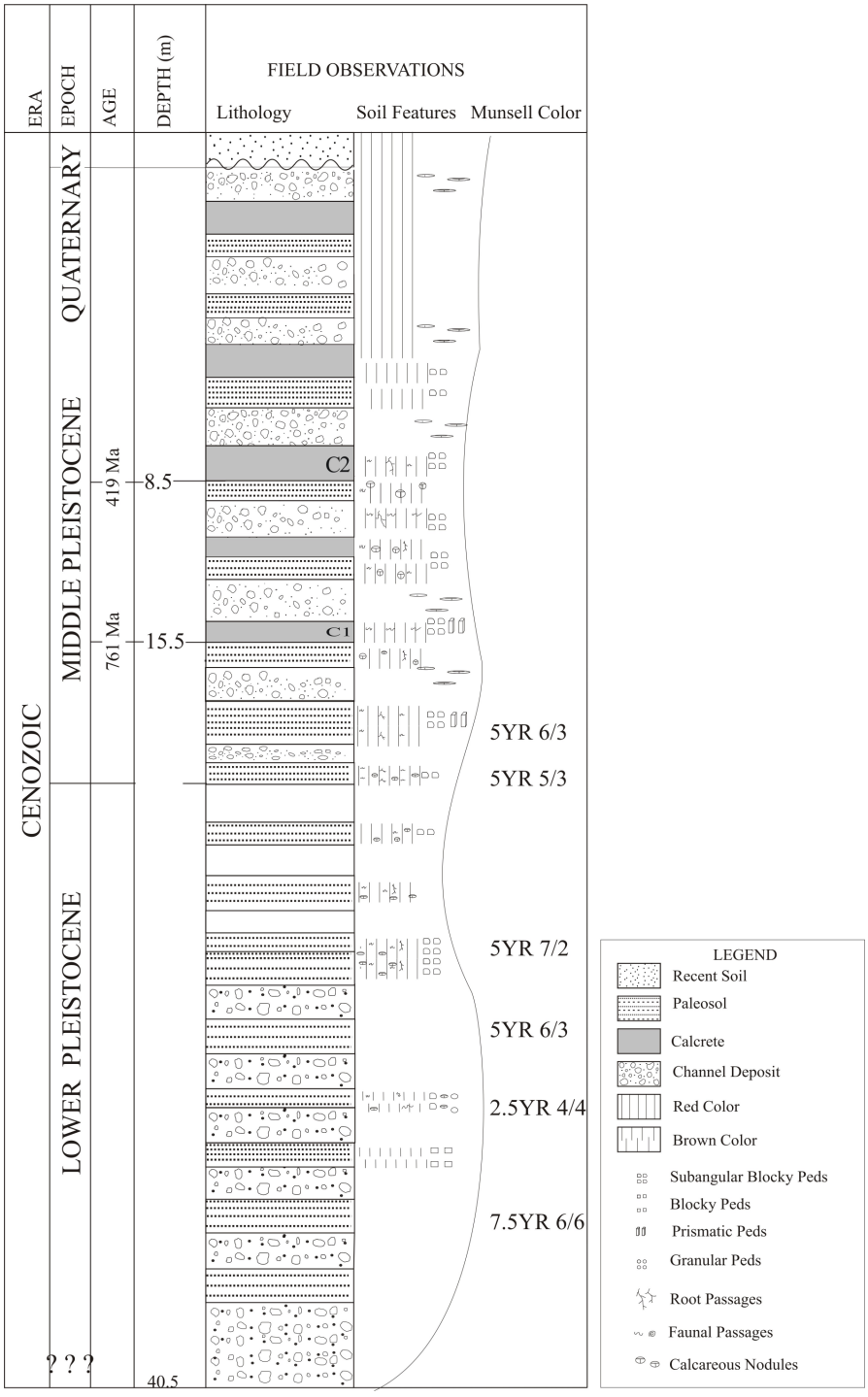

Figure 3.8. Columnar section of Bala section with field observations and soil properties.

Figure 3.9. İncek sampling site with a powdery carbonate developed within a red colored mudstone layer of Late Pliocene age.

Figure 3.10. Dodurga section showing alluvial fan deposists with channel deposits alternation.

CHAPTER 4

METHODOLOGY

4.1. FIELD SAMPLING

To have very good proxy data, four field trips were performed around Ankara. The best places to see the paleosol development were selected in Karahamzalı and Bala regions. Calcrete developments within red colored paleosols were also identified in İncek, Çiğdem and METU areas. Calcretes within grayish-yellowish siliciclastic rocks of Dodurga were also recognized and sampled. The paleosols in Karahamzalı and Bala sections were investigated on the basis of color changes and mottling revealing the horizon developments. The calcrete morphologies and the contact relationships between calcretes and the paleosols were also recorded during the field studies.

150 samples from paleosols and their carbonates (calcretes) were collected from the newly opened fresh surfaces of ourcrops/road cuts and also by means of drilling operations. The drilling operation for Karahamzalı section was done from ground to 27 m depth (Figure 4.1 a,b). For Bala section it is totally 25m depth from the ground (Figure 4.2 a,b). The samples, immediately after collected, are identified according to Munsell Color Scale in the field without the drying effect.

4.2. THIN SECTION PREPARATION

The first step to begin sample preparation is to identify the hand specimen to understand the properties of the material which is going to be studied. Therefore, each hand specimen studied with binocular to see macroscopic features closely.

Figure 4.1. Drilling operation in Karahamzalı sampling site.

The thin sections of Karahamzalı samples were prepared firstly at Thin Section Preparation Laboratory in Department of Geology at University of Western Ontario, Canada. And then, at the Thin Section Preparation Laboratories of Çukurova University and Middle East Technical University. Calcretes from Dodurga and Çiğdem areas were indurated in nature so that their thin sections were easily made at Thin Section Preparation Laboratory in Geological

Engineering Department at Middle East Technical University. During thin section preparations, the suitable standards for the soils and calcretes were applied according to the methods given by Retallack (2001) and FitzPatrick (1993).

Figure 4.2. Drilling operation in Bala sampling site.

Other than soil thin sections, slides for pollen analysis were prepared. The pollen analysis is very important for this study to give the relative age of the samples. To do this, Dr. Zühtü Batı and Ass. Prof.Dr. Nurdan Yavuz Işık have defined the most appropriate samples and they selected and analysed them. It has a long-saturation period with a careful solvation and saturation techniques. Then, the slides were prepared. For this study 15 samples from Karahamzalı and 15 samples from Bala sections were selected. Unfortunately, no well preserved pollen was identified in Bala samples. On the other hand, the samples from Karahamzalı section show 4 levels of well-preserved pollens. Their age and environmental interpretations are given in Chapter 8.

4.3. ANALYTICAL TECHNIQUES

This part is composed of the explanations of the techniques employed in this study. For the mineralogical investigations, X-Ray Diffraction equipment at Department of Earth Sciences in University of Western Ontario and Department of Geological Engineering in Middle East Technical University and Scanning Electron Microscope at the Central Laboratory, Middle East Technical University were used. For the determinations of the geochemical compositions of the paleosols and their carbonates, ICP-AES technique was employed by ACME Laboratories, Canada. The $\delta^{13}C$ and $\delta^{18}O$ analyses of the carbonates were carried in Laboratory of Stable Isotope Science at University of Western Ontario, Canada. Pollen analysis for the age and environmental constraints were carried by Dr. Zühtü Batı in TPAO Pollen Laboratory and by Dr. Nurdan Yavuz Işık in 19 Mayıs University Pollen Laboratory. Electron Spin Resonance technique was applied to two calcrete nodules from Bala sections to determine their ages by radiometric dating method. This was done in ESR Laboratory of Turkish Atomic Energy Agency, Ankara by Assoc. Prof. Dr. Birol Engin and Dr. Canan Aydaş. The soil properties were all defined in the Soil Laboratories of Soil Department at Çukurova University.

4.3.1. Separation and X-ray Diffraction of the <2µm Size-Fraction

Sample preparation for detailed clay mineralogy analysis and X-ray diffraction process were carried out in the Sample Preparation Laboratory and X-ray Laboratory of Department of Earth Sciences at University of Western Ontario, Canada. Combined procedures of Brindley and Brown (1980); Jackson (1979); Moore and Reynolds (1989); Thorez (1976) and Tucker (1988) were followed during the preparation and doing X-ray diffraction.

Firstly, approximately 30 grams from each sample were disaggregated with the metal pestle and mortar without affecting the original grain size. Then, disaggregated sample was placed in a 250 ml beaker and distilled water of 250 ml was added. The sample with the beaker was zapped with the ultrasonic probe (1/2 inch horn) for three minutes to (1) separate the clay from detrital grains and (2) to put a portion of the sample into suspension. After this, the supernate was poured off into a 1000 ml separating column. The process continued until the water in the beaker is clear after sonication. At the end, 1000 ml separation column was filled with the slurry. The residual in the 250 ml beaker is dried and labeled as "residue after sonication".

The separation of less than 2µm size-fraction is defined as follows: The settling columns were capped with a rubber cork so that the slurry in the columns could be mixed easily without loosing any material. Then, the columns were left for 22 hours and 11 minutes. This time should be the settling time according to the room temperature.

The laboratory temperature at the time of experiment was 22°C so according to Table 4.1, to separate <2µm fraction, 22 hours and 11 minutes waited. After this time, the supernate was siphonned off to a depth of 30 cm by using a rubber hose with a curved glass tip on the end to siphon the supernate into a 2 liter beaker. Each time after siphon the supernate, 10 ml of bleach was added 6% sodium

hypochlorite to the 2 lt beaker to cause clay flocculation. This would help to siphon the clear water-bleach mixture before each siphon of supernate from settling columns. This siphon procedure from settling columns continued until the water in the columns looked clear after the settling time passed. When it was completed, the sludge in the settling column was the size-fraction of >2µm.

The rest collected into 2 liter beakers was the fraction of <2µm. To those beakers, 150 ml bleach was added and the beakers were placed in the water bath overnight where the temperature was set as 65°C. This helped to remove of organic matter from the samples. Then, the bleach was washed out from each sample by first doing siphon and doing centifugation. Adding distilled water to each sample made easy to wash them. Next, the samples were washed with high speed centrifuge. To do so, samples were grouped into 8 (the capacity of the high speed centifuge at a time is 8 tubes). After balancing the tubes, they were placed into high speed centrifuge for spin of approximately 14 minutes at 12,000 rpm. After first washing, the samples were collected into 4 tubes instead of 8. Adding small amounts of distilled water into each tube and mixing with them with the stir stick were the following procedures after each washing. To test whether the sample still has bleach or not, after fourth wash, the supernate from each tube was collected into a small beaker and a few drops of 1% silver nitrate solution were added. If any precipitate forms or any cloudiness occurs, the washing should continue. At the end of the washings, there were 4 tubes for each sample. One of them was labeled as "Na-saturated", 15 ml of distilled water was added into the tube and it was covered with a kim wipe and immediately placed into the freezer.

The remaining 3 tubes were used for ion saturations. One of them was labeled as "Ca-saturated" and within this tube 15 ml of 2M $CaCl_2$ solution was added. To the second one, 15 ml of 2M KCl solution was added and labelled as "K-saturated". The last tube was labeled as "Mg-saturated" and 15 ml of 2M $MgCl_2$ solution was added. These tubes were dispersed with stir stick and left overnight so that the Ca,

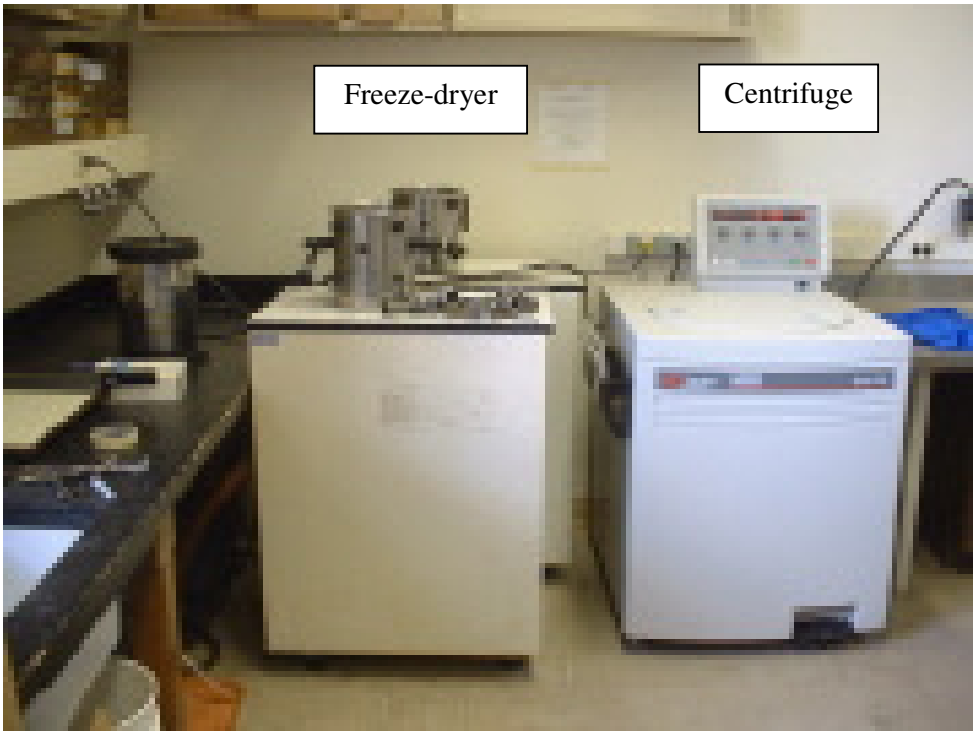

Figure 4.3. The pictures of freeze-dryer and the high-speed centrifuge in the Sample Preparation Laboratory of the Department of Earth Sciences at University of Western Ontario, Canada.

K and Mg ions were easily entered into the exchangeable sites in the clay structure. Then, the supernate was poured off. Sample remained in the tube was washed with distilled water at leat 5 times and at the end the supernate was tested with 1% silver nitrate. Like the Na-saturated tubes, 15 ml of distilled water was added to the K-, Ca- and Mg-saturated samples at the end of last washing, dispersed with stir stick and covered with a kim wipe and placed immediately in the freezer. The samples were stayed until they were frozen completely. Then they were placed into the freeze-dryer for a 3 days. After this, dry samples were removed from centrifuge tubes and put in a well labeled vial.

Disk preparation was tried on the samples but it was not a succesfull operation so glass slide was preferred. 50 mg from each freeze-dried Ca-, Mg- and K-saturated samples were placed into separate centrifuge tubes. Then, 2 ml of distilled water was added to each tube and dispersed throughly using microtip ultrasonic probe for 2 minutes. After this, the dispersed sample was taken with 2ml pipette and placed on the frosted side of the glass slide. Samples sit for at least overnight to be ready for X-ray diffractometer.

After a careful sample preparation stage, the turn into explain how to X-ray the samples in terms of their saturations. K-saturated sample slides were firstly placed into the oven which is set at 107 °C for 2 hours and the samples were X-rayed immediately after removing from the oven. This process provides 0% relative humidity. X-raying was done from 2 to 42 degrees 2 theta. Then the K-saturated slides were placed into a dessicator filled with Mg-nitrate overnight, which provides 54% relative humidity. The X-raying was done again from 2 to 42 degrees 2 theta. After this, the slides were put into the oven set at 300°C for 2 hours and scanned immediately after removing from the oven. The same procedure was carried out for the last step for K-saturated sample slides. Slides were placed into the furnace set at 550°C for 2 hours and scanned. So, the X-raying procedure for K-saturated samples were completed.

Ca-saturated sample slides were firstly put into the dessicator filled with Mg-nitrate to provide 54% relative humidity and then scanned from 2 to 42 degrees 2 theta. After this, the slides were placed into the ethylene glycol chamber and the desiccator was vacuumed and placed in the oven set at 65°C overnight. Next day, the chamber was set outside of the oven for another overnight, after, the vacuum was broken and the samples were scanned from 2 to 82 degrees two-theta.

Lastly, Mg-saturated sample slides were scanned but before X-raying the slides were placed into a dessicator filled with glycerol and again the chamber was

vacuumed and placed into oven set at 65°C for overnight and then the desiccator was sit outside of the oven for another 24 hours. Slides were x-rayed from 2 to 42 degrees two theta. Finally, all the slides were ready for detailed clay mineralogy analysis.

4.3.2. Preparation of Samples for the Stable Isotope Analysis

Samples which are x-rayed were studied in detail and the ones which include dolomite and calcite as carbonate mineral were separated for isotope analysis. This analysis was performed at Laboratory for Stable Isotope Science in Department of Earth Sciences at University of Western Ontario. A multiprep device coupled to a VG Optima dual inlet stable isotope ratio mass spectrometer was used for this procedure.

The following information is given according to the "Multiprep User Manual in Laboratory of Stable Isotope Science at Department of Earth Sciences, UWO". The Multiprep is multi-purpose sample preparation device for use with the Optima and Prism III generation of dual inlet stable isotope analysis mass spectrometers. The Multiprep comprises a temperature controlled sample rack which houses 60 small septum-capped reaction vials, a robotic autosampler and a very low-dead-volume water trap.

In the carbonate mode, carbonate material weighing as little as 10 micrograms is loaded into the reaction vial which then has the septum-lined cap screwed on. The sample vials are then loaded into the temperature controlled rack. The robotic sampler is used to pump out the vials and dispense a few drops of phosphoric acid. The CO_2 gas which is evolved from the acid-carbonate reaction, passes through the water trap and into a cryogenic CO_2 trap located close to the mass spectrometer's micro inlet system. After having been trapped the CO_2 is then introduced into the dual inlet where it is either loaded in the bellows and measured

or trapped in the inlet cold finger depending on the sample size. The most important part is the loading of samples into vials. Each sample was loaded into the vials by spatula without dropping the sample to the walls of the vials. The sample should be placed at the bottom of the vial. The sample vial caps must have a 3 mm thick silicone septum fitted and then a thin Kel-F septum fitted. When fitting the septa, the silicone septum lied flat in the bottom of the cap.

After loading, samples were placed into the storage trays. And then, the tray was placed into the oven at 50°C overnight. Then, vials were removed from the oven and placed in the Multiprep sample tray at 90°C. Then, each vial was taken one by one from the tray and introduced to the Multiprep (Figure 4.4). The valve unit houses the water trap assembly and the valve arrangement. The unit has equilibrated gases admitting and transferring parts. Main power is supplied from the mass spectrometer's power distribution panel. The whole unit is connected to the vacuum line to evacuate the system.

4.3.3. Geochemical Analysis

Fresh samples of paleosol and calcretes were selected for whole-rock geochemical analyses. The rock samples were crushed and ground at the Department of Geological Engineering of Middle East Technical University. Firstly samples were crushed to small chips by hammer and then ground by Reich Mortar Grinder in the Clay Mineralogy Laboratory at the Geological Engineering Department of METU. Finally, samples were packed as 20 g for each and sent to ACME Labs, Canada. Total abundances of the major oxides and trace elements are analysed by ICP-emission spectrometry at ACME Labs, Canada.

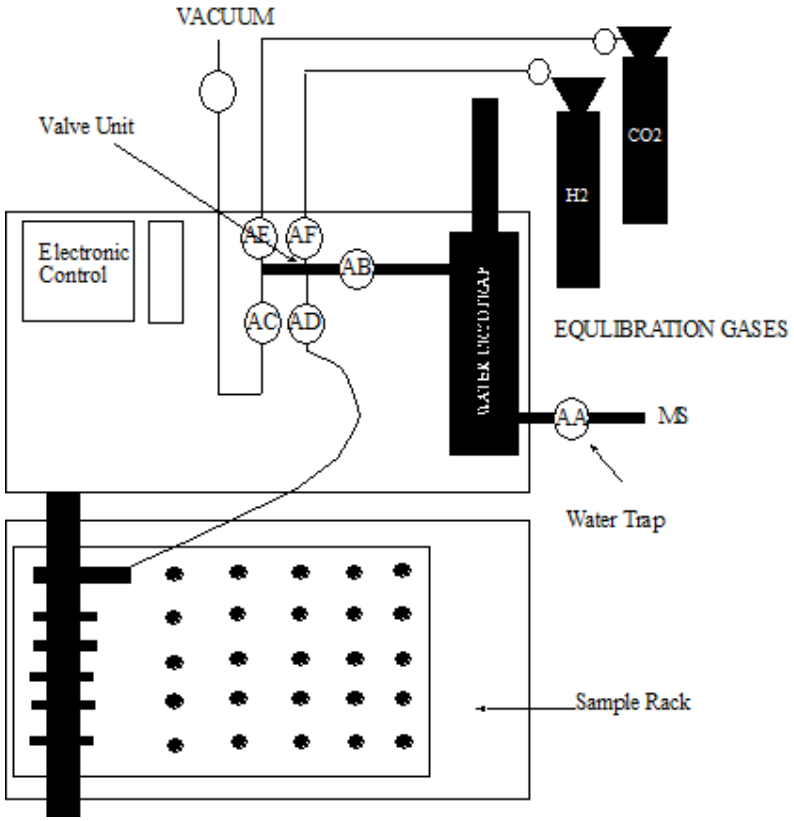

Figure 4.4. Multiprep working mechanism (from Multiprep User Manual in Laboratory of Stable Isotope Science at Department of Earth Sciences, UWO).

4.3.4. Electron Spin Resonance Technique

Electron Spin Resonance (ESR) or Electron Paramagnetic Resonance (EPR) spectroscopy is a technique for studying materials having unpaired electrons. More recently, it is recognized as a dating technique also. Literature review shows that ESR has been mostly employed to date calcite or quartz bearing materials. This technique is also used in this thesis study to date the calcite bearing calcrete nodules.

The following summary is given from Küçükuysal et al. (2011). ESR dating is based on the fact that ionizing radiation can create stable free radicals in insulating materials, like calcite and quartz. The concentration of these radicals-determined by ESR- is a function of the dose deposited in the sample along the years. ESR dating requires the measurements of two independent quantities: amount of natural radiation the sample and the annual dose due to the natural radioisotope content of the sample and can be calculated from their ratios (Ikeya, 1993). The dose rate D is calculated from the concentrations of the major radioactive elements ^{238}U,^{232}Th and ^{40}K (in K_2O) in the sample and its immediate paleosol environment, as well as the contribution by cosmic rays.

For ESR dating, firstly a fresh surface was opened through Bala section and then calcretes were sampled carefully. After calcrete nodules were extracted, surrounding red paleosols within about 30 cm radius were also sampled separately for external dose calculations. Two nodular calcrete samples which are seven meters apart from each other within the same section were selected for ESR dating. Hereafter, these samples will be designated as C1 and C2, respectively. The samples have always been kept and manipulated at normal laboratory conditions (about 21 ± 2°C, 25 ± 3 % relative humidity and ambient lighting). The calcrete nodules used for the dating experiments were separated from the red paleosols by washing with distilled water. The outer 2 mm surface of the calcrete nodules was removed by a sharp knife to eliminate the part which is affected by alpha (α) and beta (β) radiations, and the rest was prepared for ESR measurements and the detrital fraction (detrital quartz, ferro-magnetic fraction etc.) was tried to be removed as described in detail by Porat (1992). Magnetic separation eliminated some of ferrous particles and detrital quartz. The cleaned grains were etched by 0.5 % acetic acid in order to remove the mechanical-induced signal caused by the pressure in grinding. The sieve fractions of 125–180 μm for cleaned calcrete nodules were used for ESR analysis. The clean samples consist mainly of calcite and small amount of quartz, confirmed by X-ray

diffraction studies (Küçükuysal et al., 2011). The wavelength dispersive X-ray fluorescence spectrometer (XRF) (PANalytical, Advance Axios Model) available at Sarayköy Nuclear Research and Training Center (Ankara, Turkey) was used to estimate the chemical composition and trace elements contents of the calcrete samples as well as U, Th and K_2O contents within the samples and surrounding paleosols. Comparable measurements were also performed by Bruker EMX 131 X-band ESR spectrometer.

4.3.5. Scanning Electron Microscopy

Samples were selected to study under scanning electron microscope. It is held in the Central Laboratory at Middle East Technical University. Analysis were done by QUANTA 400F Field Emission Scanning Electron Microscopy with 1.2 nm resolution. Selected samples were firstly dried in air for a week and then put in an oven at 60°C overnight. Once all the water within the samples was removed, then they were coated with Au-Pd in high vacuum conditions. After coating the samples, they are investigated under SEM. During this study, Energy Dispersive X-ray Spectrometer (EDX) was also employed to have the chemical analysis of specific locations on the samples.

CHAPTER 5

MINERALOGY

The mineralogy chapter includes the determination of mineral compositions in bulk and clay fractions of the samples by X-ray diffraction analysis, the calculation of the relative abundances of the minerals and the interpretation on their presences in relation with paleoclimatic conditions. Additionally, scanning electron microscope studies are presented in this chapter to reveal the crystal shapes, sizes, micromorphologies and the textural relations between minerals. SEM also helps in detection of some minerals whose existence could not be determined by XRD because of their low quantity and poor crystallinities.

Among the minerals found in paleosols and calcretes, clay minerals have a very important role for the paleoclimate studies. They are the minerals with particle diamaters less than 2μm. Because of their fine sizes, their recognition under microscope is rather difficult. However, X-ray diffraction analysis allows us to analyse the clay minerals in detail. They are generally found at the surface of the Earth and can be formed either at the water-sediment interface or as a result of the interaction of aqueous solutions and rocks (Velde, 1995). Clay minerals play an important role in the geochemical cycle. This cycle is the evolutionary succession that occurs during weathering, transportation, sedimentation, diagenesis, metamorphism and genesis of crystalline rocks. Clays belong within the first four stages of this cycle (Millot, 1970).

As Chamley (1989) and Millot (1970) stated, weathering is one of the most important processes resulting in the formation of the clay minerals. Evolving with time, weathering processes produce soils where clay minerals are hosted. Intensity of weathering is strongly dependent on the lithology, climate and morphology

(Chamley, 1989) therefore clay mineral composition of the weathering profiles and soils are controlled by the climatic conditions. Additionally, as Chamley (1989) pointed out clay minerals in fluvial deposits are generally detrital in origin and so are used to understand the provenance of fine grained sediments and composition and climate of the source terrain. This relation between clay minerals and climate is used to reconstruct the past climates. There are certain climates which favour the formation of certain clay minerals. It is directly related to the conditions allowing the development of soils, biochemical activity and vegetation. Therefore it is apparent that climate is really an important factor producing good proxy data to reconstruct the climate of the past.

Clay minerals can be of three origins: inherited, transformed or neoformed within the soil. Millot (1970) defines those three types of clays as follows: inherited clays are the results of direct erosion of continental rocks or reworking of soils. Transformed clays, on the other hand, are the products of physico-chemical transformation of inherited material during sedimentation. Finally, neoformed clays are formed from the dissolved materials in water. Diagenesis is another process which strongly affects the clay minerals. Therefore after deposition, since sedimentary evolution continues, clays also face with futher changes. That is why diagenetic clays should also be considered as another type of clay minerals besides the three major classes (Millot, 1970).

Inherited clays carry information about the provenance of the deposit however neoformed clays reflect the formation conditions since it is formed in situ. Transformed clays, on the other hand, have the signatures of both source area and the chemical environment. Therefore, according to the purpose of the study, clay minerals can be used to infer the past climatic conditions.

As stated in the Methodology Chapter of this thesis, clay minerals were analysed by separating the clay fraction from the whole soil firstly. Qualitative and semi-

quantitative results of X-ray diffraction studies will be given in this chapter. Qualitative determination of the clay minerals were conducted according to Brindley (1980), Thorez (1976) and Chen (1977).

There are three groups of samples analysed for mineralogical composition. The first group is the samples of Karahamzalı section including outcrop samples and drilling samples. Group II samples are from Bala area. Bala section, because of its topographical relief, could not be well-sampled on the outcrop but drilling was performed in the Bala area. Therefore a profile from the surface to 25 m depth could be sampled. The third group is composed of samples from İncek, Dodurga, Çiğdem and METU. Those samples are rather different than the Karahamzalı section since they do not represent a well developed paleosol profile but show calcrete development within the silty-clayey host rock.

All the samples, both paleosols and calcretes, were examined in terms of their mineralogical compositions by X-ray diffraction analyses. According to the purpose of the study, two types of size fractions were separated. The first group of powder diffraction sample was separated by grinding the sample representing the bulk mineralogy of the samples. The second group is less than 2µm in diameter which is separated by the sedimentation method according to the Stoke's Law (defined in methodology chapter). Both fractions were qualitatively and semi-quantitatively investigated in this contribution.

5.1. MINERALOGY OF THE KARAHAMZALI SECTION

In Karahamzalı area, sampling was carried out in two parts; first sampling was from outcrop and the second one was obtained from the surface to 25m depth by drilling. Samples are from red colored paleosols and their calcretes. 42 levels including paleosols and their carbonates were sampled at Karahamzalı section.. At the bottom of the paleosols and their carbonates, a basaltic rock was found by the

drilling operation at 25 meter depth. K–41 is the sample number of this basaltic body. On the XRD diagram of the K–41 sample, only smectite is recognized (Figure 5.1). Above this basaltic body, red-brownish colored paleosols and their calcretes are alternating with channel deposits. Quartz (3.34 Å and 4.26 Å) as a non-clay component of the Karahamzalı section is present in all of the samples except the basaltic sample (K–41).

Calcite, the other non-clay mineral in Karahamzalı section, was detected at the middle to lowermost part of the Bala section. It gives 3.03 Å reflection which is typical of calcite (Figure 5.2). In the middle to lower parts of the section, dolomite is present in six samples, three of them also include calcite.

Dolomite has a distinct 2.89 Å reflection in Karahamzalı section. Dolomite is present in almost all samples in the upper parts of the section where calcite is completely absent. Additionally, plagioclase as a detrital mineral is present all through the section and recognized with its 3.2 Å reflection (Figure 5.3).

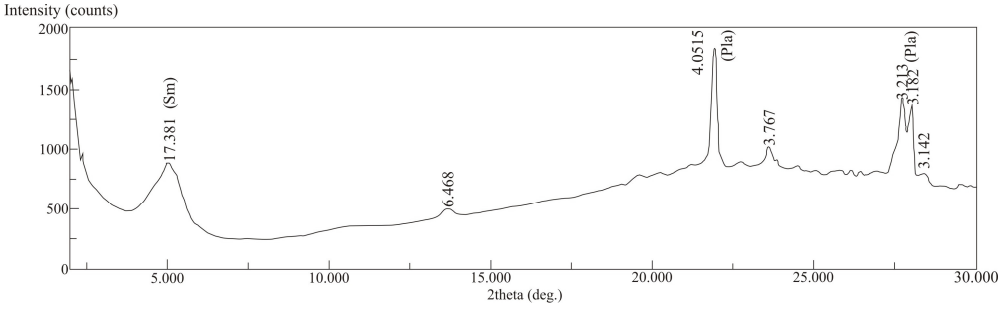

Figure 5.1. X-Ray diffraction of ethylene glycol solvated K-41 basaltic substrate (Sm: Smectite; Pla: Plagioclase)

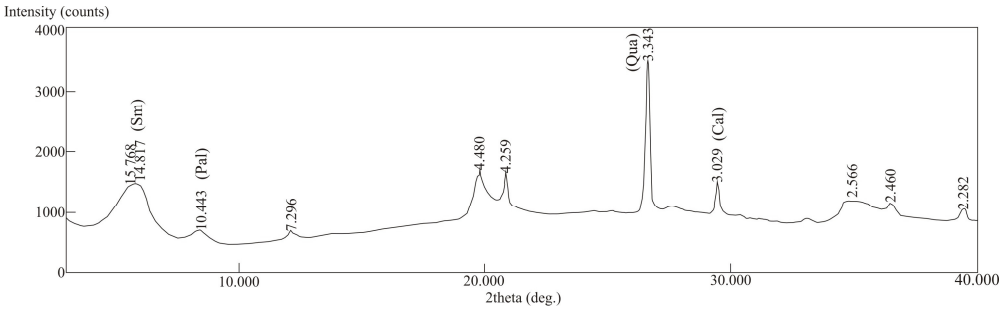

Figure 5.2. X-ray diffraction of powder paleosol from the lower part of the Karahamzalı Section (Sm: Smectite; Pal: Palygorskite; Qua: Quartz; Cal: Calcite).

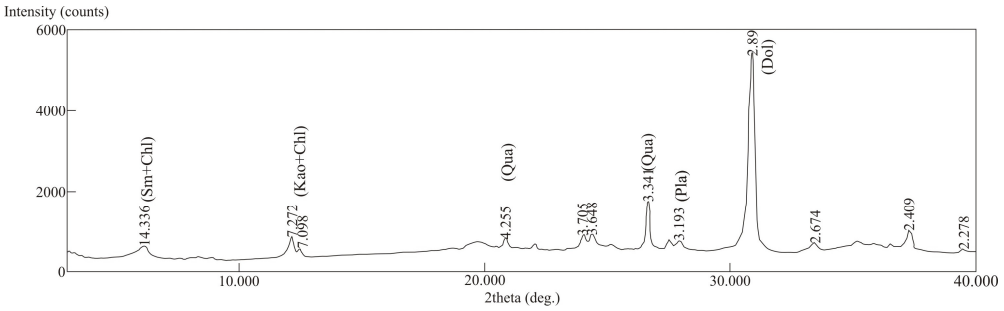

Figure 5.3. X-ray diffraction of powder paleosol (carbonate-rich) from the Karahamzalı Section (Sm: Smectite; Chl: Chlorite; Kao: Kaolinite; Qua: Quartz; Pla: Plagioclase; Dol: Dolomite).

The clay-fraction of the studied samples of Karahamzalı section reveal the presence of smectite, chlorite, kaolinite, illite and palygorskite in a decreasing order in Karahamzalı section. Smectite, the dominant clay mineral found in the section is present in all samples including K–41 the basaltic body. It was identified by the 12 Å - 14 Å peaks which shift to 17 Å by ethylene glycol solvation (Figure 5.4). Ethylene glycol solvation technique was applied to the samples in the mid-lower part of the samples, but, to the samples in the upper parts of the section, Mg-saturation and glycerol solvation technique was also

employed at the UWO, XRD Laboratory. This technique gives a detailed information on the type of swelling clay minerals. According to the Mg-saturation and glycerol solvation, smectite peak at 14.2 Å remains stable at 14.2 – 14.3 Å reflections. This behaviour is typical of beidellite type smectite mineral (Thorez, 1976). This was also confirmed by Ca-saturation at relative humidity of 54% and Ca-saturation with glycol solvation treatments. The smectite of this section has a 14.2 Å reflection at Ca-saturation at relative humidity of 54% which shifts to 17 Å peak by Ca-saturation and glycol solvation. Smectite collapsed to 10.1 Å reflection by K-saturation and heating treatments. Crystallinity of smectites is a parameter produced by Biscaye (1965) to use smectite to have correlations between v/p ratio with stratigraphical position, depth of the samples and the diagenetic effects on the samples. It is measured on the XRD pattern of glycolated sample. Height of 17 Å reflection above the background is measured as "p" and the depth of the valley on the low angle side of the 17 Å diffraction is shown as "v". If the v/p ratio is close to 1, then it is well-crystallized smectite; if it is close to 0, it is poorly crystallized smectite. In Karahamzalı section, the v/p ratio is generally between 0.3 and 0.5 which means the smectites in this area are poorly to moderately crystallized. This information is consistent with the detrital origin of smectites within the Karahamzalı section.

Kaolinite and chlorite are the two clay minerals present in all samples except the basaltic rock (K–41) underlying the paleosols (Figure 5.4). Kaolinite and chlorite have some reflections overlapping each other. However, as Thorez (1976) stated, chlorites have strong d(001) at 14 Å and d(003) at 4.7 Å peaks which do not occur in kaolinites. Also, heating to 550 °C for an hour causes dehydroxylation of the hydroxide sheet which is seen as an increase in the intensity of the d(001) reflection of chlorites (Moore and Reynolds, 1989). Heating to 550°C in K-saturated samples or in unsaturated samples causes the collapse of kaolinite where chlorite would still have the 14 Å and 7.3 Å reflections.

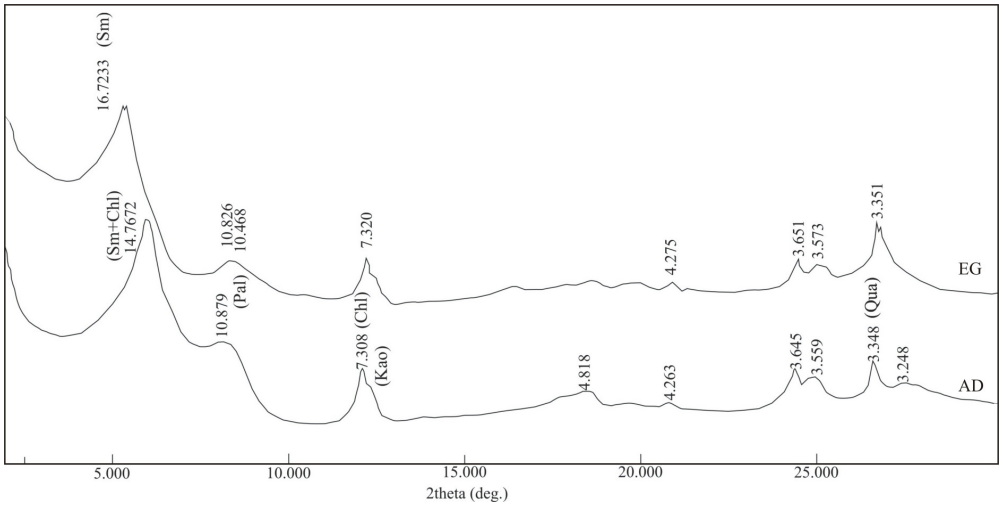

Figure 5.4. X-ray diffraction of air dried and ethylene glycol solvated K-1 paleosol from the Karahamzalı Section. (Sm: smectite; Chl: chlorite; Pal: palygorskite; Qua: quartz; AD: air dried; EG: ethylene glycol solvated).

Illite is the easiest to differentiate among others. Its basal reflections are stable with all treatments and heatings. Therefore, 10 Å d(001) remains constant througout the saturations. It is almost absent in the lower section samples but appeared with its 10 Å reflection in the upper section samples but abruptly disappeared in the lower parts of Karahamzalı section.

The other mineral present in the clay fraction of the samples is palygorskite (Figure 5.2). It is easily recognized with its 10.4–10.5Å reflection. This peak collapses to 10.1 Å by heating to 550°C. To get over with the confusion on the presence of palygorskite, SEM studies were also carried out to reveal its existence with its fibrous morphology. Its presence is very important in paleoclimatic reconstruction studies. Therefore, it is also used as a proxy data for the paleoclimate reconstruciton of the region in this contribution. According to the peak intensities of the minerals on XRD diagrams in the Karahamzalı section, the relative amounts of the non-clay minerals and the total amount of clay minerals within the bulk composition were calculated according to the method of

Gündoğdu (1982). According to this method, intensity factors of 0.35, 0.74, 1.62, 1 and 14.63 are used for quartz (3.34Å), calcite (3.04Å), feldspar (3.18–3.20Å), dolomite (2.89Å) and total clay minerals (4.53Å), respectively. The results listed in Table 5.1 are plotted with respect to depth of the section (Figure 5.5). Quartz is present throughout the section however it shows a decreasing trend towards the upper part of the section and reaches almost a constant value close to the upper levels. Its abundance is between 2.6% to 11.6%. Dolomite appears in the lower parts of the section at a very low quantity and then disappears at some levels. However, it shows an increasing trend towards the upper part of the section where calcite is absent. Where calcite is present, the abundance of dolomite varies from a maximum of 66.3% to a minimum of 3.4%. Dolomite is found with calcite only at the bottom of the section. This trend was checked and confirmed by XRD and also by staining test under the microscope. Feldspars, like calcite, are much more abundant at the bottom of the section and are at lower values close to the upper levels. Its abundance ranges from 3.4% to 11.2% through the section. Total clay mineral amounts gathered from XRD diagrams are generally higher than 40%. The minimum value is 33.7% and the maximum is 94.4% for clay mineral abundance. Changes in the amount of clay minerals with respect to depth reveals an opposite trend with the dolomite versus the depth line.

The peak intensities of the clay minerals in the Karahamzalı section were used to quantify the amounts of smectite, chlorite, kaolinite, illite and palygorskite. The method of Biscaye (1965) was followed during the calculation of amounts of clay minerals. According to this method, 1, 1, 2, 0.5 and 1 are used as intensity factors for kaolinite (7Å), chlorite (14Å), illite (10Å), smectite (17Å) and palygorskite (10.4Å), respectively. The relative amount of clay minerals in the clay fraction of the samples through the Karahamzalı section is listed in Table 5.2. They are plotted versus depth (Figure 5.6). Smectite plots a zigzag pattern with enrichments and depletions. Its highest content is almost 100% at the bottom of the section but it shows depletion up to the section reaching almost an abundance of 8.7%.

Kaolinite and illite, the detrital phases, plot almost the same trends on the diagrams. Kaolinite abundance ranges between 3.2% and 25.6%; similarly illite has 4.3% to 38.9% abundance throught the section. Chlorite, the other detrital mineral found in the section, show a opposite trend with respect to kaolinite and illite. Its lowest value is 11.1% whereas it is 84.6% at maximum in the section. Palygorskite plots exactly an opposite trend line to smectite and chlorite. The best line for palygorskite abundance through the section shows an increasing trend towards the top of the section. It starts with 4.7% abundance and reaches to 47.2% at maximum.

5.2. MINERALOGY OF BALA SECTION

The selected succession in Bala is very similar to one in Karahamzalı within the region in that it has red mudstone levels including calcretes which are alternating with the thick channel deposits. 18 levels were sampled from Bala succession and 10 of them were X-rayed to define their bulk mineral compositions and the clay fractions. From top to bottom, samples are numbered as B–1 to B–17 and Bc, respectively.

Almost all the samples have the same clay and non-clay minerals in the Bala succession. As the non-clay minerals, quartz, feldspar and calcite are identified within a size fraction of less than 63 μm (Figure 5.7). Quartz was found by the presence of two prominent peaks at 4.27 Å and 3.34 Å. Feldspars, on the other hand, were determined by the most intense peak at 3.2 Å. Calcite, the presence of which is very important for this study, was determined with the sharp and intense peak at 3.03Å.

Table 5.1. Semi-quantitative analysis on Karahamzalı samples.

Sample	Quartz	Calcite	Feldspar	Dolomite	Clay	Total
U13	4.1	0.0	0.0	52.3	43.6	100.00
U12	11.9	0.0	0.0	0.0	88.1	100.00
U11	8.5	0.0	0.0	0.0	91.5	100.00
U10	2.6	1.7	0.0	66.3	29.4	100.00
U8	6.4	2.2	0.0	4.1	87.3	100.00
U7	3.0	0.0	0.0	46.9	50.1	100.00
U6C	3.9	0.0	0.0	49.1	47.0	100.00
U6S	6.6	0.0	5.8	0.0	87.6	100.00
U5	6.1	0.0	5.2	29.8	59.0	100.00
U4	6.2	0.0	11.2	19.5	63.0	100.00
U3	9.5	0.0	5.5	0.0	85.0	100.00
U2	5.2	0.0	0.0	33.2	61.5	100.00
U1	7.1	0.0	3.6	0.0	89.2	100.00
A1	6.3	0.0	0.0	43.1	50.6	100.00
A2	11.2	0.0	4.2	0.0	84.6	100.00
A3	6.6	0.0	0.0	49.3	44.0	100.00
A4	7.4	0.0	0.0	17.6	75.0	100.00
A5	8.8	3.4	0.0	0.0	87.7	100.00
A6	8.7	3.7	0.0	37.0	50.6	100.00
A7	8.1	0.0	9.9	0.0	82.0	100.00
A14	9.8	0.0	3.4	0.0	86.8	100.00
A15	6.4	0.0	0.0	23.7	69.9	100.00
K-1	4.4	3.5	11.2	8.3	72.6	100.00
K-2	4.3	6.4	9.0	4.6	75.6	100.00
K-4	4.8	0.0	3.7	57.7	33.7	100.00
K-5	3.3	0.0	6.7	29.3	60.7	100.00
K-6	5.0	3.5	8.4	0.0	83.1	100.00
K-9	3.3	0.0	6.5	21.6	68.5	100.00
K-12	5.0	25.5	10.7	0.0	58.8	100.00
K-13	4.9	3.0	8.1	3.9	80.1	100.00
K-15	4.5	3.7	7.7	4.6	79.5	100.00
K-16	2.8	0.0	10.7	0.0	86.4	100.00
K-19	5.6	0.0	0.0	0.0	94.4	100.00
K-21	4.6	0.0	7.9	5.4	82.1	100.00
K-24	5.5	0.0	7.5	0.0	87.0	100.00
K-27	5.5	3.4	0.0	5.7	85.3	100.00
K-30	3.9	12.8	8.1	6.9	68.2	100.00
K-33	4.2	11.3	7.9	4.2	72.4	100.00
K-35	5.0	3.3	7.7	0.0	84.1	100.00
K-37	4.3	2.9	6.9	0.0	85.9	100.00
K-39	4.1	3.2	7.1	0.0	85.6	100.00
K-40	4.5	4.0	0.0	0.0	91.5	100.00
K-41	0.0	3.1	43.9	0.0	53.0	100.00

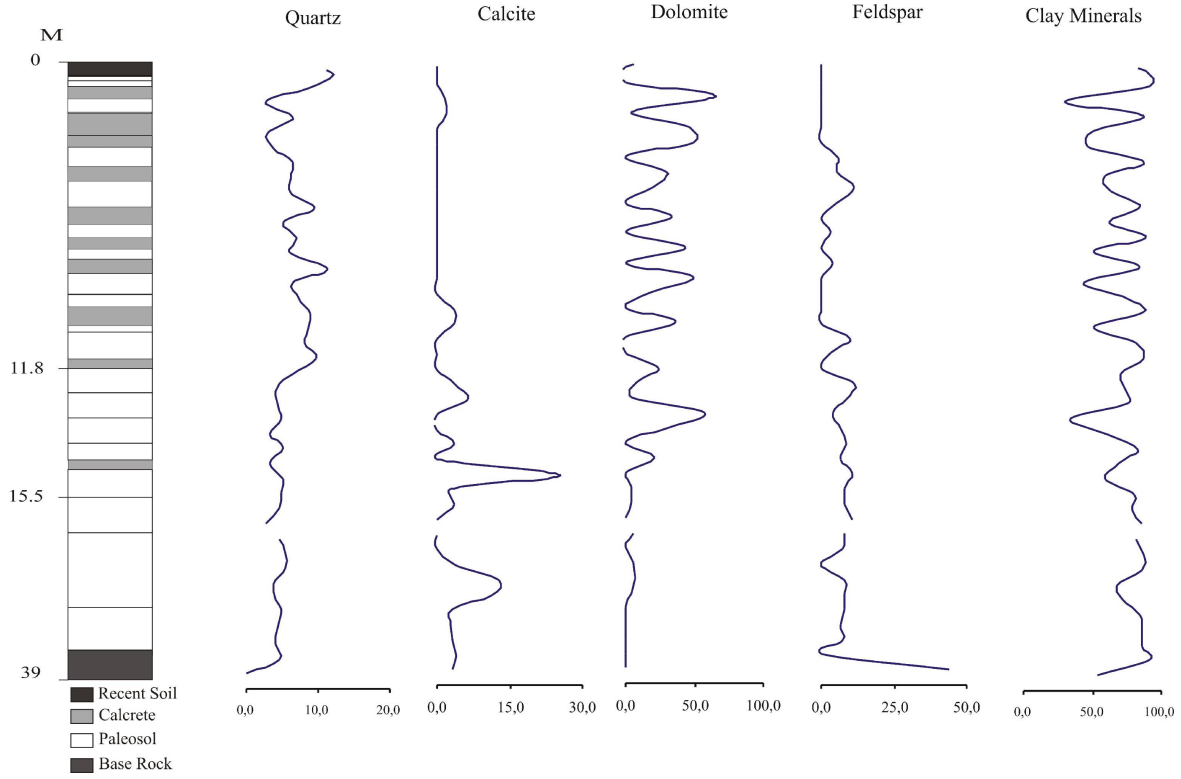

Figure 5.5. Changes in amounts of bulk mineral compositions (wt in %) of the Karahamzalı section with respect to depth (m).

Table 5.2. Semi-quantitative analysis of clay fraction of samples from Karahamzalı section.

	Smectite	**Chlorite**	**Palygorskite**	**Kaol**	**Illite**	**SUM %**
U-13	68.9	16.2	0.0	9.5	5.4	100.0
U-12						
U-11						
U-10	22.4	17.9	37.3	13.4	9.0	100.0
U-8	19.5	16.1	16.1	20.7	27.6	100.0
U-7	29.5	17.6	13.2	20.3	19.4	100.0
U-6S	44.5	21.1	0.0	16.7	17.6	100.0
U-6C	43.6	23.6	0.0	18.2	14.5	100.0
U-5	45.4	26.4	6.2	11.5	10.6	100.0
U-4	53.1	25.5	0.0	11.2	10.2	100.0
U-3	8.7	14.2	47.2	15.7	14.2	100.0
U-2	27.8	27.8	0.0	19.4	25.0	100.0
U-1	15.6	17.7	15.6	30.2	20.8	100.0
A-1	41.7	25.0	5.8	14.2	13.3	100.0
A-4	31.3	20.5	22.3	17.0	8.9	100.0
A-5	14.8	15.1	19.4	20.6	30.1	100.0
A-6	28.4	18.2	11.9	17.5	23.9	100.0
A-7	23.3	20.9	8.7	22.7	24.4	100.0
A-14	32.9	21.7	4.7	21.7	19.0	100.0
A-15	43.9	21.9	8.8	16.7	8.8	100.0
K-1	20.3	51.1	10.5	9.0	9.0	100.0
K-2	34.1	33.0	8.8	11.0	13.2	100.0
K-5	40.9	34.1	6.8	9.1	9.1	100.0
K-6	21.2	15.4	13.5	26.9	23.1	100.0
K-9	42.5	30.0	7.5	10.0	10.0	100.0
K-12	23.1	20.5	0.0	25.6	30.8	100.0
K-13	22.2	11.1	5.6	22.2	38.9	100.0
K-15	47.1	17.6	11.8	11.8	11.8	100.0
K-16	0.0	84.6	0.0	15.4	0.0	100.0
K-19	30.0	20.0	13.3	10.0	26.7	100.0
K-21	36.7	23.3	10.0	10.0	20.0	100.0
K-24	33.3	27.5	11.8	11.8	15.7	100.0
K-27	40.7	25.9	7.4	11.1	14.8	100.0
K-30	44.9	29.0	0.0	14.5	11.6	100.0
K-33	37.5	18.8	0.0	18.8	25.0	100.0
K-35	69.0	13.8	6.9	3.4	6.9	100.0
K-37	57.4	19.7	6.6	3.3	13.1	100.0
K-39	64.9	17.5	7.0	3.5	7.0	100.0
K-40	67.7	16.1	6.5	3.2	6.5	100.0
K-41	100.0	0.0	0.0	0.0	0.0	100.0

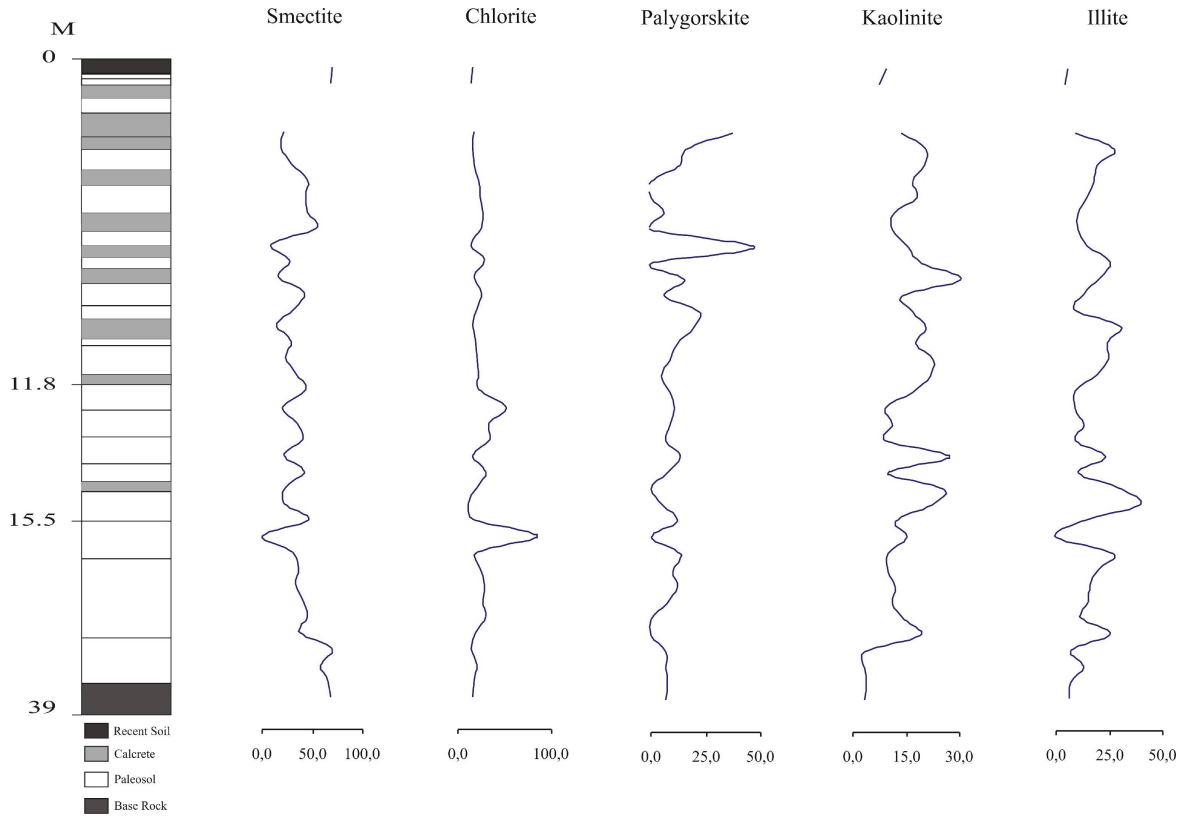

Figure 5.6. Changes in amounts of clay minerals of samples (wt in %) in the Karahamzalı section with respect to depth (m).

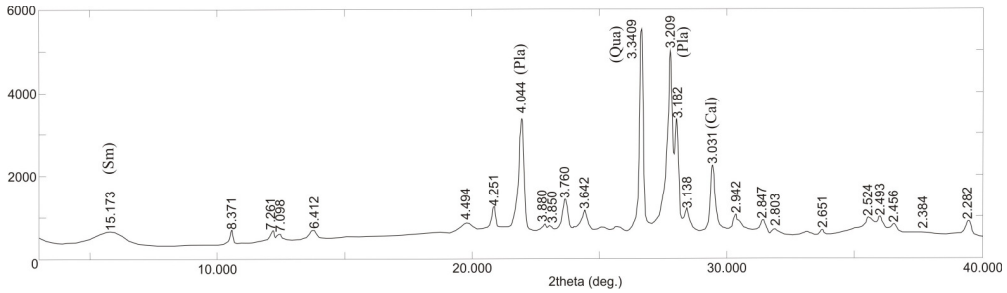

Figure 5.7. X-ray diffraction of powder B-2 sample from the Bala section (Sm: smectite; Pla: plagioclase; Qua: quartz; Cal: calcite).

Clay fractions of the samples were x-rayed using air-drying, ethylene-glycol solvation and heating treatments according to the methods of Thorez (1976), Bailey (1991) and Moore and Reynolds (1997). The clay minerals determined were smectite, kaolinite, illite and chlorite. Palygorskite was also identified in the clay fraction. Smectite, the major clay mineral found in the Bala section, was identified by the shift of the peak at 14.6 Å to 17.7 Å by ethylene glycol solvation (Figure 5.8). This behaviour is typical of smectite. It also collapses to 10.1 Å - 10.2 Å peaks after heat treatments of 300°C and/or 550°C. Crystallinity of smectites was also calculated for the Bala section (Biscaye, 1965). The ratio of v to p is generally less than 0.4 which means the smectites in this area are poorly crystallized (Figure 5.9).

Illite, kaolinite and chlorite are all present in small quantities in the samples (Figure 5.10). Illite was detected by the presence of 10.1 Å peak. However, it is hardly recognized on the diagrams because of its weak reflections. It is not affected by ethylene glycol solvation and heat treatments, therefore, its basal reflection could be seen on each treatment (Figure 5.10). It also overlaps with smectite and palygorskite when the basal reflections of these two minerals collapse to 10.1 Å by heating. Kaolinite was identified with its basal reflection at 7.13 Å which is only affected by heating to 550°C (Figure 5.10). It collapses and

disappears by the 550°C heating treatment. The relatively small amount of chlorite in the samples somewhat difficult to identify. The crystallinty is not so poor, the basal reflection at d(001) 14 Å, d(002) of 7.30 Å, d(003) of 4.7 Å are recognized in Bala section (Figure 5.10).

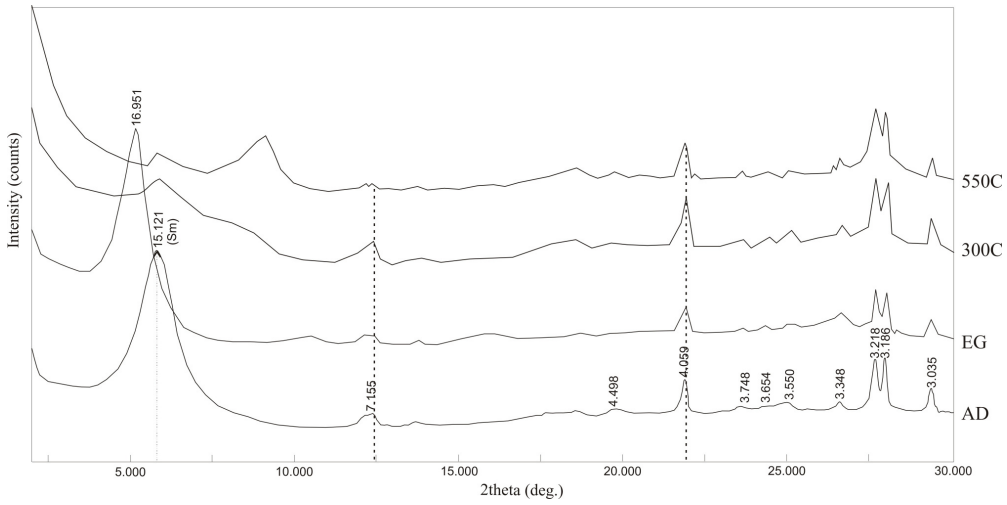

Figure 5.8. X-ray diffraction pattern of the B-2 sample from the Bala section (Sm: smectite; AD: air dried; EG: ethylene glycol; 300° and 550°C: heating treatments).

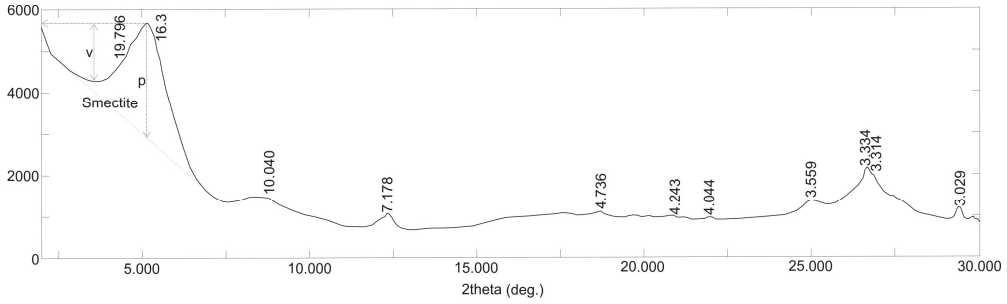

Figure 5.9. X-ray diffraction pattern showing v/p ratio indicating smectite crystallinity.

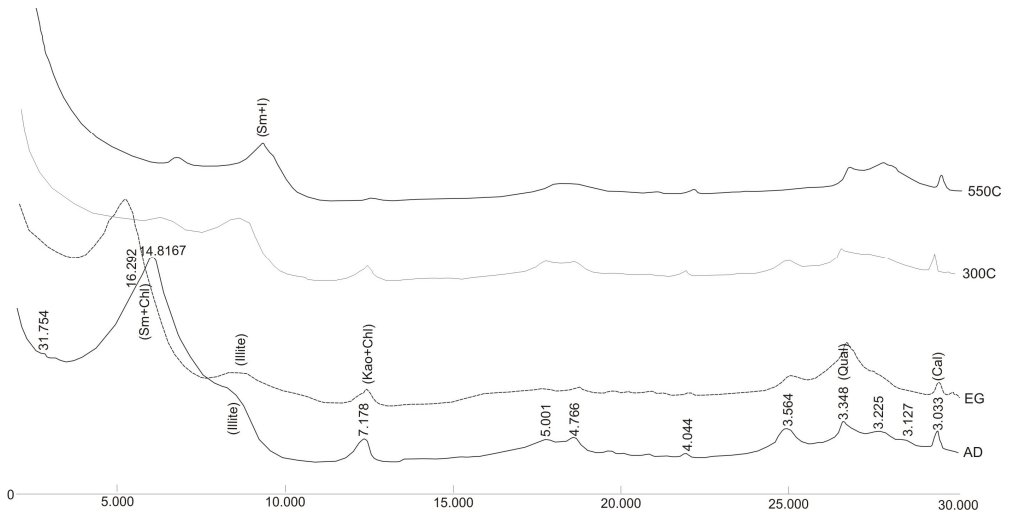

Figure 5.10. X-ray diffraction pattern of the sample with AD, EG and heating treatments of the Bala section (Sm: smectite; Chl: chlorite; Kao: kaolinite; Qua: quartz; Cal: calcite; AD: aird dried; EG: ethylene glycolated: 300°C and 550°C : heating treatments).

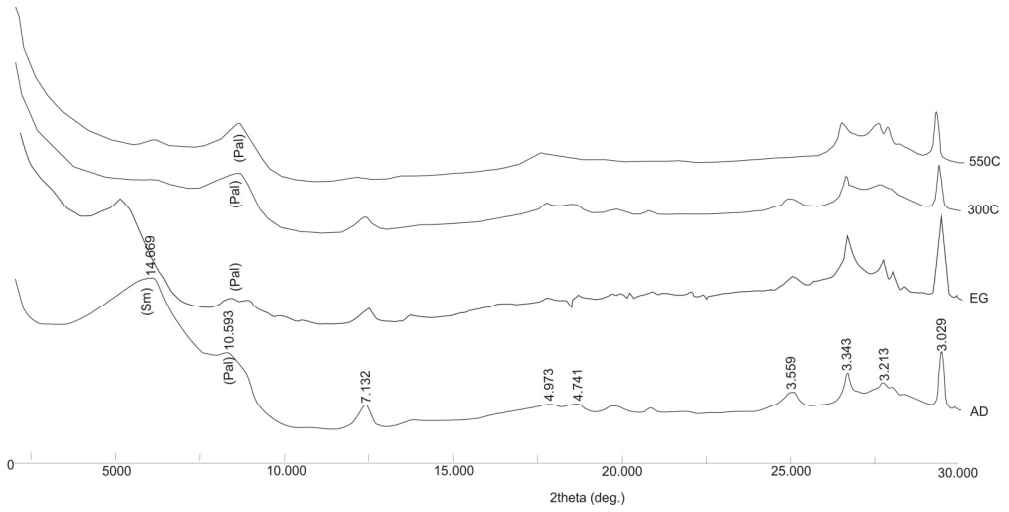

Figure 5.11. X-ray diffraction pattern of palygorskite bearing sample from the Bala section (Sm: smectite; Pal: palygorskite; AD: air dried; EG: ethylene glycolated; 300°C and 550°C: heating treatments).

Palygorskite is recognized with its peaks at 10.4Å and 6.4Å (Figure 5.11). Palygorskite is not affected by glycol and glycerol solvations however its 10.4 Å peak collapses to 10 Å by heating to 550°C (Figure 5.11). Palygorskite is present in almost all samples except B–10 and B–14. It should be mentioned here that palygorskite can be even present in these two samples but X-ray diffraction might not detect it because of its small amount and weak crystallinity. In this case SEM (Scanning Electron Microscope) Analysis can be used to identify its presence.

According to the method of Gündoğdu (1982), the mineral abundances in the bulk fraction (size fraction of less than 63µm) were determined and the results are listed in Table 5.3. Relative amounts of the minerals are plotted with respect to depth (Figure 5.12). Quartz is almost present all through the section with almost constant amount at the bottom with a slight increase at the top. Its abundance is in a very narrow range of 4.7% to 8.6%. Feldspar shows a slight increase at the middle and at the top of the section. Its abundance is 8.9% at minimum and 24.1% at maximum. Calcite, on the other hand, starts with a constant amount at the bottom, then shows an increase at the middle of the section. Towards the top, calcite increases as expected. The amounts of calcite ranges between 4.5% and 16.7%. Calcite and quartz plot almost opposite trends in relative abundance vs depth plots. Where calcite shows an increasing pattern, quartz represent a decreasing trend. At the top where calcite is high in amount, quartz is relatively lower. Total clay mineral abundance is usually higher than 60% through the section.

The relative abundances of clay minerals were determined by the method of Biscaye (1965). The results are listed in Table 5.4. The relative abundances versus depth diagrams of clay minerals in Bala section are also plotted (Figure 5.13). Smectite, the most abundant clay mineral, shows both enrichment and depletion through the section presenting zig zag pattern. Its abundance in between of 21.4% and 95.2%. It is relatively higher at the bottom of the section and decreases

towards the top. All other clay minerals except palygorskite plots almost opposite trends in abundance versus depth diagrams. Chlorite with 3.6%-16.7%, kaolinite with 3.6% to 21.2% and illite with 5.9% to 28.6% amounts are present through the section. The amount of palygorskite, on the other hand, increases towards the top of the section with 2.9% minimum and 14.3% maximum values.

Table 5.3. Semi-quantitative analysis of bulk composition of samples from Bala section.

Sample	Quartz	Calcite	Feldspar	Gypsum	Clay	Total
B-1	5,2	14,6	9,7	0,0	70,6	100,00
B-2	8,6	7,4	24,1	0,0	60,0	100,00
B-4	5,3	8,1	8,9	0,0	77,7	100,00
B-5	7,0	4,5	12,1	0,0	76,5	100,00
B-10	5,1	14,6	17,8	0,0	62,6	100,00
BC	4,8	16,7	14,6	0,0	63,9	100,00
B-14	5,9	11,7	15,2	0,0	67,3	100,00
B-15	4,7	7,5	16,0	0,0	71,7	100,00
B-16	4,7	9,5	14,1	0,0	71,7	100,00
B-17	6,2	8,8	20,5	0,0	64,5	100,00

Table 5.4. Semi-quantitative analysis of clay fraction of samples from Bala section.

Sample	Smectite	Chlorite	Palygorskite	Kaolinite	Illite	TOTAL
B1	21,4	25,0	14,3	10,7	28,6	100,0
B2	81,8	3,6	3,6	3,6	7,3	100,0
B4	44,4	16,7	13,9	8,3	16,7	100,0
B5	37,2	25,6	11,6	7,0	18,6	100,0
B10	47,1	23,5	2,9	20,6	5,9	100,0
BC	68,0	0,0	8,0	8,0	16,0	100,0
B14	48,5	21,2	3,0	21,2	6,1	100,0
B15	95,2	0,0	0,0	4,8	0,0	100,0
B16	79,6	0,0	4,1	8,2	8,2	100,0
B17	64,3	17,9	3,6	7,1	7,1	100,0

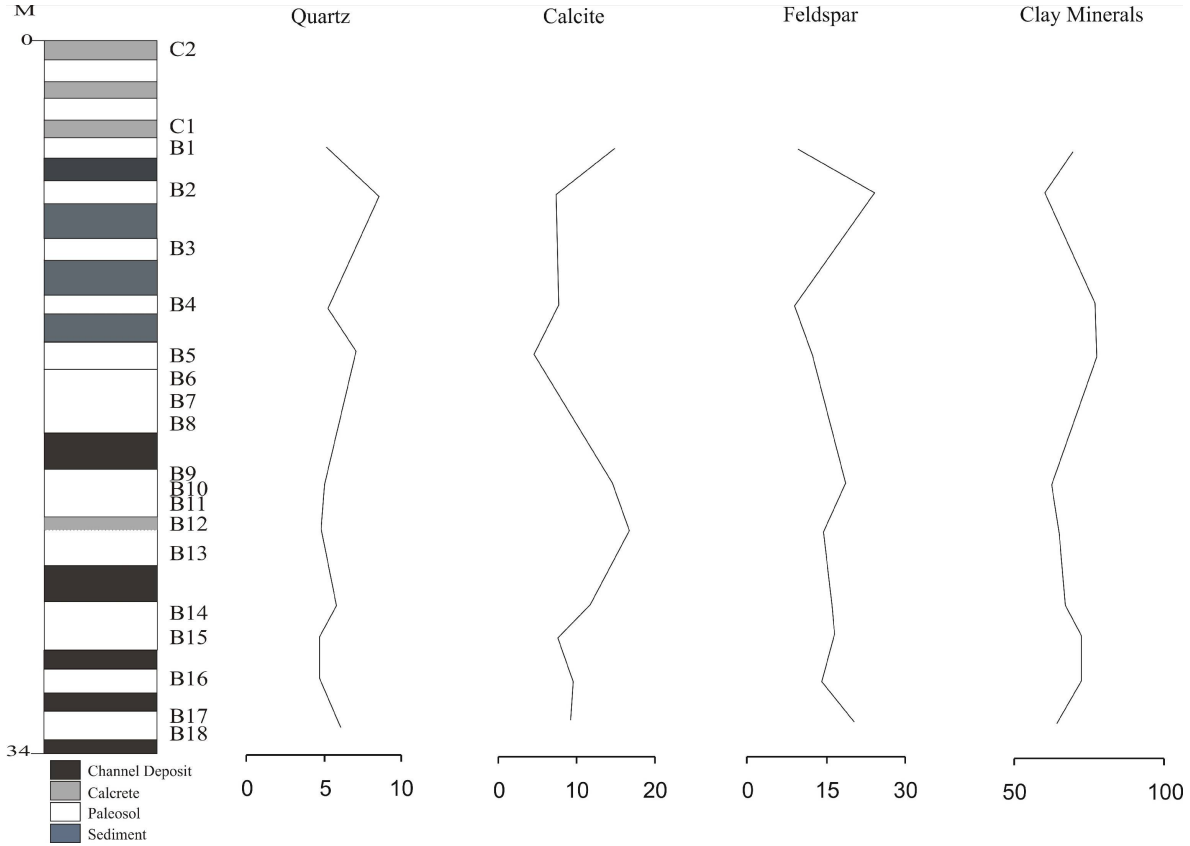

Figure 5.12. Changes in amounts of bulk mineral compositions of Bala section with respect to depth.

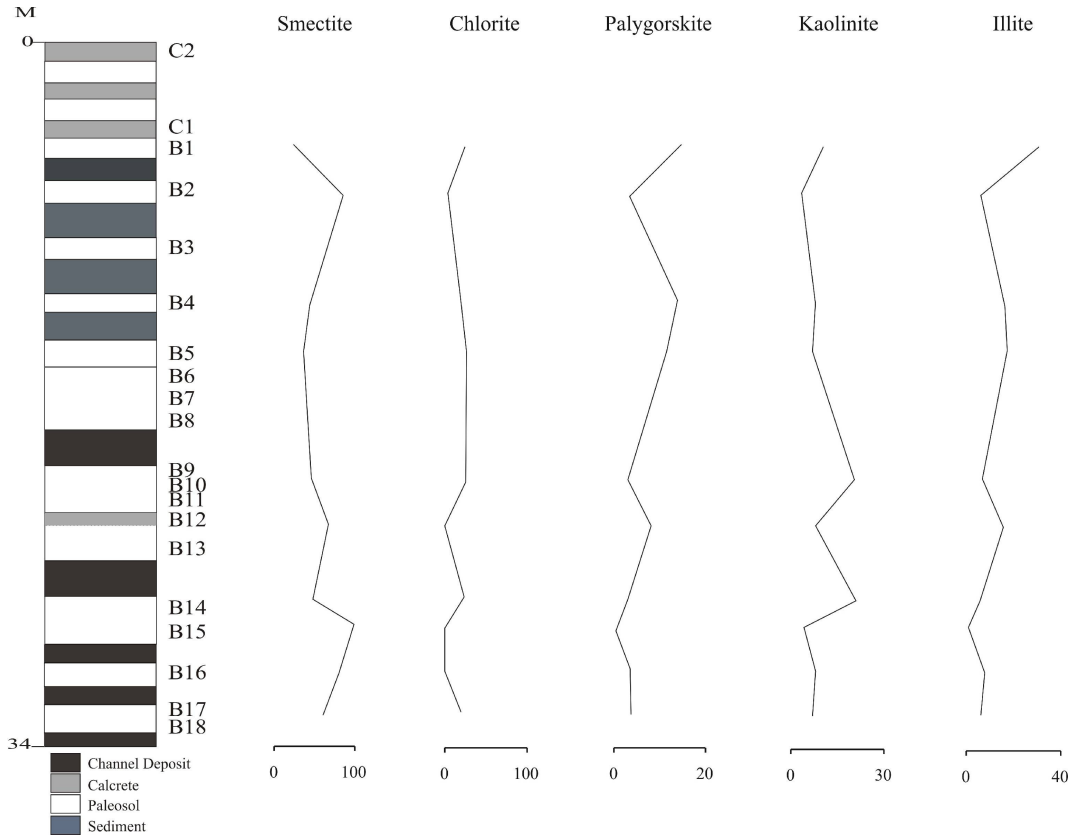

Figure 5.13. Changes in amounts of clay fraction of samples in Bala section with respect to depth.

5.3. MINERALOGY OF İNCEK, DODURGA, METU, ÇİĞDEM SAMPLES

The third group of samples were from İncek, Dodurga, METU and Çiğdem. They were analyzed by X-ray diffractometer. 20 samples were collected from different locations. Five of them are from Çiğdem (S-1, S-2, 14, 370-1, 370-2); four from İncek (I-1, I-2, I-3, I-4); ten from Dodurga (D-D, D-1, D-1a, D-1b, D-T1, D-T2, DT1, D-2D, D-2a,D-Dc); and one from METU Campus (K-1).

Samples from Çiğdem area are from caliche levels and their host rocks. S-1 and S-2 samples are nodular calcretes which have quartz, calcite and feldspar in their compositions. 4.26Å, 3.35Å for quartz, 3.03Å for calcite and 3.19Å for feldspar are the reflections identified on X-ray diagrams of S-1 and S-2 samples (Figure 5.14). Similarly, samples of 370–1, 370–2 and 14 have only calcite, quartz and feldspar as mineral constituents (Figure 5.15). K-1 which is from METU Campus is also another calcrete sample including the same mineral assemblages; quartz at 4.26Å, calcite at 3.03Å and feldspar at 3.19Å (Figure 5.15).

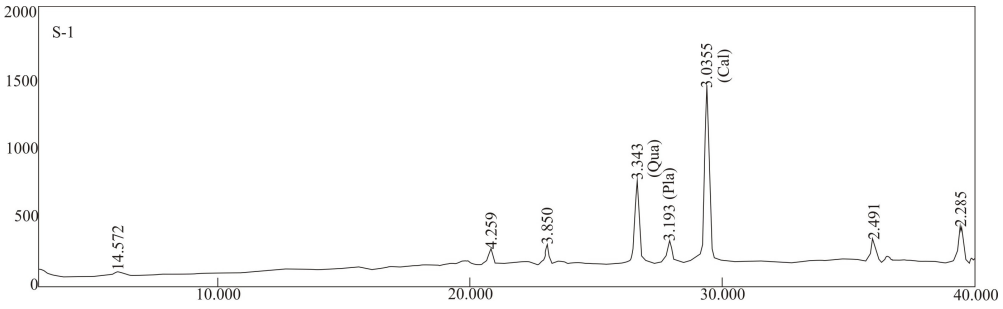

Figure 5.14. X-ray diffraction pattern of a calcrete sample from Çiğdem area (Qua: quartz; Pla: plagioclase; Cal: calcite).

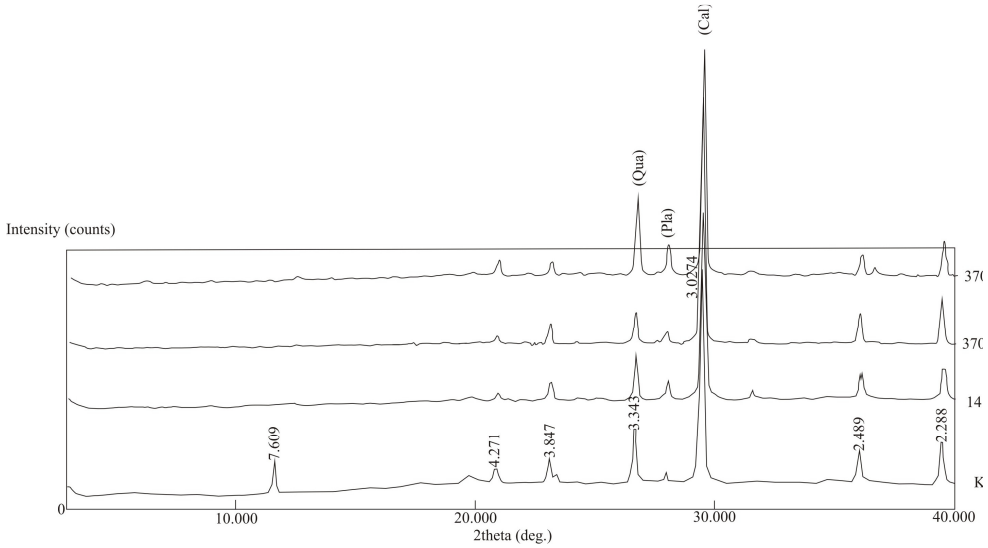

Figure 5.15.X-ray diffraction patterns of K–1, 14, 370–1 and 370–2 samples from Çiğdem and METU areas (Qua: quartz; Pla: plagioclase; Cal: calcite).

All Dodurga samples include quartz, calcite and feldspar as non-clay components (Figure 5.16). Smectite, illite and kaolinite form the clay-fractions of the Dodurga paleosol samples (Figure 5.17). Calcretes in this area are different than those from Çiğdem and METU in that they include also smectite in their compositions. Smectite is present with its 15.2 Å peak which shifts to 17.2 Å by ethylene glycol solvation (Figure 5.17). Illite is identified with its 10 Å reflection which is not affected by the treatments (Figure 5.17). Kaolinite, on the other hand, is found by the collapse of 7.1 Å peak by heating to 550°C (Figure 5.17).

İncek, another sampling site, has 4 horizons all of which include quartz and calcite except I–1 which also contains feldpsar (Figure 5.18). In clay fraction of the İncek samples, smectite is found with the shift of 15 Å peak to 17 Å by ethylene glycol solvation. Kaolinite collapses by heating to 550°C and so that was identified easily. Illite is present with 10 Å reflection during all the treatments (Figure 5.19).

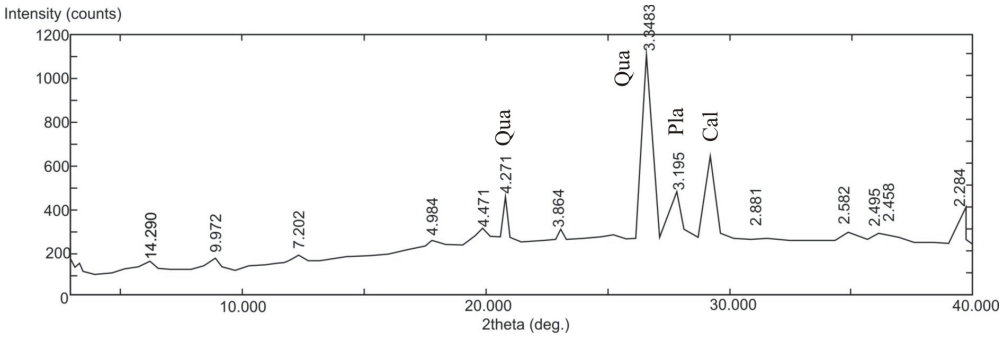

Figure 5.16. X-ray diffraction pattern of powder Dodurga sample (Qua: quartz; Pla: plagioclase; Cal: calcite).

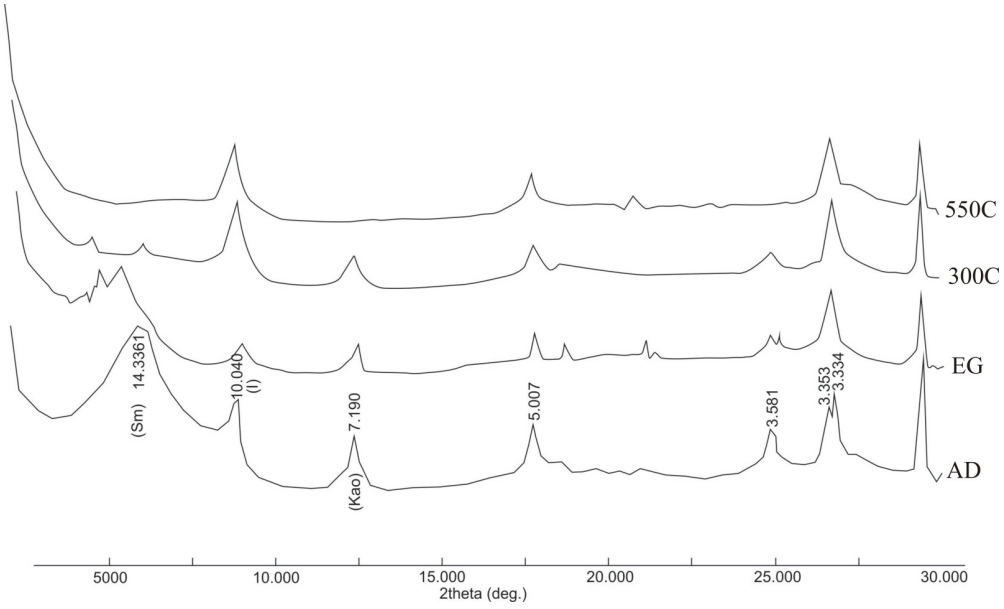

Figure 5.17. X-ray diffraction pattern of clay fraction of Dodurga sample (Sm: smectite; I: illite; Kao: kaolinite; AD: air dried; EG: ethlene glycol; 300°C and 550°C: heat treatments).

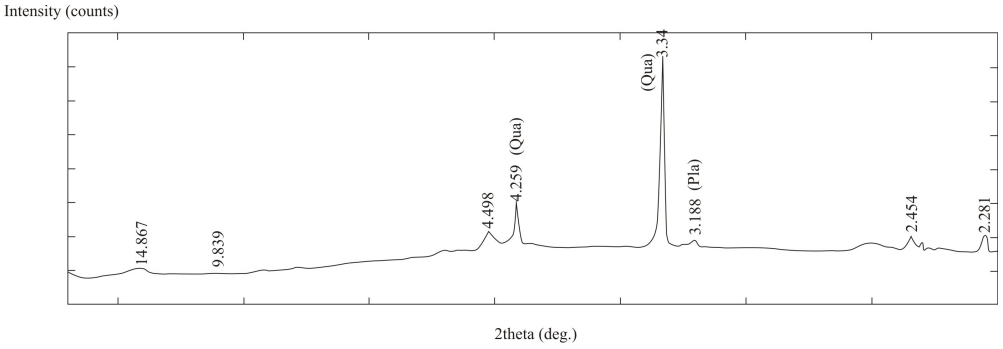

Figure 5.18. X-ray diffraction pattern of paleosol sample from İncek area (Qua: quartz; Pla: plagioclase).

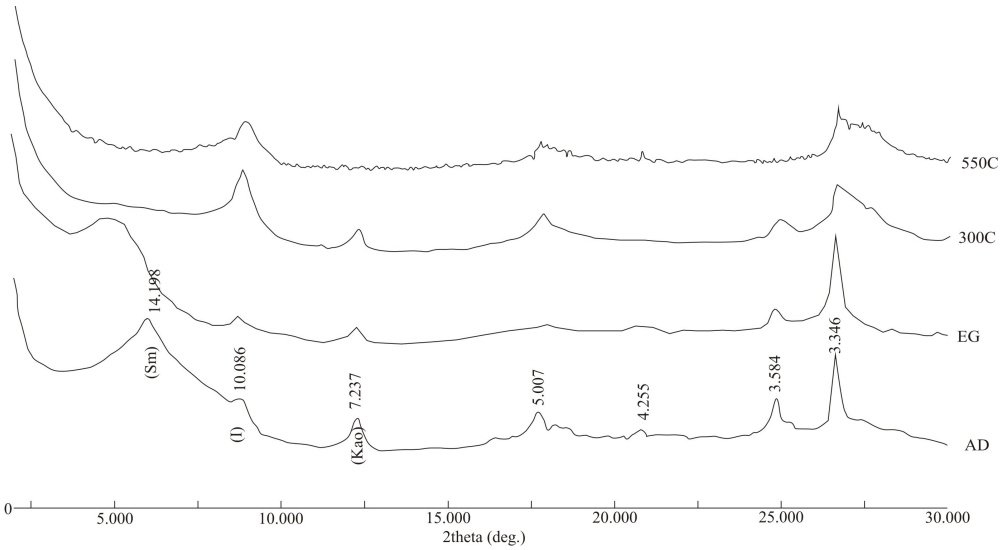

Figure 5.19. X-ray diffraction pattern of a paleosol from İncek area (Sm: smectite; I: illite; Kao: kaolinite; AD: air dired; EG: ethylene glycol; 300°C and 550°C: heating treatments).

The total non-clay and clay mineral abundances were calculated with the methods of semi-quantitative analysis. For the size fraction of less than 63 μm, the mineral abundances were calculated by using Gündoğdu (1982), same with the previous calculations.

The results are listed in Table 5.5. Quartz abundance is lowest in İncek with 1.6% and highest in Dodurga with 24.1%. On the other hand, calcite has the lowest value in Dodurga with 8.5% and highest in İncek with 98.4%. The relative abundance of feldspar ranges netween 7.6% to 27.2% in these sampling sites.

The mineral abundances in clay fraction of İncek, Dodurga, Çiğdem and METU areas were determined by the method of Biscaye (1965). The results are listed in Table 5.6. Smectite appears as the most abundant clay mineral within the samples with 20% lowest and 100% highest values. Kaolinite abundance is less than 30% while illite is almost higher than 20% in all samples. Palygorskite with its very low amount could not be detected by X-ray diffraction anaylsis but in sample I–4 (İncek sample) it is detected with an 18.2% value.

5.4. SCANNING ELECTRON MICROSCOPE INVESTIGATIONS

Selected samples from each sampling site were investigated in terms of their micromorphological and textural relationships by Scanning Electron Microscope. This study improves the knowledge about the presence of some minerals with low quantitites and poor crystallinities which can not be detected by other measurements and also helps to define the characteristic crystal properties like crystal shape, morphology and under- or overgrown textures. SEM analysis is conducted with EDX analysis to reveal the chemical composition of the studied and pictured points/minerals. Samples belonging to different sampling sites are given separately.

Table 5.5. Semi-quantitative analysis of bulk composition of samples from İncek, Dodurga, METU, Çiğdem locations.

Sample	Quartz	Calcite	Feldspar	Gypsum	Clay	Total
14	9.2	70.2	20.5	0.0	0.0	100.00
I4	1.6	98.4	0.0	0.0	0.0	100.00
I3	2.6	97.4	0.0	0.0	0.0	100.00
I2	2.7	97.3	0.0	0.0	0.0	100.00
I1	6.6	0.0	8.6	0.0	84.7	100.00
S2	12.5	63.0	24.5	0.0	0.0	100.00
S1	14.5	59.5	26.0	0.0	0.0	100.00
K1	3.6	23.2	7.9	4.9	65.3	104.87
D-DC	12.9	72.1	15.1	0.0	0.0	100.00
D-1D_0D	15.5	57.4	27.2	0.0	0.0	100.00
D-1b	6.5	8.5	11.4	0.0	73.7	100.00
D-1a	6.1	7.6	12.4	0.0	73.9	100.00
D-T1	6.9	82.7	10.4	0.0	0.0	100.00
D-T2	5.9	86.6	7.6	0.0	0.0	100.00
DT-1	5.6	86.6	7.8	0.0	0.0	100.00
370-1	6.2	77.7	16.1	0.0	0.0	100.00
370-2	11.4	62.3	26.2	0.0	0.0	100.00
D-2	17.3	56.1	26.5	0.0	0.1	100.00
D-2asagi	14.1	60.6	25.2	0.0	0.0	100.00
D-D	24.1	53.9	21.9	0.0	0.1	100.00

Table 5.6. Semi-quantitative analysis of clay minerals from İncek, Dodurga, METU, Çiğdem locations.

Sample	Smectite	Palygorskite	Kaolinite	Illite	SUM %
D-1b	38.5		20.5	41.0	100.0
D-1a	30.6		20.4	49.0	100.0
D-T1	57.1		14.3	28.6	100.0
D-T2	33.3		22.2	44.4	100.0
D-D	61.1		5.6	33.3	100.0
I-4	36.4	18.2	9.1	36.4	100.0
I-3	50.0		16.7	33.3	100.0
I-2	42.9		28.6	28.6	100.0
I-1	65.2		0.0	34.8	100.0
D-Dca	71.4		9.5	19.0	100.0
D-1Dodurga	25.0		25.0	50.0	100.0
DT-1 Trk	100.0				100.0
D-2Dodurga	25.0		25.0	50.0	100.0
D-2asagi	20.0			80.0	100.0

5.4.1. SEM Study on Karahamzalı Samples

X-ray diffraction study revealed the presence of clay and non-clay minerals within the samples of Karahamzalı section. SEM investigations show the micromorphological relations between those minerals. Toward the top of the section as revealed by semi-quantitative analysis on clay fraction. abundance of palygorskite increases. This is confirmed with the SEM studies in that samples at the bottom of the section do not show any fibrous mineral formations. Palygorskite with 0.1 μm width and 1–1.6 μm long fibers were detected in especially calcrete samples. They are distributed randomly over dolomite and other clay minerals (Figure 5.20). Palygorskite fibers form bridge-like structures between grains and also cover the surface of dolomite grains (Figure 5.21). This form of palygorskite also causes the development of small pore spaces.

Unlike the bottom to middle levels of the Karahamzalı section, dolomite is the only carbonate facies found. They are observed with perfect rhombohedral shapes (Figure 5.22). Different than calcretes in Karahamzalı section, paleosol samples have high clay mineral contents. Illite as another fibrous mineral found in a paleosol level of A–2 shows development of fibers on smectite surfaces (Figure 5.23). In this view, relatively thick and short fibers of illite are recognized with the thin and long fibers of palygorskite, both covers the smectite surfaces. Smectites, on the other hand, are recognized with their corn flake morphologies and are almost covered with palygorskite fibers (Figure 5.24). Chlorite, with its almost constant value throughout the Karahamzalı section, shows the sheet-like morphology within the smectite (Figure 5.25). Another SEM picture reveals the dissolution of feldspars within the paleosol sample of A–7. It also shows the development of clay minerals over detrital feldspar grains, indicating the disturbed clay surfaces by dissolution The palygorskite fibers also form a thin sheet over smectite surfaces (Figure 5.26).

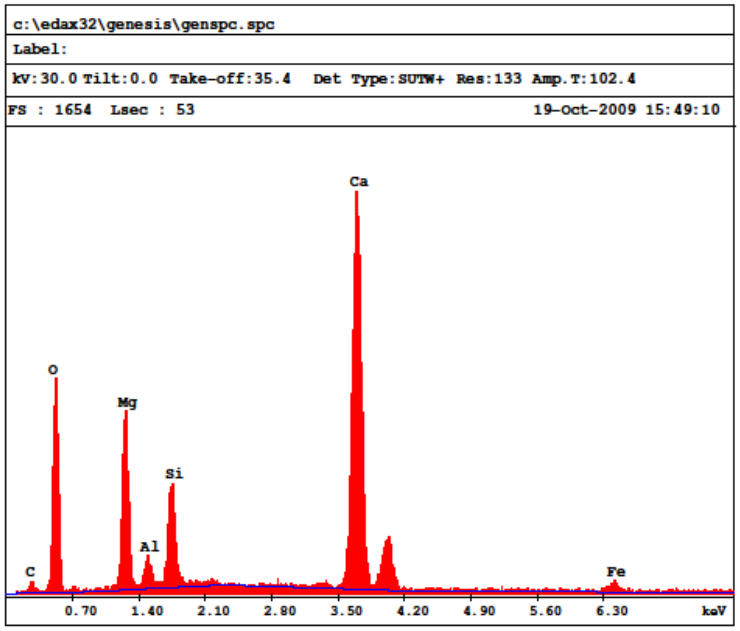

EDAX ZAF Quantification (Standardless)
Element Normalized
SEC Table : Default

Element	Wt %	At %	K-Ratio	Z	A	F
C K	6.40	10.44	0.0141	1.0330	0.2128	1.0008
O K	51.46	63.00	0.0951	1.0185	0.1814	1.0004
MgK	13.36	10.76	0.0446	0.9819	0.3392	1.0027
AlK	2.36	1.71	0.0080	0.9540	0.3536	1.0040
SiK	6.27	4.37	0.0284	0.9828	0.4593	1.0034
CaK	19.18	9.37	0.1733	0.9533	0.9471	1.0007
FeK	0.97	0.34	0.0083	0.8819	0.9750	1.0000
Total	100.00	100.00				

Figure 5.20. SEM-EDX on Karahamzalı paleosol revealing palygorskite fibers on dolomites.

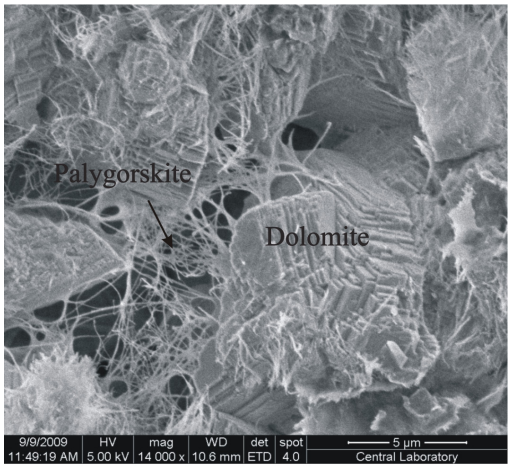

Figure 5.21. Bridge-like morphology of palygorskite fibers on paleosols of the Karahamzalı section.

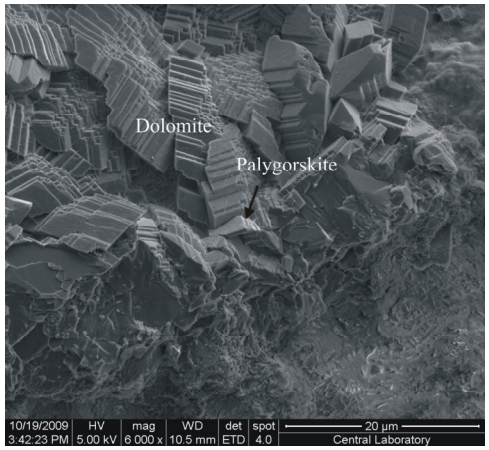

Figure 5.22. Rhombohedral dolomites forming calcretes of the Karahamzalı section.

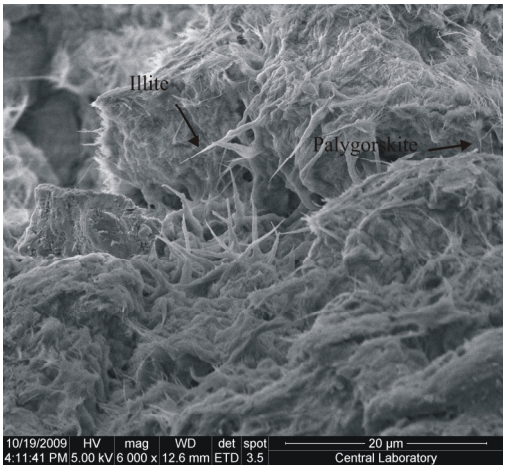

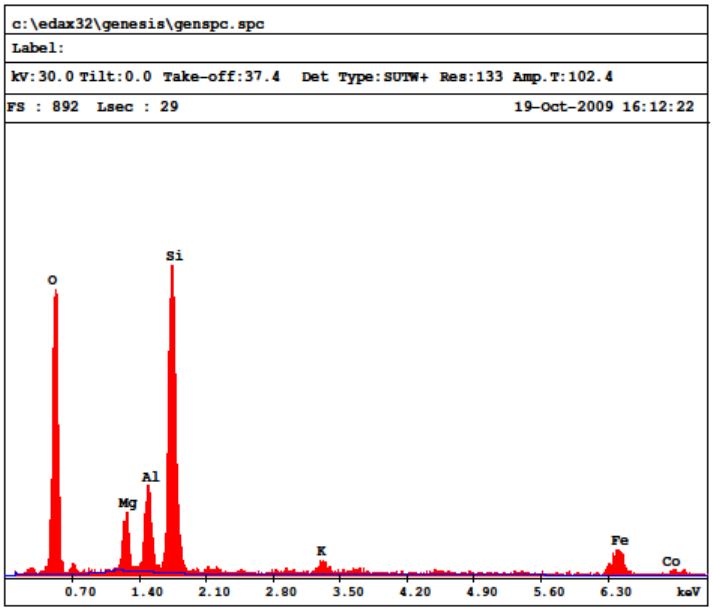

EDAX ZAF Quantification (Standardless)
Element Normalized
SEC Table : Default

Element	Wt %	At %	K-Ratio	Z	A	F
O K	55.67	69.47	0.1885	1.0220	0.3311	1.0006
MgK	5.68	4.67	0.0205	0.9853	0.3639	1.0075
AlK	7.47	5.53	0.0319	0.9573	0.4411	1.0101
SiK	25.60	18.20	0.1254	0.9862	0.4966	1.0003
K K	1.04	0.53	0.0078	0.9344	0.8036	1.0021
FeK	4.14	1.48	0.0369	0.8848	1.0062	1.0000
CoK	0.41	0.14	0.0036	0.8680	1.0117	1.0000
Total	100.00	100.00				

Figure 5.23. Short and thick illite fibers together with long and thin palygorskite fibers developed within Karakamzalı paleosols.

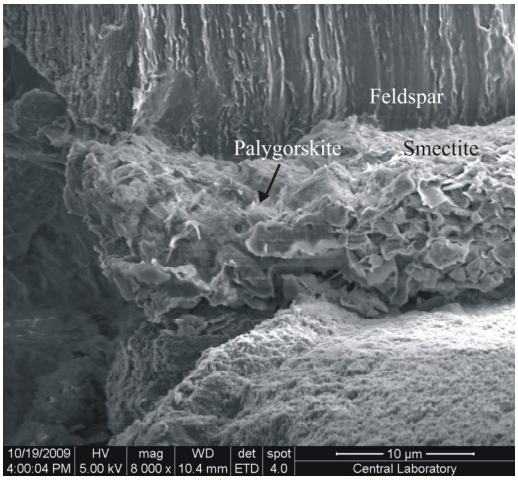

Figure 5.24. SEM image of paleosols from Karahamzalı section revealing the presence of smectite with corn-flake morphology covered by palygorskite fibers; feldspar grain next to them.

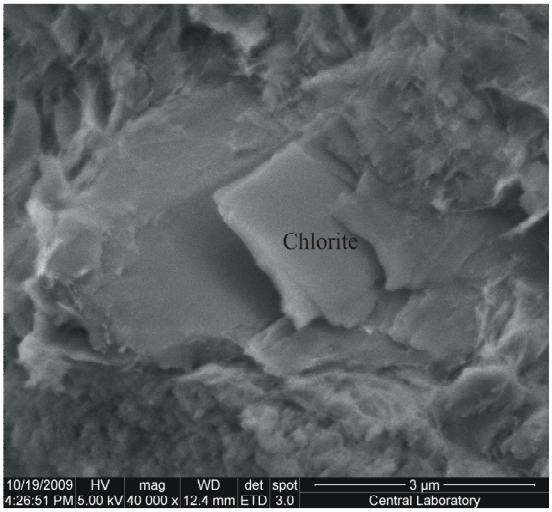

Figure 5.25. SEM image of chlorite observed with its flaky morphology within the Karahamzalı paleosols.

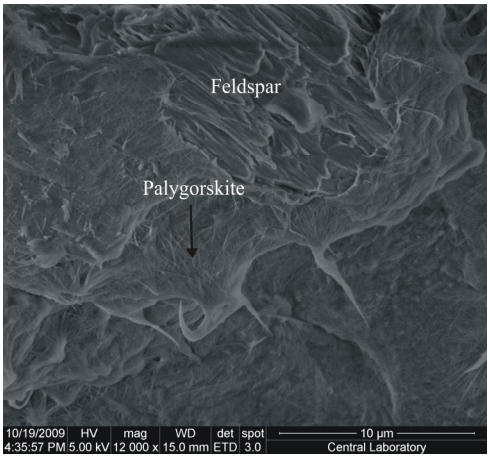

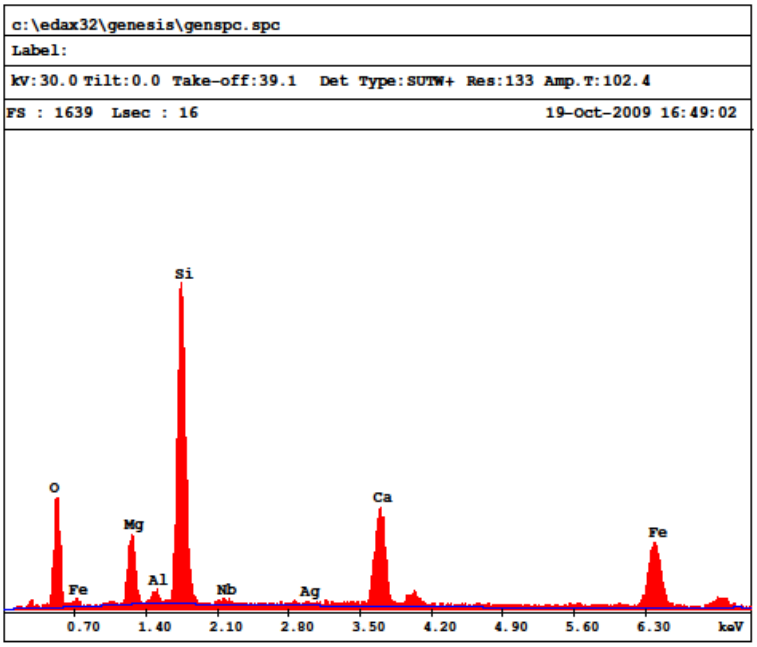

EDAX ZAF Quantification (Standardless)
Element Normalized
SEC Table : Default

Element	Wt %	At %	K-Ratio	Z	A	F
O K	37.28	54.78	0.0821	1.0376	0.2120	1.0008
MgK	9.28	8.98	0.0313	1.0001	0.3351	1.0067
AlK	1.29	1.13	0.0049	0.9717	0.3834	1.0117
SiK	28.69	24.02	0.1444	1.0010	0.5016	1.0021
NbL	1.24	0.31	0.0067	0.8524	0.6284	1.0030
AgL	0.55	0.12	0.0041	0.8074	0.9078	1.0123
CaK	9.27	5.44	0.0766	0.9745	0.8421	1.0076
FeK	12.40	5.22	0.1089	0.8998	0.9759	1.0000
Total	100.00	100.00				

Figure 5.26. SEM image of a feldspar grain and palygorskite on Karahamzalı paleosols with EDX analysis.

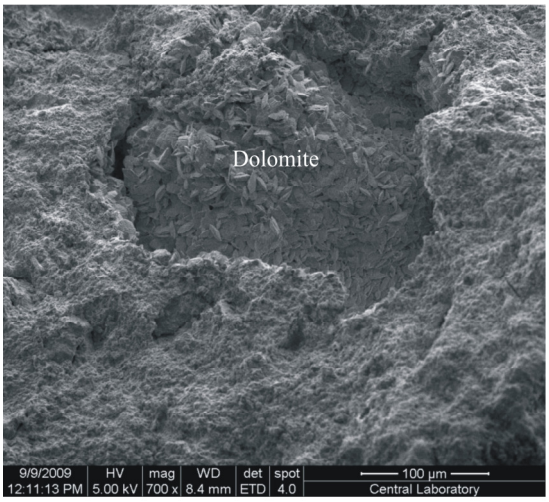

Figure 5.27. SEM image of dolomites filling the pore space within Karahamzalı paleosol.

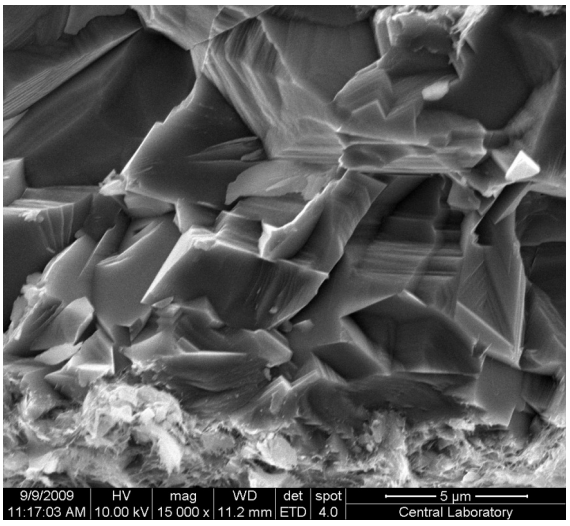

Figure 5.28. SEM image of dolomites with their fresh surcaes not covered with any palygorskite fiber.

Dolomites are recognized within the pore spaces of calcretes around which clay minerals are found (Figure 5.27). In some levels where the amount of dolomite is relatively lower than the others, dolomite crystals have relatively fresh surfaces. They are not yet covered with palygorskite fibers (Figure 5.28).

5.4.2. SEM Study on Bala Samples

Samples from Bala section are generally paleosols, since they were sampled by drilling operation from the ground to 25 m depth. Calcretes, as subaerial exposure surfaces, are mostly recognized within horizons very close to the surface. Therefore, this drilling operation supplied may paleosol horizons and only one calcrete level. On the other hand, the calcretes are very often above the sampled levels. However, it was really hard to sample each calcrete and paleosol level from the outcrop, that is why 2 calcrete and paleosol samples from the outcrop and 18 levels from drilling operation. Like Dodurga samples, Bala samples have also calcite as carbonate mineral. Clay minerals form the matrix on which detrital grains are floating and pedogenic palygorskite lies as a thin sheet (Figure 5.29). Quartz and feldpsars are recognized as detrital minerals. Different than Karahamzalı and other samples, pyrite crystals are also recognized by the SEM (Figure 5.30) . Smectite is the dominant clay mineral found in the Bala paleosols (Figure 5.31). Its EDX analysis reveals a composition of Si 42.72%, O 37.14%, Na 4.37% Mg 1.75% and Al 14.01% weights. Quartz is euhedral to subhedral and cemented to the clayey matrix. EDX analysis on a specific point of the subhedral grain shows very high contents of Si and O revealing the presence of quartz. Its fresh surface is very clear with well developed conchoidal fracture surfaces (Figure 5.32). Subhedral feldspar grains are also observed in the paleosol matrices (Figure 5.33). Palygorskite fibers are randomly distributed over the clayey matrix and overlying the feldspar grains. Illite fibers, on the other hand, are also present at the edges of the smectitic host. EDX analysis reveal the presence of feldspars,

smectite, palygorskite and illite minerals (Figure 5.33). In the same sample (B3), a quartz grain is recorded with EDX analysis. The formation of authigenic clay minerals is also observed with a nodular crystalline form (Figure 5.34). Palygorskite fibers coat calcite grains in the calcrete sample (BC) within the Bala section (Figure 5.35).

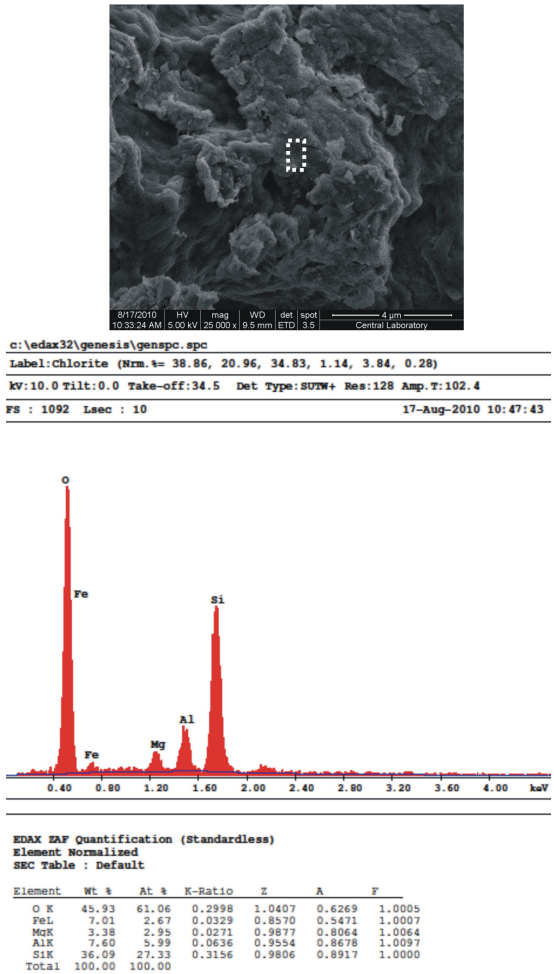

Figure 5.29. SEM image of clay minerals and palygorskiye fibers developed within Bala paleosols.

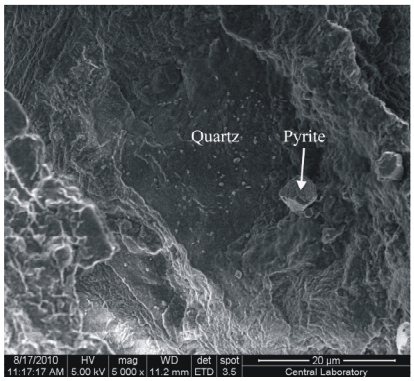

c:\edax32\genesis\genspc.spc

Label:Chlorite (Nrm.%= 38.86, 20.96, 34.83, 1.14, 3.84, 0.28)

kV:20.0 Tilt:0.0 Take-off:36.1 Det Type:SUTW+ Res:128 Amp.T:102.4

FS : 650 Lsec : 17 17-Aug-2010 11:30:33

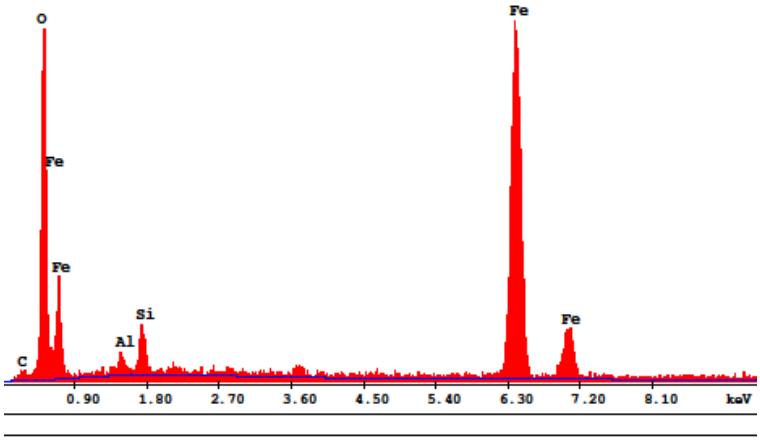

EDAX ZAF Quantification (Standardless)
Element Normalized
SEC Table : Default

Element	Wt %	At %	K-Ratio	Z	A	F
C K	3.55	9.47	0.0077	1.1262	0.1931	1.0006
O K	22.92	45.86	0.1098	1.1070	0.4314	1.0027
AlK	1.30	1.54	0.0051	1.0297	0.3797	1.0012
SiK	3.06	3.48	0.0162	1.0594	0.4995	1.0011
FeK	69.17	39.64	0.6561	0.9438	1.0050	1.0000
Total	100.00	100.00				

Figure 5.30. SEM image of a detrital quartz and cubic pyrite of Bala sample.

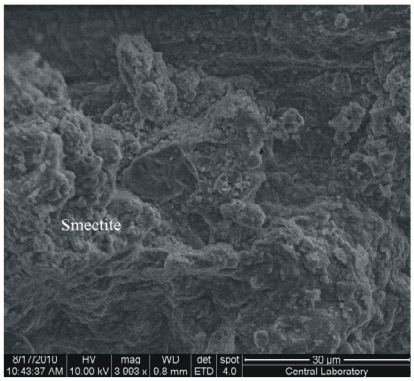

c:\edax32\genesis\genspc.spc

Label:Chlorite (Nrm.%= 38.86, 20.96, 34.83, 1.14, 3.84, 0.28)

kV:10.0 Tilt:0.0 Take-off:34.8 Det Type:SUTW+ Res:128 Amp.T:102.4

FS : 908 Lsec : 13 17-Aug-2010 10:56:43

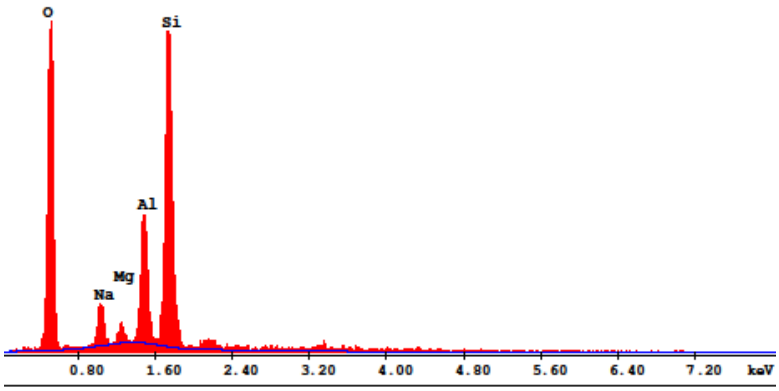

EDAX ZAF Quantification (Standardless)
Element Normalized
SEC Table : Default

Element	Wt %	At %	K-Ratio	Z	A	F
O K	37.14	50.20	0.2236	1.0406	0.5784	1.0004
NaK	4.37	4.11	0.0328	0.9665	0.7718	1.0047
MgK	1.75	1.56	0.0147	0.9871	0.8423	1.0092
AlK	14.01	11.23	0.1220	0.9549	0.9012	1.0120
SiK	42.72	32.90	0.3721	0.9802	0.8886	1.0000
Total	100.00	100.00				

Figure 5.31. SEM image of smectite developed on Bala sample.

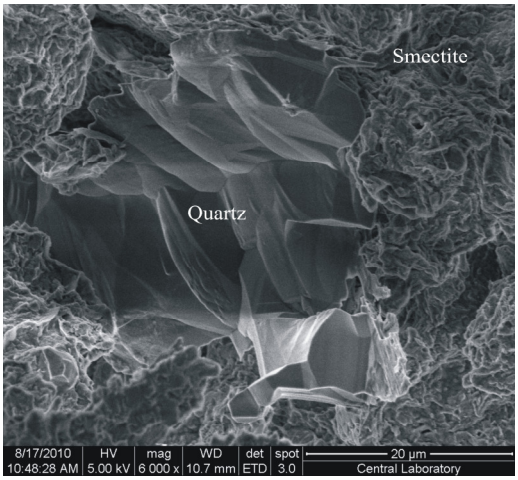

Figure 5.32. SEM image of fresh quartz grain with conchoidal fracture surfaces together with smectite on Bala sample.

5.4.3. SEM Study on İncek, Dodurga, Çiğdem and METU Samples

Samples of İncek, Dodurga, Çiğdem and METU have calcite as a carbonate mineral. This is also confirmed with the appearance of rhombohedral calcite crystals in SEM images. Because of the mineralogic, chemical and morphological similarities, Dodurga calcrete samples have been selected to reveal the presence of minerals by SEM study.

DT–2 is a calcrete sample from Dodurga area. It has calcite as carbonate mineral and palygorskite is not seen in both XRD and SEM analysis. EDX analysis also reveals that the carbonate mineral is pure calcite. Figure 5.36 shows the contact between grain and matrix. The micritic cement is composed of calcite. Calcite crystals form the cement and have subhedral to euhedral forms (Figure 5.36).

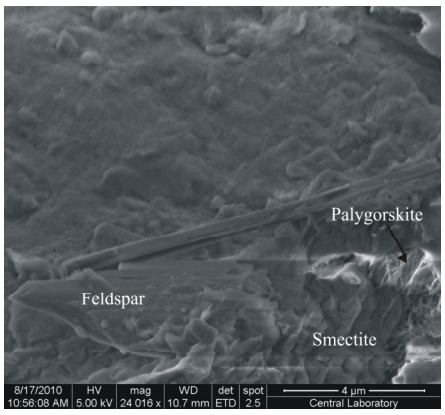

c:\edax32\genesis\genspc.spc

Label:Chlorite (Nrm.%= 38.86, 20.96, 34.83, 1.14, 3.84, 0.28)

kV:20.0 Tilt:0.0 Take-off:35.6 Det Type:SUTW+ Res:128 Amp.T:102.4

FS : 1050 Lsec : 10 17-Aug-2010 11:10:11

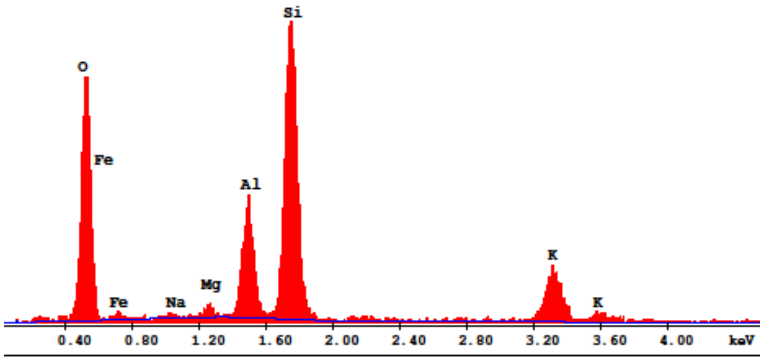

EDAX ZAF Quantification (Standardless)
Element Normalized
SEC Table : Default

Element	Wt %	At %	K-Ratio	Z	A	F
O K	46.80	62.68	0.1491	1.0342	0.3079	1.0005
FeL	6.13	2.35	0.0169	0.8866	0.3110	1.0010
NaK	0.60	0.56	0.0021	0.9679	0.3666	1.0041
MgK	1.26	1.11	0.0065	0.9922	0.5137	1.0080
AlK	9.66	7.67	0.0609	0.9630	0.6481	1.0106
SiK	28.56	21.80	0.1917	0.9911	0.6766	1.0011
K K	6.99	3.83	0.0586	0.9403	0.8890	1.0018
Total	100.00	100.00				

Figure 5.33. SEM image of feldspar grain surrounded by smectite and palygorskite fibers on Bala paleosol (EDX on feldspar).

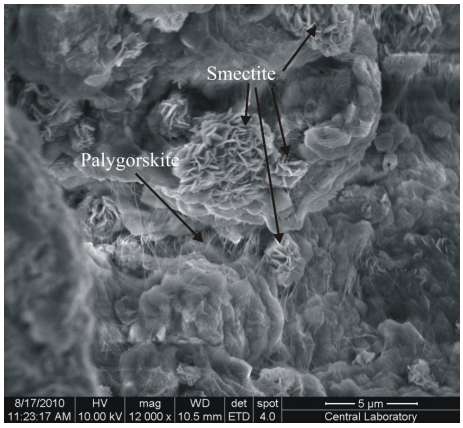

c:\edax32\genesis\genspc.spc

Label:Chlorite (Nrm.%= 38.86, 20.96, 34.83, 1.14, 3.84, 0.28)

kV:20.0 Tilt:0.0 Take-off:35.5 Det Type:SUTW+ Res:130 Amp.T:51.2

FS : 962 Lsec : 11 17-Aug-2010 11:41:24

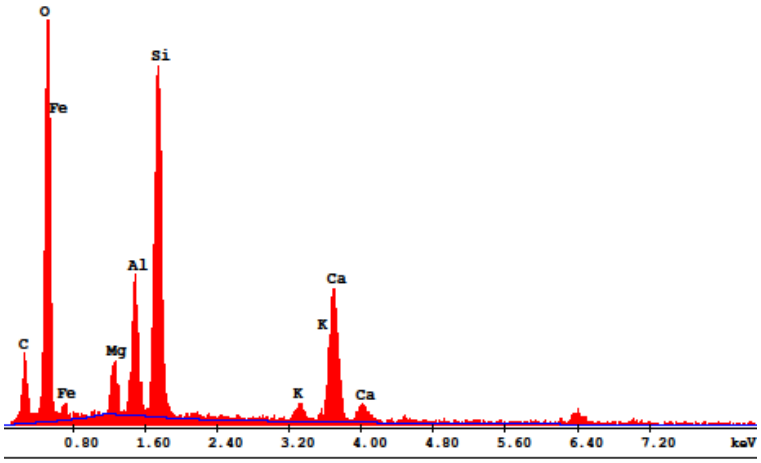

EDAX ZAF Quantification (Standardless)
Element Normalized
SEC Table : Default

Element	Wt %	At %	K-Ratio	Z	A	F
C K	19.44	29.84	0.0417	1.0400	0.2060	1.0005
O K	42.53	49.01	0.1038	1.0226	0.2386	1.0004
FeL	7.38	2.44	0.0194	0.8766	0.2997	1.0005
MgK	2.21	1.68	0.0108	0.9812	0.4971	1.0042
AlK	5.14	3.52	0.0307	0.9523	0.6235	1.0058
SiK	14.24	9.35	0.0978	0.9801	0.6999	1.0014
K K	0.91	0.43	0.0081	0.9291	0.9419	1.0182
CaK	8.14	3.75	0.0749	0.9512	0.9630	1.0044
Total	100.00	100.00				

Figure 5.34. SEM image of Bala paleosol revealing authigenic formation of clay mineral most possibly smectite with fibrous palygorskite.

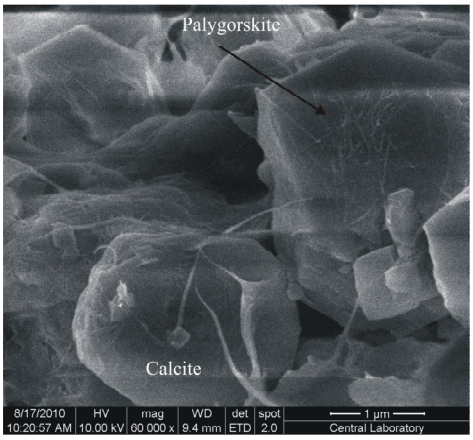

Figure 5.35. SEM image of palygorskites developed on calcite grains.

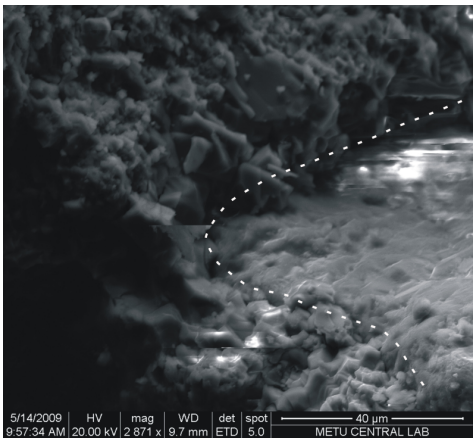

Figure 5.36. SEM image of Dodurga calcrete revealing the contact between calcite and clay minerals.

Calcite and clay minerals are found together as cement and (Figure 5.37). Calcite crystals are found within the pore spaces of the calcretes and paleosols (Figure 5.38). Also EDX analysis justified the pure calcite as Ca, C and O (Figure 5.38).

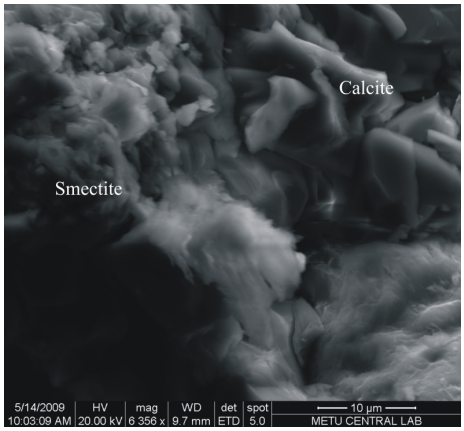

Figure 5.37. SEM image of clay minerals and calcite forming the cement of Dodurga sample (EDX on smectite).

5.5. DOLOMITE AND ITS STOICHIOMETRY

In hot and arid, non-marine, near-surface environment, pore waters are generally oxidizing and chemical leaching is less extreme. Two major processes operating under this climate are the formation of red colored beds and the development of calcretes. Other processes are feldspar dissolution and reprecipitation as overgrowths, gypsum cementation and alteration of volcanic grains to zeolites. (Tucker, 1988). As a very brief and a clear definition stated by Warren (2000), dolomite is not a simple mineral; it can form as a primary precipitate, a diagenetic replacement, or as a hydrothermal metamorphic phase, that requires permeability, a mechanism that facilitates fluid flow, and a sufficient supply of magnesium. Dolomite can form in lakes, on or beneath the shallow seafloor, in zones of brine reflux, and in early to late burial settings. It may form from seawater, from continental waters, from the mixing of basinal brines, the mixing of hypersaline brine with seawater, or the mixing of seawater with meteoric water, or via the cooling of basinal brines

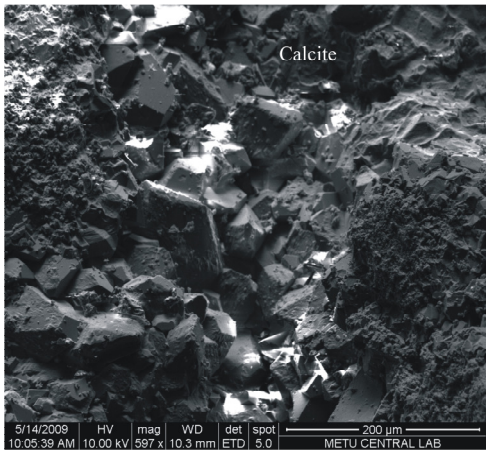

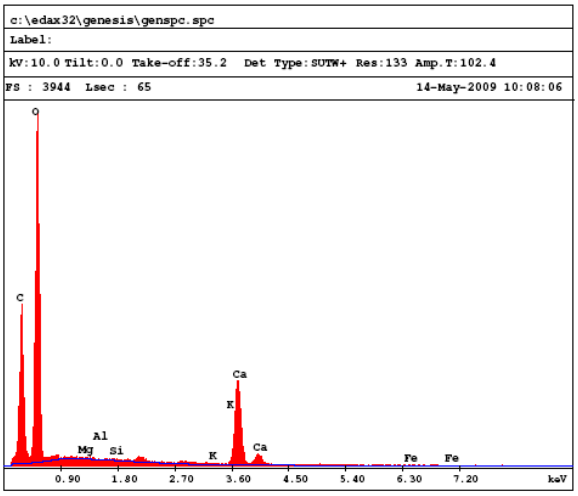

EDAX ZAF Quantification (Standardless)
Element Normalized
SEC Table : Default

Element	Wt %	At %	K-Ratio	Z	A	F
C K	21.27	31.47	0.1431	1.0440	0.6437	1.0007
O K	50.56	56.16	0.1938	1.0205	0.3756	1.0000
MgK	0.00	0.00	0.0000	0.9672	0.7676	1.0005
AlK	0.00	0.00	0.0000	0.9359	0.8572	1.0012
SiK	0.14	0.09	0.0013	0.9609	0.9159	1.0026
K K	0.23	0.10	0.0022	0.9021	1.0019	1.0697
CaK	26.61	11.80	0.2458	0.9196	1.0041	1.0003
FeK	1.18	0.38	0.0096	0.8121	0.9984	1.0000
Total	100.00	100.00				

Figure 5.38. SEM image of rhombohedral calcites in Dodurga sample.

Bacterial metabolism may aid the process of precipitation in settings where sulfate-reducing species flourish and microbial action may control primary precipitation in some hypersaline anoxic lake settings.

Structurally, dolomite is a rhombohedral carbonate consisting of alternating layers of carbonate anions and cations. Ideally, the mineral dolomite is stoichiometric but it never occurs as such, naturally (Süzen and Türkmenoğlu, 2000). It is commonly non-stoichiometric. By definition, non-stoichiometric compounds are chemical compounds with an elemental composition that cannot be represented by a ratio of well-defined natural numbers, and therefore violate the law of definite proportions. They contain crystallographic point defects, such as interstitial atoms and vacancies, which result in excess or deficiency of an element, respectively. Since solids are overall electrically neutral, the defect in an ionic compound is compensated by a change in the charge of other atoms in the solid, either by changing their oxidation state, or by replacing them with atoms of different elements with a different charge. Non-stoichiometric dolomites have an excess of Ca^{+2} up to Ca:Mg 58:42, or less commonly an excess of Mg^{+2} up to $Ca_{48}Mg_{52}$. The effect of Ca^{+2} substitution for Mg^{+2} is to increase the cation lattice spacing and XRD is often used to determine this and give the Ca/Mg ratio, by measurement of the position of the d_{104} peak relative to a standard. This non-stoichiometric property of dolomites can be used to infer the depositional environment (Tucker, 1988).

From the Karahamzalı section, samples containing dolomite are selected by X-ray diffraction analyses. After determining the samples, they were analysed in terms of their petrographical properties and Ca:Mg ratio, Ca^{+2} excess, degree of ordering.

Firstly, Ca:Mg ratio of the samples are calculated. The results are listed in Table 5.7. A-1 and U-7 samples from the Karahamzalı section represent Ca:Mg ratio as

58:42 and the rest show greater values, which indicates Ca^{+2} excess in their chemistry (Table 5.7).

Table 5.7. Table listing the samples including dolomite and their Ca:Mg ratio calculations.

Samples	MgO	CaO	Atomic Weight of Ca	Atomic Weight of Mg	Total Ca+Mg	Ca Amount in %	Mg Amount in %	Ca:Mg
U13	16.72	20.84	8.35	4.01	12.36	67.54	32.45	67-32
U10	17.91	22.16	8.87	4.29	13.17	67.38	32.61	67-32
U7	20.34	16.88	6.76	4.88	11.64	58.08	41.91	58-42
U6	18.29	16.9	6.77	4.38	11.16	60.67	39.32	61-39
A1	16.12	13.53	5.42	3.86	9.29	58.35	41.64	58-42
A3	14.97	16.42	6.57	3.59	10.17	64.68	35.31	65-35
A6	16.8	16.39	6.56	4.02	10.59	61.96	38.03	62-38
A15	15.18	13.6	5.44	3.64	9.09	59.93	40.06	60-40

Then, according to the method of Lumsden (1979) was employed to find out the N_{CaCO3}:

$$N_{CaCO3} = Md + B$$

where N is the mole of $\%CaCO_3$, M is 333.33, d is d_{104} spacing measured in angstrom unit, and B is -911.99. The results are 51,3% and 54,7% for the dolomite including samples (Table 5.8). Tucker (1988) explained that based on stoichiometry, texture and whether associated with evaporites or not, three different groups of dolomites are identified by Lumsden and Chimahusky (1980) and Morrow (1978, 1982). They are type I-coarsely crystalline, sucrosic dolomites which are generally nearly stoichiometric (mode 50.0-51.0% $CaCO_3$), type II–fine grained dolomites not associated with evaporites which are also nearly

stoichiometric (mode 51.0-52.0% $CaCO_3$) and type III-finely crystalline dolomites associated with evaporites which are generally Ca-rich (54-56% $CaCO_3$). Group I dolomites are generally of late diagenetic burial origin and the near stoichiometry could reflect slow growth from dilute solutions, possibly aided by elevated temperatures. Groups II and III are usually early diagenetic, near-surface in origin which is directly related with the salinity, Mg/Ca ratio of dolomitizing solutions with a climatic control important for groups II and III (Tucker, 1988). The Ca excess calculation (51,3% and 54,7%) on the samples from the studied succession shows that the dolomites pointing their origins as type II and type III. But other parameters-degree of ordering and Mg:Ca ratios- should also be calculated to draw the outline of the dolomites.

Table 5.8. Table showing the dolomite included samples with their d_{104} and Nca_{CO3} calculations.

Samples	d_{104}	N_{CaCO3}
U13	2,9	54.7
U10	2.9	54.7
U7	2.89	51.3
U6	2.89	51.3
A1	2.89	51.3
A6	2.89	51.3
A15	2.9	54.7

XRD data from dolomites can be useful in providing a more detailed knowledge of the crystal structure and chemistry, and that can be used to distinguish between different types of dolomites within one carbonate formation. XRD of dolomites also gives information on the ordering of the crystals. As a result of segregation of the cations into separate sheets in the dolomite crystals, a set of superstructure reflections corresponding to d_{021}, d_{015} and d_{101}, which is not present in the structurally similar calcite (Tucker, 1988). The sharpness and the relative intensities of these ordering peaks can be used to give a measure of the degree of

ordering of the dolomite crystal. The greater the ratio of the heights of the ordering peak 015 to diffraction peak 110, the higher the degree of ordering (Tucker, 1988). The ordering ratio of dolomites indicates their origin whether primary precipitation or not (Süzen and Türkmenoğlu, 2000).

All the naturally occurring dolomites are ordered to an extent with modern dolomites showing reflections due to poor ordering compared with many ancient ones. Dolomite which are non-stoichiometric are generally less well ordered than "ideal" dolomite, through the occurrence of some Ca ions in the Mg sheet. In practice, all naturally occurring dolomites are ordered to some extent with most modern dolomites showing poor ordering reflections, compared with many ancient dolomites (Tucker, 1988).

The abundance of Mg^{+2} ions in the fluids would result in near stoichiometric dolomite. The calcian dolomites of group III are thought to be formed from solutions with lower Mg/Ca ratios. Samples from the Karahamzalı section have low to moderate ordering degree and also confirm their Ca-rich character.

Petrographic examination of the thin sections reveals that the dolomite occurs in two modes in the Karahamzalı section. The first type of dolomites are named as group III in Tucker (1988) study. Group III dolomites are cement precipitated in intercrystalline pores as a thin and clear outer rim or zone around a single or cluster of clasts and also in some fenestral voids as pore-lining and space-filling crystals.

The second type of dolomite found in the studied succession is called as Group II dolomites by Tucker (1988). It is basically micrite cement on which floating grains are seen. It has a cloudy apperance and it is finer in size relative to Group III dolomites. Both Goup II (Figure 5.39b) and Group III (Figure 5.39b) dolomites are early diagenetic and near-surface in origin. The climatic control is very

important on the formation of these type of dolomites. Group II dolomites is associated with evaporites which indicates direct relation with the arid climatic condition. They have Mg excess which result in high Mg/Ca ratios. On the other hand, Group II dolomites have Ca excess and they are calcian dolomites thought to formed from solutions with lower Mg-Ca ratios during humid periods of climate of the region.

According to the textural classification of dolomites (Tucker, 1988), the studied Group III dolomites show mostly xenotopic-nonplanar textures. Dolomites show xenotopic textures where anhedral crystals with curved to serrated and irregular crystal boundaries. It is a mosaic of subhedral to anhedral crystals of dolomites. They are found to be cement as outer rim around clasts, lining the intercrystalline pores, filling a fenestral voids and pore filling material in the studied samples (Figure 5.39).

Magnesium can come from a number of sources: from the chemical reworking of nearby and perhaps earlier dolomites, from structural Mg expelled during the montmorillonite-to-illite transformation, and from the deep subsurface dissolution of salts (Tucker, 1988). It is also stated in Tucker (1988) that early dolomite precipitation may be related to near-surface evaporation. Magnesium for later dolomite precipitation may be derived from clays or dissolution of magnesium-rich silicates.

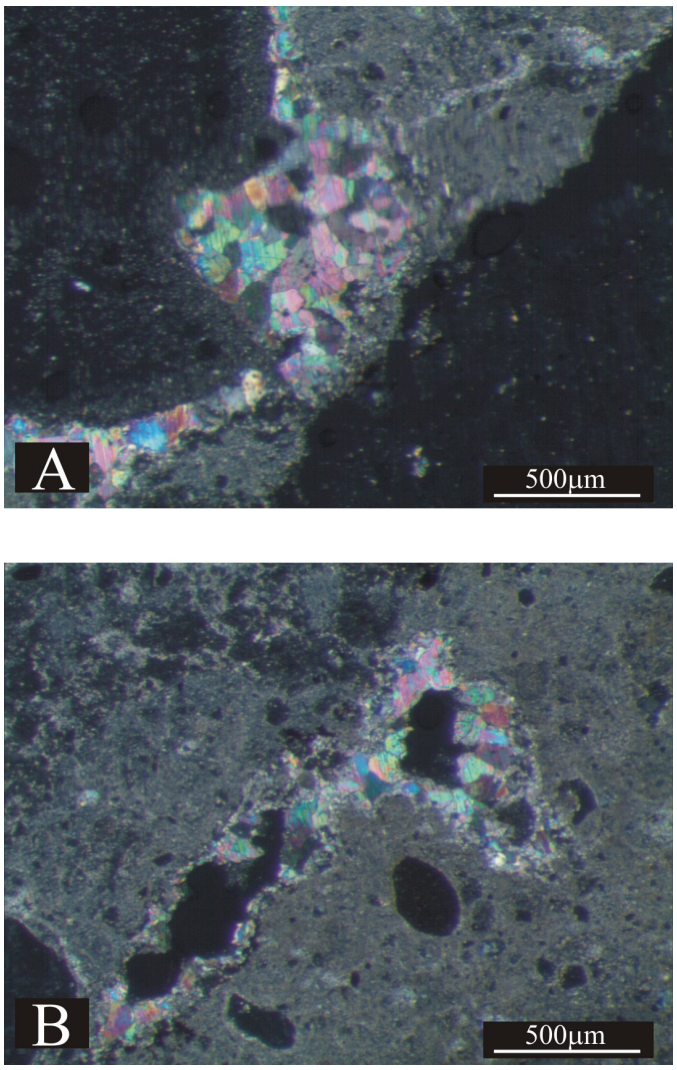

Figure 5.39. Photomicrographs of dolomites found in Karahamzalı samples revealing their a) Group III and b) Group II characteristics.

CHAPTER 6

MICROMORPHOLOGY

6.1. THIN SECTION DESCRIPTIONS

This chapter includes the descriptions of the thin section analyses of the paleosols and their calcretes. Petrographic and soil micromorphological samples were collected from calcretes of Bala and Karahamzalı successions and from the other sampling sites (Çiğdem, METU, İncek and Dordurga). The calcrete samples collected were mainly of indurated nature. However, paleosol samples, due to their unconsolidated character, were massive.

This chapter primarily begins with the explanation of the terminology used in this part of the study. After that, it defines the paleosols and its carbonates of the study area in terms of their textural and micromorphologic properties.

Micromorphological descriptions of the samples from the Bala section were not conducted due to the artefacts development in the thin sections. Thus the section is described by the mineralogical and geochemical properties of the paleosols to be compared with the Karahamzalı section.

6.2. TERMINOLOGY

Basically, the soil and Micromorphology terminologies are followed from the Soil Survey Manual (1993), FitzPatrick (1993) and Bullock et al. (1985). The studies of Esteban and Klappa (1983) and Wright and Tucker (1991) pointing out to the basic micromorphologic properties of calcretes are referred in this chapter. Soil includes the horizons near the surface that differ from the underlying rock material as a result of interactions, through time, of climate, living organisms,

parent materials, and relief. Parent material refers to unconsolidated organic and mineral materials in which soils form (Soil Survey Staff, 1993). The soil profile term refers to the vertical cut through the soil including calcrete levels. A soil horizon, on the other hand, is a layer which can be distinguished from adjacent layers by diagnostic features. Soil fabric, by definition, deals with the total organization of a soil, expressed by spatial arrangements of the soil constituents, their shape, size and frequency (Bullock et al., 1985). Bullock et al. 1985 also defined the soil structure as a feature which should be considered with the size, shape and arrangement of primary particles and voids in both aggregated and non-aggregated material and the size, shape and arrangements of any aggregates present. The individual particles whether resolvable or not under optical microscope are named as the basic components of soils. The groundmass is referred to as the coarse and fine material which forms the base material of the soil other than pedological features. Micromass, on the other hand, is used for the finer material in the groundmass (Bullock et al. 1985). Discrete units in soils which can be differentiated from the adjacent material by concentration of one or more components such as organic matter, crystals, chemical components are termed as pedofeatures (Bullock et al., 1985) which are the keys to easily understand the soils.

6.3. MICROMORPHOLOGY OF THE KARAHAMZALI PALEOSOLS AND CALCRETES

The first sampling site was the Karahamzalı Section. The cementing material is the fine grained carbonate mineral, the size of which possibly suggests relatively rapid precipitation. The grains are formed from mineral and rock fragments. The most common mineral is quartz with feldspars (Figure 6.1). Rock fragments are composed of volcanic, clastic sedimentary and metamorphic fragments. The mineral and rock fragments have subangular to subrounded edges implying that the source of those clasts are not so far away from their source area (provenance).

The carbonate nodules are also common in the calcretes of the Karahamzalı section. The mineral and rock fragments, voids and dissolution channels are surrounded by carbonate minerals which is a typical feature of calcretes (Figure 6.2a,b and c). Manganese dioxide coatings also rim some grains and also occur as dense compound infillings (Figure 6.3a) and loose discontinous clusters within the voids (Figure 6.3b).

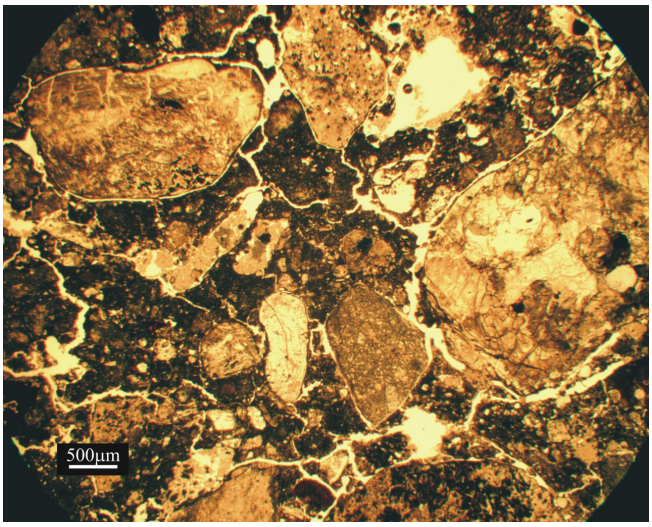

Figure 6.1.The general view of the caliche sample of the A-15 level from Karahamzalı section. Weathered feldspar grain with subangular edges and andesitic rock fragment with subrounded structure are cemented by dense micritic carbonate minerals. Iron oxide and manganese dioxide coatings are also visible around the grains.

Cracks and faunal passages in the calcretes are filled by coarse grained carbonate minerals (Figure 6.4a,b and c). Well crystallised microspars can be easily recognized by their optical properties. The elongated, generally U-shaped voids are assumed to be left from faunal activity (Figure 6.4 and b). Some are filled with compound dense sparry carbonate minerals. The walls of the voids were also

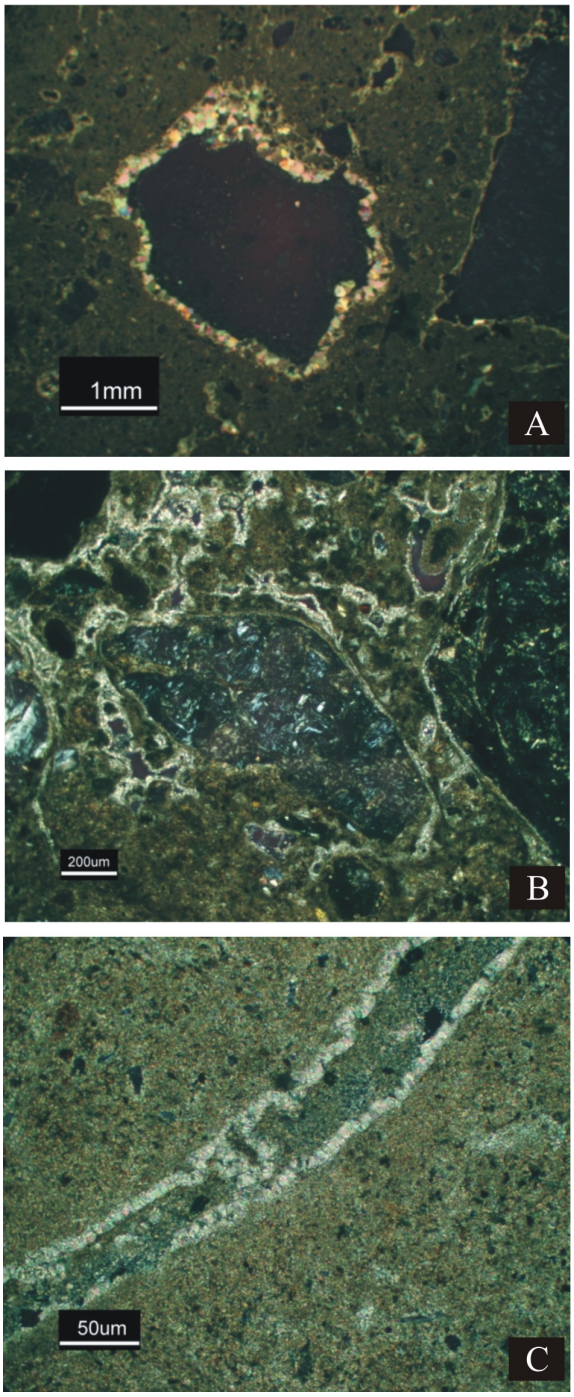

Figure 6.2. Micritic carbonate minerals lining (a) the voids, (b) grains and (c) the channels of Karahamzalı paleosol.

coated with carbonate minerals of finer size. Some of the faunal voids are coated with fine grained carbonate minerals and filled with loose discontinous clusters (beaded) of manganese dioxide.

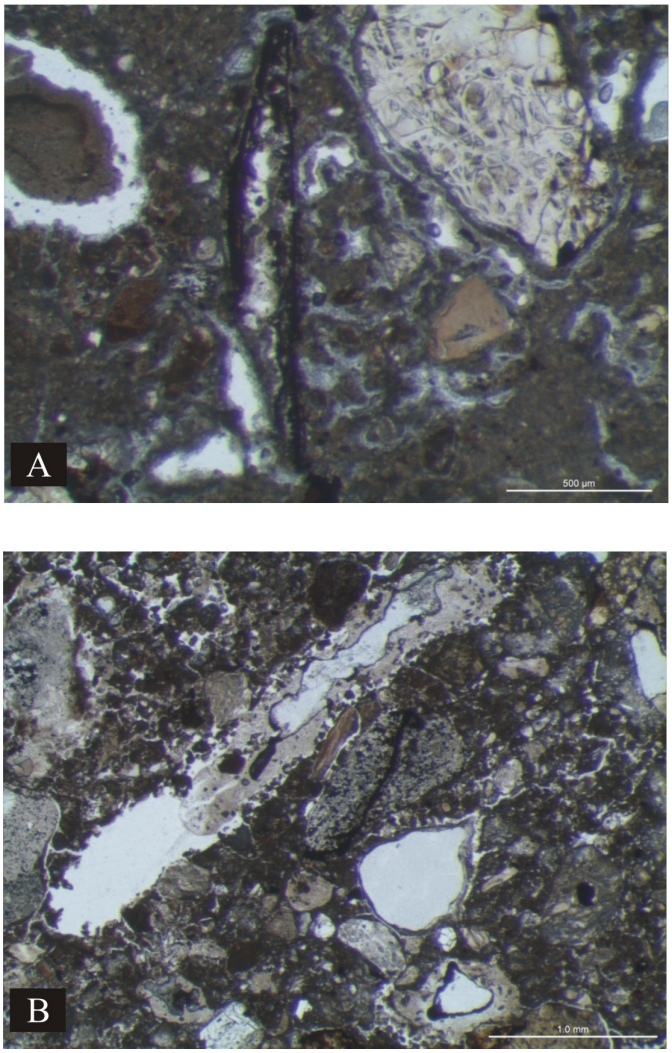

Figure 6.3. Photomicrographs of (a) dense and continous infilling of MnO_2 within a void space and around a feldspar fragment within a calcrete sample of Karahamzalı succession; (b) clusters of broken/beaded MnO_2 coatings within a void space in calcrete sample of the Karahamzalı succession with probable organic infill.

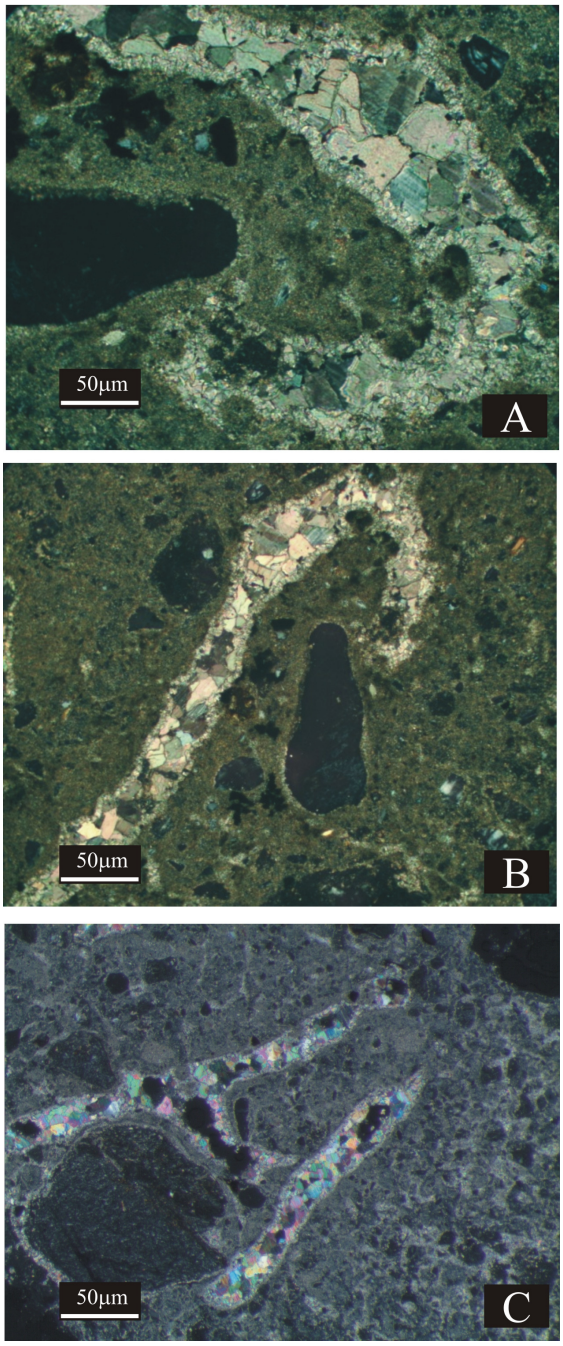

Figure 6.4. Photomicrographs of sparry carbonate mineral infillings within the void spaces of calcretes in Karahamzalı succession (a,b) U-shaped lining of the voids are filled with coarse grained carbonates; (c) two almost parallel void spaces surrounding a rock fragment are filled with sparry carbonate and include MnO_2 clusters.

Carbonate nodules (Figure 6.5), as distinctive features of paleosols and their carbonates, and some voids (Figure 6.5) are surrounded by carbonate minerals having distinct sharp and angular edges as dog-tooth cement (Figure 6.5). There are also some pore spaces developed due to dissolution during the periods of leaching of soil formation. These spaces are left unfilled due to the repeated leaching processes within the succession. As typically occurs to other voids and grains, these openings within the calcretes of the Karahamzalı section are lined by coarse grained carbonate minerals (Figure 6.6).

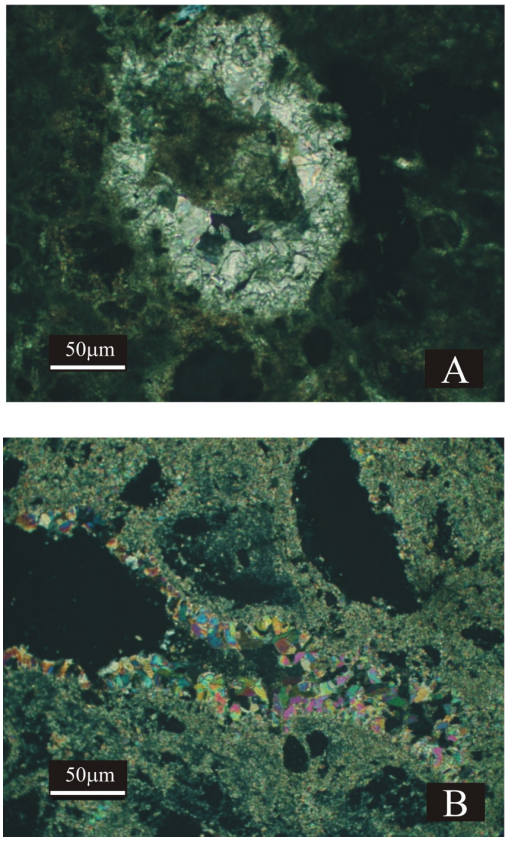

Figure 6.5. Sparry carbonate minerals (a) surrounding a carbonate nodule and (b) coating the void space left from faunal activity. The sparry carbonates with sharp edges are the dog-tooth cement.

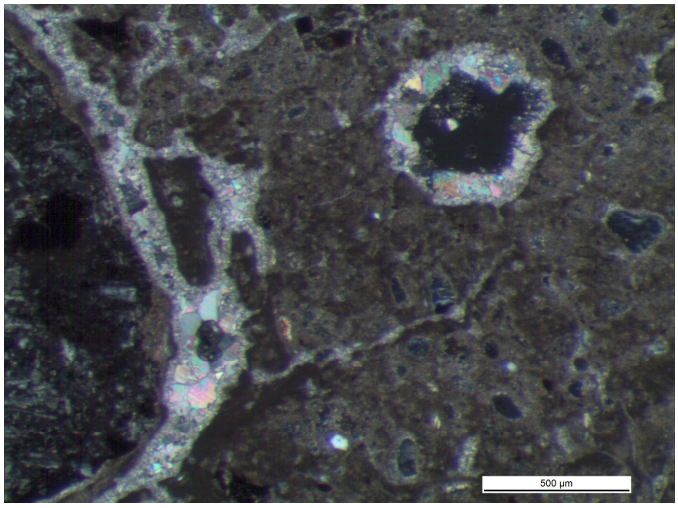

Figure 6.6. Pore spaces developed due to dissolution processes remain unfilled but surrounded by coarse grained carbonate minerals.

Calcretes developed within the reddish-brown colored paleosols in the Karahamzalı section have a distinct reddish-brown color as a primary feature which can easily be recognized due to the mode of horizonation of the paleosols. Throughout the section, the paleosols have almost the same color, whereas the color of the upper paleosol levels seem to be redder. The paleosols like the calcretes in the succession include gravels but the amount and the size of these are different than in the paleosols. Rock fragments are finer with lower amounts compared to the calcrete levels.

The fabrics (microstructure) of all thin sections were studied to understand the arrangement of the constituents in the matrix. The arrangement of the peds within the lower horizons of the Karahamzalı succession integrates from a subangular blocky (Figure 6.7) to prismatic structure. The peds are bound by angular and subrounded surfaces (Figure 6.7). Through the upper levels of the succession, the shapes of the peds change to subangular blocky and to granular, where primary peds are more or less in similar sizes as well as the secondary smaller ones

indicating more advanced physical soil formation (Figure 6.8) than the lower layers as seen in figure 6.7. In general, the microstructure of the paleosols within the Karahamzalı succession are subangular blocky to granular and prismatic. The peds of the paleosols (measure of the degree to which adjacent faces are moulds of each other) are also well accomodated at the lower levels (Figure 6.7) in the succession (measure of the degree to which adjacent faces are moulds of each other), but varies from partial (Figure 6.8a) to unaccomodated (Figure 6.8b) towards the upper parts of the succession. As pointed out by Bullock et al. (1985), voids occur in four different positions within paleosols: between aggregates, within aggregates, across aggregates and within non-aggregated material. Bullock et al. (1985) classified the voids as packing voids, vughs-vesicles, channels-chambers and planes. According to this classification, paleosols within the Karahamzalı succession can be classified as planar voids observed as crack patterns (Figure 6.9) and chambers connected with channels (Figure 6.10). Chambers are near spherical voids (Figure 6.10a) connected to channels. Channels are, on the other hand, elongated voids having smooth walls.

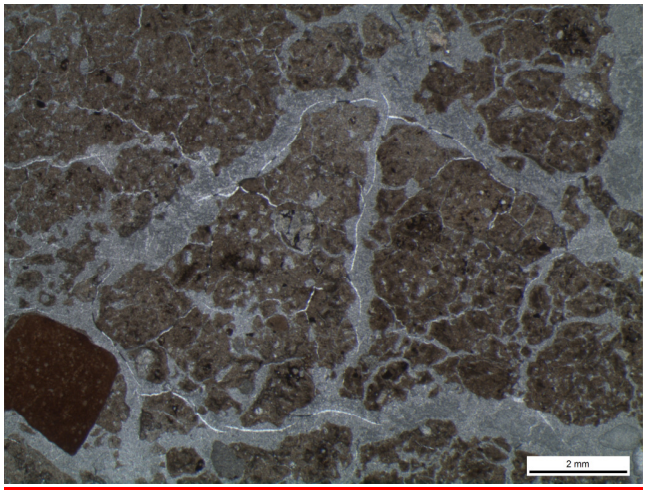

Figure 6.7. Subangular blocky microstructure and well accommodated ped structure of the paleosols within the Karahamzalı succession. The photographs belong to the samples from the A-5 levels.

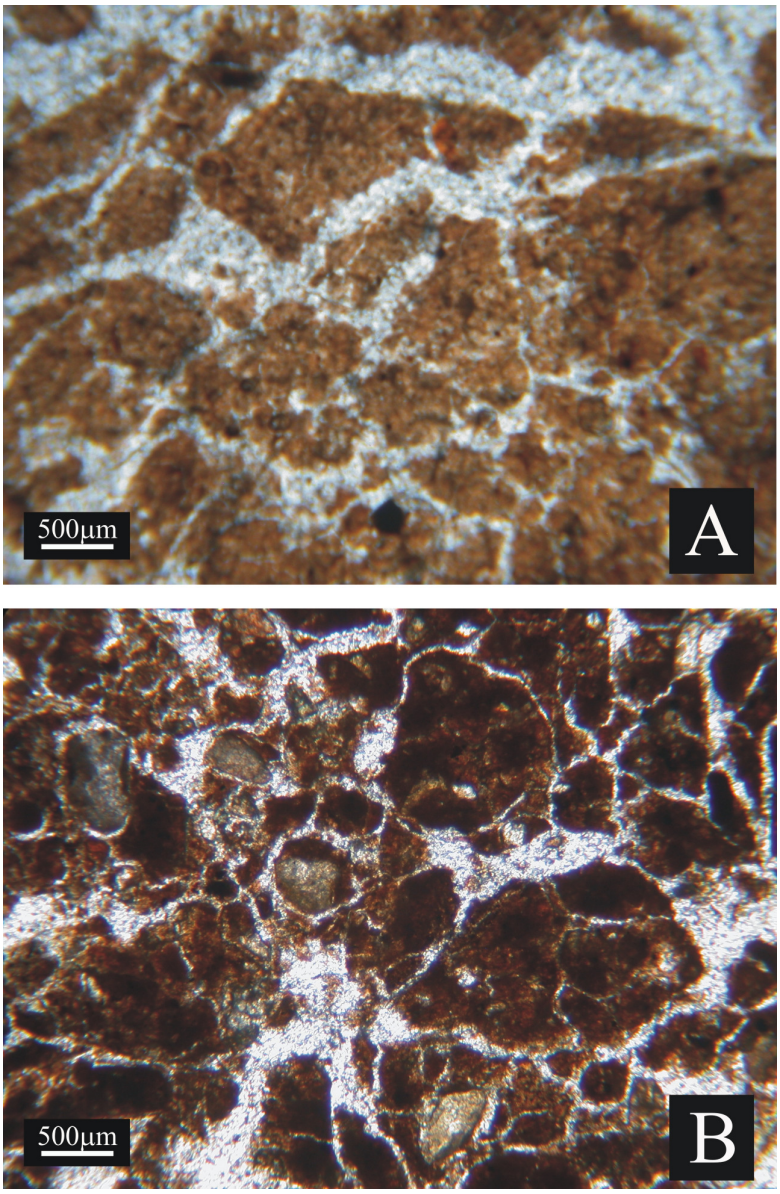

Figure 6.8. Photomicrographs of (a) the primary partially accommodated subangular blocky peds and (b)granular to subangular smaller partially accommodated peds of the paleosols within the Karahamzalı succession.

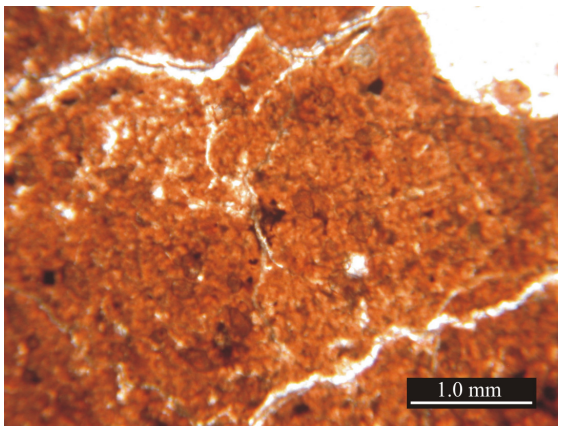

Figure 6.9. The voids morphologically classified as planar voids within the paleosols of the Karahamzalı succession.

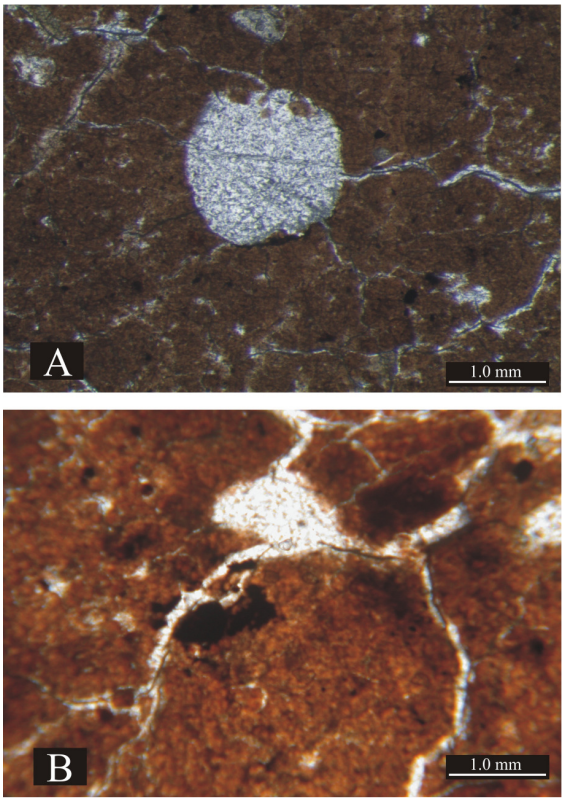

Figure 6.10. (a) spherical and (b) oval faunal chambers connected to elongated channels of Karahamzalı paleosols.

Some features specific to soil/paleosol formations are called pedofeatures. The first important parameter is the presence of microstructural units of paleosols. The next are the clay coatings, clay skins or so called cutans. The cutans are found as illuviated clay features in the paleosol matrix.

Floating grains as mentioned by Tucker (1991) are the detrital mineral and rock fragments of layers of fluvial origin. Polysynthetic quartz grains (Figure 6.11a), feldspars surfaces with weathering features (Figure 6.11a), rock fragments of volcanic origin (Figure 6.11b), cherts, clastic sedimentary rocks, basaltic and metamorphic rocks are observed at hand specimens and thin sections (Figure 6.11b).

Other pedofeatures observed in the paleosols of the Karahamzalı succession are the coatings and infills of MnO_2 along with carbonate minerals. The difference between coating and infilling is that if the void is filled with more than 90%, then it is infilling. But if this amount is smaller than 90%, it is called as coating, instead (Bullock et al., 1985).

Despite the definition of Bullock et al. (1985), concerning the difference between a clay coating and an infill based on the amount of void fill as a 90% void fill being an infill and less than 90% being a coating, a great many controversial discussions may be raised against this view, leading us to rule out this percent-wise designation. MnO_2 is generally present as loose discontinous coatings (Figure 6.12b) within the voids and coatings of grains together with illuviated clay (Figure 6.12a). Infillings in the matrix consist of MnO_2 coatings lining pores.

One of the diagnostic features of the paleosol is the presence of remnants of root fragments penetrating through the cracks present with faunal excrements (Figure 6.13a,b,c and d).

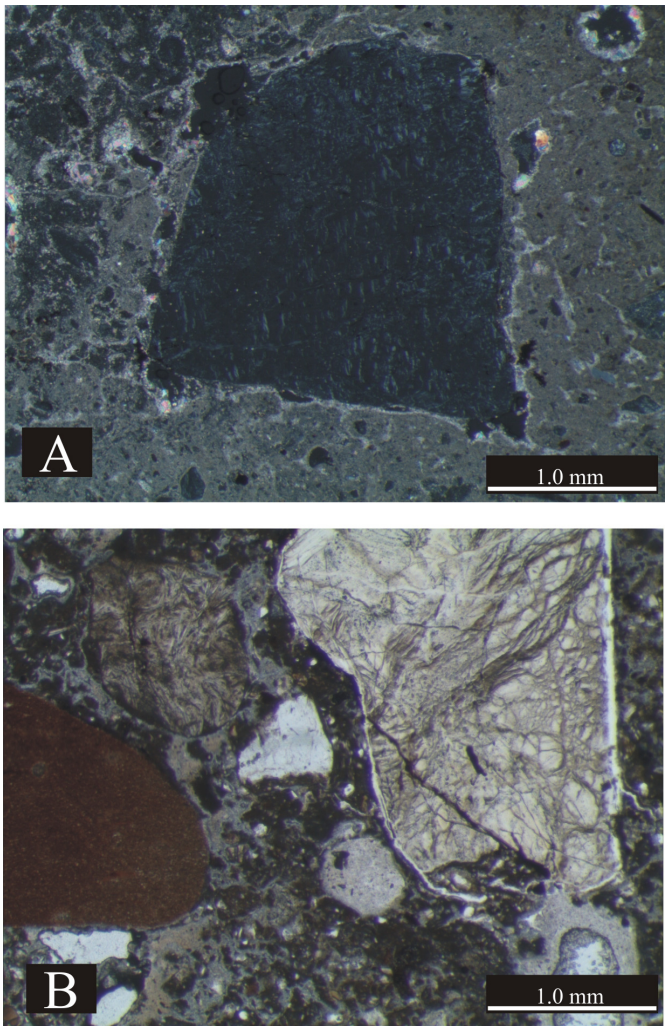

Figure 6.11. Feldspar fragments floating in the calcrete sample (a) quartz and feldspar grains and rock fragments of andesite floating in the Karahamzalı paleosol sample (b).

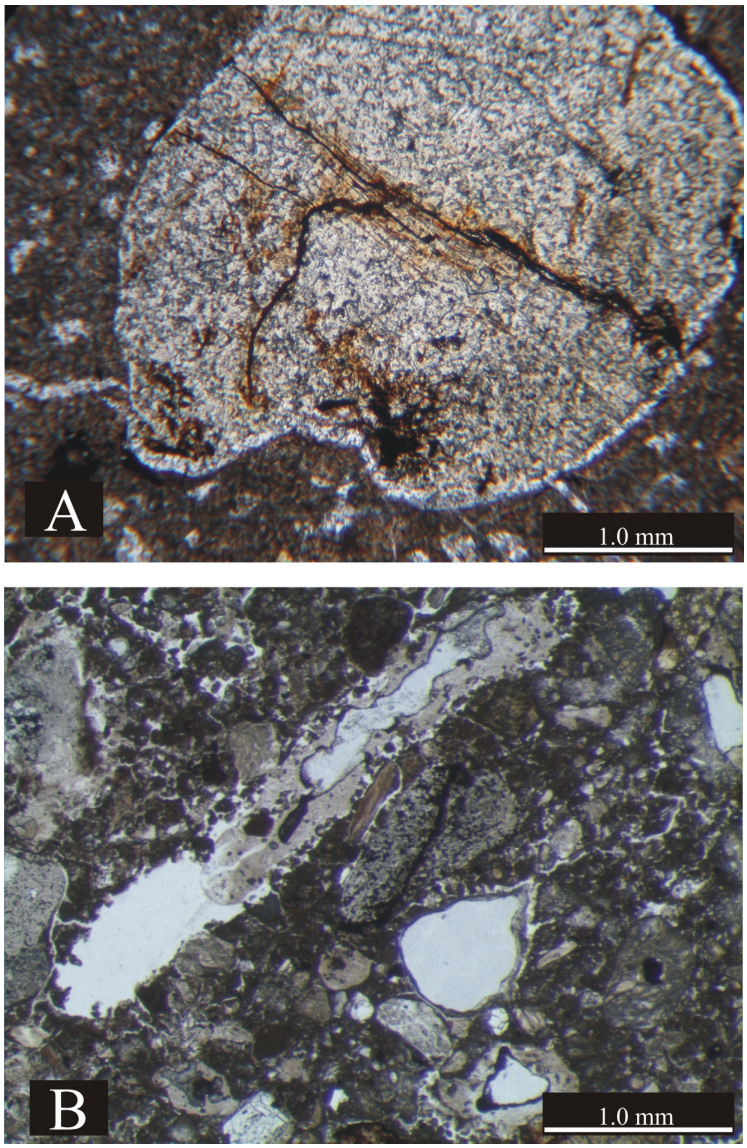

Figure 6.12. MnO_2 and clay coatings as (a) external quasi-coating of a carbonate in a paleosol sample of the calcrete sample of the Karahamzalı section.

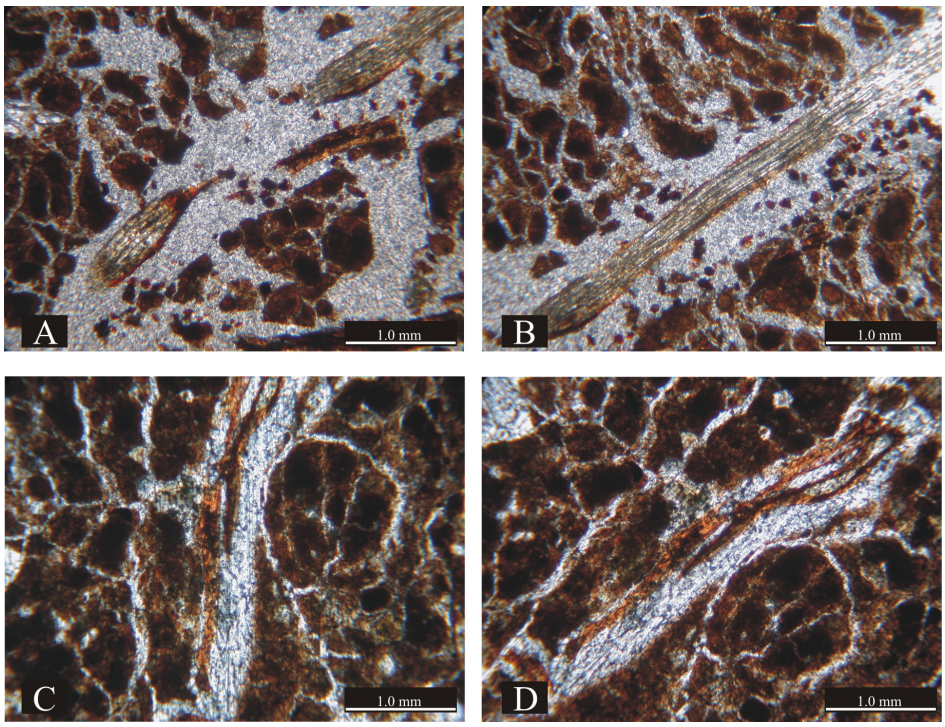

Figure 6.13. Plant parts fecal excrements within the U-11 paleosol sample of Karahamzalı succession.

Additionally, the secondary carbonate linings are also accepted as important features of paleosols and their carbonates. The Karahamzalı succession is a good example for paleosols and calcretes, both having secondary carbonate rims around floating grains, voids and carbonate nodules. This fabric feature indicates the presence of pedogenic formation in the calcretes of the Karahamzalı succesion. The geometric relationship of the U-shaped voids within the calcretes of the Karahamzalı succession directly implies to the evidence of the presence of past bioturbation. This is a prime phenomenon for classifying the calcretes of the study as beta calcretes according to the Tucker (1991). The presence of expandable clay minerals are easily identifiable via the shrink-swell structures present in the paleosol samples of the Karahamzalı succession (Figure 6.14). The spheroidal features developing in subangular aggregates determined in the Karahamzalı

paleosol layer (Figure 6.15) may possibly imply to the maturity of the soils (Kapur et al. 1987).

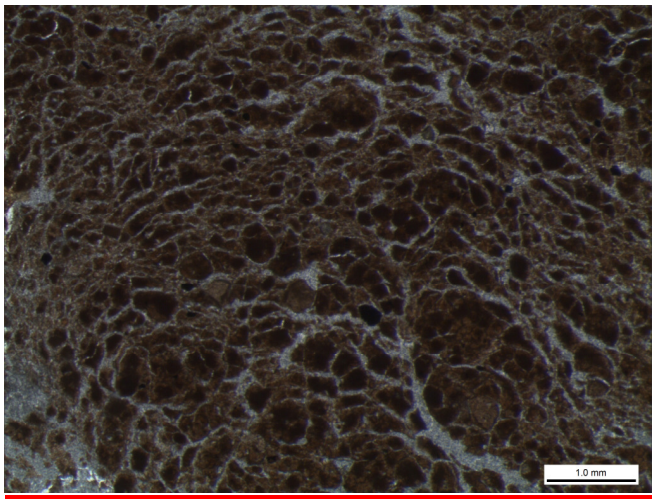

Figure 6.14. The disturbance within the paleosol matrix due to the expandable clay mineral contents of the paleosol of the Karahamzalı section.

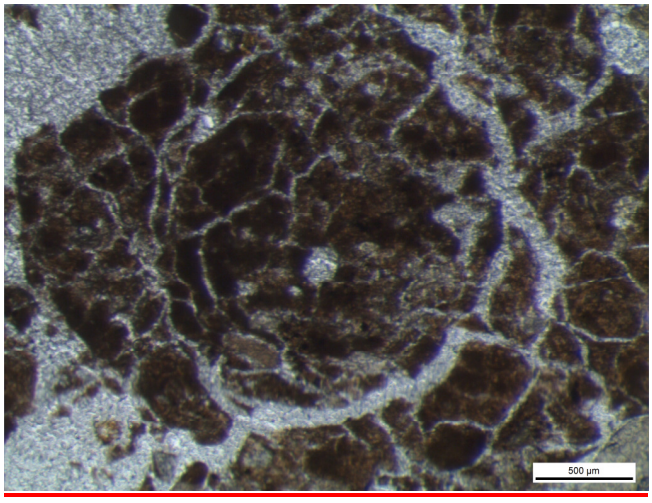

Figure 6.15. Spheroidal microstructure of the paleosol in Karahamzalı section. (Spheroidal microstructural units develop in subangular aggregates).

6.4.PETROGRAPHY OF OTHER SAMPLES

Other samples were selected from different locations from where there has been no definite profile development observed. The samples are from İncek, Dodurga, METU, Çiğdem areas. The first random sampling site was the İncek area where a shallow paleosol development and a calcrete level was observed. However, calcretes of this site are diffuse and in powdery form. The paleosols of the İncek site have angular blocky structural units recognized in the field. Their photomicrographs are presented here in X4 and X10 objectives under plane polarized light (PPL).

The other random sampling site was the Dodurga area, where different calcrete samples were collected for the study. Calcretes from the Dodurga area were determined to be very similar to the calcretes of the Bala area. The cement of the Dodurga calcrete is dominantly composed of micritic calcite crystals (Figure 6.16). This property is also observed during field studies that calcretes highly react (effervesce) with 10% HCl acid.

Floating grains are composed of both mineral and rock fragments. Mineral grains of quartz, feldspar and hematite, rock fragments of shale, chert, siltstone and of metamorphic origin are observed under the microscope (Figure 6.16). Rock fragments have subrounded edges implying to distant sources to the deposition site (Figure 6.16b), but mineral grains, especially quartz, are angular indicating that the quartz is transported from a nearby source (Figure 6.16c).

Rock fragments and minerals are surrounded by sparry calcite crystals (Figure 6.16c). Cemented dog-tooth sparry calcites surrounding the grains and void spaces are angular and similar to the calcretes in the Karahamzalı section (Figure 6.16c). A clay cutan is also observed in the calcrete sample of the Dodurga area (the scarcity of this feature is most probably bound to the presence of expandable clay minerals, i.e., smectite). Iron oxide was also observed surrounding grains (Figure

6.17) and present as linings on the grains and micritic cement. These properties of the calcretes of the Dodurga site lead us to classify them as the alpha calcretes.

Therefore, it is right to point that Dodurga calcretes have the features of alpha calcretes (Tucker, 1991). The walls of the elongated void spaces are abundantly coated with sparry calcite crystals (Figure 6.16c) and organic material residues (humified materials).

MnO_2 clusters have developed along the outer rims of the elongated void reflecting a humid pedogenic phase following the intra-void consequtive processes (wet-dry climatic minor and/or major cycles/fluctuations) of clay cutan illuviation and the deposition of the humified organic material (Figure 6.18).

The shape of the voids and the humified organic residues possibly imply that the calcretes in the Dodurga area may also consist of the features of the beta calcretes.

Some voids of irregular shape are filled with chalcedony in calcretes (Figure 6.19) indicating an arid soil environment laden with large amounts of silica that may be deposited within the matrix as cementing material (FitzPatrick, 1993).

Mineral grains and rock fragments are surrounded by sparry calcite crystals and cemented with micrite (Figure 6.20).

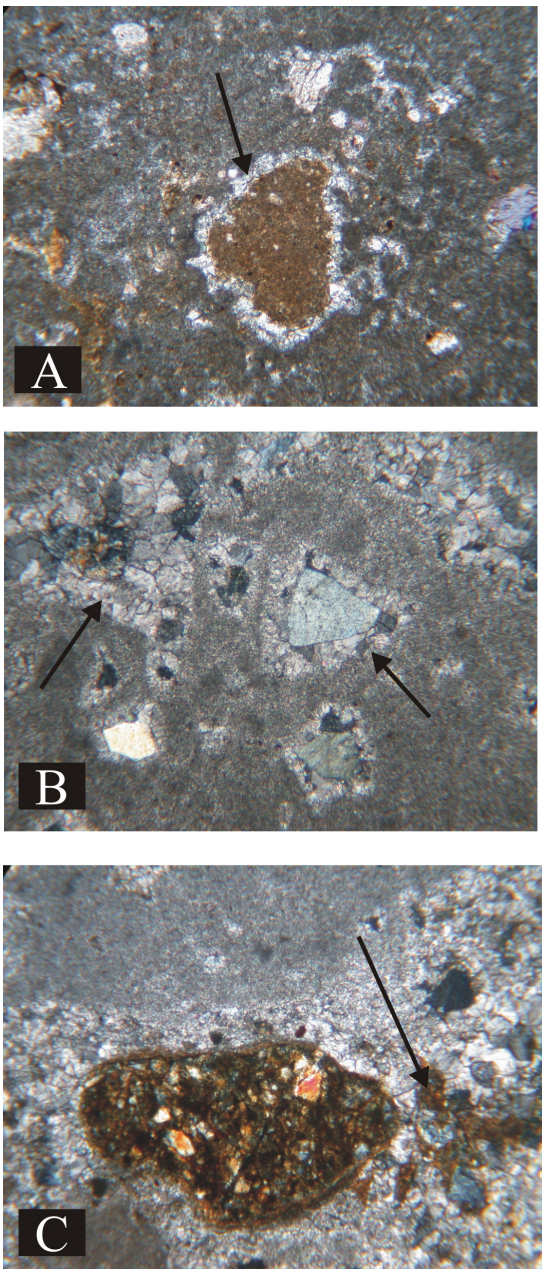

Figure 6.16. Photomicrographs of the calcretes of the Dodurga-Türkkonut area revealing (a) Micritic calcite cement and microspar surrounding the rock fragment; (b) dog-tooth cement type microspar development, and (c) presence of calcite together with clay illuviations. Iron oxide linings are also observable in calcrete samples (X4, PPL).

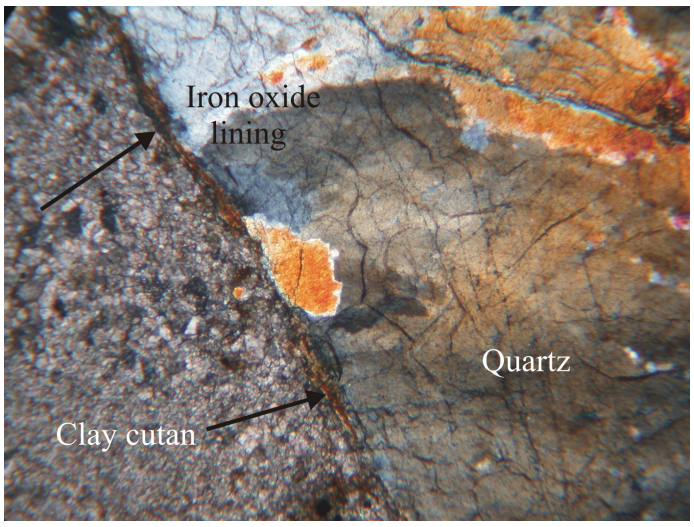

Figure 6.17. Iron oxide lining and clay cutans, micritic cement and polycrystalline quartz grain of Dodurga calcrete (X10, PPL).

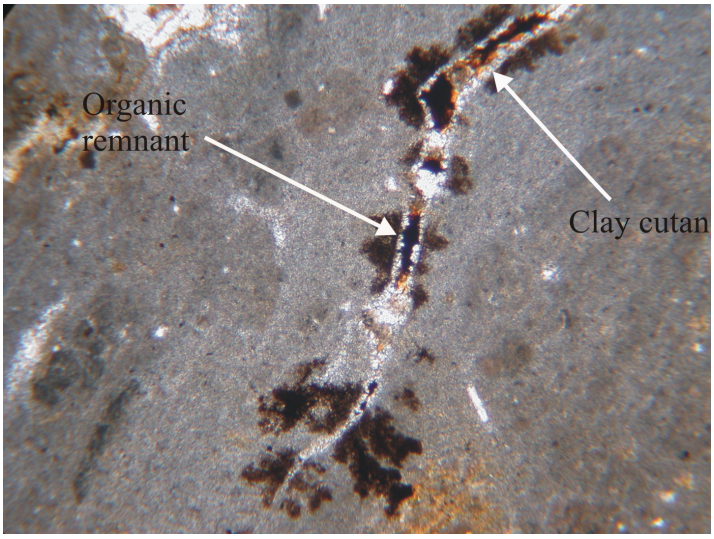

Figure 6.18. The elongated voids surrounded by sparry calcite crystals and infilled with humified material (X4, PPL).

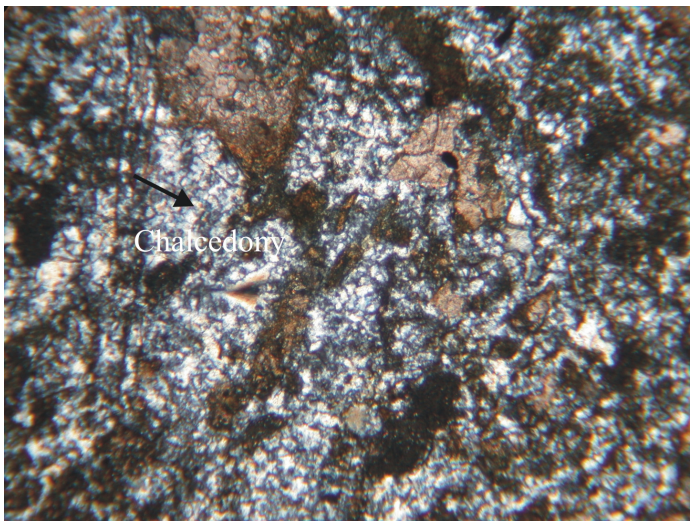

Figure 6.19. Chalcedony infilling within an irregular shaped void of calcrete from the Dodurga area (X10, PPL).

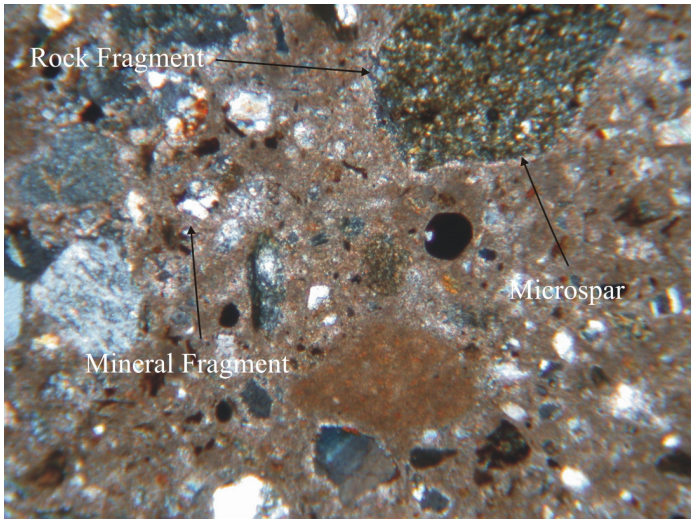

Figure 6.20. Mineral grains and rock fragments surrounded by sparry calcite crystals and cemented with micrite. Rare subrounded to oval fragments in calcrete of Dodurga area (X4, PPL).

The rare subrounded to oval fragments may be the features standing for an earlier calcrete formation (unpublished data, S. Kapur-Univ. of Çukurova, Adana, Turkey, C. Zucca-Univ. of Sassari, Italy and F. Previtali-Univ of Milan/Bicocca, Italy) as broken and partly incorporated fragments. The calcretes were determined within the brown colored siltstone levels (D-1) in the Dodurga area. Quartz, feldspar and opaque minerals are the dominant minerals found within the siltstone matrix (Figure 6.21). On the other hand the siltstone matrix is determined to comprise unfilled pore spaces (Figure 6.21). It also illustrates the formation of secondary vermiform kaolinite along with completely kaolinised feldspars indicating the highly humid past/palaeo-climatic conditions inducing soil formation. The siltstone matrix is cemented by micritic calcite and iron oxide along with prominent development of clay cutans in elongated pores (Figure 6.22), where the latter indicates the occurrence of the consequtive climatic cycles/fluctuations. Fine grained clastic sedimentary rock fragments (Figure 6.23) with rounded edges point to the distant source of these fragments. However, the mineral grains have subangular edges (Figure 6.23) with probable nearby sources to the Dodurga area.

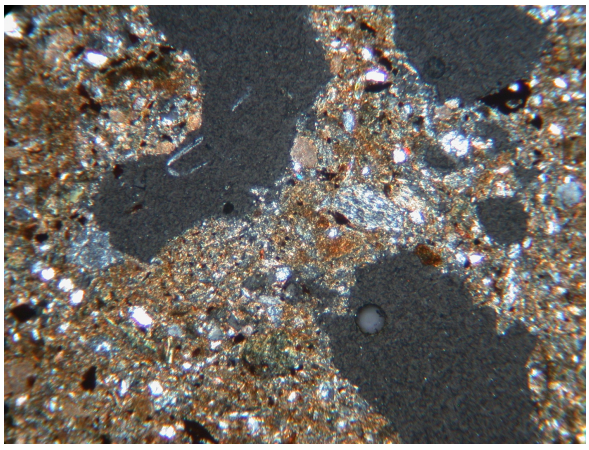

Figure 6.21. Pore spaces lined by secondary vermiform kaolinite and feldspars weathered to kaolinite (X4, PPL).

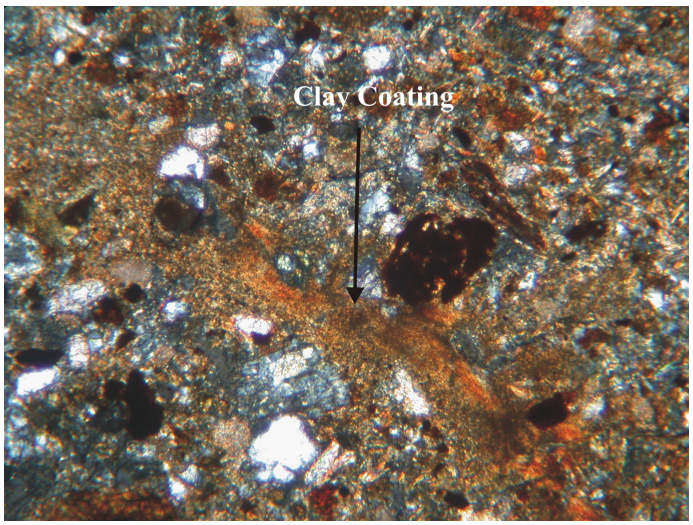

Figure 6.22. Clay coatings in the siltstone matrix from the Dodurga area (X10, PPL).

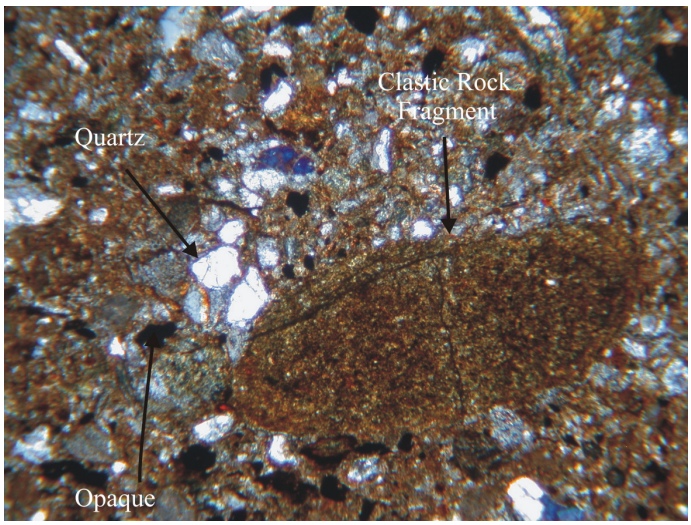

Figure 6.23. A fine grained clastic rock fragment with rounded edges and quartz and feldspar grains with subangular edges (X4, PPL).

Calcrete samples from the Çiğdem area are uniform in matrix similar to those of the Dodurga and Bala areas. Calcretes from the Çiğdem area are densely cemented with micritic calcite (Figure 6.24). Mineral and rock fragments which are enveloped by sparry calcites are the major components of the calcretes (Figure 6.24). The rock fragments as in the other calcrete samples are subrounded and the mineral grains are angular (Figure 6.24).

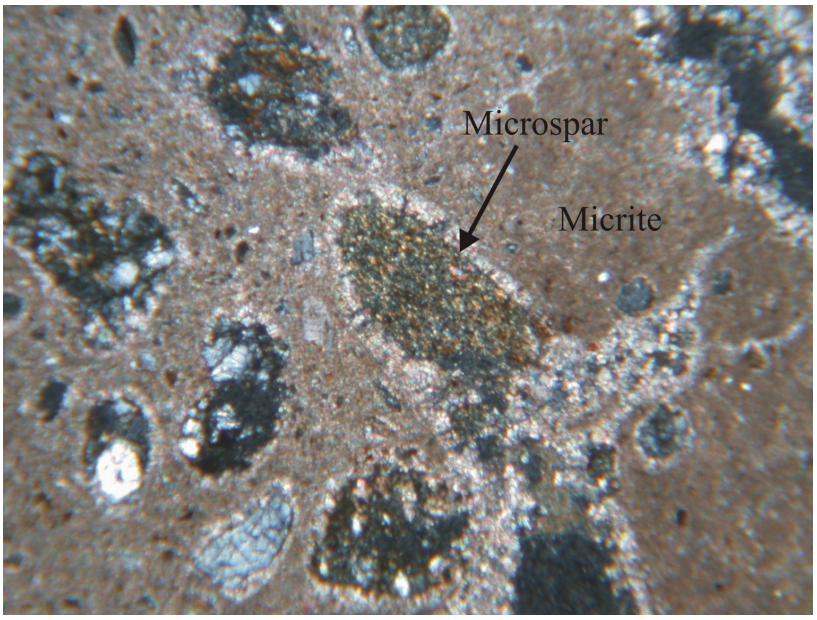

Figure 6.24. Dense micritic cement and sparry calcite surrounding the fragments of the Çiğdem area (X4, PPL).

The sparry calcites surrounding the fragments are in different forms within the calcrete samples of the Çiğdem area. They are observed as long-prismatic/bladed/fibrous crystals with sharp angular edges (Figure 6.25a,b). Both these phenomena are the evidence of vadose zone precipitation.

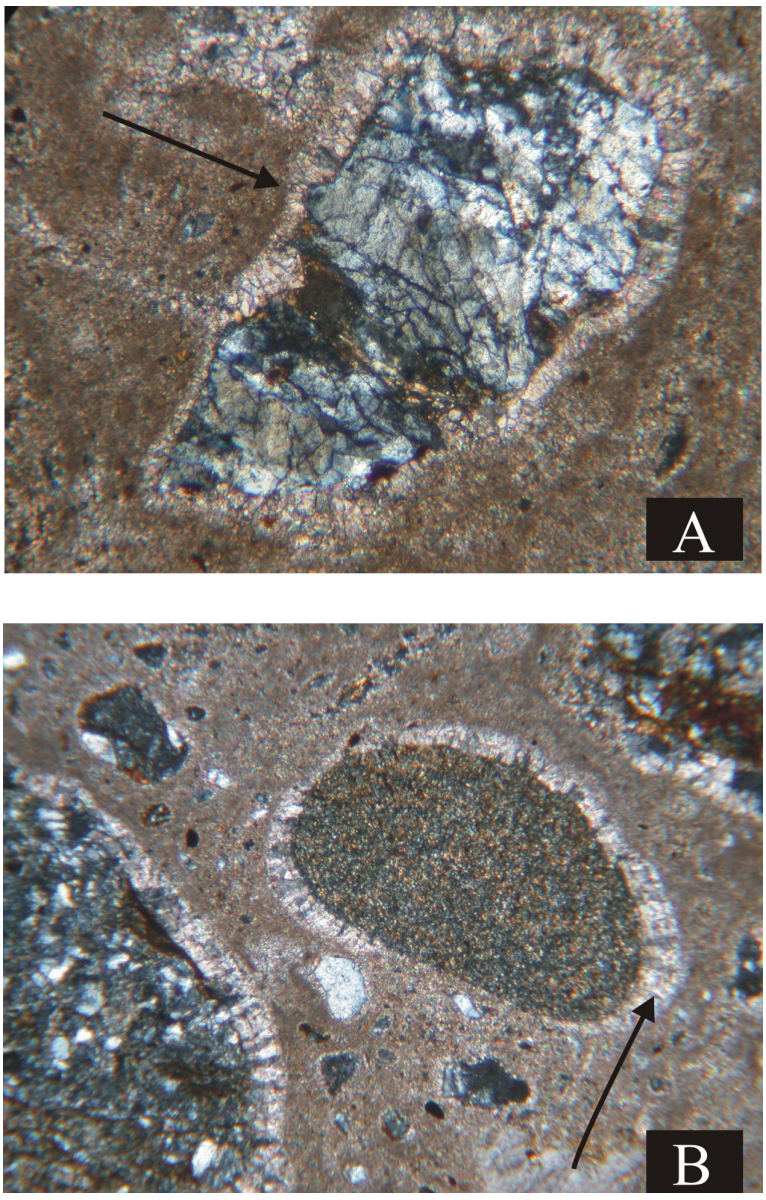

Figure 6.25. Different forms of sparry calcites coating the rock fragments of the calcretes from Çiğdem area. (a) long-prismatic form, (b) fibrous form both pointing to the vadose zone of precipitation (X4, PPL).

CHAPTER 7

GEOCHEMISTRY

7.1. INTRODUCTION

The mineralogical and chemical compositions of the paleosols are strongly controlled by the geochemical activities of the soil solution. Therefore, the geochemical characteristics of the paleosols and their carbonates are clearly important proxies revealing the climatic history of the soil. Major oxide concentrations are given as weight percentages of the whole rock, while trace element abundances are reported as parts per million. Variations of these elements within each sample series as a function of depth from the base of a presumed paleosol to its top are shown in the figures below. Both element abundances and molecular weathering ratios are used as proxy data to interpret the weathering and pedogenesis intensities on paleosols of the studied areas. All the variations of major oxides, trace elements and the quantitative analysis of molecular weathering ratios are plotted against depth to reveal the changes throughout the sections.

Like many studies on paleosol geochemistry (Retallack, 1997; 2001), more recently Sheldon and Tabor (2009) stated that different proxies based on geochemical analyses can be used to infer the pedogenic processes revealing the effect of chemical weathering in paleosols (Table 7.1). Hydrolysis, oxidation, hydration, salinization and calcification can all be defined by the whole rock geochemical compositions of the paleosols. Hydrolysis, by definition, is the reaction of carbonic acid with a cation rich carbonate grain to produce clay and cations. Clays can accumulate in the soil while cations are leached or taken up by plants in solution (Retallack, 2001). To measure the prevalence of the hydrolysis

reactions in soils, their acidity should be measured by pH which can be estimated from the stability fields in the fence diagram of Krumbein and Garrels (1952).

Hydrolysis can be assessed by the molecular weathering ratios of alumina/bases, alumina/silica and barium/strontium (Retallack, 2001). As Retallack (1997) stated, the values of alumina to bases can reach 100 or more in strongly developed soils (Oxisols and Ultisols), but are less than two in moderately to well developed fertile soils (Alfisols and Mollisols).

The clayeyness or the clay movements within the soil profile stands for the translocation of fine smectitic material with depth and is determined by the ratio of Al_2O3 to SiO_2.

Trace element abundances vary considerably among different paleosols and parent materials. Geochemistry of trace elements in paleosols are used also to reveal weathering intensity, evaluating leaching and for provenance. Leaching can be quantified by the ratio of Ba to Sr. High ratio of Ba/Sr implies to more leaching conditions. Both Ba and Sr are alkaline earth elements and have the same atomic radii however Sr is more soluble than Ba. Therefore under most conditions, Sr is leached more readily (Sheldon and Tabor, 2009). This ratio ranges from near 10 in acidic, sandy soils (Spodosols) to near two in most rocks and soils (Retallack, 1997).

Hydration or dehydration reactions, as indicated by Retallack (2001) involve the addition or loss, respectively the water that is structurally part of a mineral. Normally, the degree of hydration reactions can be calculated by Mössbauer spectroscopy for iron oxyhydrates and X-ray diffraction for clays.

Hydration of minerals in paleosols, on the other hand, is revealed by the ratio of silica to iron and alumina. This ratio is high in quartz-rich paleosols with few

hydrated minerals, on the contrary, this ratio is low in clayey ferruginous soils, which may have been full of iron oxyhydrates and hydrated clays (Retallack, 2001).

Salinization in paleosols can not be measured directly by electrical conductivity as in modern soils. Therefore, molecular weathering ratio of soda to potash, alkalis to alumina and soda to alumina are used to assess the degree of salinization. This study uses Na_2O / K_2O ratio for salinization. The salts common in soils of very dry climates include halite, gypsum and mirabilite. Additionally, very saline soils have the phyllosilicates of palygorskite and sepiolite. Salinization can be indicated by soda to potash ratios greater than one or less than one.

Calcification is another important process that generally occurred in paleosols of well-drained of semi-arid to subhumid regions. The process of Calcification involves little loss of nutrient cations andthe overall soil pH is alkaline. Soils of this kind is fairly fertile supporting grassy woodland vegetation with abundant soil fauna. In more drier regions, they support desert vegetation (Retallack, 2001). Calcification can be quantified with the ratio of calcium and magnesium to alumina.

A reaction in which an element suffers electron loss when forming a compound is named oxidation, reversly, electron gain is due to a reduction process. Reduction generally occurs in waterlogged or buried soils. However, oxidation occurs strictly in well-drained soils. The measure of the extent of oxidation and reduction reactions in modern soils is Eh (Retallack, 2001). Low negative Eh means soil can readily donate electrons and is reducing. On the other hand, high positive Eh is found in oxidizing soils with a high demand for electrons. These reactions produce color effect on the soil appearance. Reducing soils (strong negative Eh) are usually bluish greenish gray. However, the oxidized soils with high positive Eh values, are warm brownish red colored. Molecular weathering ratios of ferrous

to ferric iron, total iron to alumina and total iron and manganese to alumina can be used to chemically characterize the oxidation state of the paleosol (Retallack, 2001). North American soil data can be used as reference Standard with total iron to alumina ratio of 0.4 (Marbut, 1935). The values can reach to 1.2 in ferruginous (spodic) horizons, 1.9 in clayey (argillic) horizons and 1.5 in red and deeply weathered (oxic) horizons.

In addition to the molecular weathering ratios, Nesbitt and Young (1982) proposed a measure of degree of chemical weathering and named it as Chemical Index of Alteration (CIA) calcultaed by the ratio of Al_2O_3 to (Al_2O_3+CaO+K_2O+Na_2O). The CIA is a measurement of the weathering of feldspar minerals and their hydration to form clay minerals. As the clay content increases Al should also increase, whereas Ca, K, and Na contents should decrease, leading to higher CIA values (Sheldon and Tabor, 2009). Considering the post-burial addition of potash by metasomatism, Maynard (1992) suggested another index. CIA-K is almost similar to CIA index except it has no K in the calculation. As alteration progresses, the index values also increases. Magnesium index is also very similar measure for the chemical alteration and calculated by using MgO and Al_2O_3 values.

Sheldon and Tabor (2009) explained the importance of U and Th as potential proxies since they are both relatively immobile during weathering except under intense conditions (Li, 2000) or where there is a strong redox gradient. U is leached away during pedogenesis and Th remains in the upper horizons of paleosols with low U/Th ratio than parent material. This indicates very intense weathering and a strong redox gradient. If U is redistributed by leaching, then U/Th ratio should be expected to be high in Bw/Bt horions. Oppositely, if pedogenesis is not effective and if there is no strong redox gradient then the U/Th ratio is expected to be constant all through the profile. Nb is also stated in Sheldon and Tabor's (2009) study as a trace element of interest. Nb has a similar chemical

behaviour to V, Ti and Zr which are all immobile during weathering. Therefore, they can be used as index elements for variation diagrams. Rare Earth Elements are also sensitive to the environmental conditions therefore can be used for paleosol studies. Solubility of REEs is low at neutral pHs (Li, 2000). Increasing solubility results from more acidic pHs (Tyler, 2004). Sheldon and Tabor (2009) stated that their leaching behavior varies according to regional humidity. The ratios of Sm/Nd, La/Ce, Yb/Lu and Ti/Al are also used to determine the provenance of the paleosols.

Table 7.1. Molecular weathering and pedogenesis ratios (Retallack, 2001 and Sheldon and Tabor, 2009).

Ratio	**Formula**	**Pedogenic Process**
Al/ ΣBases	$Al_2O_3/(CaO+MgO+K_2O+Na_2O)$	Hydrolysis
Clayeyness	Al_2O_3/SiO_2	Hydrolysis
Base Loss	Ba/Sr	Leaching_Hydrolysis
Gleization	FeO/Fe_2O_3	Oxidation
Gleization	ΣFe/Al	Oxidation
Gleization	ΣFe+Mn/Al	Oxidation
Silica/Sesquioxides	$SiO2/ (Fe_2O_3+Al_2O_3)$	Hydration
Base Loss	Base/Ti	Leaching
Provenance	Ti/Al	Acidification(~pH)
Alkalis to Alumina	$(K_2O+Na_2O)/Al_2O_3$	Salinization
Soda to Potash	Na_2O/K_2O	Salinization
Parent Material	La/Ce, Sm/Nd, U/Th	Acidification (~pH)

7.2. GEOCHEMISTRY OF KARAHAMZALI SECTION

The results of the whole rock geochemical analysis of paleosols and their carbonates in the Karahamzalı Section (only the outcrop samples) are listed in Table 7.2, 7.3 and 7.4. The major and trace element contents are given in weight percentages and in parts per million, respectively. The molecular weathering ratios and chemical index of alteration values are calculated according to the given formulas in part 7.1. Due to the resistancy for mobilization, Ti is accepted as a normalizing element for major and trace element contents within sections. The values are plotted against depth to reveal the changes in the paleosols.

SiO_2 values of the Karahamzalı Section ranges between 47.1% and 51.41% for paleosols and between 16.86% to 31.03% for calcrete levels (Table 7.2). The amount is relatively higher down to the section, and shows slight depletion towards the top. The relative abundance of SiO_2 is directly related with the leaching conditions that have occurred during soil formation (Gay and Grandstaff, 1980) therefore its high abundance at the bottom and the relative decrease at the top can be interpreted as revealing moderate leaching during soil formation. SiO_2 is part of the quartz and clay mineral structures. As given in Table 5.2, the abundance of quartz and clay minerals gathered from XRD patterns are consistent with the geochemical variations. Ti-normalized values of SiO_2 concentration through Karahamzalı section reveals its increase in calcrete levels close to the surface horizons (Figure 7.1).

Al_2O_3 is assumed to be retained in a soil profile during weathering because aluminum compounds are relatively insoluble under normal pH conditions, and most of the aluminum is incorporated in clay minerals (Birkeland, 1974). The concentration of aluminum therefore should increase in a soil profile, while other components are removed due to leaching. The composition of Al_2O_3 through the section varies from 8.31% to 10.96% for paleosols and 2.52% to 5.58% for calcrete levels. It is high in soil layers, revealing its insolubility caharacteristics

and the composition of alumina which do not show any significant variation within paleosol levels however its amount is low in calcrete levels. This explanation is also consistent with the high clay mineral abundance in paleosols and low amounts in the calcrete levels. Ti-normalized concentration of Al_2O_3 follows almost the same trend with that of SiO_2 (Figure 7.1).

Fe_2O_3 varies in response to oxidation/reduction reactions and illuvial translocation of iron-bearing compounds through a soil profile. The composition of Fe_2O_3 ranges from 8.12% to 9.18% in paleosols and from 2.48% to 5.03 in calcrete layers through the Karahamzalı section. It is recognizable that the Fe composition throughout the section is relatively high at the bottom of the section revealing the addition of Fe from the basaltic parent rock. According to the Ti-normalized values, Fe_2O_3 is nearly constant at depth, but high in calcrete levels close to the surface (Figure 7.1).

Mg and Mn generally follow the same trends as iron, reaching their highest concentration along with iron in the presumed B horizon of each profile. However, in the Karahamzalı section, it is not the case, because the Karahamzalı section contains dolomite as the carbonate mineral which leads to the higher concentration of MgO and differs the concentration trends of MgO vs depth. The amount of MgO ranges from 6.33% to 15.2% in paleosol levels and from 15.2% to 20.3% in calcrete levels. Its abundance fluctuates between the paleosol and calcrete levels. Due to the dolomite content of calcretes in Karahamzalı section, the Ti-normalized MgO concentrations show enrichment at calcrete levels (Figure 7.1).

Ca has contributed to the formation of calcretes and therefore accumulated in the B horizon of the paleosol. Due to the presence of dolomite, CaO is expected to follow the same trend throughout the Karahamzalı section. Its abundance ranges from 0.61% to 2.24% for paleosols and from 13.5% to 22.2 for calcrete levels. As

a general trend, it increases towards the top with the increasing calcrete levels. Ti-normalized CaO plot is almost the same with MgO in enrichments of calcrete levels (Figure 7.1).

Na and K are more readily mobilized elements released by weathering therefore they would be expected to have lower values in the surface horizons of a paleosol relative to underlying horizons. It is the case for the Karahamzalı section indicating weathering intensity. The amount of Na_2O varies from 0.13% to 0.31% for paleosols and from 0.05% to 0.22% for calcrete levels. K_2O, likely, reveals contents of 1.11% to 1.37% for paleosol and 0.27% to 0.71% for calcrete levels through the Karahamzalı section. Their abundances versus depth diagrams reveal the parallel tendency between them (Figure 7.1). Ti-normalized contents show that Na is generally low in the upper horizons due to leaching, but shows 3 shifts in calcrete levels. K, on the other hand, is almost constant throughout the section. It is well correlated with the presence of clay minerals and feldspars in paleosols and their carbonates (Figure 7.1).

Ti has a distribution comparable to that of Si, presumably reflecting a similar resistance to mobilization, though it occurs in much lower concentrations. Its abundance is from 0.67% to 0.77% for paleosols and 0.17% to 0.40% for calcrete levels. The content of TiO_2 throughout the Karahamzalı section is lower than 1, representing its low quantity due to a cut off sediment influx during pedogenesis. The highest quantity of TiO_2 throughout the section is at the bottom revealing the Ti contribution from basaltic parent rock (Figure 7.1).

P_2O_5 contents, which are generally used as direct measures for the biological activity in soils, has very low concentrations throughout the Karahamzalı section with 0.17% to 0.19% for paleosols and 0.04% to 0.11% for calcrete levels. Although the traces of faunal activites can be found in paleosols and calcretes of the Karahamzalı section, there is no organic remnant found in the samples. P_20_5

versus the depth diagram (Figure 7.1) shows that it has almost the same trend with MgO versus the depth plot. Both MgO and P_2O_5 are high in calcrete samples the latter confirming that biological activities common in calcretes of the paleosols.

MnO, which is a very important parameter used for assessing the wet conditions during pedogenesis. Therefore, it is expected that the MnO content is very low in calcrete levels since they are the products of arid climatic conditions. Ti-normalized MnO versus the depth diagram follows a decreasing trend towards the top of the section with slight enrichments in calcrete levels (Figure 7.1). It is, like P_2O_5, has very low quantity through the section with 0.17% to 0.19% in paleosols and 0.04% to 0.11% for calcerete levels.

Loss on ignition (LOI) amounts were relatively high in calcrete levels with 28% to 37% and low in paleosol levels with 17% to 19% contents. This also has a parallel tendency with depth as MgO, CaO and P_2O_5 which are highly concentrated within the calcrete levels.

Al, Ti and Cr have been commonly accepted as immobile elements during paleosol developments. Therefore, to reveal the weathering intensity of the trace elements, they can be used for normalization. Thus, Ti has been used as an element for normalization of the trace element contents of the Karahamzalı samples. Ti-normalized variations of trace elements are plotted with respect to depth (Figure 7.2). Trace element concentrations of Co, Cs, Ga, Nb, Th, Zr, V, Hf and Rb are nearly constant in all samples through the Karahamzalı section, whereas variability is slightly higher for Ba, Sr, U and Y (Figure 7.2). Ba, Sr, U and Y are all positively correlated with calcrete levels with negative trends in paleosols throughout the Karahamzalı section. The greatest variability is measured for U and Sr elements in the upper calcrete horizons of the section (Figure 7.2).

The rare earth elements (REE) are the most useful of all trace elements as indicators of pedogenesis. As accepted to be immobile phase during weathering, REE are also normalized to Ti to show their weathering behaviours (Figure 7.3). The LREE of Ce and Pr are the only elements which remain nearly constant through the section. Others show zig-zag patterns with enrichments in calcrete horizons and relative depletions in the paleosol levels. All of them remains nearly constant in surficial levels. The major shift in REE contents versus depth diagrams is recorded in the A3 calcrete sample for all REE except Ce and Pr (Figure 7.3).

REE concentrations in rocks are usually normalized to a common standard to reveal the contribution from the provenance. As Rollinson (1993) stated, REE are insoluble and present in very low concentrations in river water.

The REE content in the sediment is dominantly controlled by the chemistry of its source. On the other hand, diagenesis and weathering has little influence on the redistribution of the REE. Upper Crust (Figure 7.4a) and Shale-European (Figure 7.4b) normalized REE patterns of the Karahamzalı samples reveal that the paleosols and their carbonates are all uniform in REE chemistry according to the standards with depleted values lower than 1.

To reveal the provenance conditions of the Karahamzalı paleosols, Ti/Al is employed to reveal the sediment influx rate. Additionally, U/Th, Sm/Nd, La/Ce and Yb/Lu were calculated (Figure 7.5).

According to McLennan and Taylor (1991), the geochemical differences between elements, such as La and Th (indicative of felsic igneous source) or Sc and Cr (indicative of mafic source) can be used. Ti/Al ratio is almost constant throughout the section implying to a cut of sediment influx supporting pedogenesis.

Table 7.2. Weight percentages of common oxides in paleosols and calcrete levels of Karahamzalı Section.

Sample / Analyte	SiO_2	Al_2O_3	Fe_2O_3	MgO	CaO	Na_2O	K_2O
U13 (Recent soil)	18,33	3,7	3,26	16,7	20,8	0,09	0,56
U12 (Soil)	48,61	9	8,62	13,4	0,98	0,22	1,21
U11 (Soil)	48,98	10,08	8,31	8,5	2,24	0,17	1,24
U10 (Calcrete)	17,06	2,52	2,48	17,9	22,2	0,05	0,27
U7 (Calcrete)	22,27	3,09	3,74	20,3	16,9	0,12	0,41
U6 (Calcrete)	23,08	4,11	3,8	18,3	16,9	0,22	0,53
U-6 (Soil)	47,1	8,31	8,5	15,2	1,21	0,31	1,11
U3 (Calcrete)	16,86	3,46	3,26	17,2	21,8	0,07	0,51
U1 (Soil)	50,36	10,96	9,18	6,33	0,75	0,13	1,37
A1 (Calcrete)	29,46	5,5	4,61	16,1	13,5	0,21	0,68
A2 (Soil)	51,55	10,72	8,37	7,2	0,93	0,18	1,33
A3 (Calcrete)	25,58	4,99	3,91	15	16,4	0,1	0,55
A5 (Soil)	51,41	9,95	8,12	9,21	0,61	0,18	1,32
A6 (Calcrete)	26,73	4,58	4,16	16,8	16,4	0,17	0,66
A7 (Soil)	49,26	9,41	8,53	12,1	0,92	0,3	1,35
A14 (Soil)	50,03	9,42	8,67	11,4	0,7	0,25	1,23
A15 (Calcrete)	31,03	5,58	5,03	15,2	13,6	0,17	0,71

Sample / Analyte	TiO_2	P_2O_5	MnO	Cr_2O_3	LOI	Sum
U13 (Recent soil)	0,3	0,12	0,08	0,031	36	99,7
U12 (Soil)	0,69	0,08	0,19	0,162	16	99,7
U11 (Soil)	0,69	0,04	0,16	0,173	19	99,8
U10 (Calcrete)	0,17	0,06	0,04	0,095	37	99,7
U7 (Calcrete)	0,23	0,05	0,06	0,137	32	99,6
U6 (Calcrete)	0,29	0,09	0,07	0,081	32	99,6
U-6 (Soil)	0,67	0,1	0,18	0,191	17	99,7
U3 (Calcrete)	0,28	0,12	0,08	0,029	36	99,6
U1 (Soil)	0,77	0,03	0,19	0,183	19	99,8
A1 (Calcrete)	0,38	0,1	0,09	0,108	29	99,6
A2 (Soil)	0,7	0,05	0,17	0,171	18	99,8
A3 (Calcrete)	0,32	0,07	0,08	0,098	33	99,7
A5 (Soil)	0,7	0,05	0,18	0,12	18	99,8
A6 (Calcrete)	0,33	0,1	0,09	0,092	30	99,6
A7 (Soil)	0,74	0,07	0,18	0,15	17	99,7
A14 (Soil)	0,69	0,06	0,18	0,178	17	99,7
A15 (Calcrete)	0,4	0,11	0,11	0,093	28	99,7

Table 7.3. Trace element concentrations in paleosols and calcretes of Karahamzalı Section (in ppm).

Sample / Analyte	**Ba**	**Be**	**Co**	**Cs**	**Ga**	**Hf**	**Nb**	**Rb**	**Sn**
U13 (Recent soil)	132	<1	25	1	4,8	1	5,8	17	<1
U12 (Soil)	224	<1	69	3	11	3	15	44	1
U11 (Soil)	206	<1	57	4	13	3	15	52	1
U10 (Calcrete)	140	<1	20	1	3,3	1	5,2	10	<1
U7 (Calcrete)	135	<1	31	1	4	1	5,6	12	<1
U6 (Calcrete)	177	<1	32	1	5,8	1	7,4	17	<1
U-6 (Soil)	196	<1	82	2	10	3	17	36	<1
U3 (Calcrete)	124	<1	28	1	4,7	1	5,8	17	<1
U1 (Soil)	198	1	68	4	13	3	19	56	1
A1 (Calcrete)	184	<1	39	1	6,5	1	9,4	24	<1
A2 (Soil)	188	<1	65	4	13	3	18	51	1
A3 (Calcrete)	178	<1	32	1	6,1	2	8,3	20	<1
A5 (Soil)	189	1	65	3	13	3	19	53	1
A6 (Calcrete)	168	<1	35	1	5,8	1	9,6	22	<1
A7 (Soil)	201	1	70	3	12	3	20	48	1
A14 (Soil)	213	<1	69	3	12	3	17	45	1
A15 (Calcrete)	167	<1	45	2	7,3	2	9,8	25	<1

Sample / Analyte	**Sr**	**Ta**	**Th**	**U**	**V**	**W**	**Zr**	**Y**
U13 (Recent soil)	292	0	1	1	43	0,5	38,7	8,7
U12 (Soil)	88,7	1	4	2	104	0,8	97,6	16
U11 (Soil)	87,6	1	5	1	100	1,1	108	17
U10 (Calcrete)	315	0	1	1	34	<0.5	28,3	5,9
U7 (Calcrete)	344	0	1	1	53	<0.5	33,6	6
U6 (Calcrete)	412	0	2	1	47	<0.5	46,3	11
U-6 (Soil)	124	1	5	1	95	0,6	111	12
U3 (Calcrete)	288	0	2	1	39	<0.5	41	7,9
U1 (Soil)	112	1	6	1	97	1,1	138	14
A1 (Calcrete)	358	1	3	1	58	0,5	65,8	14
A2 (Soil)	64,5	1	6	1	91	0,9	122	12
A3 (Calcrete)	387	1	3	1	45	<0.5	58,9	20
A5 (Soil)	64,7	1	5	2	91	0,9	126	15
A6 (Calcrete)	280	1	3	1	53	2	61,4	8,4
A7 (Soil)	70,8	1	5	2	98	0,8	129	14
A14 (Soil)	86,1	1	5	1	93	0,8	114	13
A15 (Calcrete)	174	1	4	1	57	<0.5	70,2	15

Table 7.4. REE concentrations in paleosols and calcretes of the Karahamzalı Section (in ppm).

Sample / Analyte	La	Ce	Pr	Nd	Sm	Eu	Gd	Tb	Dy	Ho	Er	Tm	Yb	Lu
U13 (Recent soil)	9	15	2	8	1,5	0	1,5	0,2	1	0,27	1	0,1	1	0,1
U12 (Soil)	18	38	4,5	17	3,3	1	3,2	0,4	3	0,56	2	0,2	1	0,2
U11 (Soil)	22	44	5,3	20	3,7	1	3,6	0,5	3	0,6	2	0,2	2	0,3
U10 (Calcrete)	6,4	11	1,4	6	1	0	1	0,2	1	0,17	0	0,1	0	0,1
U7 (Calcrete)	7	12	1,6	7	1,1	0	1,1	0,2	1	0,2	1	0,1	1	0,1
U6 (Calcrete)	13	18	2,8	11	1,9	1	1,8	0,3	2	0,36	1	0,2	1	0,2
U-6 (Soil)	17	37	3,9	16	2,9	1	2,7	0,4	2	0,46	1	0,2	1	0,2
U3 (Calcrete)	8,9	14	1,9	8	1,5	0	1,5	0,3	1	0,28	1	0,1	1	0,1
U1 (Soil)	23	46	5,3	22	3,9	1	3,4	0,6	3	0,56	2	0,2	2	0,2
A1 (Calcrete)	17	25	3,7	14	2,6	1	2,7	0,4	2	0,48	1	0,2	1	0,2
A2 (Soil)	22	44	5,1	19	3,5	1	3,2	0,5	3	0,49	1	0,2	1	0,2
A3 (Calcrete)	15	21	3,2	12	2,6	1	2,7	0,5	3	0,61	2	0,3	2	0,3
A5 (Soil)	23	44	5,2	20	3,7	1	3,4	0,6	3	0,57	2	0,2	2	0,2
A6 (Calcrete)	11	22	2,6	10	1,9	0	1,7	0,3	2	0,3	1	0,1	1	0,1
A7 (Soil)	21	42	4,9	19	3,5	1	3,2	0,5	3	0,54	2	0,2	1	0,2
A14 (Soil)	19	38	4,4	17	3,3	1	2,9	0,5	3	0,51	1	0,2	1	0,2
A15 (Calcrete)	19	23	3,5	14	2,5	1	2,4	0,4	2	0,46	1	0,2	1	0,2

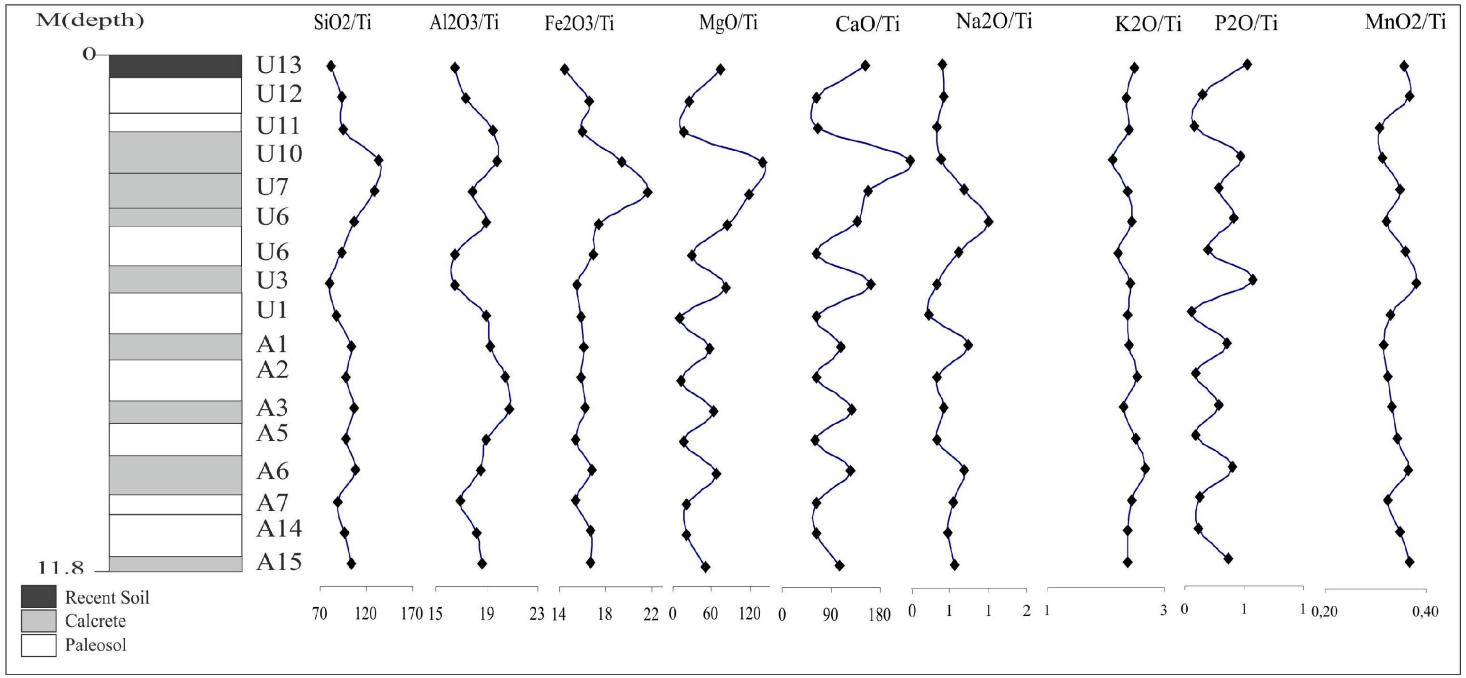

Figure 7.1. Ti-normalized major oxide values of Karahamzalı samples.

U/Th, on the other hand, shows very dramatic shifts, especially in the surficial calcrete levels. Th, which is expected to be leached during pedogenesis, has a low concentration, leading to a high U concentration in calcrete horizons.

Sm/Nd is constant throughout the section. The La/Ce ratio is depleted towards the top, supporting more mafic contribution to the region. Lastly, the Yb/Lu ratio differs than the others in that it depletes in calcerete horizons but increases in paleosol levels (Figure 7.5).

Rollinson (1993) explained the importance of trace elements in assessing the provenance Analysis of sedimentary rocks, therefore mentioned the study of Culler et al. (1988) in which La/Co, Th/Co, La/Sc and Th/Sc ratios are good indicators of felsic and mafic provenances. La and Th are more abundant in felsic igneous suites, on the other hand, Sc and Co are rich in mafic rocks. According to the information given above, the ratios are plotted against depth (Figure 7.5). La/Co and Th/Co ratios versus depth diagrams plot almost parallel trends, implying low concentration of La and Th with respect to Co meaning that mafic contribution from parent rock is greater than felsic contribution. Likely, La/Sc and Th/Sc ratios have very low concentrations pointing to a higher great amount of Sc incomparison with La and Th.

Additionally, a discrimination diagram of Roser and Korsch, (1988) is employed with certain fields for felsic, intermediate, mafic igneous provinces and quartzstone sedimentary provenance. The discrimination factors are calculated according to the formulas given in Rollinson (1993), page 211).

The data on this diagram shows that the provenance signature of the Karahamzalı section is on the border of intermediate igneous as well as within the mafic igneous provenances.

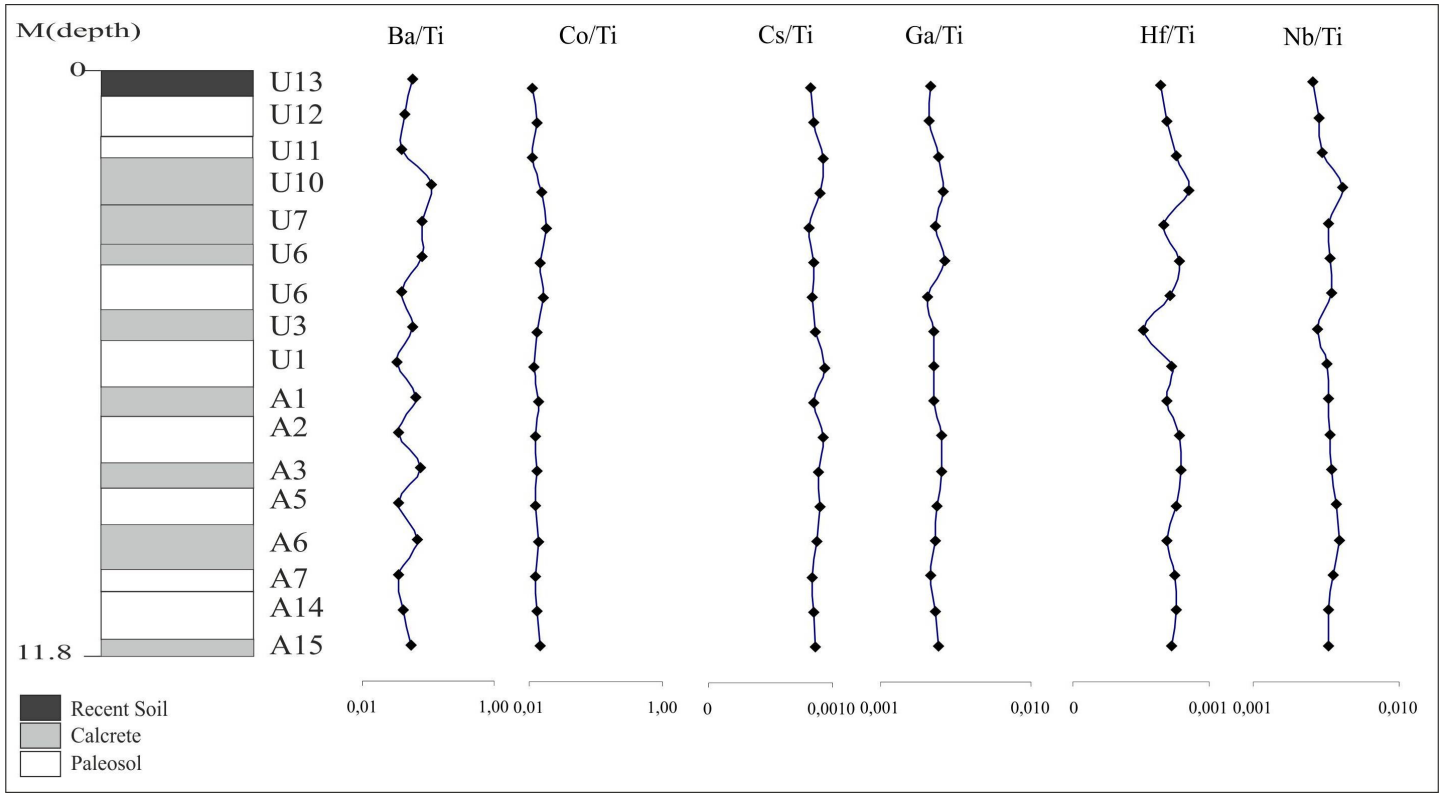

Figure 7.2. Ti-normalized trace element values of Karahamzalı samples

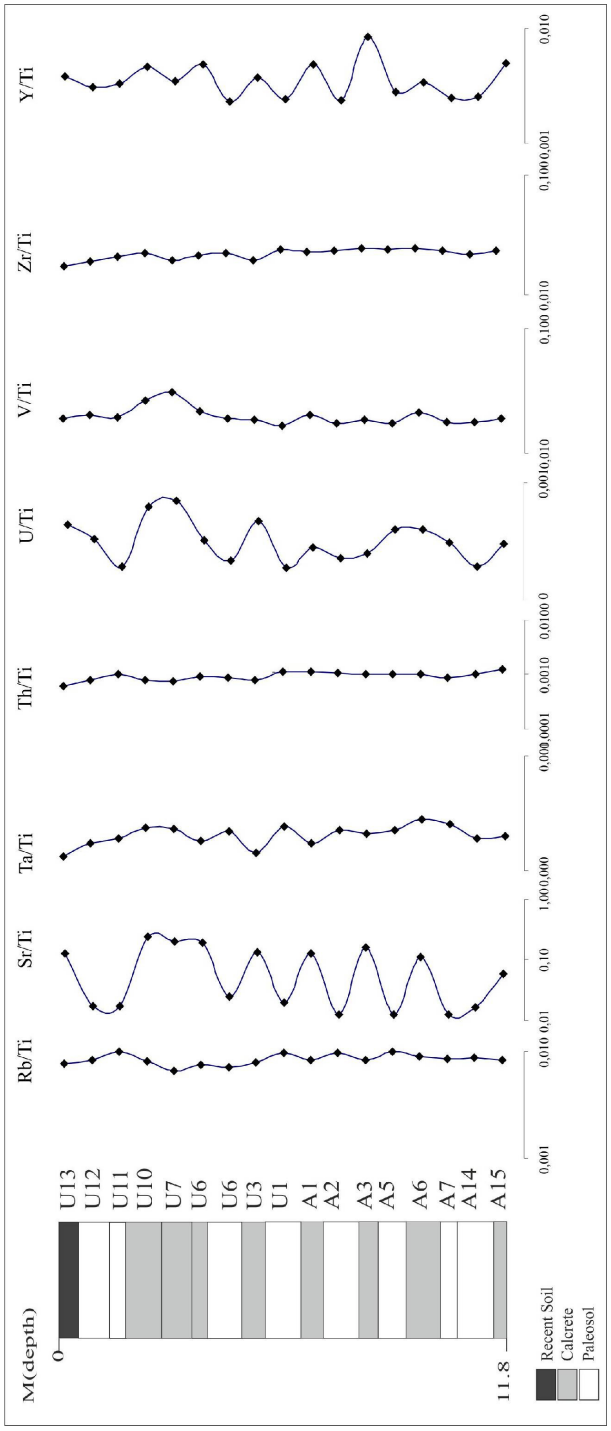

Figure 7.2 cont'd.

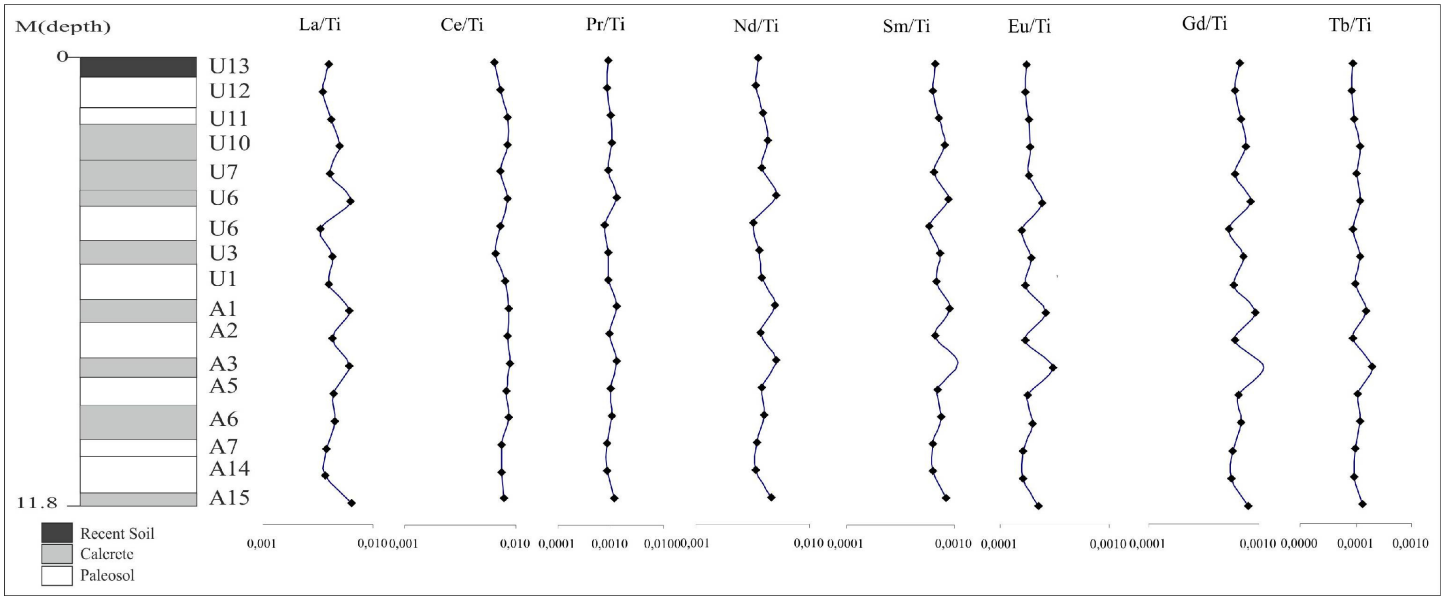

Figure 7.3. Ti-normalized REE values of Karahamzalı samples.

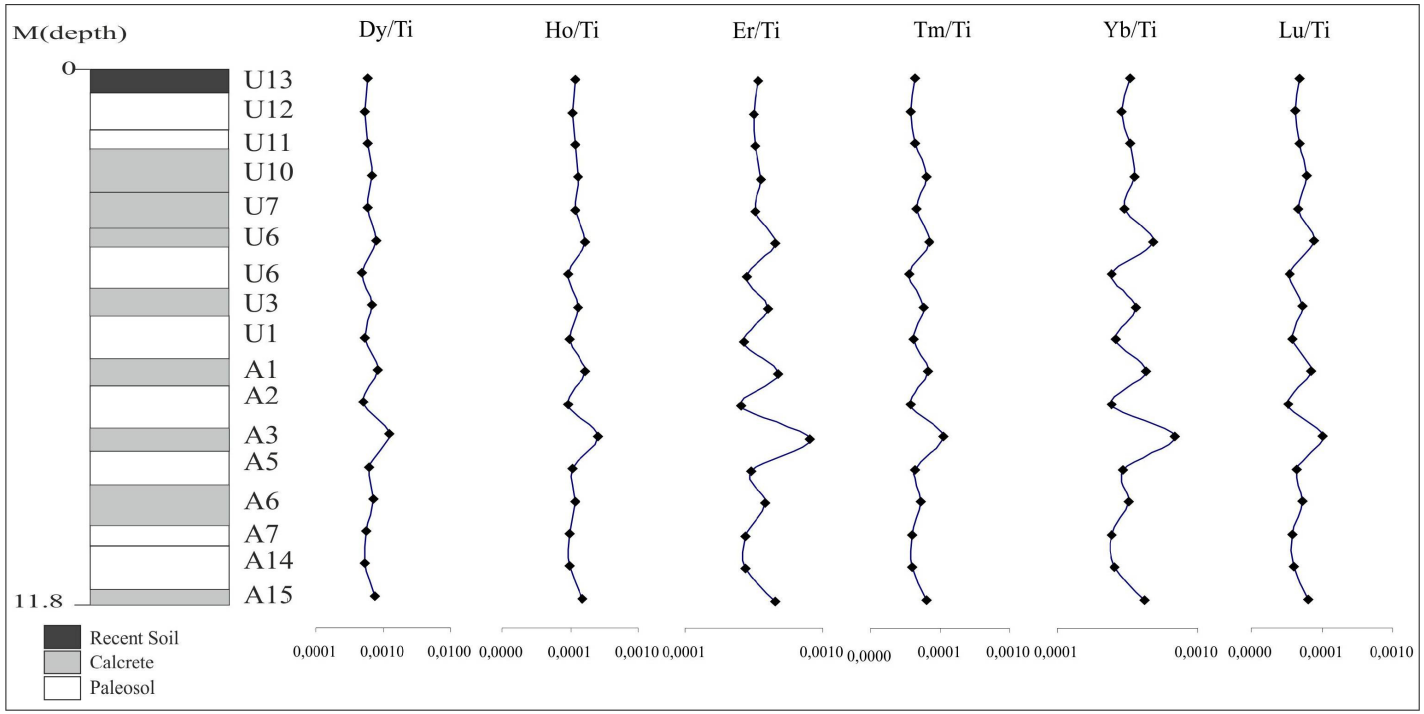

Figure 7.3 cont'd.

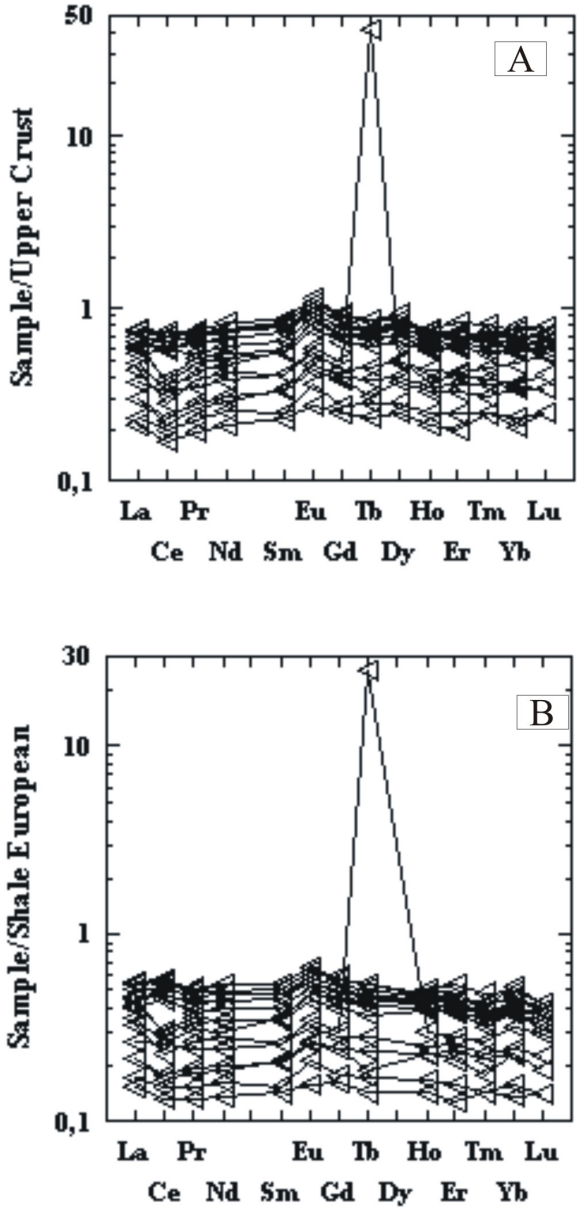

Figure 7.4. (a) Upper Crust and (b) Shale European normalized REE values of Karahamzalı samples.

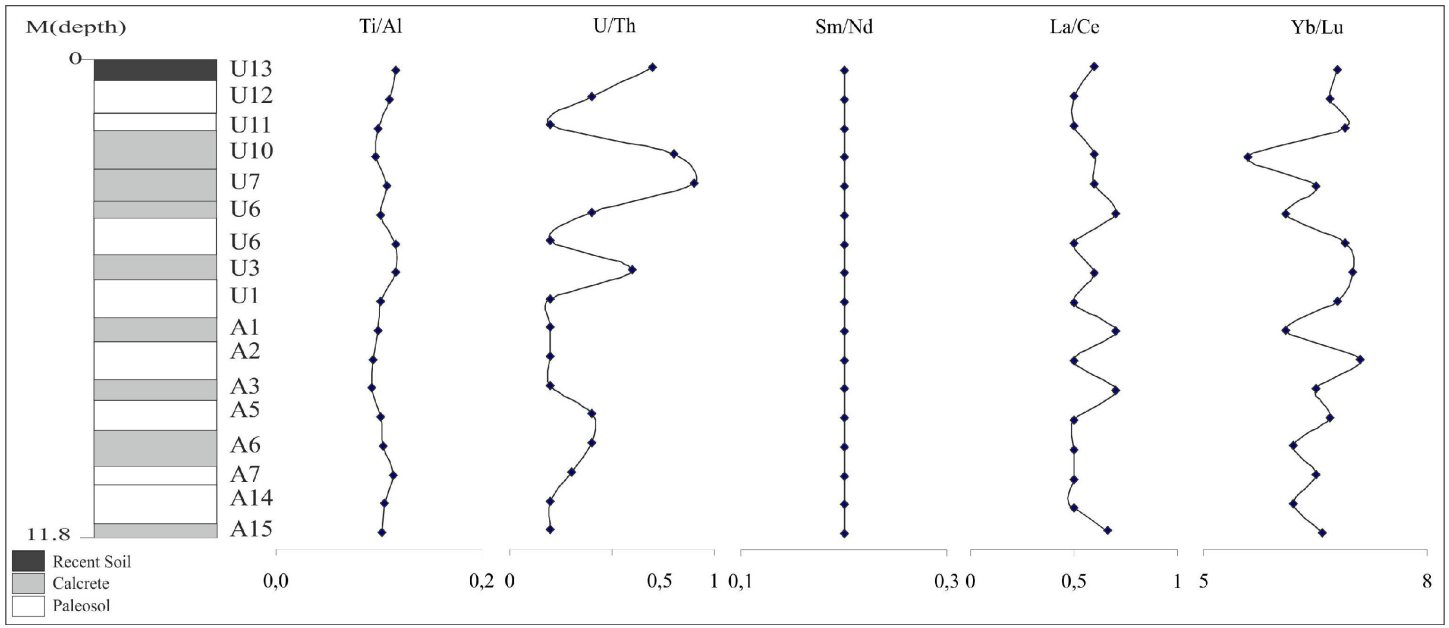

Figure 7.5. Trace element ratios of provenance estimation for Karahamzalı samples.

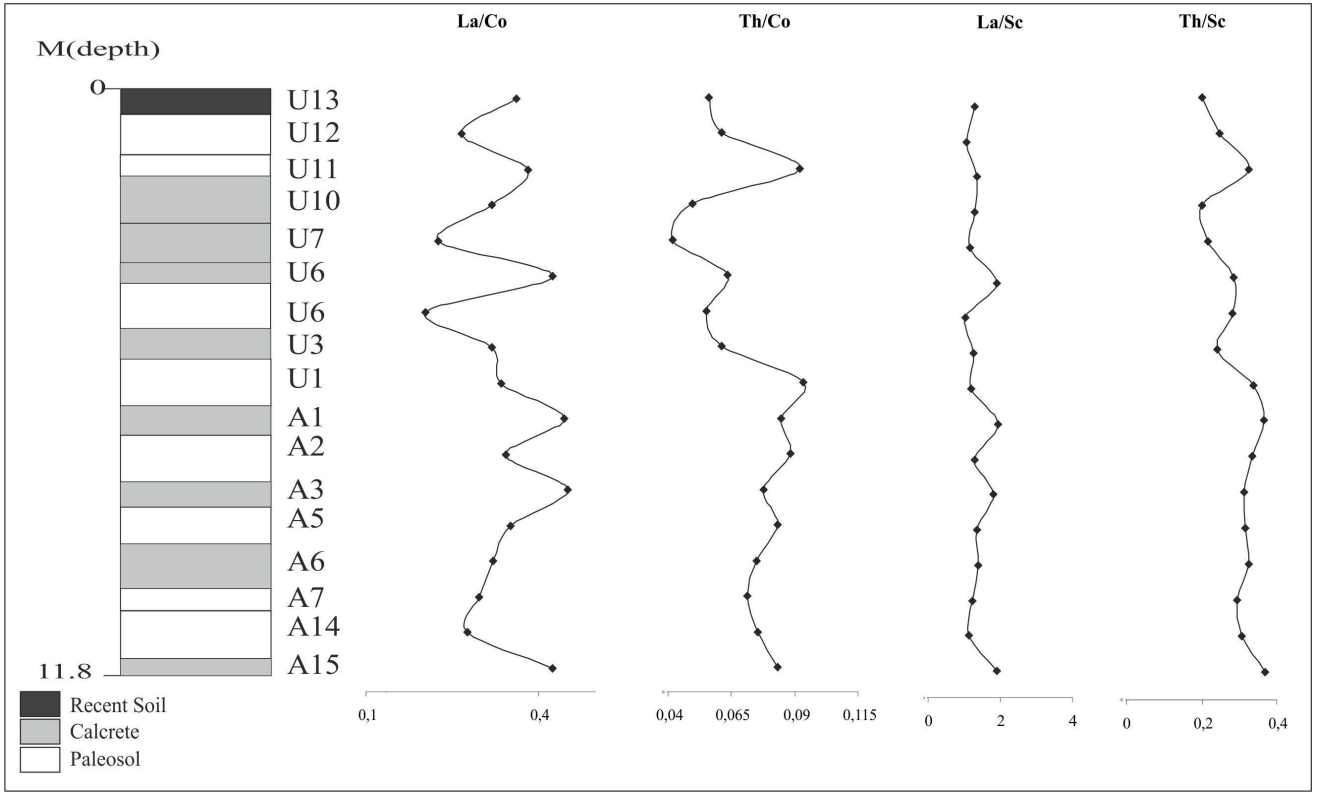

Figure 7.5. cont'd.

Based on the chemical analysis, some molecular weathering ratios are calculated. Salinization should reflect the preferential removal of sodium relative to potassium in the surface horizons. The Na_20/K_20 ratio of salinization ranges from 0.1 to 0.41 for the Karahamzalı samples. The increase towards the upper horizons is an evidence of evaporation indicating a consequent water movement in the paleosols. Salinization for the arid-climatic conditions shoul be greater than 1 however, in this case, it reaches almost 0.6 at maximum without passing a reference standard (Figure 7.6). Calcification reflected in the $(CaO + MgO/Al_20_3)$ ratio has values 0.6 at minimum and 15.9 at maximum. It is high in calcretes and low in paleosol levels throughout the section with increasing calcification values towards the surface (Figure 7.6). The other paramater is the clayeyness suggesting a clay accumulation rate varying from 0.14 to 0.22 which can be regarded as almost constant throughout the profile with a depletion trend towards the top of the section in calcrete horizons (Figure 7.6). The plot of relative base loss vs depth reflects the removal of mobile cations from the surface horizons and their accumulation at depth. Relative base loss values for Karahamzalı section range from 0.06 to 1.28 documenting the medium to high weathering of the paleosols and the leaching of carbonates throughout the section (Figure 7.6). Leaching values are consistent with the earlier studies in that it is high in paleosol levels and very low in calcrete levels. The values of leaching for the Karahamzalı Section ranges from 0.43 to 2.92. Normally leaching values are expected to be greater than 2 in well-drained soils with Na and K concentrations well correlated with the leaching trends. This the case for the Karahamzalı section since it is seasonally well-drained, the leaching values in paleosols are high. In arid conditions, the leaching values decrease leading to the precipitation of calcium and magnesium carbonates. To measure the degree of chemical weathering, a value can be obtained by calculating the chemical index of alteration (CIA) of the section in terms given by Nesbitt and Young (1982) using molecular proportions of some elements. The higher the value, the more intense is the weathering. CIA values of calcretes vary from 10.08 to 27.62, whereas those of the soils range from 73.42 to

82.97 for the Karahamzalı section. This suggests that paleosols are affected more than calcretes by weathering. Another measure for the chemical index of alteration is CIA-K which omits the K addition. This value ranges from 10.19 to 28.58 for calcretes and 80.70 to 92.6 for soils which are very similar to CIA values. The CIA and CIA-K versus depth diagrams plot paralel to each other. Considering 50 as CIA and CIA-K standard for paleosols, the studied paleosol samples are greater than 50, implying to a high degree of chemical weathering for paleosols and weak chemical alterations for calcretes. The Mg index is also used to assess the weathering affect on paleosols and is calculated as 12.3 to 27 for calcretes and 35 to 63.4 for paleosols, which are almost consistent with the CIA and CIA-K values. The base loss and leaching values through the section are well correlated with CIA, CIA-K and MgI values (Figure 7.7).

Weathering trends can be displayed on a Al_2O_3-CaO+Na_2O-K_2O (A-CN-K) triangular plot of Nesbitt and Young (1984; 1989). Rollinson (1993) summarized the trends on A-CN-K triangular diagram as follows: Initial stages of weathering form a trend paralel to the CN-A side of the diagram, whereas advanced weathering shows a marked loss in K_2O as compositions move towards the Al_2O_3 apex. The trend follow mixing lines representing the removal of alkalis and Ca in solution during the breakdown of first plagioclase and then potassium feldspar and ferromagnesian silicates. Deviations from such trends can be used to infer chemical changes resulting from diagenesis or metasomatism (Nesbitt and Young, 1984, 1989). Paleosols and their carbonates of the Karahamzalı section plot separate trend lines on the A-CN-K triangular diagram (Figure 7.7). Paleosols show a weathering trend line paralel to the CN-A side of the diagram. This, as mentioned before, implies to the early stages of weathering. Calcretes, on the other hand, plot a line paralel to the CN-A side of the diagram again, however, their compositions are very close to the Al_2O_3 apex of the diagram implying Na and Ca loss during the weathering stages (Figure 7.8). This is relevant for the advanced weathering conditions.

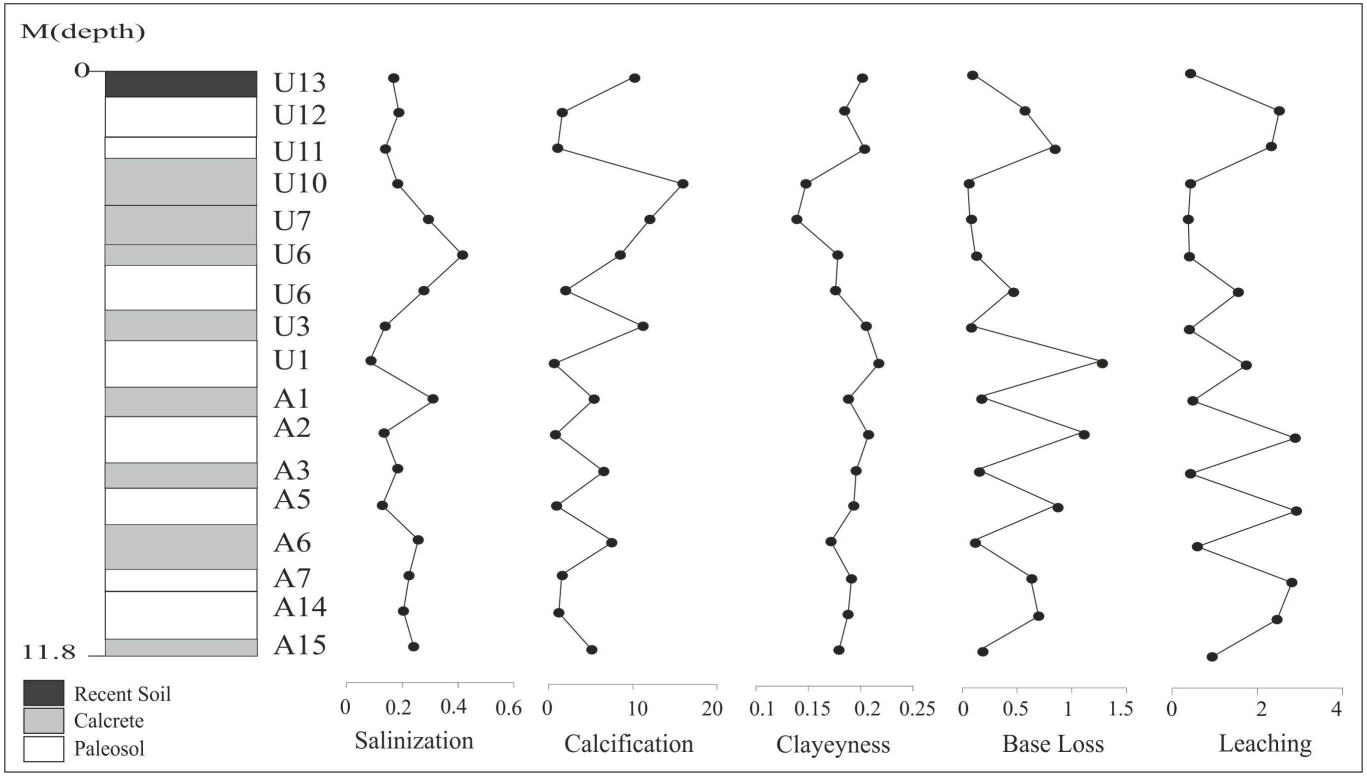

Figure 7.6. Molecular weathering ratios calculated for Karahamzalı samples.

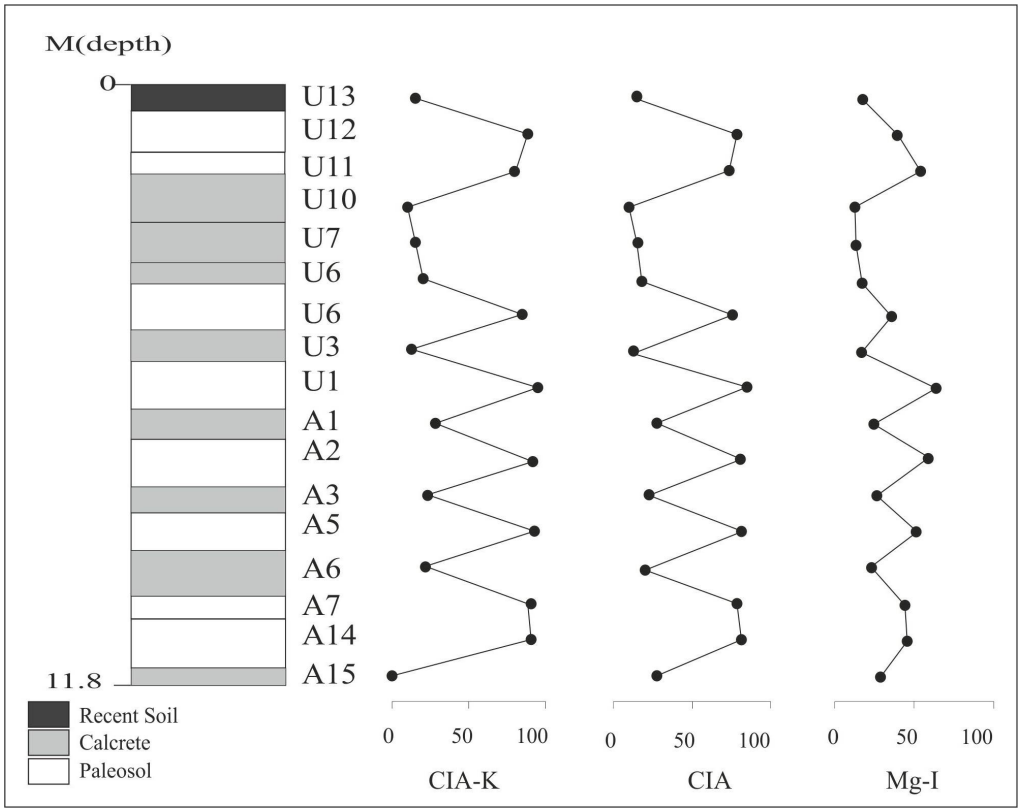

Figure 7.7.Chemical index of alteration values of Karahamzalı paleosols and carbonates.

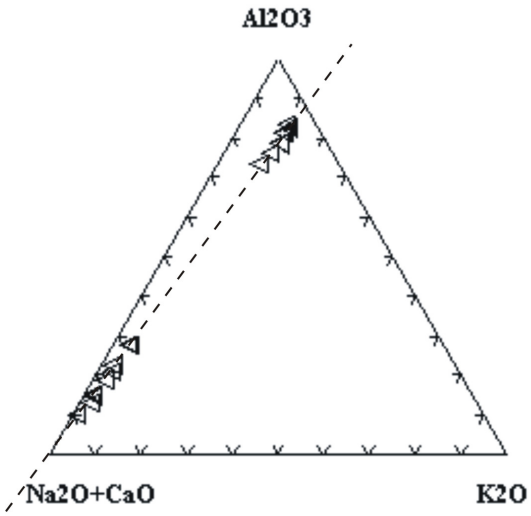

Figure 7.8. A-CN-K triangular plot of Nesbitt and Young (1984, 1989).

7.3. GEOCHEMISTRY OF BALA SECTION

The results of the whole rock geochemical analysis of paleosols and their carbonates in Bala Section are listed in Table 7.5, 7.6 and 7.7. Major and trace element contents are given in weight percentages and in parts per million, respectively. The molecular weathering ratios and chemical index of alteration values are calculated according to the given formulas in part 7.1. Due to the resistancy for mobilization, Ti is accepted as a normalizing element for major oxides and Al for trace element content within the Bala section. The values are then plotted against depth to reveal the changes.

SiO_2 values of the Bala Section range about 50% for paleosols where the C1 and C2 surface calcretes range in lower amounts from 9.18% to 24%, respectively (Table 7.5). Ti-normalized SiO_2 variation diagram shows that the amount is relatively higher down to the section showing an enrichment between B9-B14 and

B16-B18 samples (Figure 7.9), whereas it is relatively constant in the upper horizons. Knowing the positive correlation between the amount of SiO_2 and the leaching conditions, it can be concluded that leaching has affected only the upper horizons, while the bottom levels show the accumulation of silica which can be due to the increasing quartz and clay mineral contents.

The contents of Fe_2O_3 vary in a narrow range except the C2 calcrete level in the Bala section. It is approximately between 4% to 6.64% in the paleosols. These values show that Fe is almost stable in amount with slight variations in paleosol levels. It is also recognizable that in the Ti-normalized Fe variation diagram, Fe_2O_3 composition shows an enrichment at the bottom of the section positively correlating with the SiO_2 enriched levels throught the section. It is, on the other hand, relatively constant in the upper horizons with a slight enrichment in the surficial calcretes (Figure 7.9).

The MgO contents in the Bala section samples range from 2.36% to 6.18 where the C2 calcrete has the lowest content (0.98%). Compared to the Karahamzalı section, dolomite is not present in the mineral assemblages of the paleosols and their carbonates in the Bala section. Therefore, the MgO values are normally expected to be lower than that of the Karahamzalı section. Like silica and iron, MgO also shows an increasing pattern at the bottom of the section and nearly constant values towards the upper parts of the section (Figure 7.9).

CaO values of the paleosols and their Carbonates in the Bala section show an increasing pattern towards the upper part as expected in such conditions (Figure 7.9). In the paleosol levels of the Bala section, the CaO values range from 7% to 14%, however it increases in the surface horizons with the C1 calcrete having 34.01% and C2 calcrete having 47.61% CaO contents. Close to the surface, the B2 paleosol level contains 21.17% CaO confirming the occurrence of the Ca accumulation process of the B horizon.

As expected, despite the low contents towards the surface horizons, Na and K show almost constant values from the middle to the top of the section, while at the bottom an increase is determined similar to the Na and Mg. Na_2O contents are the lowest in the calcrete level with 0.22% and the highest in the paleosol level with 3.04%. Similarly, K_2O has the same tendency through the section with a narrow range throughout the paleosol. It is the lowest in surface calcretes (0.26%) and the highest in the paleosol with 1.96% (Figure 7.9).

Being one of the immobile elements in the mineral structure during the process of weathering, AI_2O_3 is expected to be constant in the weathered horizons and higher in the accumulation zone. The content of aluminum throughout the section varies from 2.65% to 16% and increases in the B horizons of the paleosols. Increase in Al is is also correlated with the high clay mineral contents. Ti-normalized concentration of Al_2O_3 follows almost the same trend with that of SiO_2, MgO, Na_2O and K_2O (Figure 7.9). The P_2O_5 contents – indicators of biological activity - are very low in the Bala section, similar to the Karahamzalı section. The amounts vary from 0.07 to 0.21 within a narrow range. The Ti-normalized diagram of P_2O_5 plots exactly the same trend with CaO as in the Karahamzalı section that the P contents are higher in the calcerete levels implying to favourable conditions of the arid environment to increased biological activity (Figure 7.9). MnO contents are very low throughout the Bala section with a slight increase in the C1 level and a constant variation at the middle and bottom. This trend is positively correlated with the Ti-normalized Fe_2O_3 diagram. It has a composition between 0.021% and 0.7% in Bala section (Figure 7.9).

Ti, the normalizing factor of the major oxides during varies from 0.1% for the surface calcretes to 0.73% for the paleosols. The variation of Ti is similar to the Karahamzalı section with less than 1% content and almost with a constant trend throughout the section. Loss on ignition (LOI) amounts ranges between 9.6% to 21.3% through the Bala section (Figure 7.9).

Table 7.5. Weight percentages of common oxides in paleosols and calcrete levels of the Bala Section.

Sample/Analyte	SiO_2	Al_2O3	Fe2O3	MgO	CaO	Na2O	K2O	TiO2
C2 (Calcrete)	9,18	2,65	1,4	0,98	47,61	0,22	0,26	0,1
C1 (Calcrete)	24	6,91	4,3	2,36	34,01	0,23	0,77	0,32
B1 (Soil)	55,57	12,54	6,03	4,48	3,47	0,77	1,63	0,66
B2 (Soil)	38,92	8,76	4	2,68	21,17	1,07	1,15	0,46
B3 (Soil)	51,41	12,23	6,55	3,77	6,5	0,79	1,94	0,74
B4 (Soil)	49,27	11,68	6,22	3,7	7,22	0,72	1,82	0,7
B5 (Soil)	54,72	12,26	6,41	3,77	3,76	1,14	1,78	0,71
B6 (Soil)	54,35	12,5	6,64	4,02	4,25	0,87	1,96	0,73
B7 (Soil)	49,94	11,92	6,28	3,78	7,52	0,76	1,83	0,71
B8 (Soil)	47,3	11,64	6,1	3,75	10,16	0,76	1,67	0,7
B9 (Soil)	47,72	11,42	6,32	4,13	9,12	1,08	1,56	0,63
B10 (Soil)	51,09	9,77	6,54	6,18	9,77	1,9	0,97	0,46
B11 (Soil)	55,04	15,98	4,54	3,33	6,09	3,04	1,13	0,42
B12 (Soil)	47,52	9,4	6,07	5,61	13,52	1,71	0,9	0,47
B13 (Soil)	49,34	9,78	5,18	4,51	12,94	1,55	1,19	0,45
B14 (Soil)	52,68	14,88	4,84	3,72	8,15	2,84	1,37	0,39
B15 (Soil)	52,87	13,14	5,77	3,02	7,39	1,47	1,59	0,7
B16 (Soil)	54,84	12,84	5,81	4,09	7,4	2,05	1,4	0,53
B17 (Soil)	56,08	12,97	5,44	3,97	7	2,44	1,39	0,48
B18 (Soil)	54,87	12,69	5,75	3,81	7,45	2,08	1,4	0,54

Sample/Analyte	P2O5	MnO	Cr2O3	Ni	Sc	LOI	Sum
C2 (Calcrete)	0,07	0,021	0,02	63,2			
C1 (Calcrete)	0,08	0,7	0,065	127,6			
B1 (Soil)	0,07	0,11	0,092	322	14	14,3	99,8
B2 (Soil)	0,12	0,09	0,054	232	10	21,3	99,8
B3 (Soil)	0,13	0,13	0,09	402	16	15,5	99,8
B4 (Soil)	0,12	0,12	0,075	367	15	18,1	99,8
B5 (Soil)	0,11	0,13	0,097	376	16	14,8	99,8
B6 (Soil)	0,12	0,13	0,091	410	16	14,1	99,8
B7 (Soil)	0,13	0,12	0,074	366	15	16,7	99,8
B8 (Soil)	0,13	0,12	0,063	388	15	17,3	99,8
B9 (Soil)	0,13	0,12	0,078	352	17	17,4	99,8
B10 (Soil)	0,12	0,12	0,168	537	15	12,6	99,7
B11 (Soil)	0,1	0,16	0,052	406	9	9,7	99,7
B12 (Soil)	0,13	0,15	0,123	453	16	14,1	99,8
B13 (Soil)	0,11	0,09	0,105	376	13	14,5	99,8
B14 (Soil)	0,1	0,15	0,076	399	12	10,4	99,7
B15 (Soil)	0,21	0,13	0,048	216	13	13,4	99,7
B16 (Soil)	0,14	0,11	0,071	330	13	10,4	99,7
B17 (Soil)	0,14	0,11	0,084	332	12	9,6	99,7
B18 (Soil)	0,14	0,1	0,079	323	13	10,8	99,7

Table 7.6. Trace element concentrations in paleosols and calcretes of Bala Section (in ppm).

Sample	Ba	Be	Co	Cs	Ga	Hf	Nb	Rb	Sn
B1 (Soil)	340	1	26,1	5,3	13,5	3,6	14,6	67	2
B2 (Soil)	404	1	18,9	2,4	9,2	3	10,5	37,6	<1
B3 (Soil)	352	2	29,1	4,1	12,9	4	15	67,4	1
B4 (Soil)	332	<1	28,1	4,1	12	3,3	13,7	64	2
B5 (Soil)	384	2	29,5	3,8	13	4,1	14,3	61,3	1
B6 (Soil)	537	2	31,5	4,4	12,1	4,1	14,9	68,6	1
B7 (Soil)	345	1	29	4,4	12,7	3,5	14,9	64,4	2
B8 (Soil)	369	1	29,5	4,2	12,4	4,1	13,9	58,3	1
B9 (Soil)	350	1	29,7	3,8	10,7	3,4	12,5	53,7	1
B10 (Soil)	465	<1	41,7	1,2	9,5	2,1	8,9	26,8	<1
B11 (Soil)	1324	<1	19	1,6	14,1	5,7	11,6	26,8	1
B12 (Soil)	413	<1	33,8	1,1	9,1	2,3	8,8	24,2	<1
B13 (Soil)	418	1	31	2	9,8	2,9	8,7	36,5	<1
B14 (Soil)	1022	2	23,1	1,8	13,3	5,3	12,4	31,9	1
B15 (Soil)	645	2	23,4	3,8	13,9	4,1	16,1	52,2	1
B16 (Soil)	719	1	26,7	2,4	12,7	3,7	13,1	40,8	1
B17 (Soil)	767	1	25,2	1,8	12,3	3,6	13,7	36,9	1
B18 (Soil)	701	1	24,9	2,7	12,9	3,3	14,3	40,9	1

Sample	Sr	Ta	Th	U	V	W	Zr	Y
B1 (Soil)	186,9	0,8	8,9	2,2	132	2,1	155,5	18,1
B2 (Soil)	239,8	0,6	6,1	1,2	75	11	103,7	14,6
B3 (Soil)	235,4	0,8	9,8	1,7	100	2	142,8	17,3
B4 (Soil)	214,7	0,8	9,3	1,8	98	1,7	133,6	17,9
B5 (Soil)	223,3	0,9	8,8	1,6	95	3,7	136,7	13
B6 (Soil)	200,4	0,9	8	1,8	96	2	145,8	16,7
B7 (Soil)	244,4	1	9	1,8	100	2,1	134	18,5
B8 (Soil)	285,7	0,9	9,6	1,8	101	1,9	153,9	17,9
B9 (Soil)	263	0,7	7,8	1,6	102	1,8	123,3	17,8
B10 (Soil)	314,5	0,5	5,4	1,3	103	2,3	87,4	13,1
B11 (Soil)	555,5	1,5	14,3	1,2	57	0,9	186,7	9,7
B12 (Soil)	341,6	0,5	4,6	1,4	108	1,7	101,8	16,2
B13 (Soil)	295,4	0,6	6,2	1,3	92	1	103,3	12,5
B14 (Soil)	544,5	1,3	13,4	1,6	72	1,5	185,1	11
B15 (Soil)	375,5	1	10,1	2,1	94	1,7	153,8	21,4
B16 (Soil)	363,9	0,9	7,9	1,7	82	2,2	142,1	14,8
B17 (Soil)	383	0,9	8,3	1,6	76	3	138,4	13,8
B18 (Soil)	371,5	1	9,1	1,5	83	2,6	135,2	14,8

Table 7.7. REE concentrations in paleosols and calcrets of Bala Section (in ppm).

Sample	La	Ce	Pr	Nd	Sm	Eu	Gd	Tb	Dy	Ho	Er	Tm	Yb
B1 (Soil)	26,3	55,7	5,85	20,2	3,79	0,99	3,04	0,54	2,86	0,63	1,72	0,26	1,81
B2 (Soil)	26,2	42,2	4,83	18,2	3,09	0,78	2,62	0,4	2,25	0,46	1,23	0,19	1,25
B3 (Soil)	28,1	58,4	6,04	21,8	4,05	1,03	3,61	0,57	3,17	0,63	1,69	0,28	1,68
B4 (Soil)	29,3	57,1	6,08	22,5	4,09	1,08	3,69	0,59	3,11	0,62	1,8	0,29	1,76
B5 (Soil)	24,4	56,3	5,21	18,5	3,45	0,85	2,76	0,45	2,34	0,5	1,33	0,19	1,37
B6 (Soil)	28,3	61,4	6,02	21,4	4,11	1,03	3,44	0,56	2,98	0,61	1,61	0,27	1,73
B7 (Soil)	31,1	61,4	6,54	23,9	4,38	1,1	3,74	0,58	3,24	0,62	1,83	0,29	1,82
B8 (Soil)	28	58,3	6,09	23,2	4,17	1,05	3,52	0,58	3,21	0,62	1,69	0,29	1,8
B9 (Soil)	27,3	54,8	5,79	21,7	3,96	1,02	3,5	0,56	3,07	0,64	1,73	0,27	1,7
B10 (Soil)	20,1	38,5	3,95	13,7	2,46	0,72	2,32	0,4	2,1	0,45	1,29	0,22	1,32
B11 (Soil)	30,7	87,4	4,76	15,6	2,19	1,05	1,94	0,29	1,54	0,32	0,95	0,16	1,01
B12 (Soil)	21,6	38,5	4,45	15,9	3,11	0,85	2,83	0,47	2,74	0,57	1,51	0,24	1,68
B13 (Soil)	19,6	36,7	3,91	13,9	2,79	0,72	2,36	0,37	2,14	0,43	1,29	0,19	1,28
B14 (Soil)	31,7	75,3	5,36	16,6	2,61	1,03	2,09	0,35	1,92	0,39	1,09	0,2	1,33
B15 (Soil)	38	70,2	7,36	26	4,49	1,22	3,79	0,64	3,41	0,69	2,04	0,31	2,07
B16 (Soil)	30,1	57,6	5,8	19,6	3,51	0,94	2,83	0,47	2,58	0,52	1,52	0,22	1,57
B17 (Soil)	31,3	55,6	5,88	19,5	3,35	0,93	2,69	0,44	2,2	0,48	1,43	0,21	1,44
B18 (Soil)	30,8	57,5	5,84	20,5	3,55	0,94	2,92	0,48	2,69	0,53	1,47	0,24	1,53

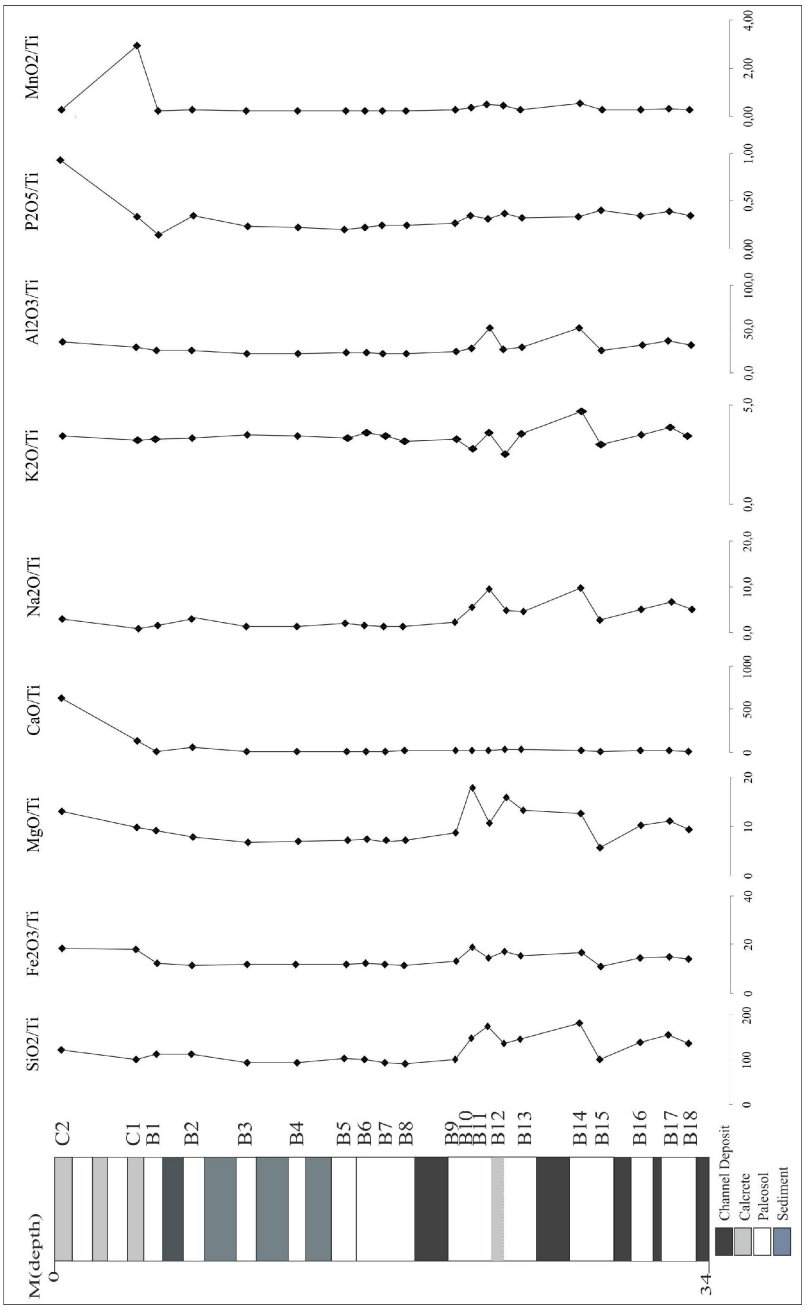

Figure 7.9. Ti-normalized major oxide values of Bala samples

In this case, Al has been used as an element for normalization for trace element contents to reveal the weathering intensity in the Bala section. Al-normalized variations of trace elements are plotted with respect to depth (Figure 7.10). Trace element contents of Cs, Ga, Nb and Hf show a parallel trend with depth, nearly constant at the top and the bottom of the section with enrichments between B6-B8 and B9 levels. Ba, Sr, Ta, Th, U and Zr are positively correlated with each other in increases recorded in the accumulation zones of the paleosols (Figure 7.10). V and Y are almost constant like Co, implying to the presence of a constant mafic content through the section. The greatest variability is measured for all elements except Co in the B8 level which is considered to be under the zone of accumulation and close to the C horizon of the paleosol. As accepted to be an immobile phase during weathering, Al is employed to show REE tendecies with respect to weathering. Rare earth elements, as expectedly, plot almost parallel trends in depth versus diagrams (Figure 7.11) They show enrichments at the same levels of B6-B7 and B10 with the other trace elements and depletions at the same horizon of B8 through the section. All of them remain nearly constant in surface levels. Concerning LREE, Sm is rather constant through the section when compared with the other REE, while still showing a slight enrichement at the B10 horizon. The major negative shift in REE concentrations versus depth diagrams is recorded in the B8 level for almost all LREE (Figure 7.11). However, HREE do not show such a negative shift in the B8 level of the Bala section. Shale-European and Upper Crust normalized REE patterns of Bala samples are plotted in Figure 7.12. They are different than that of the Karahamzalı section. The Shale-European normalized diagram shows that HREE are relatively depleted compared to LREE along with a positive Eu anomaly (Figure 7.12). The Upper crust normalized diagram reveals a positive anomaly in Eu with a depletion pattern of HREE.

Trace element concentrations in sediments result from the competing influences of the provenance, weathering, diagenesis, sediment sorting and the aqueous geochemistry of the individual elements (Rollinson, 1993). The highest

concentrations of trace elements were found in clay rich sediments. Thus, trace elements, as mentioned before, can be used to infer the geochemical processes and the sedimentary provenance. To reveal the provenance conditions of the Bala paleosols, the ratios of Ti/Al, U/Th, Sm/Nd, La/Ce and Yb/Lu are employed (Figure 7.13). Additionally the ratios of La/Sc, Th/Sc, La/Co and Th/Co are calculated since they are also the indicators of provenance (Rollinson, 1993).

The Ti/Al ratio versus the depth diagram shows constant values at the top, but reflect major depletions in the B11 and B15 levels. U/Th also plots parallel to Ti/Al diagram, showing a slight increase towards the top of the section. High U/Th ratios were determined in the B12 horizon, with visible carbonate accumulation in hand specimens. Sm/Nd is almost constant throughout the section with slight depletions at B11 and enrichment in B12. The La/Ce versus depth diagram has parallel trends with Sm/Nd but shows slight enrichment at the B2 surface level. Additionally, the Yb/Lu ratio is very similar to the Sm/Nd plot.

La/Co, Th/Co, La/Sc and Th/Sc versus depth diagrams plot parallel trends, while revealing opposite enrichment patterns to the previous provenanace ratios. They all present enrichment in B11 and B15 levels and depletion at B10, B12 and B13 levels. The enrichments can be correlated with the felsic contribution from the provenance and the depletion trends may imply to a the more mafic contribution from the parent rock. Since Th is easily leached away from the surficial horizons during weathering, The Th/Co versus depth diagram shows a constant pattern towards the top of the section. As applied to the Karahamzalı samples, a discrimination diagram of Roser and Korsch, (1988) is also employed to the Bala section. The discrimination factors are calculated according to the formulas given in Rollinson (1993, page 211). All diagrams show that the provenance signature of the Bala section is exactly within the area of a mafic igneous province and partly on quartzose sedimentary province area.

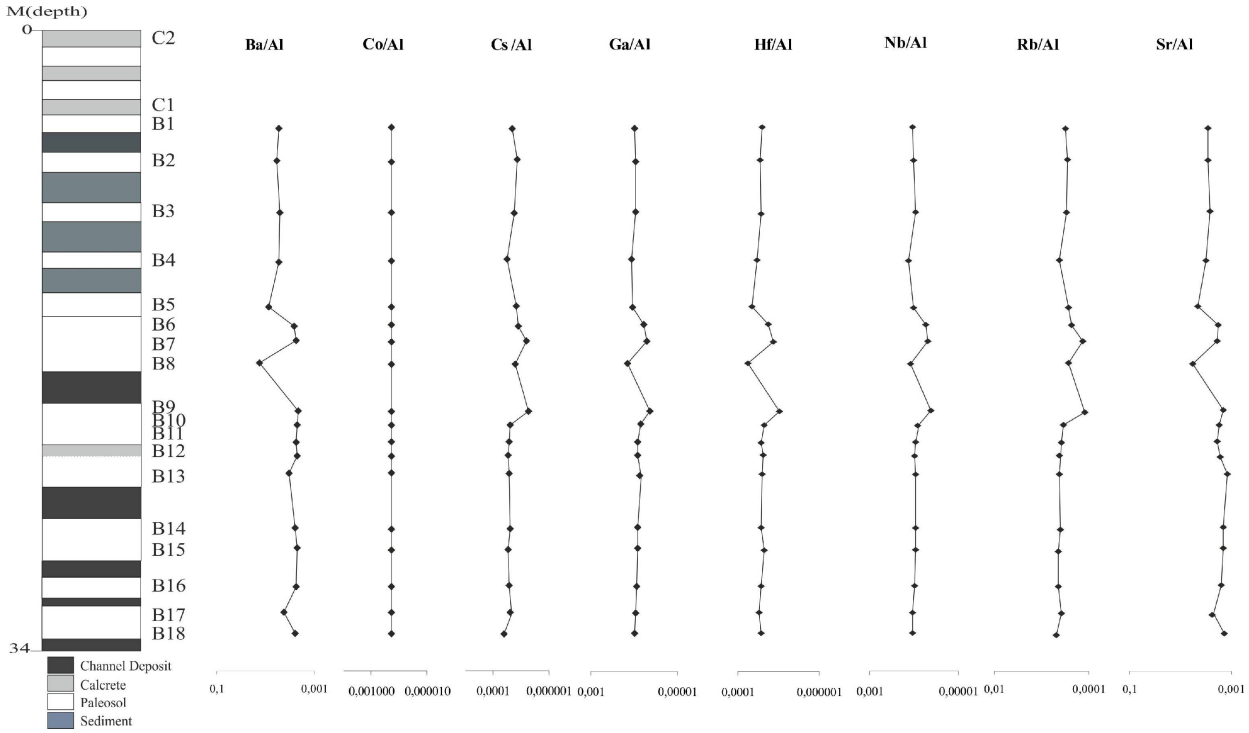

Figure 7.10. Al-normalized trace element values of Bala samples.

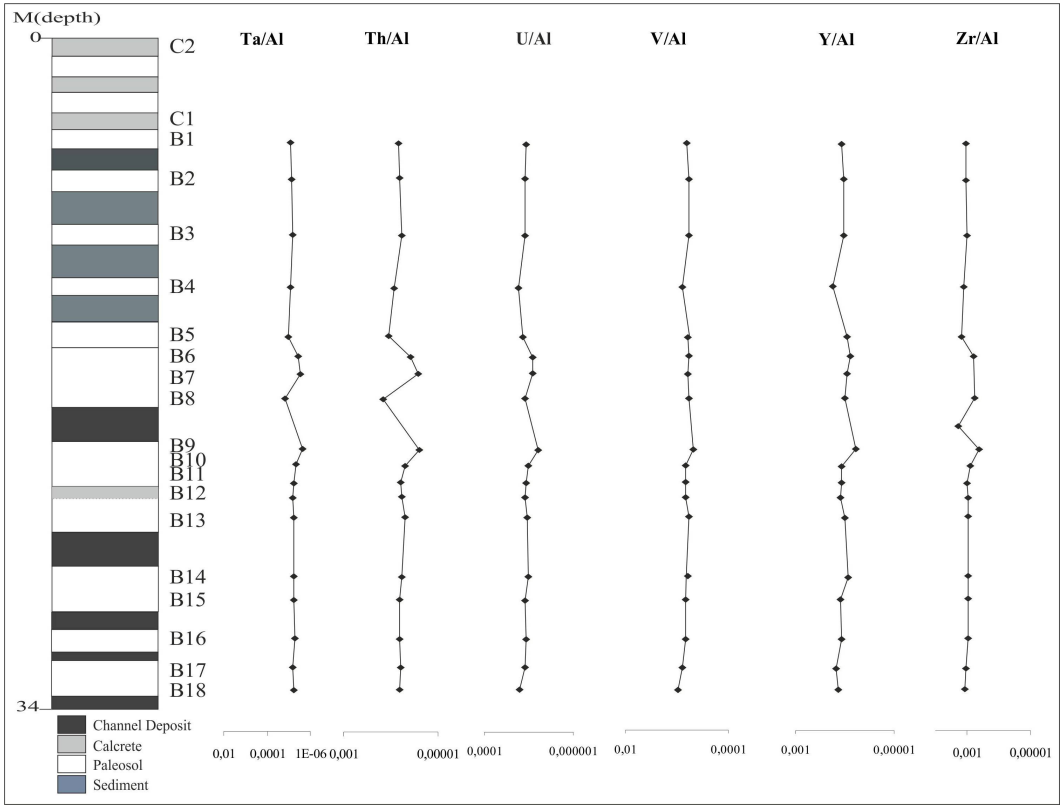

Figure 7.10 cont'd.

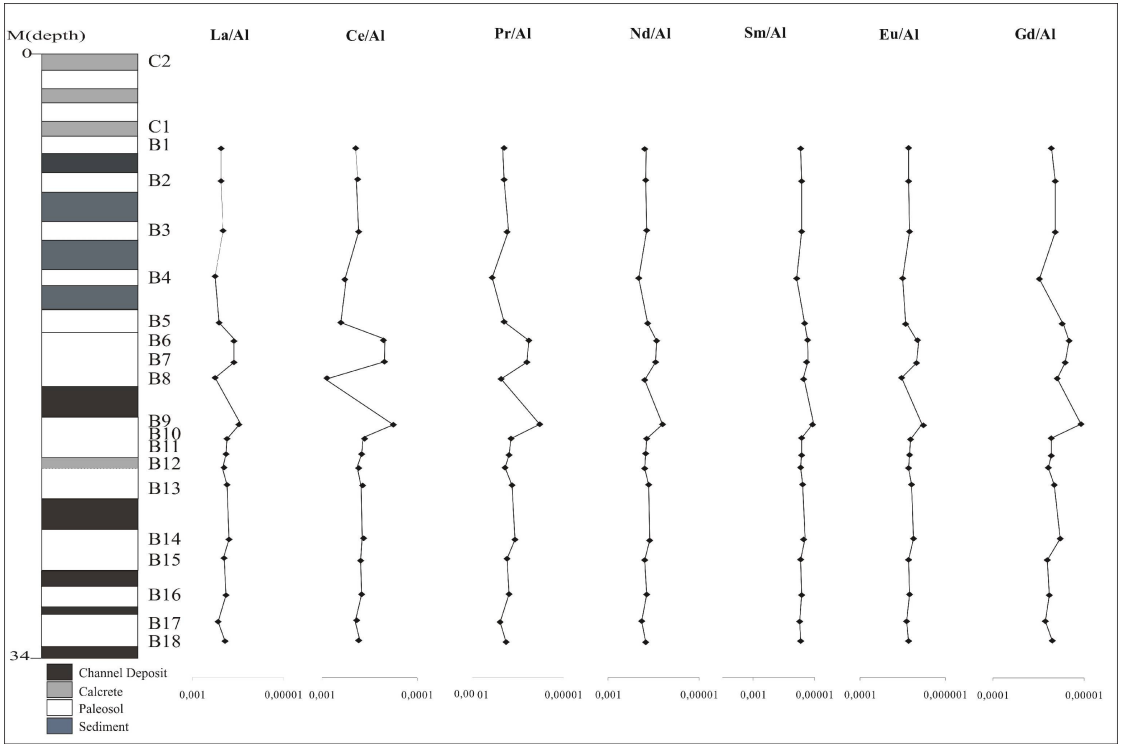

Figure 7.11. Al-normalized REE values of Bala samples.

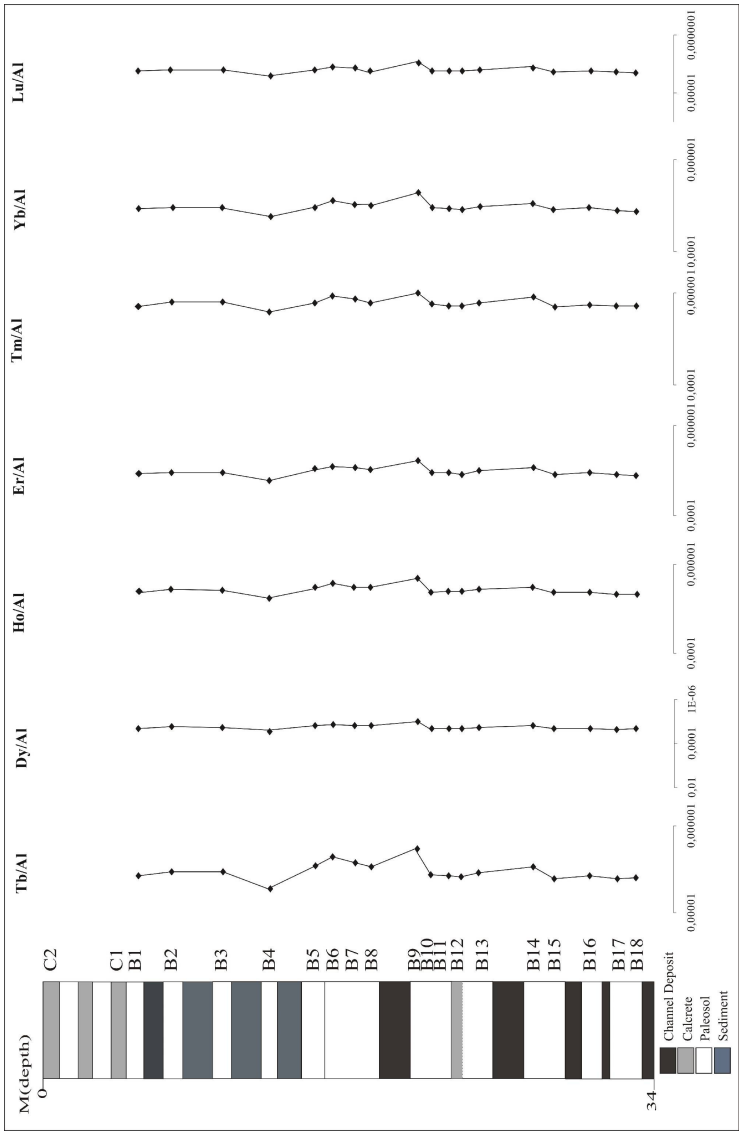

Figure 7.11 cont'd.

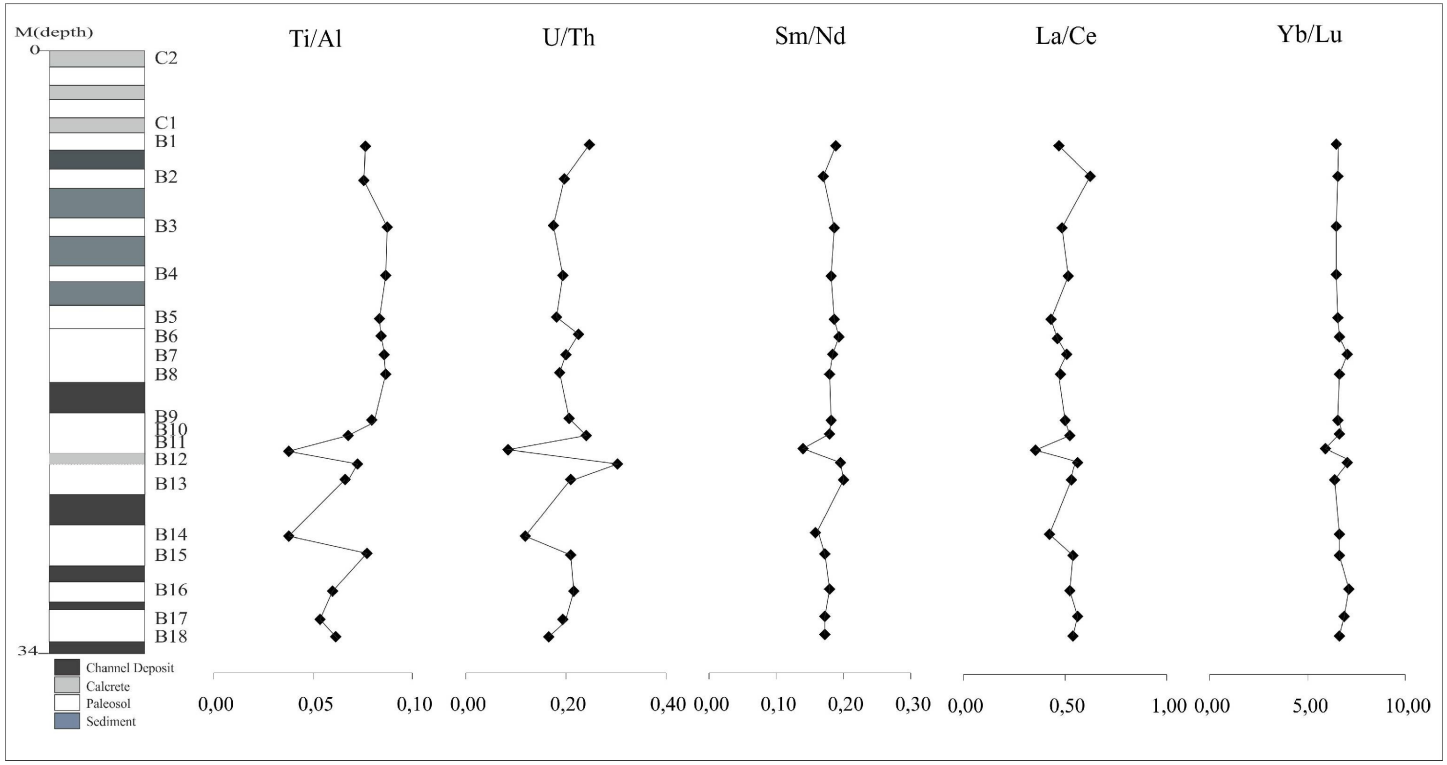

Figure 7.12. Trace element ratios of provenance estimation for Bala samples.

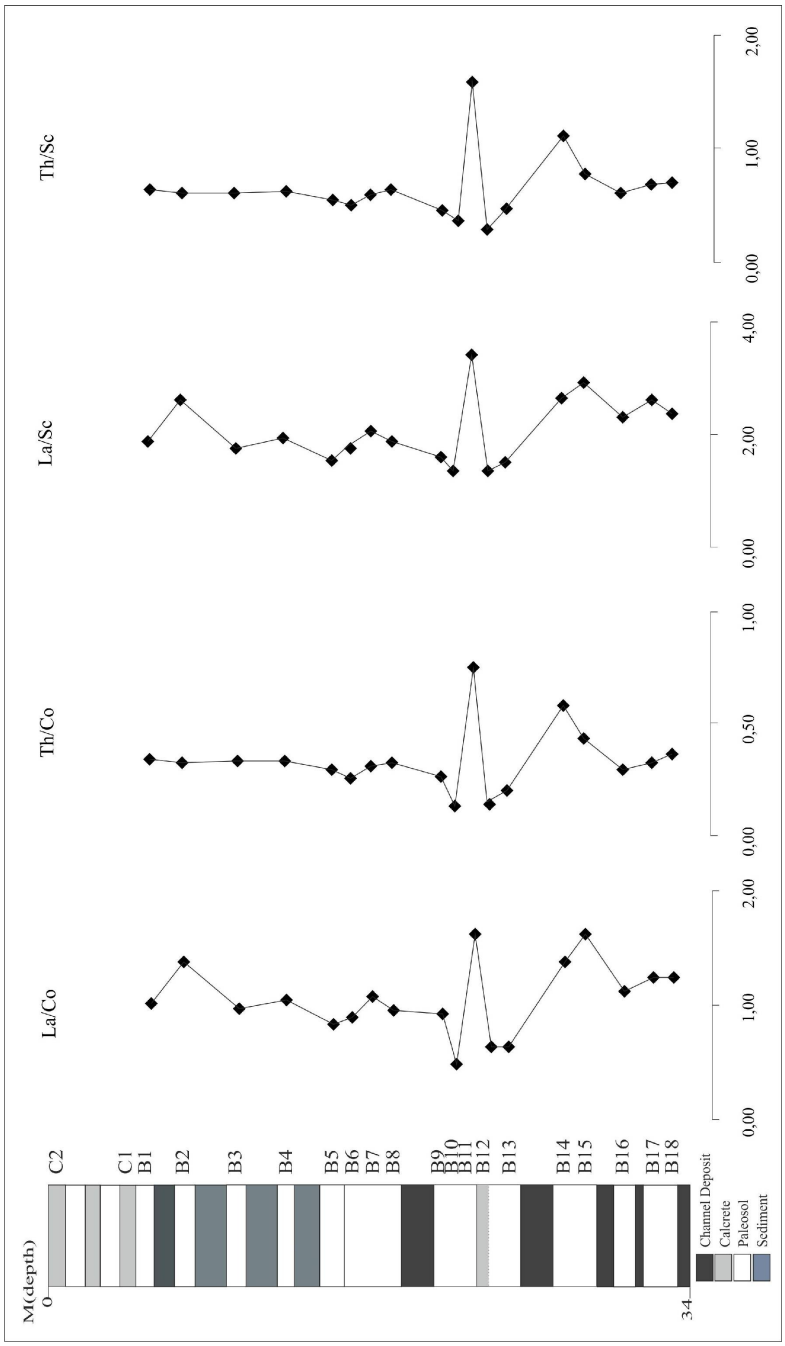

Figure 7.12. cont'd.

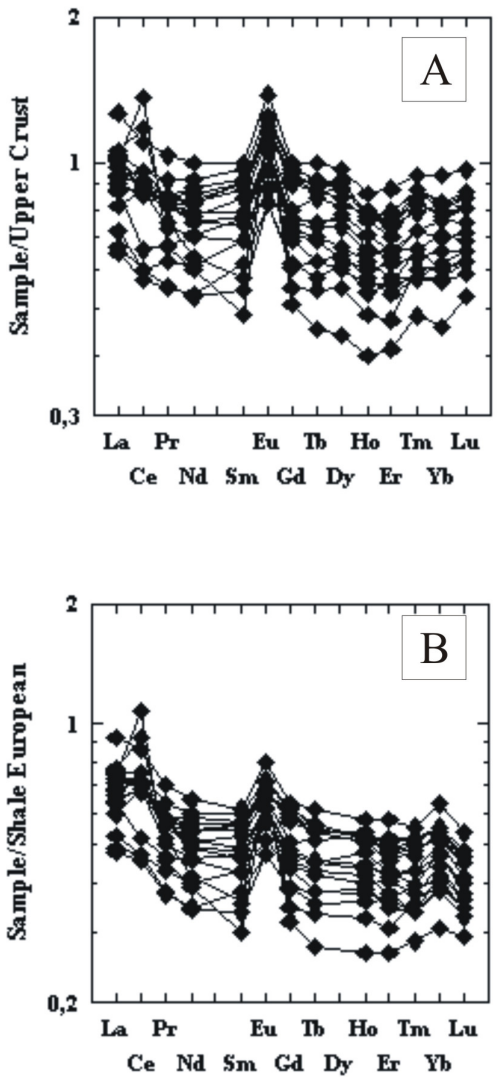

Figure 7.13. Upper Crust and Shale European normalized REE values of Bala samples.

According to the major oxide values, molecular weathering ratios which are typical for paleosols and their carbonates are calculated. Salinization, which is a good indicator for the arid conditions, reflects the relative leaching of sodium to potassium in surficial horizons. It ranges between 0.3 and 2.7 for the Bala

paleosols and calcretes. It shows an enrichment close to the upper horizons as an evidence of evaporation during the paleosol pedogenesis. Salinization for the arid-climatic conditions shoul be greater than 1, and in this case, salinization passes 2 with a positive enrichments in B11-B12 and B14 carbonate rich horizons (Figure 7.14). Calcification is very high at the top due to the presence of carbonate nodules. It also shows an enrichment at B11-B12 horizons. It is positively correlated with salinization values indicating that the saline conditions favour the accumulation of carbonates. Clayeyness, another molecular weathering ratio for paleosols, ranges between 0,15 to 0,3 which can be accepted as moderate clayeyness throughout the section (Figure 7.14). It increases in B11 and B14 argillic horizons of the paleosols. Relative base loss vs depth diagram shows a depletion in the surficial calcretes however an enrichment in the paleosol horizons. It ranges between almost 0 to 2 implying moderate weathering conditions (Figure 7.14). Leaching values present an increasing trend toward the top of the section which is consistent with the other findings. The values of leaching for Bala Section range between 1 to 3 implying 2 major shifts greater than leaching value of 2. They are in B6 and B11 horizons which can be accepted as the surficial horizons of the paleosols.

The chemical index of alteration (CIA) of the Bala section is calculated by the formula of Nesbitt and Young (1982) using molecular proportions of some elements. The higher the value, the more intense the weathering. CIA values of calcretes are 15 at maximum however the paleosol levels are generally higher than 50 CIA. The other measure for the chemical index of alteration is CIA-K is also very similar to CIA values, low for calcretes and high for paleosols. The CIA and CIA-K versus depth diagrams plot paralel to each other. Both index shows that the section experienced moderate weathering conditions in the geological past. Mg index is also gretaer than 50 except B10, B12 and B13 horizons, confirming the moderate weathering intensity (Figure 7.15).

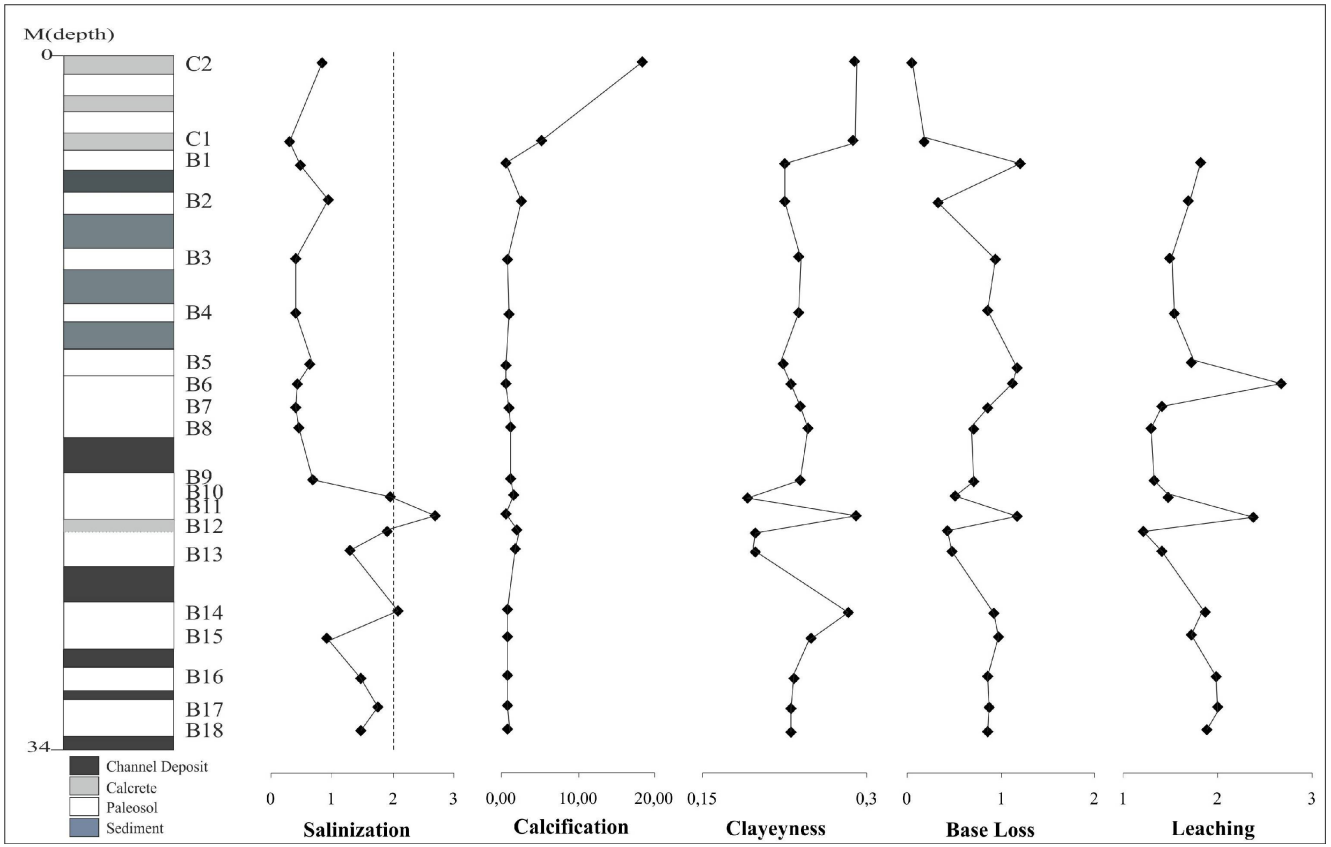

Figure 7. 14. Molecular weathering ratios calculated for Bala samples

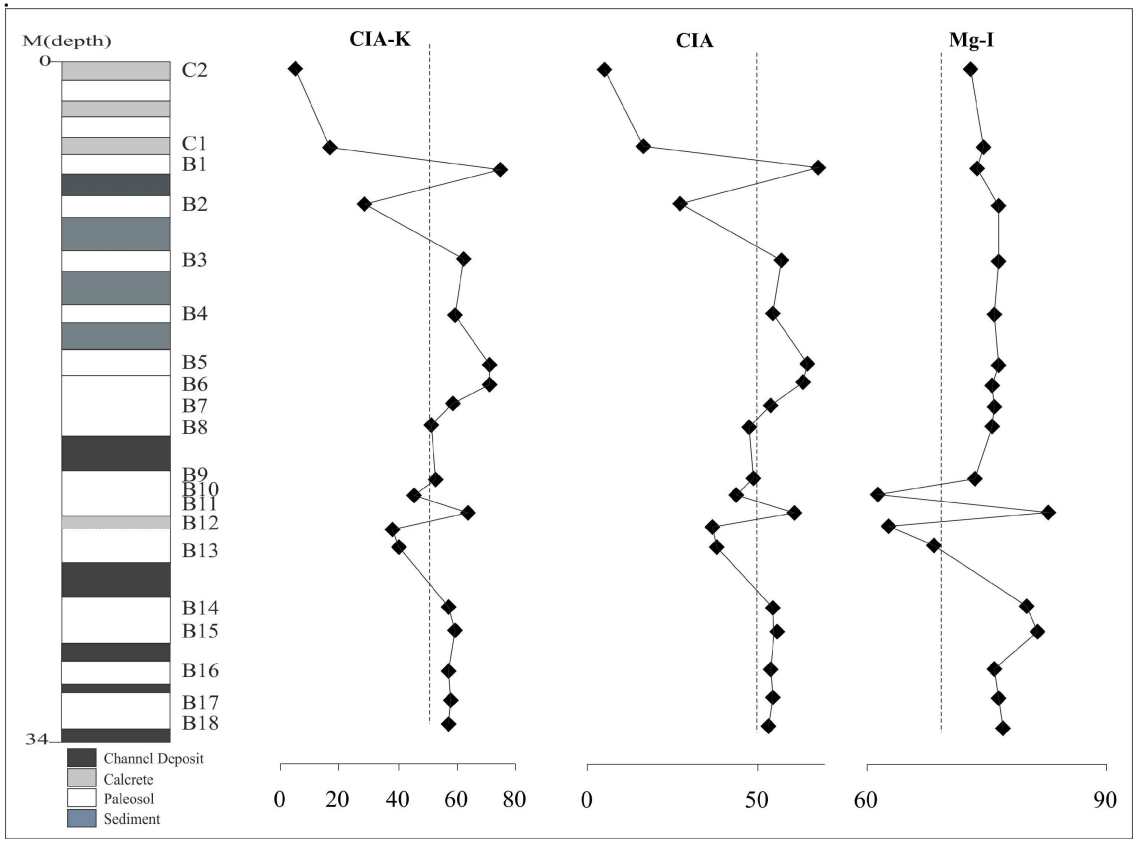

Figure 7.15. Chemical index of alteration values of Bala paleosols and carbonates

The triangular plot of Nesbitt and Young (1984; 1989) is employed on Al_2O_3-$CaO+Na_2O$-K_2O (A-CN-K) diagram. Paleosols and their carbonates of Bala section plot a single linear trend line on A-CN-K triangular diagram (Figure 7.16). It is almost parallel to CN-A side of the diagram with small K addition. This is, as mentioned before, implies moderate stages of weathering (Figure 7.16).

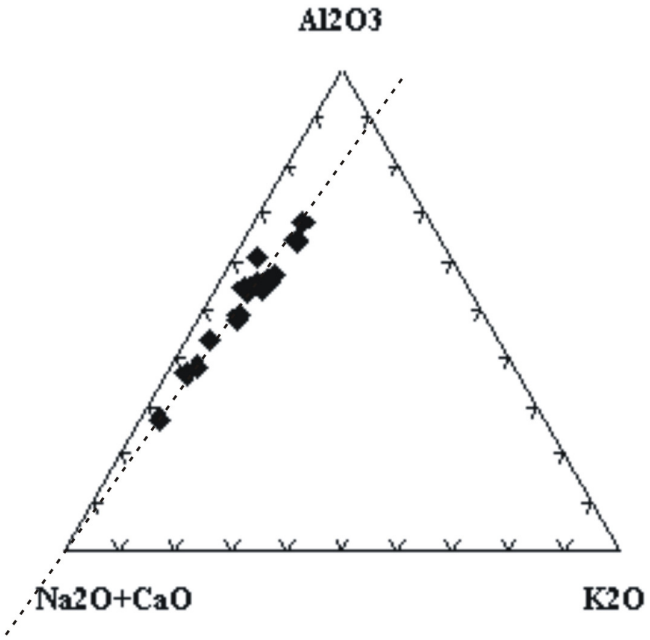

Figure 7.16. A-CN-K triangular plot of Nesbitt and Young (1984, 1989)

7.4. GEOCHEMISTRY OF CALCRETES FROM OTHER SAMPLING SITES

To compare the geochemical characteristics of the studied calcretes, different samples were collected randomly from İncek, Dodurga, Çiğdem and METU areas. Their major oxide values are plotted in a bar diagram and compared with those in

Table 7.8. Major element values of the samples from other sampling sites.

Sample / Analyte	**SiO_2**	**Al_2O_3**	**Fe_2O_3**	**MgO**	**CaO**	**Na_2O**
D-D	43,63	6,48	2,39	1,08	23,08	0,57
$D\text{-}2_{ASAGI}$	34,57	7,49	4,04	1,28	26,68	0,77
DT-1	15,14	1,97	0,9	0,63	45,2	0,21
DT-2	15,64	2,21	1,04	0,74	44,4	0,22
D1-B	50,89	12,66	5,86	2,09	10,87	0,96
D1-A	49,35	13,07	5,94	2,07	11,34	0,98
$D\text{-}D_{\ CALICHE}$	28,92	4,28	1,7	1	35,15	0,37
$D\text{-}1_{\ DODURGA}$	39,35	7,74	3,58	1,41	26,47	0,76
$D\text{-}2D_O$	37,5	8,32	3,82	1,58	25,18	0,7
DT-1 TRK	11,44	1,44	0,69	0,59	47,55	0,19
I 1	57,78	13,31	7,31	2,18	2,53	0,27
I 2	7,38	2,21	1,09	0,5	48,87	0,03
I 3	5,25	1,63	0,81	0,38	50,7	0,01
I 4	4,3	1,39	0,57	0,32	51,79	0,01
S1	32,12	7,55	3,23	1,66	27,23	0,71
S2	27,32	6,26	2,67	1,35	31,41	0,55
370-	17,59	4,66	1,98	1,07	39,49	0,35
370-	32,31	6,72	3,01	1,49	28,39	0,87
K1	30,51	7,51	3,03	1,97	26,65	0,31
14	21,75	4,95	2,12	1,43	35,58	0,37

Sample / Analyte	**K_2O**	**TiO_2**	**P_2O_5**	**MnO**	**U**
D-D	0,7	0,28	0,05	0,05	1
$D\text{-}2_{ASAGI}$	1,19	0,45	0,1	0,07	1,6
DT-1	0,22	0,1	0,04	0,01	0,4
DT-2	0,23	0,11	0,04	0,02	0,7
D1-B	1,9	0,78	0,12	0,1	2,7
D1-A	1,99	0,79	0,13	0,11	2,6
$D\text{-}D_{\ CALICHE}$	0,47	0,18	0,05	0,03	0,8
$D\text{-}1_{\ DODURGA}$	1,19	0,46	0,08	0,07	1,6
$D\text{-}2D_O$	1,3	0,49	0,11	0,07	2,1
DT-1 TRK	0,17	0,07	0,05	0,02	0,5
I 1	1,25	0,83	0,04	0,2	1,9
I 2	0,22	0,12	<0.01	0,03	0,4
I 3	0,17	0,08	<0.01	<0.01	0,3
I 4	0,14	0,07	0,01	<0.01	0,2
S1	1,01	0,39	0,1	0,06	1,2
S2	0,84	0,32	0,08	0,04	1,1
370-	0,7	0,26	0,11	0,05	1,6
370-	0,9	0,36	0,11	0,05	2,2
K1	0,87	0,39	0,06	0,15	4,9
14	0,58	0,26	0,1	0,06	1,9

Karahamzalı and Bala sections (Table 7.8). SiO_2, Na_2O, TiO_2, P_2O_5, MnO, K_2O and Sr values of the calcretes from other sampling sites are consistent with that of Karahamzalı and Bala calcretes. Al_2O_3 is similar to Bala values but Karahamzalı calcretes have slightly lower values. CaO composition of the calcretes from other sites are almost up to 50% and consistent with the Bala calcretes however these values are greater than that of Karahamzalı calcretes. MgO, on the other hand, is very high in Karahamzalı calcretes. Therefore Bala calcretes have almost similar values of MgO with the calcretes of other sampling sites. Fe_2O_3 has less contribution to the composition of calcretes than Karahamzalı section. Finally, U is higher in Dodurga calcretes.

7.5. STABLE ISOTOPE GEOCHEMISTRY

Stable isotope data are widely preferred in paleoclimatology studies since they are accepted as good proxies reflecting the changes in environmental conditions. By definition, isotopes are atoms whose nuclei contain the same number of protons but a different number of neutrons. The nuclei of unstable isotopes decay spontaneously toward the stable condition through the emission of particles and energy. However, the nuclei of stable isotopes do not undergo radioactive decay to form other isotopes. That is why, they are preferred to trace the rock-water interaction in sedimentary basins. The stable oxygen and carbon isotope compositions of secondary minerals formed by interaction with fluids during weathering, diagenesis and hydrothermal alteration carry information about the conditions of rock-water interactions. The stable isotope compositions of the minerals are shaped mostly by temperature, fluid source, crystal chemistry and rock to water ratio for the system of interest (Longstaffe, 2000).

White (2005) summarized the use of stable isotopes as follows: the stable isotopic ratios of carbon and oxygen from authigenic soil carbonate can record changes in climatic conditions and plant cover. Using these ratios from carbonate nodules

that formed in stacked paleosols within ancient fluvial deposits can provide a proxy for changing climatic conditions. The carbon isotopic composition of authigenic soil carbonate is controlled by the type of plant cover (Cerling, 1984). The formation of authigenic soil carbonate has been described and its fractionation pathways under various types of plant cover have been documented by Cerling (1984), Quade et al. (1989) and Cerling et al. (1991). Since C4 plants were not a significant part of the flora until the Miocene (Quade and Cerling, 1995) and the $\delta^{13}C$ values of a C3 cover are between –14‰ and -8‰, changes in the atmospheric $^{13}C/^{12}C$ ratio should be recorded in pedogenic carbonate (Cerling, 1984; Quade et al., 1989; Cerling et al., 1991; Koch, 1998). $\delta^{13}C$ value of modern pedogenic calcite increases with increasing proportion of grasses that use C4 photosynthetic pathway (Mack et al., 1991). Stable isotope results are measured relative to a standard, VSMOW or VPDB. They are expressed with delta notation (δ) in parts per thousand (‰ or per mil).

Rollinson (1993) pointed that a study of carbon isotopes allows the origin of carbon in the carbonate to be determined and can distinguish between marine, organic and methane related carbon. Studying oxygen isotopes in sedimentary carbonates can be used to determine the origin of fluids in equilibrium with the carbonates and provide an estimate of the temperature of the carbonate formation. Isotopic fractionations decrease with increasing temperature and so oxygen isotope thermometers might be expected to be less sensitive at high temperatures (Rollinson, 1993). Evaporation causes co-variation in C and O in soil carbonate, both becoming enriched in the heavier isotope up the profile. Pedogenic carbonate forms in isotopic equilibrium with soil CO_2, which in turn is determined by the relative proportions of C3 and C4 plants where soil respiration rates are high enough to exclude isotopic inputs from atmospheric CO_2 (Cerling, 1984, 1991; Cerling and Hay, 1986; Cerling et al., 1989; Quade et al., 1989; Cerling and Quade, 1993). Terrestrial plants employ three distinct photosynthetic pathways reflecting different carbon isotopic fractionation. The bulk of continental plants

(i.e., basically all trees, most shrubs and herbs, and cool-season and montane grasses) follow C3 photosynthetic pathway (Calvin cycle). These display a range in $\delta^{13}C$ values between -33‰ and -21‰ and averaging about -27‰ (Cerling and Quade, 1993). The higher values are associated with higher water-use efficiency in water stress (Ehleringer, 1989). The C4 (Hatch-Slack) photosynthetic pathway is less discriminating against $^{13}CO_2$ and therefore C4 plants are more higher in $\delta^{13}C$ than are C3 plants. They have $\delta^{13}C$ values between -6 and -19‰ (Deines, 1980) with an average of -13‰. C4 plants include warm season grasses, sedges, and a few halophytic shrubs and are better adapted to moisture and heath stress than C3 plants. The carbon isotope values in soil carbonates are shown to possess higher $\delta^{13}C$ values than the coexisting local biomass due to gas diffusion processes and isotopic fractionation between the soil CO_2 and precipitating carbonate. The soil carbonates formed in the presence of pure C3 vegetation are between -14 and -8‰, whereas values above -8‰ are indicative of a mixture of C3 and C4 plants (Cerling, 1984; Cerling et al., 1991; Quade et al., 1995).

7.5.1. Stable Isotope Values of Carbonates in Karahamzalı and Bala Sections

The results of isotope analysis of the carbonates in Karahamzalı and Bala sections are listed in Table 7.8 and Table 7.9, respectively. The isotopic composition of carbonates in Karahamzalı section exhibit a narrow range in $\delta^{13}C$ composition from -7.11‰ to -7.74‰ and a relative narrower range in $\delta^{18}O$ composition from -3.97‰ to -4.91‰. Changes in the isotope compositions with respect to depth is revealed by the diagram of Figure 7.18. Upward low values in $\delta^{13}C$ is observed at U10, U6C, A1, A6 and A15 levels, but $\delta^{13}C$ is enriched in U7 and A3 levels of calcretes of Karahamzalı section (Figure 7.17). Almost parallel trend to $\delta^{13}C$ is observed in $\delta^{18}O$ composition through the section in that it shows upward depletions and enrichments at the same levels with $\delta^{13}C$ except U6 (Figure 7.17). Therefore, it can be mentioned that a good covariance is observed between $\delta^{13}C$ and $\delta^{18}O$ values of carbonates in Karahamzalı section. The ranges of stable

isotope values are typical of meteoric vadose environment (James and Choquette, 1990). The $\delta^{18}O$ enrichment at the top of the section is well-correlated with the water evaporation process. The increase in $\delta^{13}C$ and $\delta^{18}O$ values of carbonates implies an increase in the temperature. The enrichments in both isotopes observed through Karahamzalı section are well correlated with the levels of high Sr compositions. Such an arid climates are generally dominated by C4-vegetation flora. The $\delta^{13}C$ values ranging around -7 indicate high input of $\delta^{13}C$ from soil respiration and typically correlate with the vegatation cover dominated by C4 plants. However, some depletion trends in $\delta^{13}C$ may also reflect the seasonal nature of plant activity showing C3:C4 association (Wright and Tucker, 1991). The $\delta^{18}O$ versus $\delta^{13}C$ diagram also plots a linear increasing trend suggesting the general increase in temperature up through the section (Figure 7.18). This trend is also common in almost all fluvial settings affected by aridity.

Table 7.9. $\delta^{13}C$ and $\delta^{18}O$ isotope compositions of Karahamzalı Section.

	$\delta^{13}C$	**$\delta^{18}O$**	**$\delta^{18}O$**
Sample	**VPDB**	**VSMOW**	**VPDB**
U-5	-7.4	26.4	-4.4
A-4	-7.7	26.2	-4.6
U-7	-7.3	26.2	-4.6
U-6c	-7.6	26.3	-4.4
A-6	-7.6	26.3	-4.5
U-2	-7.6	26.4	-4.4
A-15	-7.8	25.7	-5.0
A-1	-7.7	26.5	-4.2
A-3	-7.1	26.8	-3.9
U-10	-7.7	25.9	-4.9
U-13	-7.5	26.0	-4.7

Table 7. 10. $\delta^{13}C$ and $\delta^{18}O$ isotope compositions of Bala Section

Sample	$\delta^{13}C$ VPDB	$\delta^{18}O$ VSMOW	$\delta^{18}O$ VPDB
B-2	-5.9	23.5	-7.2
B-4	-9.2	22.8	-7.9
B-5	-8.6	22.2	-8.4
BC	-8.3	23.1	-7.6
B-15	-6.9	23.0	-7.6
B-16	-7.1	22.1	-8.6
B-17	-6.5	21.9	-8.7

The isotopic composition of carbonates in Bala section exhibit a slightly wider range in $\delta^{13}C$ composition from -5.98‰ to -9.22‰ and a narrower range in $\delta^{18}O$ composition from -7.19‰ to -8.66‰. The relative changes of the stable isotopes with respect to depth is plotted in Figure 7.19. The trends of stable isotope values in the diagram are very similar to what observed in Karahamzalı section. It starts with a depletion at the bottom levels of B16, then at the middle an enrichment is observed at B7, major depletion at B4 is recorded, finally it ends with an enrichment at the top at B2 level (Figure 7.19).

Comparing the $\delta^{13}C$ values with $\delta^{18}O$ values of Bala section, almost parallel trends are observed with an exception of BC level where $\delta^{13}C$ is higher with respect to $\delta^{18}O$ composition (Figure 7.19). Like Karahamzalı section, a good covariance can be mentioned between $\delta^{13}C$ and $\delta^{18}O$ values of carbonates in Bala section. The ranges of stable isotope values are again typical of meteoric vadose environment (James and Choquette, 1990).

The high values in both $\delta^{13}C$ and $\delta^{18}O$ values at the surficial horizons imply the effect of water evaporation process. When compared with the Sr composition of the same levels in Bala section, inreasing and decreasing trends in $\delta^{13}C$ and $\delta^{18}O$ diagrams are well-correlated with Sr enrichments and depletions, respectively. As

expected to be dominant in arid to semi-arid climates, C4-vegtation flora is favoured in the paleosols of Bala section however the wide range of $\delta^{13}C$ composition stil point the contribution of C3:C4 mixed flora in the region.

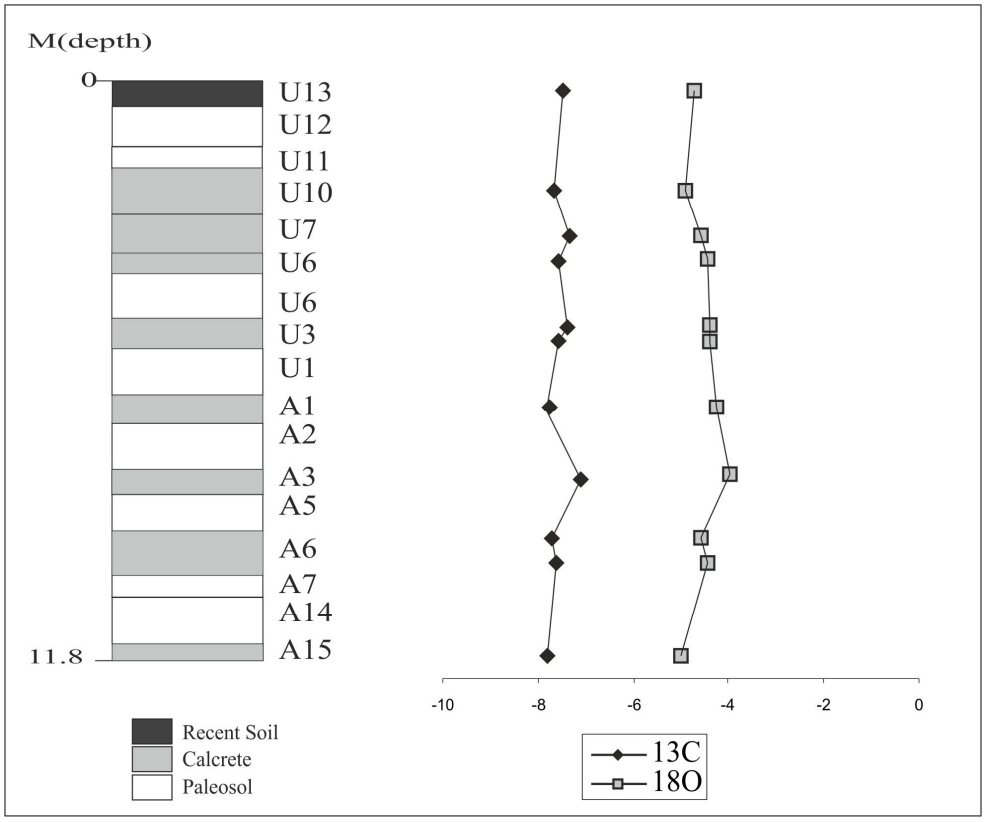

Figure 7.17. $\delta^{13}C$ and $\delta^{18}O$ values of Karahamzalı samples plotted with respect to depth.

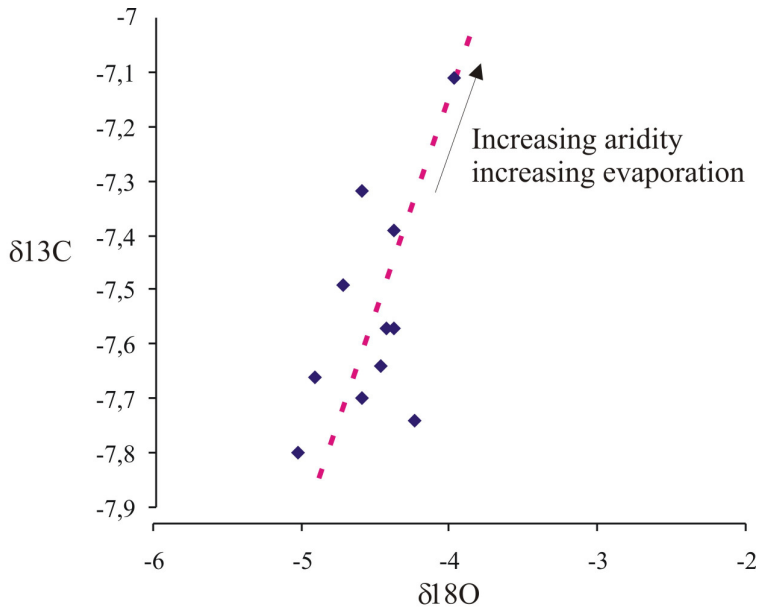

Figure 7.18. $\delta^{18}O$ versus $\delta^{13}C$ values of Karahamzalı section.

On a $\delta^{13}C$-$\delta^{18}O$ plot, the Bala data exhibit two distinct groupings. The $\delta^{18}O$ versus $\delta^{13}C$ diagram also plots 2 separate groups suggesting the general increase in temperature up through the section (Figure 7.20). Group II shows a similar trend with Karahamzalı data and can be correlated with other fluvials of arid climates. Group I, on the other hand, plots a linear trend with an increase in $\delta^{13}C$ values whilst a decrease in $\delta^{18}O$ values of the data analysed.

Although many studies have been carried about the geology of the Ankara region, assigning the age for the Cenozoic units become always problematic. The stratigraphical relations between units are considered while assessing the relative age of Neogene cover.

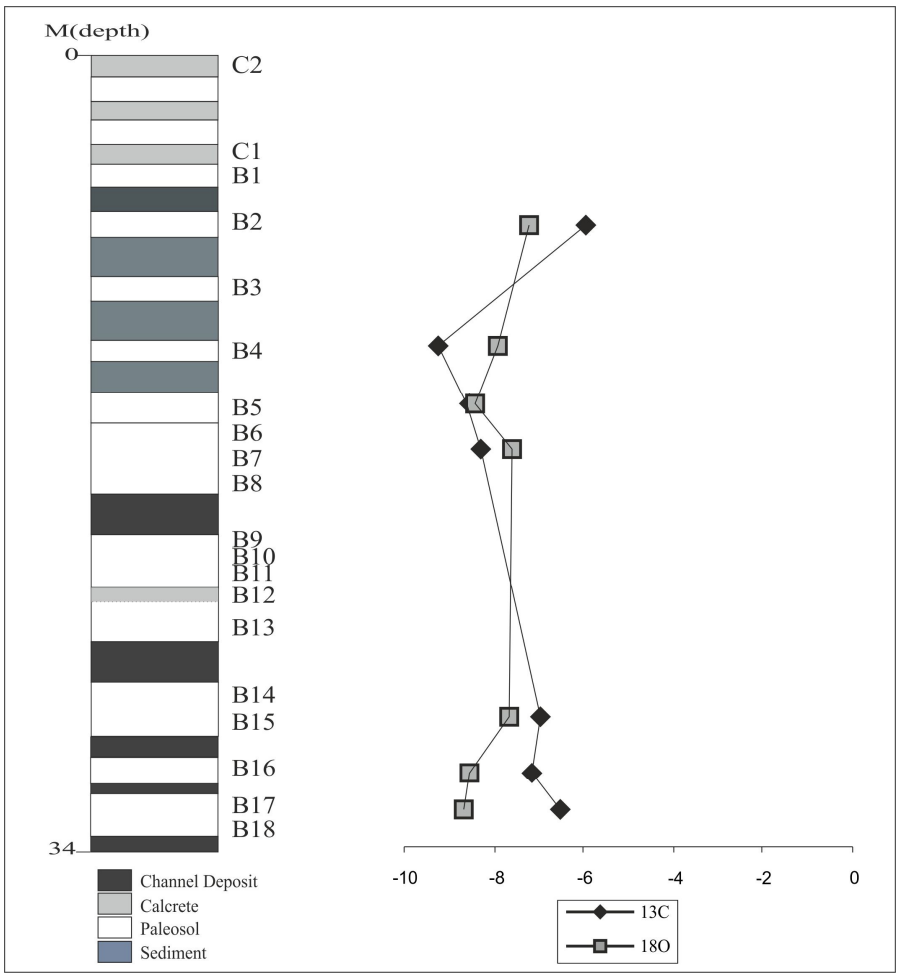

Figure 7.19. $\delta^{13}C$ and $\delta^{18}O$ values of Bala samples plotted with respect to depth.

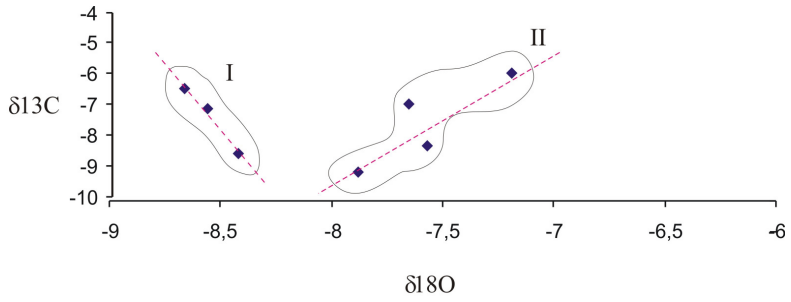

Figure 7.20. $\delta^{18}O$ versus $\delta^{13}C$ values of Bala section

CHAPTER 8

GEOCHRONOLOGY

For this study, fortunately the calcretes of Bala section are dated by ESR technique. The details of the methodology is given in Chapter 4. Two calcrete samples from paleosols of Bala sections were selected. They were 7m apart from each other. C1 is the bottom unit and C2 is the upper calcrete. Firstly their chemical compositions are determined by XRF technique. The results are given in Table 8.1. The results are compatible with the Karahamzalı calcrete compositions.

After that, dosimetric measurements were carried out. At the end, two age data were gathered. C1, the bottom unit has 761 ± 120ka and C2 the upper one has 419 ± 64 ka. This means that the ages of the calcretes are Middle Pleistocene. It belongs to the Ionian stage. The ages found by ESR are also consistent with their stratigraphic positions. The proposed ages until now for the units are Pliocene.

The same region was examined in terms of its pollen content however there is no well preserved pollens identified in this study. The Karahamzalı calcretes, on the other hand, do not include that much calcite which is not enough to measure its ESR signal. Therefore, this area was only examined by its pollen content and the result is compared with the Pliocene aged basement rock.

From 15 samples seleceted for pollen Analysis, only 4 of them have well preserved pollens. The results are given in Table 8.3. The pollens which are not detrital suggest an age younger than Late Miocene/Pliocene to recent.

Table 8.1. The geochemical compositions of the calcretes from Bala section (Küçükuysal et al., 2011).

Composite	C1 (wt %)	C2 (wt %)
$CaCO_3$	60.70	84.98
SiO_2	24.00	9.18
Al_2O_3	6.91	2.65
MgO	2.36	0.98
Na_2O	0.23	0.22
P_2O_5	0.08	0.07
SO_3	0.01	0.01
TiO_2	0.32	0.1
Fe_2O_3	4.30	1.40
Element	**C1 (ppm)**	**C2 (ppm)**
Mn	547.7	166.0
Cr	221.3	57.9
Cu	20.1	6.4
Ni	127.6	63.2
V	48.3	17.4
Zn	38.2	19.0

According to the studies of Velichko and Nechaev (2005) and Akgün et al. (2007) the environmental interpretations of the pollens found as follows: Artemisia is present in semi-arid to arid climatic conditions. Compositae likes the sun and also favours semi-arid to arid conditions. Quercus, unlike the others is generally found in cold climates. The pollen which are dominant in this region clearly shows arid conditions occurred during the time interval derived from pollen analysis.

Table 8.2. The radioactivity and dating results of C1 and C2 samples (Küçükuysal et al., 2011).

Nodular Calcrete							
	^{238}U (ppm)	^{232}Th (ppm)	K_2O (%)	Internal dose rate D_{Int} (mGy/year)	^{238}U (ppm)		
C1	1.8 ± 0.2	5.8 ± 0.7	0.77 ± 0.03	Oca.82	2.8 ± 0.4		
C2	1.3 ± 0.2	2.7 ± 0.3	0.26 ± 0.03	0.93	3.1 ± 0.4		
Paleosol Surrounding Calcretes							
	^{232}Th (ppm)	K_2O	External dose rate D_{Ext} (mGy/year)	Total annual dose rate $D=D_{Int}+D_{Ext}$	D_E	ESR age (ka) D_E/D	
		(%)		(mGy/year)	(Gy)		
C1	10.7 ± 1.3	1.58 ± 0.04	0.65	2.47 ± 0.36	1880 ± 207	761 ± 120	
C2	11.4 ± 1.4	1.71 ± 0.05	0.67	1.60 ± 0.21	671 ± 67	419 ± 64	

Table 8.3. Pollen results of Karahamzalı paleosols.

Samples	Pollens Included
2	Compositae (tubuliflorae-type) Compositae (tubuliflorae-type) Compositae (liguliflorae-type) Graminae Umbelliferae *Periporopollenites multiporatus* *Pityosporites* spp. *Quercus* spp.
4	Compositae (tubuliflorae-type) Compositae (tubuliflorae-type) Compositae (liguliflorae-type) *Laevigatosporites haardtii* *Periporopollenites multiporatus* *Pityosporites* spp. *Quercus* spp. Graminae Umbelliferae Dipsacaceae *Artemisia*
9	Compositae (tubuliflorae-type) Compositae (tubuliflorae-type) Compositae (liguliflorae-type) *Laevigatosporites haardtii* *Periporopollenites multiporatus* *Pityosporites* spp. *Quercus* spp.
12	Compositae (tubuliflorae-type) Compositae (liguliflorae-type) *Laevigatosporites haardtii* *Periporopollenites multiporatus* *Pityosporites* spp.

CHAPTER 9

DISCUSSION

9.1. AGE CONSTRAIN

Although Ankara region has been widely studied by many workers in terms of its geology, the age of the relatively young units could not be dated by radiometric geochronological methods. In literature, the ages of the studied sections have been given in terms of their stratigraphical positions.

For Karahamzalı section, the red-brown colored paleosols have been accepted to belong Gölbaşı Formation and on the basis of its stratigraphy, the Pliocene age has been assigned recently by Dönmez et al. (2008). For the thesis study, all geochronological methods which could be potentially suitable for the dating of this time interval have been searched. At the end, only pollen analysis and micromammalian remnants are found to be the solution. The same site has been researched by micromammalian experts and they could not get any remnants yet. As explained in Chapter 8, the pollen give an age of Pliocene to present, which is a broad range to emphasize an exact age of the section. According to the stratigraphic position of the paleosols, they are underlain by Evciler basalt (coeval with Bozdağ Basalt). This unit was dated with K-Ar technique and given an age of Middle Miocene by Akçay et al. (2008). The Bozdağ basalt, on the other hand is given an age of Pliocene with its stratigraphical position and it is the age equivalent unit for Evciler Basalt in the region. Therefore, the age of the underlying volcanic unit is accepted as Mio-Pliocene for this study. The geomorphological study carried by Erol (1983) has assigned a formation age of the paleosols as Pliocene to Late Pleistocene.

For Bala section, pollen analysis were also performed, however, there is no well-preserved pollen identified within the paleosols of Bala section. Fortunately, the calcretes of the paleosols in Bala section are formed from calcite which allow us to use Electron Spin Resonance technique to date the calcretes and give the age of the paleosols. This technique finds two different ages for two different calcretes within the same section but from different levels. The age of the lower calcrete is 761±120 ka and that of upper one is found to be 419±69ka. Both ages point a time of Middle Pleistocene period, Ionian Stage. Those two calcretes are at the middle of the section. By drilling operation up to 25m depth from the ground, only paleosols and channel deposits were cut. Unfortunately, the basement rock could not be sampled from this location. However, with the help of field work, Bozdağ Basalt is found to be the possible base rock of the section. The age of the this unit is given as Pliocene by Akyürek et al. (1997).

The samples from other sampling sites, like Karahamzalı and Bala samples, have not been dated by geochronological methods. Their ages are assigned to be Plio-Quaternary in many studies (Aras, 1991, Koçyiğit and Türkmenoğlu, 1991).

9.2. AN APPROACH TO THE MINERALOGY

The clay mineral composition of weathering profiles and soils largely depends on the climatic conditions existing on land at successive periods of the geological history. Because of this, the clay minerals can be used to reconstruct the past climates (Chamley, 1989).

When the relative abundances of calcite, dolomite, palygorskite and smectite were compared with respect to the depth of the Karahamzalı section (Figure 9.1), it is observed that only calcite is the mineral with a constant abundance at the upper levels of the section. The other minerals fluctuate level by level. Palygorskite has a general increasing pattern up to the section providing the increasing aridity. At

the same time, smectite shows a general decreasing pattern towards the top. Dolomite, similar to palygorskite has a general increasing trend towards to the top of the section and abundant in the calcrete levels (Figure 9.1). As smectite decreases in amount, palygorskite becomes enriched, possibly suggesting the smectite weathering as one of the sources of Mg for the palygorskite formation. It is also somewhat true for dolomite abundance that where the amount of smectite lowers, dolomite becomes abundant. For the formation of dolomite, Mg is also needed. Therefore, this trend also implies that smectite may also be one of the Mg sources for dolomite formation. Additionally, scanning electron images of the palygorskites in the Karahamzalı section show that palygorskites cover the dolomites and form bridge-like structures. This also confirms the formation of palygorskire from the soil solution enriched in Mg. Dolomites are generally found within the pore spaces with rhombohedral forms and covered with palygorskites implying that they were formed before palygorskite formations. As pedogenic minerals, palygorskite and dolomite are accepted to be formed during paleosol development. Therefore, these two minerals can be used for the paleoclimate reconstruction study. Their relative abundances through the section may indicate the climatic conditions during the soil development. The other minerals are all detrital and can not be used to infer the paleoclimate of the paleosols.

The clay minerals present in Bala paleosols and their carbonates are almost the same with that of Karahamzalı section (Figure 9.2). Smectite is the dominant clay mineral in the clay fraction. It shows alternation of enrichment and depletion patterns with a general decreasing trend towards the top of the section. Palygorskite, on the other hand, is found to be the pedogenic mineral like in Karahamzalı samples. Its amount increases towards the top providing aridity conditions. Its amount highers while smectite's lowers in the paleosols of the Bala section (Figure 9.2). This relationship may also point the smectite as a possible source of Mg for the formation of palygorskite. It is also confirmed with the scanning electron microscope images of the Bala samples that calcite

rhombohedras are covered with palygorskite fibers and they also form bridge-like structures pointing the formation from soil solution. Calcite shows a similar pattern to palygorskite which presents the possibility of calcite forming from soil solution as a secondary mineral carrying pedogenic history of the paleosols in the Bala section.

SEM image of B3 level of the Bala section clearly shows the remnants of the biological activity on the paleosols of the Bala section. This is also a good parameter to use for the classification of the calcretes in terms of faunal and floral activities.

Samples from the other sampling sites have only calcite in the calcretes as carbonate mineral and do not include palygorskite in their compositions. This study can not recognize the palygorskite fibers in the calcretes of Dodurga, Çiğdem, İncek and METU areas by XRD and SEM Analysis. However, Aras (1991) indicates the presence of palygorskite fibers in the red colored mudstones of Çiğdem area. In the bulk fraction of the calcretes, calcite, quartz and feldspar are found in calcretes, and in addition to them clay minerals are present in the paleosols.

One of the paleosol from Çiğdem area has also gypsum in its composition which also points that the red colored paleosol of Late Pliocene-Pleistocene age has experienced an aridity which favours evaporation leading to the development of gypsum.

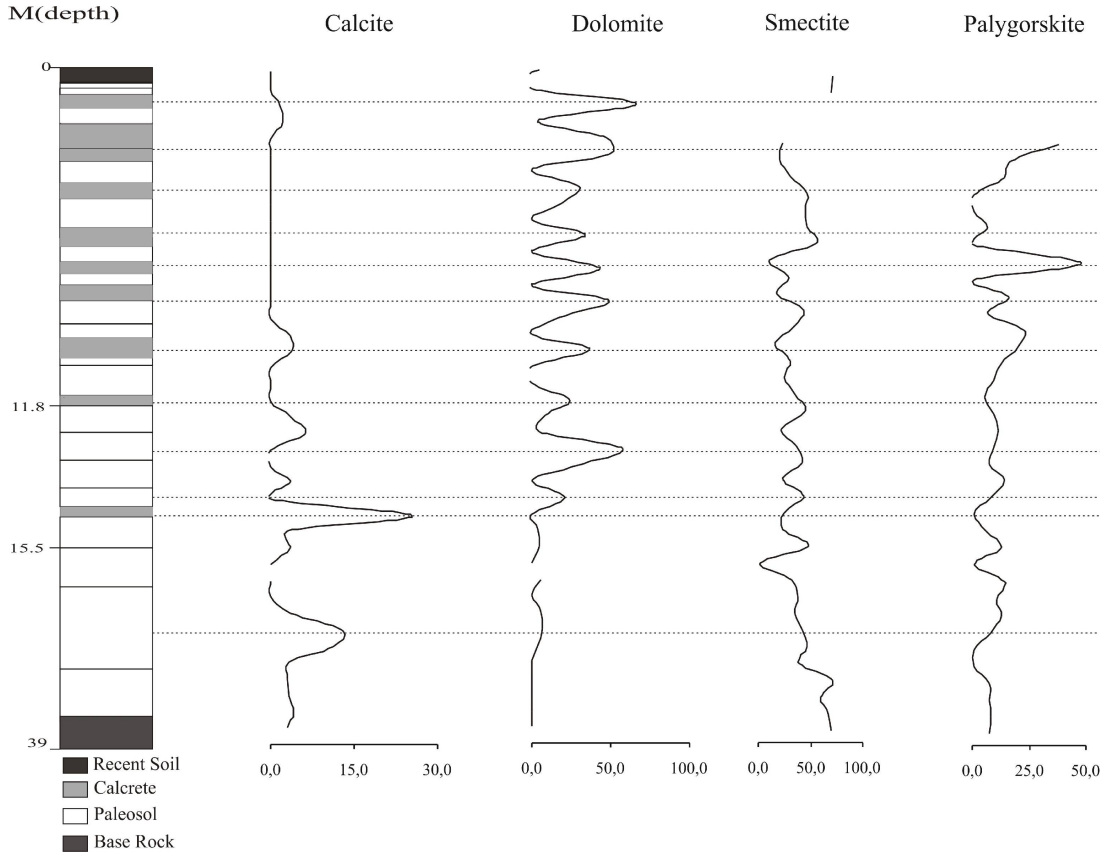

Figure 9.1. Relative changes between calcite, dolomite, palygorskite and smectite with respect to depth in Karahamzalı section.

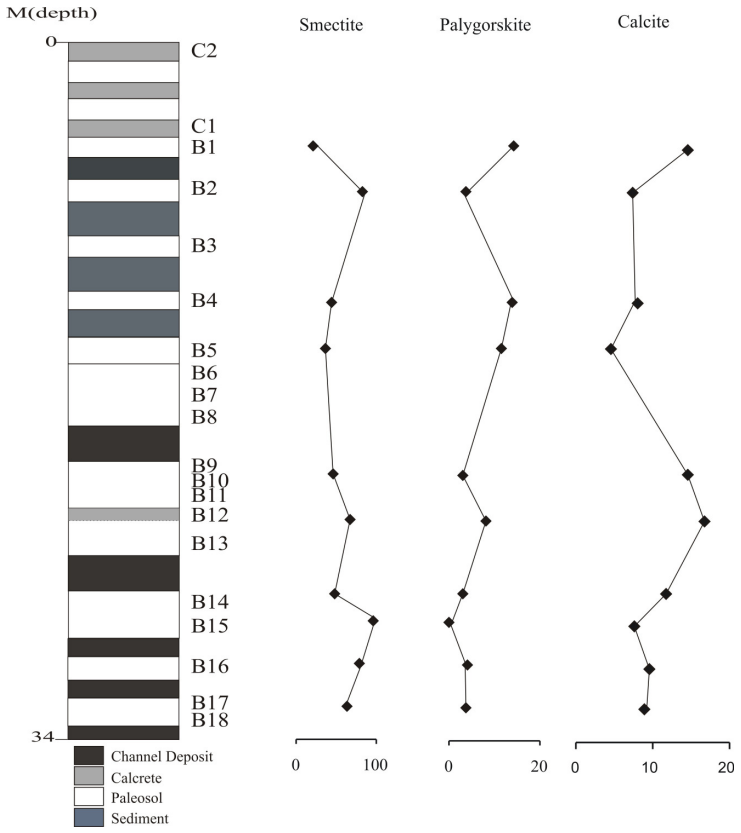

Figure 9.2. Relative changes between smectite, palygorskite and calcite with respect to depth in Bala section.

9.3. AN APPROACH TO THE GEOCHEMISTRY

9.3.1. Karahamzalı Data

Generally titanium is the best proxy for terrigenous components in sediments, therefore Ti-normalized ratios eliminate the effect of dilution by biogenic and authigenic elements on the variation patterns of the element records. During chemical weathering titanium is released from the primary minerals but it is precipitated before it is carried out of the sample mass (Wei et al., 2004). Due to its conservative nature in a weathering profile it is selected as a normalizing factor in this study.

Ti-normalized major oxide and trace element values are compared with the stable isotope values of the samples from Karahamzalı section. The major oxides of SiO_2/Ti, MgO/Ti, Fe_2O_3/Ti, CaO/Ti, MnO/Ti, P_2O_5/Ti and Al_2O_3/Ti ratios exhibit similar patterns as those of the $\delta^{18}O$ and $\delta^{13}C$ isotope values. Generally during warm-interpluvial periods, these ratios exhibit high values and during cold-pluvial periods they show lower values. The variation of K_2O/Ti ratio is very small through the section and do not show any variation. Trace elements are also normalized with respect to titanium. The ratios exhibit both matching the isotope patterns and not. Ba, Sr, U display well matching to the patterns of $\delta^{18}O$ and $\delta^{13}C$ values of the samples from Karahamzalı section. On the other hand, Hf, Nb, Cs, Ga and Y are negatively correlated with the isotope values. Co, Th, V, Zr and Rb show very weak variation through the section.

For Karahamzalı data, it can be stated that the behaviours of the major oxide/Ti ratios agree well with their behaviours during chemical weathering. As Wei et al. (2004) stated, Fe is expected to be enriched in advanced weathering conditions relative to Ti. On the other hand, K and Mg are easily removed from primary minerals during chemical weathering, but combined in weathering profile. Na is

also removed from the primary minerals and show low concentration in weathering profile. Wei et al. (2004) summarizes the behaviours of the elements during low degree of chemical weathering as high contents of Al, Fe, K, Mg but low content of Na.

SiO_2/Ti, MgO/Ti, Fe_2O_3/Ti, CaO/Ti, MnO/Ti, P_2O_5/Ti and Al_2O_3/Ti ratios of the data in Karahamzalı section are higher in warmer periods and lower during cooler conditions. Na_2O/Ti ratio shows opposite behaviour for the climatic periods. These patterns may indicate that the chemical weathering was stronger during warm periods than cold ones. On the basis of the chemical nature of Mn, it is expected to be fluctuate between warm to cool periods. Mn coatings are very common in calcrete and paleosol samples which indicate warm and wet conditions. Therefore high Mn/Ti ratio can also be interpreted as high in warm and wet conditions but low in cool and dry periods. During chemical weathering, Ba behaves similar to Mg, Rb; Cs are similar to K and Ga is similar to Al. Rb/Ti, Cs/Ti and Ga/Ti ratios are in aggreement with the chemical weathering mechanism through Karahamzalı section. This indicates that the chemical weathering at the source area dominantly affects the variations of the elements. Cr_2O_3/Ti values are also in pace with the isotope values of the data in Karahamzalı section. Zr which is bonded in zircon is very resistant to weathering. This is confirmed in this study with almost constant values of Zr through Karahamzalı section. REEs/Ti, Nb/Ti, Ta/Ti and Y/Ti ratios are nearly constant through the section as expected. Molecular weathering ratios of the paleosols and the calcretes of Karahamzalı section display a parallel behaviour between clayeyness, base loss and leaching. These values fluctuate between paleosol and calcrete levels. They are higher in paleosols levels while calcretes display lower values. Calcification and salinization are very similar to each other and increases towards the upper sections. This implies increasing aridity with increasing temperature. Chemical index of alteration values of CIA, CIA-K and MgI are all parallel to each other, their values are high within the paleosol levels, low in

calcrete levels. The highest values are greater than 50 which suggest medium degree of weathering happens within the paleosols. The values are as low as 10 for calcrete levels which points very low degree of weathering affected the calcrete levels. As Nesbitt and Young (1982) stated, chemical weathering is mainly controlled by moisture and temperature. The variation patterns of the element records of Karahamzalı section indicate that wet and warm climate occurs which results in enhanced chemical weathering during pluvial periods and dry climate exhibits with relatively weak chemical weathering during interpluvials of Late Pliocene to Pleistocene.

9.3.2. Bala Data

Ti-normalized major oxide and trace element values are compared with the stable isotope values of the samples from Bala section. The major oxides of SiO_2/Ti, MgO/Ti, Fe_2O_3/Ti, MnO/Ti, P_2O_5/Ti, K_2O/Ti and Al_2O_3/Ti ratios exhibit increasing patterns while no isotope data is available. The high values of these ratios can be assigned to the warm periods and the low values for the cold. However, CaO/Ti ratio presents almost constant value up to the section with a major shift towards a positive value supporting dry condition. At the same level Mn value is very low which confirms the hot and dry period occurred between 416 to 761 ka (Middle Pleistocene).

Trace elements are also normalized with respect to aluminum since Al is also preserved during chemical weathering. Al normalized values are compared with Ti normalized trace element ratios. There is no difference between Ti and Al normalizations. Therefore, Al normalization is used for the trace element concentrations of Bala section. The ratios exhibit both matching the isotope patterns and not. Ba, Cs, Rb, Ta, Th, Sr and U display well matching the patterns of 18O values of the samples from Bala section. On the other hand, Ga, Hf, Nb are negatively correlated with the $\delta^{18}O$ values. Y, Zr and V are almost constant

through Bala section. The major oxide/Ti ratios for the Bala data agree with the chemical weathering behaviours. Fe is enriched while K and Na are depleted in weathering condition of Bala section. The upper level of Bala section has 3 mudstone layer which do not show paleosol characteristics. The major oxides/Ti ratios of these levels are constant suggesting stable chemical conditions. The bottom part of the section however has calcretes and paleosols therefore show fluctuating patterns. They are related with the chemical weathering occurred during paleosol development within the section. B10-B11 levels show major shifts to positive values of SiO_2/Ti, MgO/Ti and P_2O_5/Ti suggesting warm period. The lower part of the section at B14-B15 display depletions in these major oxides implying cooler conditions. The behaviours of major oxides and trace elements indicates the effect of chemical weathering on the elemental variations. Zr is nearly constant all through the scetion except a weak variation at the middle of the section. REEs/Ti, Ta/Ti and Y/Ti ratios, as in Karahamzalı data, nearly constant through the section with a small exceptional variations between B5-B10 levels.

Molecular weathering ratios of the paleosols and the calcretes of Bala section display a parallel behaviour between clayeyness, base loss and leaching. These values display shifts from carbonate rich levels to paleosls. High values of these ratios at B11 level indicate argillan horizon characteristic. Calcification and salinization are very similar to each other and increases towards the upper sections. This implies increasing aridity with increasing temperature. Chemical index of lateration values of CIA and CIA-K are parallel to each other. They show major shifts at B1 and B11 levels with very high values indicating high degree of chemical alteration. The general values of CIA and CIA-K are greater than 50 which indicates medium degree of weathering.

The lower values fall in the carbonate rich levels of Bala section. MgI values are very high through the section and gretaer than 60 suggesting medium to high degree of alteration. As all these values suggest, wet conditions alternate with dry

periods. This means enhanced chemical weathering occurred during pluvials while low degree of weathering happened during interpluvials.

9.4. AN APPROACH TO STABLE ISOTOPES

For both sections, there is a positive correlation between $\delta^{18}O$ and $\delta^{13}C$ values of the paleosol carbonates which indicates closed environmental conditions. It is also consistent with the constant provenance values of trace elements suggesting that through the deposition of units in Karahamzalı and Bala sections, there is no additional influx to the system. This leads to the development of the sedimentary units with similar characteristics. There are of course slight fluctuations in $\delta^{18}O$ and $\delta^{13}C$ values through the sections pointing changes in climatic conditions. Variations towards the higher ^{13}C mean ^{12}C depletion of soil water favouring dry conditions. Opposite trend implies wet conditions favouring CO_2 leaching from the soil. Because only $\delta^{18}O$ and $\delta^{13}C$ contents of the carbonates were determined due to lack of independent estimates based on fission track ages or maturation indices of fossil pollen to constrain the upper temperature limit, the temperature of the formation of the nodules has to be estimated independently. According to the mineralogical and textural evidences, it can be assumed that the formation temperature for the nodules should be well below 60°C (Mack et al., 1991).

Fluid $\delta^{18}O$ values are calculated using dolomite-water fractionation curve given by Woronick and Land (1985). Lines of equilibrium were plotted using the relationship of $1000\ln\alpha = 3.2*10^6/T^2 - 3.3$.

Assuming the carbonates of Karahamzalı section formed at 20°C, then the calculated $\delta^{18}O$ values for the formation water ranges from -7,2‰ to -8,3‰. If the soil temperature was as high as 30°C, then the $\delta^{18}O$ isotopic composition of the soil water in equilibrium with calcretes range from -4,75‰ to -5,70‰. It is observed for both temperature conditions that $\delta^{18}O$ for waters have a range of

roughly 2,5‰. Additionally, low values of $\delta^{18}O$ in the water equilibriated with calcretes is recorded in stratigraphic height except A1 level. This means, at the time of early stages of calcrete formation, the fluids responsible for the formation of carbonate accumulation were isotopically heavier, and became depleted over time as the maturity of carbonates increases. During the early stages of carbonate accumulation, it is expected that, the soil water has a $\delta^{18}O$ composition less than -4.5‰. As Mack et al. (1991) stated the waters with compositions heavier than -4‰ imply high soil temperatures, in excess of 30°C. Also, it is mentioned in the same study that if the soil temperature were as cold as 0°C, the fluid $\delta^{18}O$ values become as light as -14 to -12‰. However, temperatures of this much cold is inconsistent with the distribution of the flora in the region. If the formation temperature is assumed to be 30°C, in this case, soil waters have $\delta^{18}O$ values range between -1 to 3‰. Considering the 20°C, the $\delta^{18}O$ values of -7,2 to -8,3‰ for Karahamzalı calcretes, 30°C temperature is unlikely the soil water temperature for the carbonates of the section. On the basis of the theoretical consideration, this study suggest that the surface water responsible for carbonate accumulation have $\delta^{18}O$ values probably less than -4‰ as low as -8‰ which assumes soil depositional temperature greater than 20°C and colder than 30°C.

Fluid $\delta^{18}O$ values are calculated using the calcite-water fractionation curve given by Friedman and O'Neil (1977). Assuming the carbonates of Bala section formed at 0°C, then the calculated $\delta^{18}O$ values for the formation water ranges from -11‰ to -13,1‰. If the soil temperatures between 20°C and 30°C with an average 25°C, then the $\delta^{18}O$ isotopic composition of the soil water in equilibrium with calcretes range from -4,9‰ to -6.7‰. It is observed for both temperature conditions that $\delta^{18}O$ for waters have a range of roughly 2‰. Additionally, $\delta^{18}O$ enrichment in the water equilibriated with calcretes is recorded in stratigraphic height. This means, at the time of early stages of nodule formation, the fluids responsible for the formation of carbonate accumulation were isotopically lighter, and became enriched over time as the maturity of carbonates increases. During the early stages

of carbonate accumulation within Bala section, the soil water has a $\delta^{18}O$ composition less than -4.5‰. As Mack et al. (1991) stated the waters with compositions heavier than -4‰ imply high soil temperatures, in excess of 30°C. Also, it is mentioned in the same study that if the soil temperature were as cold as 0°C, the fluid $\delta^{18}O$ values become as light as -14 to -12‰. If the formation temperature is assumed to be 30°C, in this case, soil waters have $\delta^{18}O$ values range between -1 to 3‰. Considering the 25°C calculation, the $\delta^{18}O$ values of -4,9 to -6,7‰ are observed for Bala calcretes. Therefore, neither 0°C nor 25°C temperatures are likely the soil water temperatures for the carbonates of the Bala section. On the basis of the theoretical consideration, this study suggests that the surface water responsible for carbonate accumulation have $\delta^{18}O$ values probably less than -4‰ as low as -8‰ which assumes 20°-25°C soil depositional temperature.

9.5. INTERPRETATION OF ALL PROXY

Comparing the stable isotope values of carbonates with similar stratigraphic and pollen ages in Karahamzalı and Bala sections reveal consistent trends over time (Figure 9.3). Both data set is well correlated each other and shows 3 distinct periods presenting covariance. The period I and III shows the same characteristics with first lower values both isotopes and then followed by higher amounts. On the other hand, period II presents first higher amounts and then relatively lower values in the isotope compositions (Figure 9.3). This comparison is independent of age constraint of the paleosols and calcretes but revealing wet and dry cycles affecting the isotopic compositions of the paleosols and their carbonates.

It is very obvious in Figure 9.4 that if we compare all proxy used for Karahamzalı section, it can be concluded that the dry periods favour an increase in palygorskite and dolomite amounts while smectite decreases; CIA-K and Mg-I are low while salinity and calcification are high with increasing $\delta^{18}O$ and $\delta^{13}C$ values.

Oppositely, the wet conditions allow to have high smectite with low dolomite and palygorskite amounts, high CIA-K and Mg-I values with low salinity and calcification values leading decreasing $\delta^{18}O$ and $\delta^{13}C$ values. It is clearly shown in Figure 9.4 that the studied section shows alternating wet and dry conditions led by pluvials and interpluvials favouring the formation of red-brownish colored paleosols and their carbonates. The frequency of the dry periods are very high towards the top of the section meaning that aridity and evaporation increases towards the top of the section.

Table 9.1. The calculated $\delta^{18}O$ values of the fluids responsible for the formation of the Carbonates in Karahamzalı and Bala paleosols.

KARAHAMZALI SECTION				Calculated Fluid $\delta^{18}O$ (SMOW)	
Sample	$\delta^{13}C$	$\delta^{18}O$	$\delta^{18}O$	20°C	30°C
	VPDB	VSMOW	VPDB	VSMOW	VSMOW
U-13	-7,49	26,04	-4,72	-7,9	-5,35
U-10	-7,66	25,85	-4,91	-8,05	-5,58
U-7	-7,32	26,17	-4,59	-7,8	-5,30
U-6c	-7,57	26,35	-4,42	-7,73	-5,15
U-5	-7,39	26,4	-4,37	-7,70	-5,07
U-2	-7,57	26,4	-4,37	-7,70	-5,07
A-1	-7,74	26,55	-4,23	-7,45	-5
A-3	-7,11	26,82	-3,97	-7,2	-4,75
A-4	-7,7	26,17	-4,59	-7,8	-5,30
A-6	-7,64	26,31	-4,46	-7,74	-5,16
A-15	-7,8	25,73	-5,02	-8,30	-5,70
BALA SECTION				Calculated Fluid $\delta^{18}O$ (SMOW)	
Sample	$\delta^{13}C$	$\delta^{18}O$	$\delta^{18}O$	0°C	25°C
	VPDB	VSMOW	VPDB	VSMOW	VSMOW
B-2	-5,96	23,5	-7,19	-11	-4,9
B-4	-9,22	22,79	-7,88	-11,8	-5,8
B-5	-8,57	22,23	-8,42	-12,4	-6,4
BC	-8,32	23,11	-7,57	-11,6	-5,5
B-15	-6,99	23,02	-7,65	-11,5	-5,6
B-16	-7,15	22,08	-8,56	-13	-6,6
B-17	-6,5	21,98	-8,66	-13,1	-6,7

Comparing the proxy data of Bala section, the same conclusion can be drawn. In dry periods which are marked with gray areas favour the formation of palygorskite and calcite while smectite decreases in amount. CIA-K values are low in dry periods while salinity and calcification are high leading high values of $\delta^{13}C$ and $\delta^{18}O$.

Towards the top of the section, the aridity conditions are enough to have the calcretes while the lower levels passing arid conditions do not show well-developed nodular calcretes but have powdery calcrete formations. The wet conditions on the other hand progress the pluvials and favour the formation of eluviation zones where leaching values are high.

Having an age data on calcretes of Bala section, the results can be compared with the global data. The ages found are really important dates, since it is the time for Middle Pleistocene period that the periodicity of glacial response changes from 41,000 yrs to 100 000 yrs affecting the temperature and precipitation patterns over the European continent (Lisiecki and Raymo, 2007). This was the start of warmer periods until the Holocene. Between 450 kyr and 780kyr, the interglacial period favours arid conditions over this continent. It has been stated in Kapur et al. 1987 that the calcretes in the southern part of Turkey were formed during Middle Pleistocene interglacial periods. The calcretes dated in the Bala section are the lowest levels of the semi-mature nodular calcretes, the lower ones are not calcretes but are calcified soils. Therefore, it can be stated that the formation of calcretes in Bala section started at 761 ±120ka which is the time of climatic periodicity change. Also, this time is the time of Mid-Brunches Event which is the time for warming (Kitaba et al., 2011) (Figure 9.6).

A general schematic model is produced in this study to represent to contrasting and alternating periods as climate changed from semi-arid to more humid conditions.

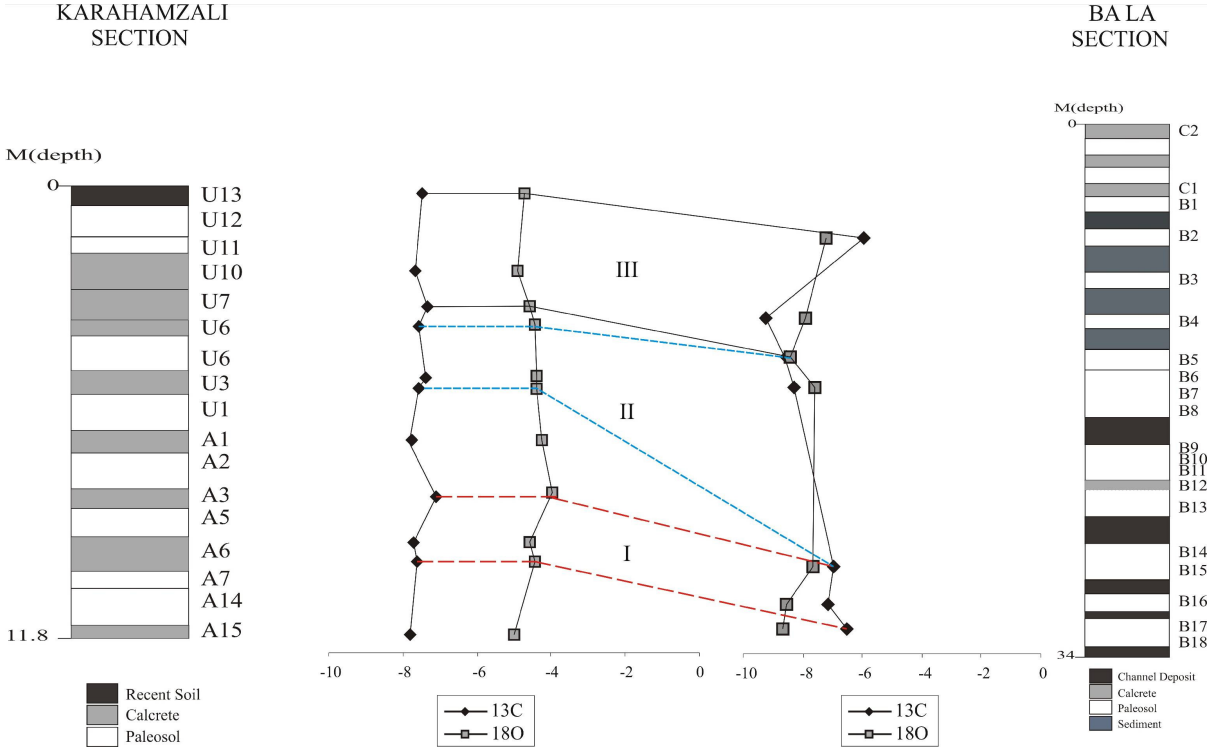

Figure 9.3. Comparison of the stable isotope values of both sections studied.

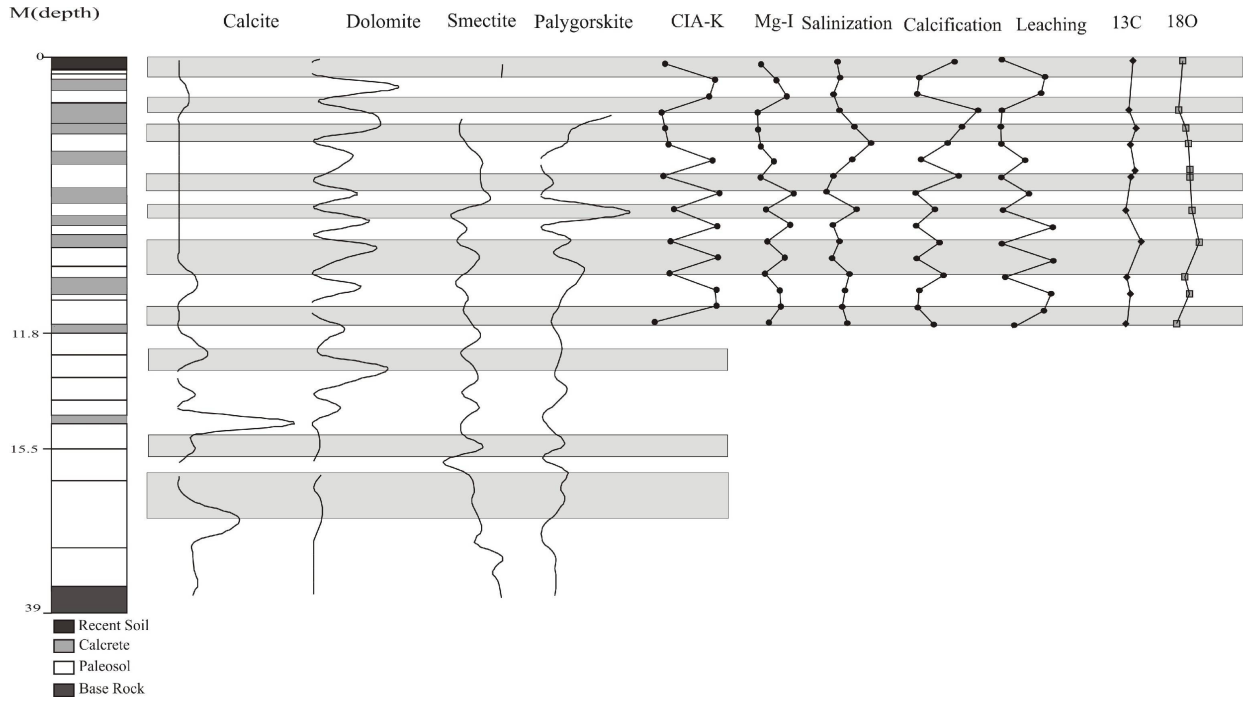

Figure .9.4. Interpretation of all proxy data of Karahamzalı section (gray areas show dry periods, the rest represents wet conditions)

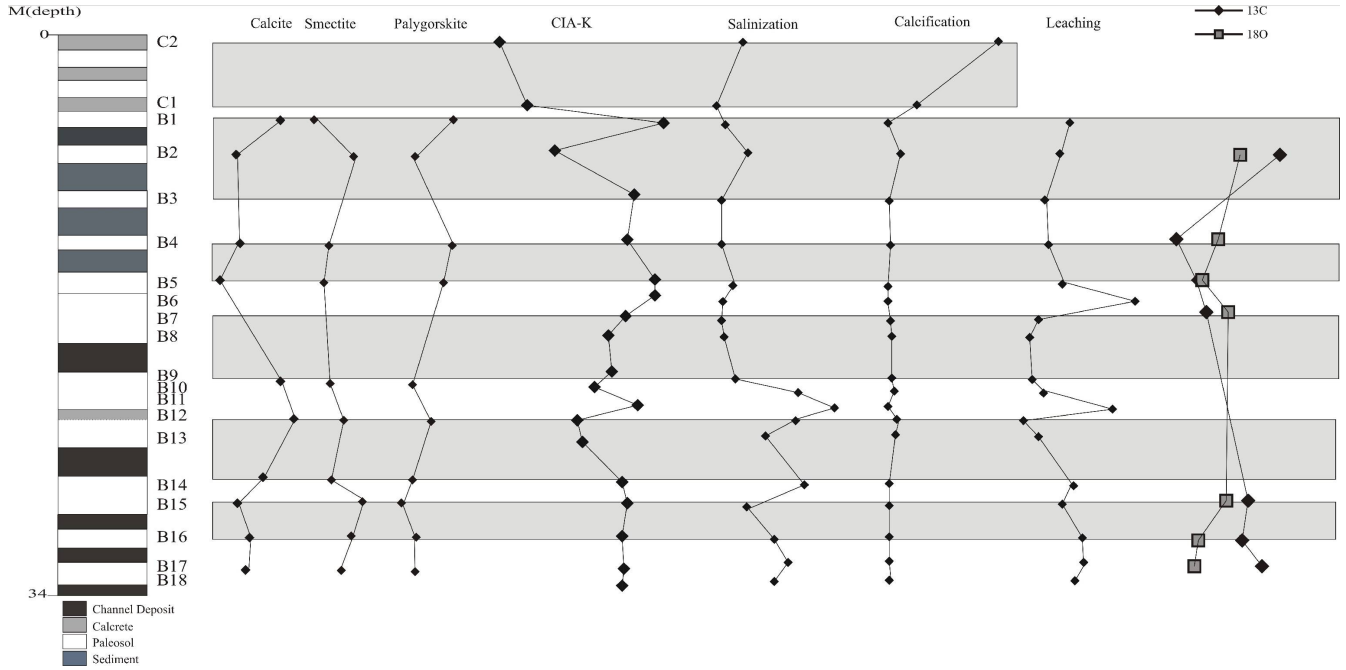

Figure 9.5. Interpretation of all proxy data of Bala section(gray areas show dry periods, the rest represents wet conditions).

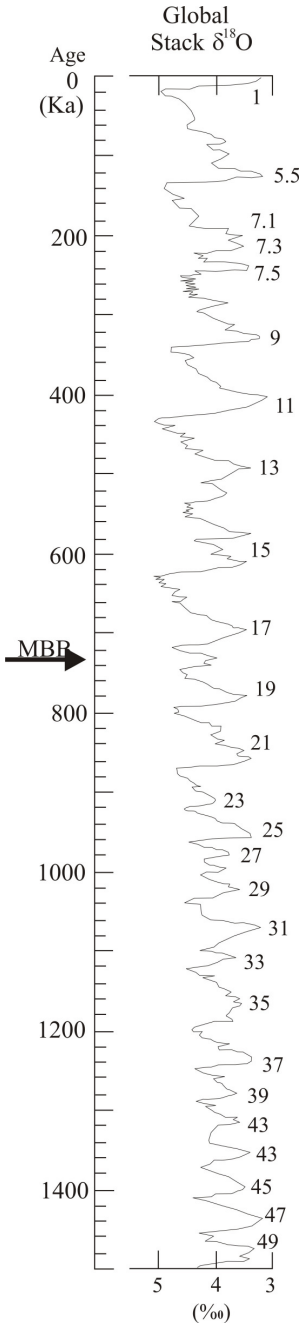

Figure 9.6. Global Stack $\delta^{18}O$ data showing marine isotope stages (Kitaba et al., 2011).

The semi-arid conditions caused the fluvial system to retreat so that the channel become thinner. The marginal alluvial fan became inactive blocking any sediment influx to the basin allowing the formation of paleosols and calcretes (Figure 9.7a) (Armenteros and Huerta, 2006). Semi-arid conditions favoured the formation of dolomite and palygorskite. The change from dry and semi-arid to wet and humid conditions support the high sediment influx to the Basin which also nourished the fluvial system. Therefore, the channels became thicher and laterally expandable. The increase in clastic input and water supply raised base level and caused the expansion of the fluvial systems which inhibit the formation of calcretes (Figure 9.7b). The wet conditions, especially in Bala section, allowed the neoformation of smectite.

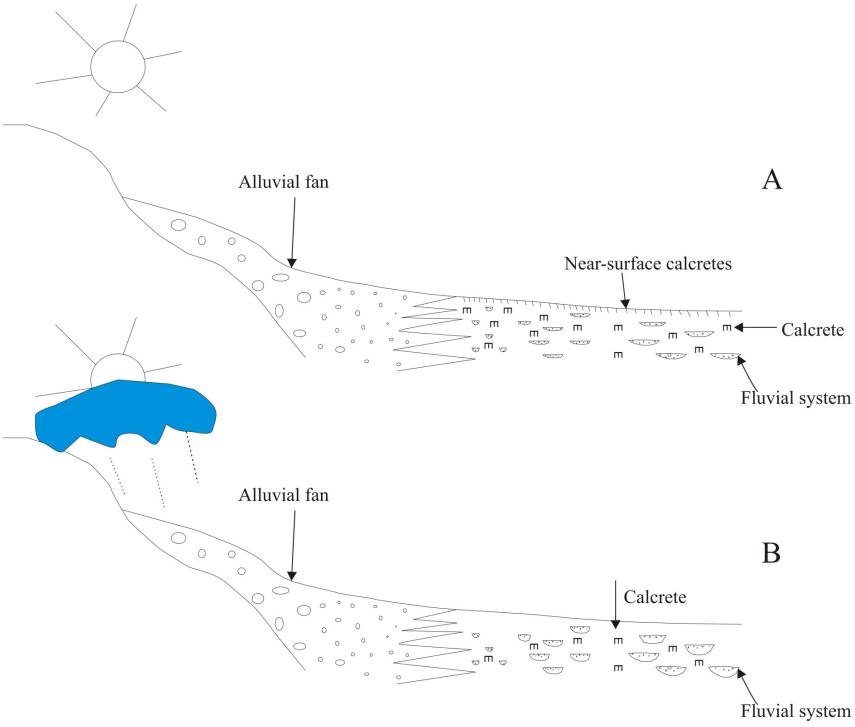

Figure 9.7. Schematic model representing (a) semi-arid, (b) wet conditions in the region (modified from Armenteros and Huerta, 2006).

CHAPTER 10

CONCLUSION

The following conclusions can be made at the end of this study.

1) Presence of pedofeatures like clay cutans, floating grains, circumgranular cracks, MnO_2 linings, secondary carbonate rims, presence of past bioturbation and remnants of root fragments document that the call the reddish alluvial/colluvial deposits in and around the Ankara region are paleosols and the carbonate concretions stand for the calcretes.
2) This study reveals that there is a consistency between the isotope values, the mineralogical compositions, the geochemical similarities and micromorphological characteristics of the paleosols and the calcretes of Karahamzalı and Bala sections.
3) Paleosols can be classified as PaleoCalcisols and PaleoCambisols due to their mineralogical and micromorphological characteristics. On the other hand, calcretes are of pedogenic origin wherein stage II-III, the semi-mature calcretes formed in the vadose zone of the depositional environment. Dolomite-bearing calcretes in the Karahamzalı section are also calcretes or dolomitic calcretes. The biological activityreflects the alpha and beta properties of the calcretes.
4) The studied calcretes are powdery to nodular and massive. Paleosols, on the other hand, show prismatic, to subangular-angular blocky to granular microstructures with horizon developments.
5) Quartz and feldspar are two common detrital minerals found both in Karahamzalı and Bala sections, and also present in other neighbouring sites. Calcite is the carbonate mineral of the Bala calcretes and for the other sampling sites. On the other hand, dolomite is determined in the Karahamzalı section.

6) Palygorskite is found to be pedogenic for both sections, but not determined in the other sites. Dolomite on the other hand is also a secondary carbonate in the Karahamzalı section. Stoichiometry studies have identified the near-surface early diagenetic origin, formed mostly by the influence of climate. The non-stoichiometric goupes II and III of dolomites (Tucker, 1988) most likely point out to the presence of dry and humid conditions respectively. Mg needed for both palygorskite and dolomite formations were most probably supplied from smectite.
7) The contents of palygorskite together with dolomite in the Karahamzalı section implies to the increase of aridity towards the top of the section. Most likely, the increase in palygorskite with calcite in the Bala section with decreasing smectite content manifests the same trend. Chlorite, kaolinite and illite are the detrital clay minerals found in the studied samples.
8) Geochemical studies state that during the formation of paleosols the influx rate was very small, not affecting the geochemical signature of the region. The provenance of both sections have the same geochemical characteristics which are stable during the paleosol development.
9) Molecular weathering ratios are in aggrement with the mineralogical data throughout the section implying high calcification and salinization in calcrete levels where high clayeyness, leaching and base loss were also recorded in the other horizons of the paleosols. The chemical index of alteration values show that the paleosols were subjected to medium and high degrees of weathering whereas low values were determined for the calcretes.
10) The reddish soils reveal that the main soil forming process in the region was calcification and the brown soils with steppe vegetation reveal a less vigorous leaching/reddening and calcification-decalcification trend.
11) The Evolution history of the calcretes in the Çukurova Basin proposed by Kapur et al. 1990 is also valid for the calcretes in the Ankara region. The

following stages are summarşzed from Kapur et al. (1990), as 1) the deposition of the Pliocene clayey sediments, 2) formation of the cuboidal structural units by cracking, 3) CO3 enrichment occurring during arid conditions followed by leaching along vertical units during the wet periods of the Pleistocene, 4) the development of the vertical calcite columns and the formation of the moderately calcareous surface soils. The decalcification of the soil and calcification leadingto the formation of the massive calcretes and 6) progressive rubefaction to red hues of 2.5YR and 10YR prevails together with the development of a massive, thin crust with a totally decalcified, friable red soil finally eroded leaving the crust outcroping at the surface.

12) The stable isotope values of the studied samples are consistent with each other indicating the formation from percolating soil-solutions under predominantly C4 to C3:C4 association type vegetation. Temperature calculations show that the paleoclimatic conditions favouring the formation of calcretes in the region are semi-arid, seasonally dry with pluvial alternations. The estimated soil depositional temperature for the formation of calcretes is calculated as approximately 25°C.
13) The proxy data of both sections are consistent with the world Pedogenic paleosols.
14) This study is the first to present radiometric age data for the calcretes of Central Anatolia, Ankara. The calculated ESR ages fall in the range of Middle Pleistocene when MBE was happened and theclimatic periodicity changes affecting the climatic control over the European continent. This period is the time dated on Bala calcretes, thus the study documents that the calcretes in the study area started to develop with MBE which leads to high temperaturesh and the formation of almost all Mediterranean type calcretes.

REFERENCES

Akarsu, İ., 1971. II. Bölge AR/TPO/747 No'lu Saha'nın terk raporu: Pet. İş. Gen. Müd., Ankara (unpublished).

Akgün, F., Kayseri, M.S., Akkiraz, M.S., 2007. Paleoclimatic evolution and vegetational changes during the Late Oligocene–Miocene period in Western and Central Anatolia (Turkey). Palaeogeography Palaeoclimatology Palaeoecology, 253, 56-90.

Akyürek, B., 1981. İç Anadolu'nun jeolojisi simpozyumu, Ankara melanjının kuzey bölümünün temel jeolojik özellikleri: TJK Yayını, 41-45, 56-58.

Akyürek, B. and Soysal, Y., 1978. Kırkağaç-Soma (Manisa)-Savaştepe-Korucu-Ayvalık (Balıkesir)-Bergama (İzmir) civarının jeolojisi, MTA Derleme No: 6432 (unpublished).

Akyürek, B., Bilginer, E., Dağer, Z. and Sunu, O., 1979a. Hacılar (K.Çubuk-Ankara) bölgesinde Alt Triyas'ın varlığı: TJK Bülteni, 22 (2).

Akyürek, B., Bilginer, E., Çatal, E., Dağer, Z., Soysal, Y. and Sunu, O., 1979b. Eldivan Şabanözü (Çankırı) dolayında ofiyolit yerleşimine ilişkin bulgular, JMO, 9.

Akyürek, B., Bilginer, E., Çatal, E., Dağer, Z., Soysal, Y. And Sunu, O., 1980. Eldivan-Şabanözü (Çankırı) Hasayaz-Çandır (Kalecik-Ankara) dolayının jeolojisi, MTA Derleme No: 6741 (unpublished).

Akyürek, B., Bilginer, E., Akbaş, B., Hepşen, N., Pehlivan, Ş., Sunu, O., Soysal, Y., Dağer, Z., Çatal, E., Sözeri, B., Yıldırım, H. and Hakyemez, Y., 1982. Ankara-Elmadağ-Kalecik dolayının jeolojisİ, MTA Derleme No: 7298 (unpublished).

Akyürek, B. And Soysal, Y., 1983. Biga Yarımadası güneyinin (Savaştepe-Kırkağaç-Bergama Ayvalık) temel jeoloji özellikleri, MTA Dergisi, 95/96, 1-12.

Akyürek, B., Bilginer, E., Akbaş, B., Hepşen, N., Pehlivan, Ş., Sunu, O., Soysal, Y., Dağer, Z., Çatal, E., Sözeri, B., Yıldırım, H. and Hakyemez, Y., 1984. Ankara-Elmadağ-Kalecik dolayının temel jeolojik özellikleri, Jeoloji Mühendisliğ,, 20, 31-46.

Akyürek, B., Akbaş, B. And Dağer, Z., 1988. 1/100 000 Ölçekli Açınsama Nitelikli Türkiye Jeoloji Haritaları Serisi, Çankırı E-16 Paftası, MTA Yayınları.

Akyürek, B., Duru, M., Sütçü, Y.F., Papak, İ., Şaroğlu, F., Pehlivan, N., Gönenç, O., Granit, S., Yaşar, T., 1997. MTA Genel Müdürlüğü Ankara F-15 Paftası, 1:100 000 ölçekli açınsama nitelikli Türkiye Jeoloji Haritaları, No.55.

Aras, İ.A., 1991. Clay Mineralogy and Sedimentological Features of the Late Pliocene Sediments in Ankara Area. M.Sc Thesis, METU, Ankara, p 87 (unpublished).

Arakel, A.V., 1982. Genesis of calcrete in Quaternary soil profiles, Hutt and Leeman lagoons, Western Australia, Paleogeography, Paleoclimatology, Paleoecology, 54, 283-303.

Arıkan, Y., 1975. Tuz Gölü Havzasının jeolojisi ve petrol olanakları, MTA Bull., 85, 17-37.

Armenteros, I. and Huerta, P., 2006. The role of clastic sediment influx in the formation of calcrete and palustrine facies: a response to paleographic and climatic conditions in the southeastern Tertiary Duero basin (northern Spain), Geological Society of America Bull., 416 119–132.

Andrews, JE., Singhvi, A.K., Kailath, A.J., Kuhn, R., Dennis, P.F., Tandon, S.K., and Dhir, P.R., 1998. Do stable isotope data from calcrete record Late Pleistocene monsoonal climate variation in the Thar Desert of India? Quaternary Research, 50, 240-251.

Atabey, E., Atabey, N., and Kara, H., 1998. Sedimentology of caliche (calcrete) occurrences of the Kırşehir region. Bulletin of the Mineral Research and Exploration, 120, 69–80.

Atalay, I., 1996. Palaeosols as indicators of the climatic changes during Quaternary period in S Anatolia. Journal of Arid Environments, 32, 23–35.

Bailey, S. W., 1991. Practical notes concerning the X-ray powder diffraction patterns of clay minerals. Clays and Clay Minerals, 39, 184-190.

Batman, B., 1978. Haymana kuzeyinin jeolojik evrimi ve yöredeki melanjın incelenmesi: I. Stratigrafi Birimleri, H.Ü. Yerbilimleri Bull., 4(1-2), 95-124.

Billard, A., 1993. Is a middle Pleistocene climatic optimum recorded in the loess-paleosol sequences of Euroasia?. Quat. Int., 17, 87–94

Bingöl, E., Akyürek, B. and Korkmazer, B., 1973. Biga Yarımadası'nın jeolojisi ve Karakaya formasyonunun bazı özellikleri. Cumhuriyet'in 50. yılı Yer Bilimleri Kongresi Tebliğleri , MTA publication, 70-77.

Birgili, Ş., Yoldaş, R. and Ünalan, G., 1975. Çankırı-Çorum havzasının jeolojisi ve petrol olanakları, MTA Report No: 5621 (unpublished).

Birkeland, P.W., 1999. Soils and Geomorphology, 3rd edn. Oxford University Press, New York, p 430.

Biscaye, P.E., 1965. Mineralogy and sedimentation of recent deep sea clay in the Atlantic Ocean and adjacent seas and oceans. Geol. Soc. Amer. Bull. 76, 803– 832.

Bradley, R.S., 1999. Paleoclimatology: Reconstructing Climates of the Quaternary. Academic Press, San Diego, p 610.

Brindley, G.W., 1980. Quantitative X-ray analyses of clays. In: Brindley, G.W. and Brown, G. (eds), Crystal Structures of Clay Minerals and Their X-ray Identification. Mineralogical Society Monograph 5, 411–438.

Bullock, P. Fedoroff, N., Jongerius, A., Stoops, G., Tursina, T. and Babel, U. 1985. Handbook of Soil Thin Section Description. Waine Research Publications, p 150.

Buol, S.W., Hole, F.D., McCracken, R.J. and Southard, R.J., 1997. Soil Genesis and Classification, Iowa State University Pres, Mes, IA, p 527.

Calvi S.W. and Kleinsorge, H., 1940. Geologische und hydrologische Beobachtungen über zent ralanotolia Ova, MTA , 19, 186-212.

Calvi S.W., Kleinsorge, H. 1940. Merkezî Anadolu ovalarının jeolojik ve hidrolojik müşahedeleri hakkindaki almanca makalenin hulâsası. Mineral Research and Exploration Bulletin. 2 (19), 184–211 (in Turkish).

Candy, I., Coope, G.R., Lee, J.R., Parfitt, S.A., Preece, R.C., Rose, J., and Schreve, D.C., 2010. Pronounced warmth during early Middle Pleistocene interglacials: Investigating the Mid-Brunhes Event in the British terrestrial sequence. Earth-Science Reviews, 103, (3-4), 183-196.

Carlisle, D., 1983. Concentration of uranium and vanadium in calcretes and gypscretes. In: Wilson, R.C.L., (Ed.), Residual deposits. Surface Related Weathering Processes and Materials. London. Geol. Soc. London and Blackwell, 185–195.

Cerling, T.E, 1984. The stable isotopic composition of modern soil carbonate and its relationship to climate. Earth and Planetary Science Letters, 71, 229–240.

Cerling, T.E. and Hay, H.L., 1986. An isotopic study of paleosol Carbonates from Olduvai Gorge, Quaternary Research, 25, 63-78.

Cerling, T.E., Solomon, D.K., Quade, J., and Bowman, J.R., 1991. On the isotopic composition of carbon in soil carbon dioxide. Geochimica et Cosmochimica Acta, 55, 3403– 3405.

Chamley, H., 1989. Clay Sedimentology, Springer, New York, p 623.

Chaput, E., 1936. Türkiye'de jeolojik ve jeomorfolojik tetkik seyahatleri. İ.Ü. Yayınları, p 324.

Chen, P.Y., 1977. Table of key lines in X-ray powder diffraction patterns of minerals in clays and associated rocks. Department of Natural Resources, Geological Survey Occasional Paper 21. Bloomington, Indiana, USA.

Cullers, R.L., Basu, A., and Suttner, L., 1988. Geochemical signature of provenance in sand-size material in soils and stream sediments near the Tobacco Root batholite, Montana, USA. Chemical Geology, 70, 335–348.

Çalgın, R., Pehlivanoğlu, H., Ercan, T. and Şengün, M., 1973. Ankara civarının jeolojisi, MTA Der. Report No: 6487 (unpublished).

Çapan, U.Z. and Buket, E., 1975. Aktepe-Gökdere bölgesinin jeolojisi ve ofiyolitli melanjı, TJK Bull., 18(1), 11-16.

Çobanoğlu, I., Bozdağ, S.¸ and Kumsar, H., 2008. Microstructural, geochemical and geomechanical properties of caliche deposits from the Adana Basin, Turkey. Bull Eng Geol Environ.

Deutz, P., Montanez, I.P., Monger, H.C., Morrison, J., 2001. Morphology and isotope heterogeneity of Late Quaternary pedogenic carbonates: Implications for paleosol carbonates as paleoenvironmental proxies. Palaeogeography, Palaeoclimatology, Palaeoecology, 166, 293–317.

Deutz, P., Montanez, I.P. and Monger, H.C., 2002, Morphologies and stable and radiogenic isotope compositions of pedogenic carbonates in Late Quaternary relict and buried soils, New Mexico: an integrated record of Pedogenic overprinting. J. Sed. Res., 72, 809–822.

Dinç, U., Şenol, S., Kapur, S., and Sarı, M., 1991. Catenary Soil Relationships in the Çukurova Region, southern Turkey. CATENA, 18, 185-196.

Dönmez, M., Akçay. A.E., Kara, H., Yergök, A.F., Esentürk, K., 2008. 1:100 000 ölçekli Türkiye Jeoloji Haritaları Kırşehir I-30 Paftası. MTA Publications No: 91, Ankara.

Eastwood, W.J., Leng, M.J., Roberts, N., and Davies, B., 2007. Holocene climate change in the eastern Mediterranean region: a comparison of stable isotope and pollen data from Lake Gölhisar, southwest Turkey. Journal of Quaternary Science, 22, 327–341.

Eren, M., 2007. Genesis of tepees in the Quaternary hardpan calcretes, Mersin, S Turkey. Carbonates and Evaporites 22, 123–134.

Eren, M., Kadir, S., Hatipoğlu, Z., and Gül, M., 2008. Quaternary calcrete development in the Mersin area, southern Turkey. Turkish Journal of Earth Sciences, 17, 763–784.

Eren, M., 2011. Stable isotope geochemistry of Quaternary calcretes in the Mersin area, southern Turkey – A comparison and implications for their origin, Chemie der Erde, 71, 31–37.

Erk, A., 1977. Ankara civarında genç Paleyozik'in Kulm fliş formasyonu, MTA Bull., 88, 73-93.

Erk, A.S., 1980. Ankara flişi, TÜBİTAK VII. Bilim Kongresi, Abstract Book, 16.

Ermolli, E.R. and Cheddadi, R., 1997. Climatic reconstruction during the Middle Pleistocene: A pollen record from Vallo di Diano (Southern Italy). Geobios, 30(6), 735-744.

Erol, O., 1956. Ankara güneydoğusundaki Elma Dağı ve çevresinin jeolojisi ve jeomorfolojisi üzerine bir araştırma. MTA Yayını, seri D, no.9.

Erol, O., 1961. Ankara Bölgesinin Tektonik Gelişmesi. TJK Bülteni, , 57–85.

Erol, O. 1973. Ankara şehri çevresinin jeomorfolojik ana birimleri. Dil, Tarih ve Coğrafya Fak. Yay. No. 240, 29 s, Ankara.

Erol, O., 1983. Türkiye'nin genç tektonik ve jeomorfolojik gelişimi. Jeomorfoloji Dergisi 11, 1–22 (in Turkish with English abstract).

Esteban, M. and Klappa, C.F., 1993. Subaerial exposure environments: Carbonate Depositional Environments (Eds.by P.A. Scholle, D.G.Bebout and C.H.Moore): AAPG.Mem.33,2-54.

FAO (Food and Agriculture Organization) (1974). Soil Map of the World. Vol. I Legend. Paris: UNESCO.

Fitzpatrick, E.A., 1993. Soil Microscopy and Micromorphology. John Wiley and Sons Ltd., p 304.

Friedman, I., O'Neil, J.R., 1977. Compilation of stable isotope fractionation factors of geochemical interest. In: Fleischer M. (Ed.), Data of Geochemistry, USGS Prof. Paper 440-KK, 1–12.

Fu, Q., Qing, H. and Bergman, K.M., 2004. Dolomitized calcrete in the Middle Devonian Winnipegosis carbonate mounds, subsurface of Southcentral Saskatchewan, Canada. Sedimentary Geology 168, 49–69.

Gay, A.L. and Grandstaffd, E., 1980. Chemistry and mineralogy of Precambrian paleosols at Elliot Lake, Ontario, Canada. Precambrian Res. 12, 349-73.

Gile, L.H., Peterson, F.F., and Grossman, R.B., 1966. Morphological and genetic sequences of carbonate accumulation in desert soils. Soil Science, 101, 347-360.

Gong, S.Y., Mii, H.S., Wei, K.Y., Horng, C.S., You, C.F., Huang, F.W., Chi, W.R., Yui, T.Z., Torng, P.K., Huang, S.T., Wang, S.W., Wu, J.C., Yang, K.M., 2005. Dry climate near the Western PacificWarmPool: Pleistocene caliches of the Nansha Islands, South China Sea. Palaeogeography, Palaeoclimatology, Palaeoecology, 226, 205–213.

Goudie, A.S., 1973. Duricrusts in Tropical Landscapes. Clarendon Press, Oxford, p. 174.

Goudie, A.S., 1983. Calcrete. In: Goudie, A.S., Pye, K. (Eds.), Chemical Sediments and Geomorphology. Academic Press, London, 93–131.

Göktürk, O.M., Fleitmann, D., Badertscher, S., Cheng,H., Edwards, R.L., Leuenberger, M., Fankhauser, A, Tüysüz, O., Kramers, J., 2011. Climate on the southern Black Sea coast during the Holocene: implications from the Sofular Cave record, Quaternary Science Reviews, doi:10.1016/j.quascirev.2011.05.007.

Göncüoğlu, M.C., Dirik, K. and Kozlu, H., 1996. General characteristics of pre-Alpine and Alpine Terranes in Turkey: Explanatory notes to the terane map of Turkey: Annales Geologique de Pays Hellenique, 37, Geol.Soc Greece, 515-536.

Gündoğdu, M.N., 1982. Geological, mineralogical and geochemical investigation of the Bigadiç Neogene volcano-sedimentary Basin, PhD thesis, Hacettepe University, Ankara, Turkey (unpublished).

Hakyemez, Y., Barkurt, M.Y., Bilginer, E., Pehlivan, Ş., Can, B., Dağer, Z. and Sözeri, B., 1986. Yapraklı Ilgaz-Çankırı-Çandır dolayının jeolojisi, MTA Derleme No: 7966 (unpublished).

Han, J., Fyfe, W.F. and Longstaffe, F.J., 1998. Climatic implications of the S5 paleosol complex on the southernmost Chinese Loess Plateau. Quat. Res., 50, 21–33.

Haug, G.H., Hughen, K.A., Sigman, D.M., Peterson, L.C., Rfhl, U., 2001. Southward migration of the Intertropical Convergence Zone through the Holocene. Science, 293, 1304–1308.

Haug, G.H., Granopolski, A., Sigman, D.M., Rosell-Mele, A., Swann, G.E.A., Tiedemann, R., Jaccard, S.L., Bollman, J., Maslin, M.A., Leng, M.J., Eglington, G., 2005. North Pacific seasonality and the glaciation of North America 2.7 million years ago. Nature 433, 821–825.

Ikeya, M., 1993. New applications of Electron Spin Resonance: Dating, Dosimetry and Microscopy. World Scientific, Singapore.

IPCC fourth assessment report: Climate Change 2007. Chapter 10, global climate projections p 100.

Jackson, M.L., 1979. Soil chemical anaylsis-advaced course, 2nd edition. Published by the author, Madison, Wisconsin, U.S.A., 895p.

James, N.P., 1972. Holocene and Pleistocene calcareous crust (caliche) profiles: Criteria for Subaerial exposure, J.Sed. Petrol., 42,817-836.

James, N.P., and Choquette, P.W., 1990. Limestones – the sea floor diagenetic environment. In: Diagenesis (Eds A. McIlreath and D.W. Morrow), Geosci. Canada Report Ser., 4, 13–34.

Jeong, G.Y., Hillier, S., and Kemp, R.A., 2008. Quantitative bulk and single-particle mineralogy of a thick Chinese loess-paleosol section: implications for loess provenance and weathering. Quaternary Science Reviews, 27, 1271-1287.

Jimenez-Espinosa, R. and Jimenez-Millan, J., 2003. Calcrete development in Mediterranean colluvial carbonate systems from SE Spain. Journal of Arid Environments, 53, 479–489.

Jones, M.D., Roberts, N., Leng, M.J., Türkes, M., 2006. A high-resolution late Holocene lake isotope record from Turkey and links to North Atlantic and monsoon climate. Geology, 34, 361–364.

Kadir, S., Eren, M., 2008. The occurrence and genesis of clay minerals associated with Quaternary caliches in the Mersin area, southern Turkey. Clays and Clay Minerals, 56, 244–258.

Kaakinen, A., Sonninen, E., and Lunkka, J.P., 2006. Stable isotope record in paleosol carbonates from the Chinese Loess Plateau: Implications for late

Neogene paleoclimate and paleovegetation. Palaeogeography, Palaeoclimatology, Palaeoecology, 237 (2-4), 359-369.

Kalkan, İ., Şaroğlu, F., Özmutaf, M., Atiker, M., Yıldırım, N., Süzük, H. and Tanıl, A., 1992. Eymir-Mogan Göllerinin Korunmasına Yönelik Jeoloji-Hidrojeoloji İncelemeleri, MTA Derleme No: 9477.

Kapur, S., Çavusgil, V.S., Fitzpatrick, E.A., 1987. Soil–calcrete (caliche) relationship on a Quaternary surface of the Çukurova Region, Adana (Turkey). In:Federoff, N., Bresson, L.M., Courty, M.A. (Eds.), Soil Micromorphology. Association Francaise pour L'Etudedusol, Paris, 597–603.

Kapur, S., Çavuşçugil, V., Şenol, M., Gürel, N. and FitzPatrick, E.A., 1990. Geomorphology and pedogenetic evolution of Quaternary calcretes in the northern Adana Basin of southern Turkey: Z. Geomorphology, N.F., 34 (1), 49-59.

Kapur, S., Yaman, S., Gökçen, S.L., Yetiş, C., 1993. Soil stratigraphy and Quaternary caliche in the Misis area of the Adana Basin, southern Turkey, Catena, 20, 431–445.

Kapur, S., Saydam, C., Akça, E., Çavuşgil, V.S., Karaman, C., Atalay, I., Özsoy, T., 2000. Carbonate pools in soil of the Mediterranean: a case study from Anatolia. In: Lal, R., Kimble, J.M., Eswaran, H., Stewart, B.A. (Eds.), Global Climate Change and Pedogenic Carbonates. Lewis Publishers, Boca Raton, Florida, 187–212.

Karakaş¸, Z. and Kadir, S., 1998. Mineralogical and genetic relationships between carbonate and sepiolite-palygorskite formations in the Neogene Lacustrine Konya Basin, Turkey. Carbonates and Evaporites, 13, 198-206.

Kasapoğlu, K.E., 1982. Ankara kenti zeminlerinin jeo-mühendislik özellikleri: Yerbilimleri, 9,19-40.

Khadkikar, A.S., Merh, S.S., Malik, J.N., Chamyal, L.S., 1998. Calcretes in semi-arid alluvial systems: formative pathways and sinks. Sedimentary Geology, 116, 251-260.

I. Kitaba, I., Harada, M., Hyodo, M., Katoh, S., Sato, H., and Matsushita, M., 2011. MIS 21 and the Mid-Pleistocene climate transition: Climate and sea-level variation from a sediment core in Osaka Bay, Japan. Palaeogeography, Palaeoclimatology, Palaeoecology, 299, 227–239

Kiper, B.O., 1984. Pliyosen'de Ankara ile Etimesgut-Batıkent Havzaları Arasında Uzanan Paleosırt. JMO Dergisi, No: 21, 34–38.

Koçyiğit, A., 1987. Hasanoğlan (Ankara) Yöresinin Tektono-Stratigrafisi: Karakaya Orojenik Kuşağının Evrimi. Yerbilimleri, 14, 269-293.

Koçyiğit, A., 1991. An example of an accretionary forearc basin from northern Central Anatolia and its implications for the history of subduction of Neo-Tethys in Turkey. Geological Society of America Bulletin, 103, 22–36.

Koçyiğit, A., 2000. General neotectonic characteristics and seismicity of Central Anatolia. Haymana-Tuzgölü-Ulukışla Basenleri Uygulamalı Çalışma, Türkiye Petrol Jeologları Derneği Özel Sayı 5, 1-26.

Koçyiğit, A., Türkmenoğlu, A., 1991. Geology and mineralogy of the so-called Ankara clay formation: A geologic approach to Ankara clay problem: In Zor, M. (Editor), Proceedings of the 5th National Symposium on Clay, Anatolia University, Eskişehir, Turkey, 112–125.

Koçyiğit, A. and Deveci, Ş., 2008. Ankara Orogenic Phase, Its Age and Transition From Thrusting-dominated Palaeotectonic Period to the Strike-slip Neotectonic Period, Ankara (Turkey), Turkish Journal of Earth Sciences, 17, 2008, 433–459.

Kraus, M.J., 1999. Paleosols in clastic sedimentary rocks: their geologic significance. Earth-Sci. Rev., 47, 41–70.

Krumbein, W.C., and Garrels, R.M., 1952. Origin and classification of chemical sediments in terms of pH and oxidation-reduction potentials. The Journal of Geology, 60 (1), 1–33.

Kutzbach, J., Martinson, D.G., McIntyre, A., Mix, A.C., Molfino, B., Morley, J.J., Peterson, L.C., Pisias, N.G., Prell, W.L., Raymo, M.E., Shackleton, N.J., Toggweiler, J.R., 1993. On the structure and origin of major glaciation cycles. Part 2: The 100,000-year cycle. Paleoceanography 8, 699–735.

Küçükuysal, C., Engin, B., Türkmenoğlu, A.G., and Aydaş, C., 2011. ESR dating of calcrete nodules from Bala, Ankara (Turkey): Preliminary results. Applied Radiation and Isotopes, 69 (2), 492-499.

Lahn, E., 1949. Orta Anadolu'nun Jeolojisi Hakkında. TJK Bülteni, CII No:1.

Leng, M.J., Roberts, N., Reed, J.M., Sloane, H.J., 1999. Late Quaternary palaeohydrology of the Konya Basin, Turkey based on isotope studies of modern hydrology and lacustrine carbonates. Journal of Paleolimnology, 22, 187–204.

Li, Y.H., 2000. A Compendium of Geochemistry. Princeton University Press, Princeton.475 pp.

Lisiecki, L.E., Raymo, M.E., 2005. A Pliocene–Pleistocene stack of 57 globally distributed benthic $\delta^{18}O$ records. Paleoceanography 20, PA1003.

Lisiecki, L. E., and M. E. Raymo, 2007. Plio-Pleistocene climate evolution: Trends and transitions in glacial cycle dynamics, Quaternary Science Reviews, 26, 56-69.

Litt, T., Krastel, S., Sturm, M., Kipfer, R., Örçen, S., Heumann, G., Franz, S.O., Ülgen, U.B. and Niessen, F., 2009. 'PALEOVAN', International Continental Scientific Drilling Program (ICDP):site survey results and perspectives. Quaternary Science Reviews, 28, 1555–1567.

Lumsden, D.N., 1979. Discrepancy between thin-section and X-ray estimates of dolomite in limestone . Journal of Sedimentary Research, 49 (2), 429-435.

Lumsden, D.N. and Chimahusky. J.S., 1980. Relationship between dolomite nonstoichiometry and carbonate facies parameters. In: Concepts and Models of Dolomitization (Ed. by D. H. Zenger, J. B. Dunham & R. L. Ethington), Spec., publs., Soc. Econ. Paleont. Miner., 28, 123–137.

Mack, G.H., Cole, D.R., Giordano, T.H., Schaal, W.C. and Barcelos, J.H., 1991. Paleoclimatic controls on stable oxygen and carbon isotopes in caliche of the Abo Formation (Permian), south-central New Mexico, U.S.A.. J. Sediment. Petrol., 61, 458–472.

Machette, M.N., 1985. Calcic soils of southwestern United States. Geol. Soc. Am. Spec. Paper, 203, 1–21.

Mack, G.H., Cole, D.R., Giordano, T.H., Schaal, W.C., and Barcelos, J.H., 1991. Paleoclimatic controls on stable oxygen and carbon isotopes in caliche of the Abo Formation (Permian), south-central New Mexico, U.S.A. Journal of Sedimentary Petrology 61, 458–472.

Mack, G.H., James, C.W., and Monger, C.H., 1993. Classification of paleosols, Geol. Soc. Am. Bull., 105, 129–136.

Maynard, J.B., 1992. Chemistry of Modern Soils as a Guide to Interpreting Precambrian Paleosols. The Journal of Geology, 100, 279-289.

McCarthy, P.J and Plint, A.G., 1998. Recognition of interfluve sequence boundaries: integrating paleopedology and sequence stratigraphy. Geology, 26, 387–390.

Morozova, T.D., 1995. T.D. Identification of paleosol types and their applicability for paleoclimatic reconstruction. GeoJournal, 36 (2/3), 199–205.

Morrow, D.W., 1978. The influence of the Mg/Ca Ratio and salinity on dolomitization in evaporite basins: Canadian Soc. Petroleum Geol. Bull., 26, 389-392.

Morrow, D.W., 1982. Diagenesis 1. Dolomite part 1. The chemistry of dolomitization and dolomite precipitation. Geoscience Canada, 9 (1), 5-13.

Millot, G., 1970. Geology of Clays. Springer, New York, N.Y., 429 p.

Müller, G., 1957. Ankara'nın güney havalisinde su bulma imkanı hakkında rapor, MTA Derleme No: 2523 (unpublished).

Nesbitt, H.W. and Young, G.M., 1982. Early Proterozoic climates and plate motions inferred from major element lutites. Nature, 299, 715-717.

Nesbitt, H.W. and Young, G.M., 1984. Prediction of some weathering trends of plutonic and volcanic rocks based thermodynamic and kinetic considerations. Geochimica et Cosmochimica Acta, 48, 1523-1534.

Nesbitt, H.W. and Young, G.M., 1989, Formation and diagenesis of weathering profiles, Journal of Geology, 97, 129-147.

Netterberg, F., 1967, Some road making properties of South African calcretes. Proceeding 4th Reg.Conf. Soil Mech. Fndn Engng., Cape Town, 1, 77-81.

Netterberg, F., 1980. Geology of southern African calcretes.I Terminology, description, macrofeatures and classification. Trans. Geol. Soc. S. Afr., 83, 255-283.

Nettleton, W.D., Brasher, B.R., Benham, E.C and Ahrens, R.J., 1998, A classification system for buried paleosols, Quaternary International, 51/52, 175-183.

Nettleton, W.D., Olson, C.G. and Wysocki, D.A., 2000, Paleosol classification: problems and solutions, Catena, 41, 61-92.

Norman, T., 1973, Ankara Melanjının yapısı hakkında, Cumhuriyet'in 50. yılı Yerbilimleri Kongresi Tebliğleri Dergisi, MTA Publications, 77-94.

Ordemir, İ., Soydemir, Ç.ve Birand, A., 1977. Swelling Problems of Ankara Clay. IXth International Conference on Soil mechanics and Foundation Engineering Proceedings, Tokyo.

Ozansoy, F., 1957. Türkiye Tersiyer Memeli Faunaları ve Stratigrafik Revizyonları. MTA Dergisi, No: 49, 11-23.

Özer, A.M., Wieser, A., Göksu, H.Y., Müller, P., Regulla, D.F., Erol, O., 1989. ESR and TL age determination of caliche nodules. International Journal of Radiation Appli- cations and Instrument. Part A: Applied Radiation and Isotopes 40, 1159–1989.

Özkaya, İ., 1982. Origin and tectonic setting of some melange units in Turkey, Journal of Geology, 90, 269-278.

Peryam, T.C., Dorsey, R.J., Bindeman, I., 2011. Plio-Pleistocene climate change and timing of Peninsular Ranges uplift in southern California: Evidence from paleosols and stable isotopes in the Fish Creek–Vallecito Basin. Palaeogeography, Palaeoclimatology, Palaeoecology, 305, 65–74.

Pisias, N.G., Moore Jr., T.C., 1981. The evolution of the Pleistocene climate: a time series approach. Earth and Planetary Science Letters 52, 450–458.

Porat, N., 1992. ESR dating of carbonate Nodules II. Israel Geological Survey Technical Progress Report TR-GSI/28/92, 13 p.

Roser, B.P., and Korsch R.J., 1988. Provenance signatures of sandstone-mudstone suites determined using discriminant function analysis of major-element data. Chemical Geology, 67 (1-2), 119-139.

Quade, J., Cerling, T.E. and Bowman, J.R., 1989. Systematic variations in the carbon and oxygen isotopic composition of Pedogenic carbonate along elevation transects in the southern Great Basin, United States, Geol. Soc. Am. Bull., 101, 464-475.

Quade, J., Cerling, T.E., 1995. Expansion of C-4 grasses in the Late Miocene of northern Pakistan — evidence from stable isotopes in paleosols. Palaeogeography, Palaeoclimatology, Palaeoecology, 115, 91–116.

Ravelo, A.C., Andreason, D.H., Lyle, M., Lyle, A.O., Wara, M.W., 2004. Regional climate shifts caused by gradual cooling in the Pliocene epoch. Nature 429, 263–267.

Retallack, G.J., 1988. Field recognition of paleosols. In: Paleosols and Weathering Through Geologic Time: Principles and Applications (Eds J. Reinhardt and W.R. Sigleo), Geol. Soc. Am. Spec. Paper, 216, 1–20.

Retallack, G. J. (1992). Comment on the paleoenvironment of Kenyapithecus at Fort Ternan. J. hum. Evol. **23,** 363–369.

Retallack, G. J. (1997). A Colour Guide to Paleosols.Chichester: Wiley.

Retallack, G.J., 2001. Soils of the past. Blackwell, Oxford. 600 p.

Roberts, N., Reed, J., Leng, M.J., Kuzucuoğlu, C., Fontugne, M., Bertaux, J., Woldring, H., Bottema, S., Black, S., Hunt, E. And Karabıyıkoğlu, M., 2001: The tempo of Holocene climatic change in the eastern Mediterranean region: new high-resolution crater-lake sediment data from central Turkey. The Holocene, 11, 721–36.

Robinson, D. And Wright, V.P., 1987. Ordered illite-smectite and kaolinite-smectite: Pedogenic minerals in a Lower Carboniferous paleosol sequence, South Wales, Clay Minerals, 22, 109-118.

Robinson, S.A., Andrews, J.E., Hesselbo, S.P., Radley, J.D., Dennis, P.F., Harding, I.C., Allen, P., 2002. Atmospheric pCO2 and depositional environment from stable-isotope geochemistry of calcrete nodules (Barremian, Lower Cretaceous, Wealden Beds, England). Journal of the Geological Society, London 159, 215–224.

Ruddiman W.F., Raymo M.E., Martinson D.G., Clement B.M., and Backman J., 1989. Pleistocene Evolution: Northern Hemisphere Ice Sheets and North Atlantic Ocean. Paleoceanography, 4, 353–412.

Salomons, W., Goudie, A., and Mook, W.G., 1978. Isotopic composition of calcrete deposits from Europe, Africa and India. Earth Surface Processes, 3, 43–57.

Salomons, W.,Goudie, A. and Mook, W.G., 1978. Isotopic composition of calcrete deposits from Europe, Africa and India, Earth Surf. Proc., 3, 43-57.

Schellenberger, A. and Veit, H., 2006. Pedostratigraphy and pedological and geochemical characterization of Las Carreras loess-paleosol sequence, Vale de Tafi, NW Argentina. Quaternary Science Reviews, 25, 811-831.

Schmidt, C.G., 1960, Mem. 365-367 no'lu ruhsatlarının nihai terk raporu, Petrol İş. Gen. Müd., Ankara (unpublished).

Sezer, G.A., 1998. Cation Exchange Capacity and Contaminant Uptake Properties of Some Natural Clays as Potential Landfill Liners. M.Sc Thesis, METU, Ankara, p 116 (unpublished).

Sezer, G.A., Türkmenoğlu, A.G. ve Göktürk, E.H., 2003. Mineralogical and sorption characteristics of Ankara Clay as a landfill liner. Applied Geochemistry, 18, 711–717.

Sheldon, N.D. and Tabor, N.J., 2009. Quantitative paleoenvironmental and paleoclimatic reconstruction using paleosols. Earth-Science Reviews, 95 (1-2), 1-52.

Singer, A., 1980. The paleoclimatic interpretation of clay minerals in soils and weathering profiles. Earth Sci. Rev., 303-326.

Soil Survey Staff (1975) Soil Taxonomy. US Department of Agriculture Handbook, 436, p 754.

Soil Survey Staff (1998) Keys to Soil Taxonomy. US Department of Agriculture Natural Resources Conservation Service, Washington, DC, p 325.

Singer, A., 1980. The paleoclimatic interpretation of clay minerals in soils and weathering profiles. Earth Science Reviews, 303-326.

Süzen, M.L. and Türkmenoğlu, A.G., 2000. Lacustrine mineral facies and implications for estimation of paleoenvironmental parameters: Neogene intervolcanic Pelitçik Basin (Galatean Volcanic Province), Turkey. Clay Minerals, 35, 461-475.

Şen, Ş.; Heintz, E. and Gingsburg, L., 1974. Çalta fosil yataklarında yapılmış kazıların ilk sonuçları. M.T.A. Derg., no. 83, Ankara.

Şen, Ş., 1978. Anadolu'da Pliyosen Rodentia faunasının ilk incelemesi. MTA Sayı 89, 78-85.

Şen, Ş. Ve Rage, J.C., 1979. Çalta (Ankara) Pliyosen Omurgalı Faunası Türkiye Jeol. Kur. Bült., 22, 155-160.

Tabor, N.J., 2002. Paleoclimate Isotopic Proxies Derived from Paleozoic, Mesozoic, Cenozoic Paleosols and Modern Soils. University of California, PhD Thesis, p 213.

Tankut, A., 1985. Basic and ultrabasic rocks from the Ankara Melange, Turkey: Dixon, J.E. ve Robertson, A.H.F., ed., The Geological Evolution of the Mediterranean da.,'Special Publication of the Geological Society, 17, Blackwell Scientific Publications, 884, 449-454.

Tekkaya, İ., 1974. Türkiye'de Yeni Bulunan Omurgalı Fosiller ve Fosil Yatakları. MTA Dergisi, No: 83, 109–113.

Thorez, J., 1976. Practical Identification of Clay Minerals, 89 p.

Tzedakis, P.C., 1994. Vegetation change through glacial–interglacial cycles: a long pollen sequence perspective. Philosophical Transactions of the Royal Society of London. Series B 345, 403–432.

Tzedakis, P.C., Hooghiemstra, H., Pälike, H., 2006. The last 1.35 million years at Tenaghi Philippon: revised chronostratigraphy and long-term vegetation trends. Quaternary Science Reviews 25, 3416–3430.

Tucker, M., 1988. Techniques in sedimentology. Oxford: Blackwell Scientific Publications, 394 pp.

Tucker, M.E., 1991. Sedimentary Petrology: An Introduction to the Origin of Sedimentary Rocks. Blackwell Science, Oxford.

Tyler, G., 2004. Rare earth elements in soil and plant systems – a review. Plant and Soil 267, 191–206.

Ufnar, D.F., Gonzalez, L.A., Ludvigson, G.A., Brenner, R.L. and Witzke, B.J., 2001. Stratigraphic implications of meteoric sphaerosiderite $\delta^{18}O$ compositions in paleosols of the Cretaceous (Albian) Boulder Creek Formation, NE British Columbia Foothills, Canada. J. Sediment. Res**.,** 71, 1017–1028.

Ufnar, D.F., 2007. Clay coatings from a modern soil chronosequence: A tool for estimating the relative age of well-drained paleosols. Geoderma, 141 (3-4), 181-200.

Ünalan, G., Yüksel, V., Tkeli, T., Gönenç, O., Seyit, Z. and Hüseyin, S., 1976. Haymana-Polatlı yöresinin (güneybatı Ankara) Üst Kretase-Alt Tersiyer stratigrafi ve paleocoğrafik evrimi, TJK Bull., 19 (2).

Üveges, J.B., Horváth, Z., Michéli, E., Mindszenty, A., Németh, T., 2003. Reconstructing Quaternary pedogenesis in a paleosol sequence in Hungary. Quaternary International, 106-107, 61-71.

Velde, B., 1995. Origin and mineralogy of clays, Springer Verlag, Berlin. p 334.

Velichko, A. A., and Nechaev, V. P., (eds). 2005. Cenozoic climatic and environmental changes in Russia. Geological Society of America, Special Paper 382; 226.

Vitali, F., Longstaffe, F.J., McCarthy, P.J., Plint, A.G., Glen, W., Caldwell, E., 2002. Stable isotopic investigation of clay minerals and pedogenesis in an interfluve paleosol from the Cenomanian Dunvegan Formation, N.E. British Columbia, Canada Chemical Geology, 192 (3-4), 269-287.

Wick, L., Lemcke, G., Sturm, M., 2003. Evidence of Lateglacial and Holocene climatic change and human impact in eastern Anatolia: high resolution pollen, charcoal, isotopic and geochemical records from the laminated sediments of Lake Van, Turkey. The Holocene, 13 (5), 665–675.

Woronick, R.W. and Land, L.S., 1985. Late burial diagenesis, Lower Cretaceous Pearsall and Lower Glenn Rose Formations, South Texas. Soc. Econ. Paleontol. Mineral. Spec. Publ., 36, 265-275.

Wright, V.P., Tucker, M.E., 1991. Calcretes. Blackwell Scientific Publications, Oxford, p. 351.

Wright, V. P. and Robinson, D., 1988. Early Carboniferous floodplain deposits from South Wales: a case study of the controls on palaeosol development.Journal of the Geological Society, London, 145,847-857.

Wright, V.P., 1990. A micromorphological classificationof fossil and recent calcic and petrocalcic microstructures In: Soil Micromorphology: A Basic and Applied Science (Ed. By L.A. Douglas), Developments in Soil Science, 19, 401-407.

Yoldaş, R., 1982. Tosya (Kastamonu) ile Bayat (Çorum) arasındaki bölgenin jeolojisi, İst. Üniv. Fen. Fak. Genel Jeo. Kürsüsü, 331 p (Unpublished PhD Thesis).

Yüksel, S., 1970. Etude geologıque de la region d'Haymana (Turquie centrale): These, Fac.Sci. Univ. Nancy, France (unpublished).

Zachos, J., Pagani, M., Sloan, L., Thomas, E., Billups, K., 2001. Trends, rythms, and abberations in global climate 65 Ma to the present. Science, 292, 386–392.

CURRICULUM VITAE

Surname, Name: Küçükuysal, Ceren

Nationality: Turkish (TC)

Date and Place of birth: 5 June 1979, Ankara

Marital Status: Married

Phone: +90 533 474 77 62

Fax : +90 312 285 42 71

E-mail: ceren@mta.gov.tr

EDUCATION

Degree	Institution	Year of Graduation
MS	METU, Geological Engineering	2005
BS	METU, Geological Engineering	2002
High School	Cumhuriyet Lisesi, Ankara	1996

WORK EXPERIENCE

Year	Place	Enrollment
2010-	MTA	Engineer
2002- 2010	METU	Research Assistant
2000 July	MNG İnşaat	Intern Student
2000 July	TPAO	Intern Student

FOREIGN LANGUAGES

Advanced English, Fair Spanish

PUBLICATIONS

Küçükuysal, C., Engin, B., Türkmenoğlu, A.G., Aydaş, C., 2011. ESR dating of calcrete nodules from Bala, Ankara (Turkey): Preliminary results. Applied Radiation and Isotopes, 69, 492–499.

Nicoll, K. and Küçükuysal, C. Emerging Multi-Proxy Records of Late Quaternary Paleoclimate Dynamics in Turkey and the surrounding region. Submitted to Turkish Journal of Earth Sciences.

Küçükuysal, C., Türkmenoğlu, A.G., Kapur, S., Yılmaz, İ.Ö. 2010. Swelling Clay Paleosols As Indicators of Seasonal Drynesss During Plio-Quaternary in Ankara, Turkey. GSA Tectonic Crossroads: Evolving Orogens of Eurasia-Africa-Arabia Abtsract Book, p14.

Küçükuysal, C., Türkmenoğlu, A.G., Yılmaz, İ.Ö., Kapur, S., 2010. Mineralogic and Geochemical Properties of Calcretes in Ankara: Indicators of the Paleoclimatıc Conditions. 7th International Symposium on Eatsern Mediterranean Geology Abstract Book, p116.

Küçükuysal,C. Türkmenoğlu,A.G., Yılmaz,İ.Ö., 2009. Clay minerals as paleoclimaye indicators of Pliocene-Pleistocene time range,Ankara area, Turkey.

"14th International Clay Conference, Micro et Nano:Science Mare magnum, Book of Abstracts", Vol.II, p.198.

Atakul, A., Küçükuysal, C., Sayıt, K., Süer, S., 2007. Süs Taşları. ODTÜ Yayıncılık, 108s.

İpekgil, C., Aras, A., Türkmenoğlu, A.G., 2006. Occurrence of palygorskite in caliche deposits of Pliocene sediments in Ankara region, Turkey. Abstracts, Fourth Mediterranean Clay meeting, 5–10 September2006, METU, Ankara",66-67.

İpekgil, C. and Lünel, A.T., 2005. Beypazarı-Oymaağaç Granitoid: Its geology, petrography, geochemistry and tectonic significance. IESCA Proceedings, 137–142.

İpekgil, C., Lünel, T., 2005. Beypazarı-Oymaağaç Granitoid- Its Geology, Petrography, Geochemistry and Tectonic Significance. International Earth Sciences Colloquium on Agean Region (IESCA, 2005) Abtsract Book.

HOBBIES

Swimming, Traveling, Photography